



UNIVERSITY OF
BIRMINGHAM

**EXPLORING THE POTENTIAL OF HIGH MASS RESOLUTION AND
MASS ACCURACY MASS SPECTROMETRIC TECHNIQUES TO
TRACK THE ENVIRONMENTAL METABOLISM AND FATE OF BFRS:
APPLICATION TO THE AMBIENT ENVIRONMENT**

by

Aristide Paolo Ganci

MSc, BSc

A thesis submitted to the University of Birmingham for the degree of

DOCTOR OF PHILOSOPHY (Ph.D)

Division of Environmental Health Risk Management
College of Life and Environmental Sciences
School of Geography, Earth and Environmental Sciences
The University of Birmingham
Edgbaston, B15 2TT
United Kingdom
May 2018

UNIVERSITY OF
BIRMINGHAM

University of Birmingham Research Archive

e-theses repository

This unpublished thesis/dissertation is copyright of the author and/or third parties. The intellectual property rights of the author or third parties in respect of this work are as defined by The Copyright Designs and Patents Act 1988 or as modified by any successor legislation.

Any use made of information contained in this thesis/dissertation must be in accordance with that legislation and must be properly acknowledged. Further distribution or reproduction in any format is prohibited without the permission of the copyright holder.

Acknowledgments

I would like to express my gratitude to my supervisor Prof. Stuart Harrad for giving me the opportunity to conduct this PhD thesis. He was always available with a good advice and supported me where necessary, while allowing me to work independently. Also special thanks to Dr. Mohamed Abdallah who always had an open ear for my questions and gave me a lot of good hints and suggestions. Moreover, I would like to thank Dr. Thomas Möhring and the team of Thermo Fisher Scientific in Bremen for their support during my secondment, as well as the team in Dreieich under Dr. Michal Godula. Thanks to the European Commission for the financial support and making this ELUTE project possible.

I would like to thank all the other people of the POPs group in Birmingham for a good time together in the office and laboratory. Especially Dan for some fruitful discussions, Nina and Jennifer for a great atmosphere in the office, as well as Salim and Chris for letting me use their GCxGC-TOF system. Special thanks also to Dr. Christopher Vane from BGS for providing me the sediment samples.

A very unique thanks to Leon and Hoang, for being such great ELUTE project companions, but even more, friends and flatmates. Without them, this experience would have been way less exciting and memorable.

Last but not least thanks to my parents and my sister, who always encouraged and supported me in all my decisions, my friends in Vienna for cheering me up in the final phase of this thesis, as well as Alessia for being such a caring and wonderful person.

Abstract

This thesis investigates levels, sources, and transformation products of both legacy BFRs (LBFRs), and several novel BFRs (NBFRs). To accurately target these emerging pollutants in environmental matrices, an analytical method based on liquid chromatography coupled to high resolution mass spectrometry was developed. Sediment samples taken along the River Thames revealed the presence of both legacy and novel compounds, with concentrations of selected NBFRs approaching those of LBFRs. Tentative sources in the industrial area of London were identified, along with the presence of hydroxylated transformation products of polybrominated diphenyl ethers (PBDEs). Further, the employed technique facilitates the precise identification of metabolites and degradation products formed through *in vitro* and photodegradation studies. This provides valuable insight into the transformation mechanisms of NBFRs, including hydroxylation and debromination reactions. While 2,3,4,5-tetrabromobenzoic acid (TBBA) was the major metabolite of 2-ethylhexyl-2,3,4,5-tetrabromobenzoate (EH-TBB), 1,2-dibromo-4-(1,2-dibromoethyl)cyclohexane (DBE-DBCH) was biotransformed to monohydroxy-DBE-DBCH and monohydroxy-triDBE-DBCH in trout liver microsomes. Photolysis of investigated NBFRs resulted in the formation of lower brominated species through stepwise reductive debromination as a main pathway. In addition, the use of mass defect plots and bromine isotopic pattern assist in the identification of relevant unknown chemicals within complex mixtures of halogenated compounds in dust and sediment samples.

Table of Contents

Chapter I - Introduction	1
1.1. General background on PBDEs and NBRs.....	1
1.2. Legislative regulation on brominated flame retardants	2
1.3. Novel brominated flame retardants (NBRs).....	3
1.3.1. Environmental fate.....	5
1.3.2. 1,2-Bis(2,4,6-tribromophenoxy)ethane (BTBPE)	10
1.3.3. Decabromodiphenyl Ethane (DBDPE)	11
1.3.4. Bis(2-ethylhexyl)tetrabromophthalate (BEH-TEBP) and 2-ethylhexyltetrabromo- benzoate (EH-TBB).....	12
1.3.5. 2,3,4,5,6-pentabromoethylbenzene (PBEB).....	13
1.3.6. 2,3,4,5,6-pentabromotoluene (PBT)	14
1.3.7. 1,2-dibromo-4-(1,2-dibromoethyl)cyclohexane (DBE-DBCH).....	14
1.3.8. 2,3-dibromopropyl-2,4,6-tribromophenyl ether (TBP-DBPE).....	15
1.4. Behaviour and fate of NBRs and their transformation products.....	20
1.5. Transformation products of NBRs.....	21
1.5.1. Abiotic transformation processes	22
1.5.2. Biological transformation processes	23
1.6. Analysis of NBRs using high resolution mass spectrometry and mass defect filtering..	25
1.6.1. Types of Mass Spectrometer scans	25
1.6.2. Hyphenated chromatography/mass spectrometry analytical approaches	26
1.6.3. Mass defect and transformation products.....	29
1.6.4. Unknown screening approaches	36
1.7. Aims and Objectives.....	38
Chapter II - Materials and Methods.....	39
2.1. Chemicals	39
2.1.1. Sediment analysis.....	39
2.2. Sampling.....	40
2.2.1. Sediment Sampling.....	40
2.2.2. Total organic carbon (TOC) determination	42
2.2.3. Dust sampling.....	42
2.2.4. Master standard-mixture for multi-residue analysis.....	42
2.2.5. In vitro biotransformation of NBRs by trout liver microsomes	43
2.2.6. Photodegradation experiments	45
2.3. Extraction and Clean-up	48
2.3.1. Sediment	48
2.3.2. Dust	49
2.3.3. In vitro biotransformation of BFRs by trout liver microsomes (TLM).....	49
2.3.4. Photodegradation	50
2.4. Instrumental Analysis	50
2.4.1. Analytical method description	50
2.4.2. Maintenance of the instrument	60

2.4.3.	GCxGC-TOF mass spectrometer	63
2.5.	Qualification/Quantification	63
2.5.1.	Qualification	63
2.5.2.	Quantification.....	64
2.5.3.	QA/QC Criteria.....	65
2.6.	Data analysis.....	69
2.6.1.	Mass defect plots	69
2.6.2.	Statistical analysis.....	70
2.6.3.	Enzymatic kinetics	71
2.6.4.	Qualification and Quantitation using XCalibur and Trace Finder	71
2.6.5.	Unknown Screening using Compound Discoverer	71
Chapter III - A Comparison of Two High Mass Resolution Mass Spectrometric Methods for Screening for Halogenated Compounds in Complex Mixtures		75
3.1.	General overview.....	75
3.2.	Mass defect measurements	76
3.2.1.	Workflow.....	77
3.2.2.	PBDEs and PCBs.....	80
3.2.3.	NBFRs, HBCDDs and TBBPA.....	81
3.2.4.	OPFRs and Dechloranes	81
3.2.5.	Remarks.....	83
3.2.6.	PAHs	84
3.3.	Mass defect plot of dust sample.....	84
3.3.1.	PBDEs, HBCDDs and TBBPA	86
3.3.2.	PCBs.....	86
3.3.3.	Bromophenols, chlorophenols and mixed bromo-chloro phenols.....	86
3.3.4.	Chlorinated paraffins (CPs).....	87
3.3.5.	Other tentative compounds.....	88
3.4.	Mass defect plots of a sediment sample.....	88
3.4.1.	Internal standards	90
3.4.2.	PBDEs, HBCDDs and NBFRs	90
3.4.3.	PCBs.....	90
3.4.4.	Chlorinated paraffins.....	90
3.4.5.	Other tentative compounds.....	91
3.4.6.	Conclusion	91
3.5.	GCxGC-TOF/MS measurements.....	92
3.5.1.	Variable ionization energies	95
3.6.	Impact of collision energy and fragmentation in the HRAM Orbitrap	96
3.7.	Conclusions.....	98
Chapter IV - Legacy PBDEs and NBFRs in Sediment Samples of the River Thames.....		100
4.1.	General overview.....	100
4.2.	Sediment analysis	101
4.2.1.	Levels and trends of PBDEs and NBFRs in sediments.....	101
4.2.2.	TOC.....	102
4.2.3.	PBDEs	105

4.2.4.	HBCDDs and TBBPA	106
4.2.5.	NBFRs	107
4.3.	Spatial trends in concentrations of PBDEs and NBFRs.....	110
4.4.	PBDE / NBFR patterns	116
4.5.	Screening for degradation products and other low production volume NBFRs	118
4.5.1.	Hydroxylated BDEs	119
4.6.	Conclusion	123
Chapter V – Photochemical transformation reactions of NBFRs		126
5.1.	Overview	126
5.1.1.	PBDEs, HBCDDs and TBBPA	126
5.1.2.	NBFRs	128
5.1.3.	Calculations and QA/QC	129
5.2.	Exposure Experiments.....	132
5.2.1.	Indoor exposure	132
5.2.2.	Outdoor solar irradiation exposure.....	132
5.2.3.	UV-exposure.....	133
5.3.	Degradation products	134
5.3.1.	EH-TBB (2-ethylhexyl-2,3,4,5-tetrabromobenzoate).....	134
5.3.2.	BEH-TEBP (bis(2-ethylhexyl)tetrabromophthalate)	138
5.3.3.	BTBPE	141
5.3.4.	DBDPE.....	145
5.4.	Conclusions.....	149
Chapter VI – <i>In vitro</i> biotransformation of NBFRs by trout liver microsomes.....		151
6.1.	Overview	151
6.1.1.	PBDEs, HBCDDs and TBBPA	152
6.1.2.	NBFRs	153
6.2.	Screening for metabolite formation of NBFRs	154
6.2.1.	EH-TBB and BEH-TEBP	154
6.2.2.	Temperature studies for EH-TBB.....	159
6.2.3.	BTBPE	160
6.2.4.	DBE-DBCH.....	161
6.3.	Kinetic studies on DBE-DBCH.....	163
6.4.	Conclusion	167
Chapter VII – Summary and future perspectives		169
7.1.	Summary and Conclusions	169
7.2.	Research gaps and future perspective	173
References		175
Appendix I		190
Appendix II		197
Appendix III		205

List of Figures

Chapter I - Introduction

Figure 1-1. Comparison of ionization modes (APCI, APPI and ESI) for LC-MS systems, based on molecular weight and compound polarity, adapted from [150]	28
Figure 1-2. Halogen isotope patterns of Br ₃ , Cl ₃ and Br ₂ Cl ₂ , M = molecular ion peak, M+2, +4, +6, +8 = isotope peaks	30
Figure 1-3. Halogen isotope patterns of chlorinated, brominated and mixed-halogenated compounds, adapted from Vetter <i>et al.</i> [163]	31
Figure 1-4. Mass defect plot using the H/Cl transformed Kendrick mass scale of an extract of Lake Ontario lake trout, adapted from Jobst <i>et al.</i> [164] DDT= dichlorodiphenyltrichloroethane; PCN = polychlorinated naphthalene; PCBs = polychlorinated biphenyls; PCDPes = polychlorinated diphenyl ethers	34
Figure 1-5. Different levels of confidence in the identification process of compounds by high resolution mass spectrometry, adapted from Schymanski <i>et al.</i> [22]	37
Figure 1-6. Different approaches for identification of compounds and levels of confidence, adapted from Schymanski <i>et al.</i> [184]	37

Chapter II - Materials and Methods

Figure 2-1. Sampling locations (yellow diamonds) of surface sediments along the Thames Estuary. Stars represent the main discharge locations of sewage effluents; 1. Mogden; 2. Abbey Mills; 3. Beckton STP; 4. Crossness STP; 5. Long Reach STP; 6. Tilbury STP. Red shaded area shows the main industrial discharge area on the Thames (samples 13-34). The Teddington Lock on the left divides the river Thames in to a tidal and non-tidal part. Adapted from Lopes dos Santos and Vane [185]. STP – sewage treatment plants	41
Figure 2-2. Schematic of indoor exposure experiment	45
Figure 2-3. Schematic of outdoor exposure experiment	46
Figure 2-4. Location of the outdoor exposure experiment (red circle) on the University of Birmingham campus	47
Figure 2-5. Schematic of UV exposure experiment	48
Figure 2-6. Excerpt from an extracted ion chromatogram for selected PBDEs measured in APCI in a 200 pg μL^{-1} standard solution	55
Figure 2-7. Excerpt from an extracted ion chromatogram for selected NBFRs measured in APCI in a 200 pg μL^{-1} standard solution	55
Figure 2-8. Excerpt from an extracted ion chromatogram for selected BFRs measured in APCI in a 200 pg μL^{-1} standard solution	56
Figure 2-9. Excerpt from an extracted ion chromatogram for Dechloranes measured in APCI in a 200 pg μL^{-1} standard solution	56
Figure 2-10. Excerpt from an extracted ion chromatogram for OPFRs (pos.), HBCDDs (neg.) and TBBPA (neg.) measured in HESI in pos./neg. switching mode in a 200 pg μL^{-1} standard solution	57

Figure 2-11. Excerpt from an extracted ion chromatogram for PCBs measured in APCI in a 200 $\mu\text{g mL}^{-1}$ standard solution.....	57
Figure 2-12. Excerpt from an extracted ion chromatogram for selected PBDEs measured in APCI in an extracted dust sample.....	58
Figure 2-13. Excerpt from an extracted ion chromatogram for HBCDD and selected NBFrs measured in APCI in an extracted dust sample.....	58
Figure 2-14. Excerpt from an extracted ion chromatogram for selected PBDEs measured in APCI in the sediment SRM 1944.....	59
Figure 2-15. Excerpt from an extracted ion chromatogram for HBCDD and selected NBFrs measured in APCI in the sediment SRM 1944.....	59
Figure 2-16. Results of an acceptable mass accuracy calibration in positive (A) and negative (B) ESI mode, with rms = (internal- / external ppm).....	61
Figure 2-17. ESI Positive Ion Calibration Solution Spectra - Formulation: caffeine (20 $\mu\text{g mL}^{-1}$), MRFA (1 $\mu\text{g mL}^{-1}$) and Ultramark 1621 (0.001 %) in an aqueous solution of acetonitrile (50 %), methanol (25 %) and acetic acid (1 %). Caffeine @195, MRFA @524, Ultramark @1222, 1422, 1622.....	62
Figure 2-18. ESI Negative Calibration Solution Spectra - Formulation: sodium dodecyl sulfate (SDS) (2.9 $\mu\text{g mL}^{-1}$), sodium taurocholate (5.4 $\mu\text{g mL}^{-1}$) and Ultramark 1621 (0.001 %) in an aqueous solution of acetonitrile (50 %), methanol (25 %) and acetic acid (1 %). SDS @265, sodium taurocholate @514, Ultramark @1280, 1380, 1480, 1580, 1680, 1780.....	62
Figure 2-19. Isotope pattern of EH-TBB standard (80 pg), measured (top) and simulated with Xcalibur (bottom).....	64
Figure 2-20. Five-point calibration curve for EH-TBB.....	65
Figure 2-21. Workflow of Compound Discoverer to screen for unknown compounds.....	72
Figure 2-22. Example for a result from a Compound Discoverer workflow to screen for DBE-DBCH metabolites in a trout liver microsome <i>in-vitro</i> study, A: list of hits and identified parameters, B: extracted ion chromatogram of sample vs. control measurement, C: mass spectrum of the identified compound (monohydroxy-DBE-DBCH) together with isotope pattern matching (green boxes).....	73
Chapter III - A Comparison of Two High Mass Resolution Mass Spectrometric Methods for Screening for Halogenated Compounds in Complex Mixtures	
Figure 3-1. Screen capture from Xcalibur workflow for the identification of compounds, including the observed accurate mass taken from the mass defect plot (1), the extracted ion chromatogram (2), the experimental isotope pattern and mass-to-charge value (3), the predicted elemental composition (4) based on the employed settings, the simulated theoretical isotope pattern and mass-to-charge value (5), with a subsequent calculated mass deviation value in ppm (3) and the resulting tentative compound identification (6), after conducting a ChemSpider database search.....	78
Figure 3-2. Mass defect plot of master mix containing 200 $\mu\text{g mL}^{-1}$ of PBDEs, HBCDDs, TBBPA, NBFrs, Dechloranes, OPFRs and PCBs.....	79
Figure 3-3. Mass defect plot of master mix only showing PBDEs and PCBs.....	80

Figure 3-4. Mass defect plot of master mix only showing NBFRs, HBCDDs and TBBPA.....	82
Figure 3-5. Mass defect plot of master mix only showing OPFRs and Dechloranes.....	82
Figure 3-6. Mass defect plot of simulated isotopic patterns of brominated (hexaBDE), chlorinated (Dec 602) and mixed compounds (Dec 604) to visualise the slope of the isotopic cluster	83
Figure 3-8. XICs of bromophenols (mono-, di- and tri-), chlorophenols (mono-, di- and tri-) and mixed phenols (chlorobromo and chlorodibromo) in an extracted dust sample.....	87
Figure 3-9. Mass defect plot of extracted sediment sample transformed with H/Br scale 78/77.91051	89
Figure 3-10. GCxGC-TOF results for master mixture standard measured at 70 eV containing 200 $\mu\text{g } \mu\text{L}^{-1}$ of PBDEs, HBCDDs, TBBPA, NBFRs, Dechloranes, OPFRs, PCBs and PAHs ...	93
Figure 3-11. GCxGC-TOF results measured at 12 eV for standard containing 200 $\mu\text{g } \mu\text{L}^{-1}$ of only NBFRs	94
Figure 3-12. GCxGC-TOF spectrum for HCDBCO measured at 12 and 70 eV, M^+ =molecular ion	95
Figure 3-13. Fragmentation of decaBDE standard in different measurements on LC-orbitrap employing selected normalized collision energies (10, 20 and 30).....	97
Figure 3-14. Fragmentation of decaBDE standard in a single measurement on LC-Orbitrap at stepped collision energies (SCE) of 10, 20 and 30	97
Chapter IV - Legacy PBDEs and NBFRs in Sediment Samples of the River Thames	
Figure 4-1. TOC content from surface sediments of the Thames Estuary.....	102
Figure 4-2. Average PBDE congener profile in all sediment samples. BDE-209 is on a different scale. Average percent contributions are indicated above each congener with error bars representing the standard deviation.....	104
Figure 4-3. Average HBCDD diastereomer profile in industrial and non-industrial area	111
Figure 4-4. HBCDD diastereomer profile of 3 sampling sites (location nr. 18, 31 and 34) with comparatively high HBCDDs concentrations.	111
Figure 4-5. Spatial trends for Σ_{12} BDEs, HBCDDs and TBBPA (top) and Σ_{12} BDEs, BEH-TEBP, BTBPE and TBP (bottom) measured (in $\mu\text{g } \text{kg}^{-1}$ organic carbon) along the river Thames, with an approximate distance from Teddington Lock.....	112
Figure 4-6. Concentrations ($\mu\text{g } \text{kg}^{-1}$ organic carbon) of Σ_{12} PBDEs in River Thames sediments at each sampling location. Stars represent the main discharge locations of sewage effluents; 1. Mogden; 2. Abbey Mills; 3. Beckton STP; 4. Crossness STP; 5. Long Reach STP; 6. Tilbury STP. Adapted from Lopes dos Santos and Vane [185]. STP – sewage treatment plants	114
Figure 4-7. Concentrations ($\mu\text{g } \text{kg}^{-1}$ organic carbon) of BDE-209 in River Thames sediments at each sampling location. Stars represent the main discharge locations of sewage effluents; 1. Mogden; 2. Abbey Mills; 3. Beckton STP; 4. Crossness STP; 5. Long Reach STP; 6. Tilbury STP. Adapted from Lopes dos Santos and Vane [185]. STP – sewage treatment plants	115

Figure 4-8. Comparison of an average PBDE profile in the industrial area (dotted) and outside the industrial area (white) to a technical penta / octa / deca BDE mix (black) – technical mixture values adapted from La Guardia et al. [233].....	117
Figure 4-9. XICs of 2-HO-BDE28 (C ₁₂ H ₇ Br ₃ O ₂) standard (bottom) measured in HESI, including the trace of a dibrominated impurity (top)	120
Figure 4-10. MS ² fragmentation spectra of a 2-HO-BDE28 standard at retention time 5.67	120
Figure 4-11. MS ² fragmentation spectra of a sediment sample (nr. 22) at retention time 5.67	121
Figure 4-12. MS ² fragmentation spectra of impurity in the 2-HO-BDE28 standard at retention time 5.21	121
Figure 4-13. MS ² fragmentation spectra of a sediment sample (nr. 21) at retention time 5.21	121
Figure 4-14. XICs of 6-HO-BDE47 (C ₁₂ H ₆ Br ₄ O ₂) standard (bottom) measured in HESI, including the trace of 3 different dibrominated impurities (top)	122
Figure 4-15. MS ² fragmentation spectra of a 6-OH-BDE47 standard at retention time 6.46	122
Figure 4-16. MS ² fragmentation spectra of a sediment sample (nr. 21) at retention time 6.42	122

Chapter V - Photochemical transformation reactions of NBFRs

Figure 5-1. Temperature profile for indoor exposure experiment (05.08.-29.08.2017), solid line: dark control, dotted line: exposed samples	130
Figure 5-2. Temperature profile for outdoor exposure experiment (08.08.-29.08.2017), located at N 52° 27' 3" latitude and W 1° 55' 50" longitude; solid line: dark control, dotted line: exposed samples.....	130
Figure 5-3. Solar irradiation data in W/m ² (measured at Coleshill, UK – located at N 52° 28' 57" latitude and W 1° 41' 46" longitude – obtained from MetOffice) for outdoor exposure time period, black arrows indicate the five sampling points.....	131
Figure 5-4. Cumulative irradiation in W/m ² of five samples taken during outdoor exposure	131
Figure 5-5. XICs of EH-TBB and identified photodegradation products P1 (tribrominated) and P2 (dibrominated) in methanol after 22 h of UV-C irradiation.....	136
Figure 5-6. XICs of EH-TBB and identified photodegradation products P1 (tribrominated) and P2 (dibrominated) in methanol after 9 h of outdoor solar exposure.....	136
Figure 5-7. Relative amount of EH-TBB and its debromination products in methanol at different UV-C irradiation times	137
Figure 5-8. XICs of BEH-TEBP and its photodegradation products P1 (tribrominated), P2 (dibrominated) and P3 (monobrominated) in methanol after 22 h of UV-C irradiation	139

Figure 5-9. XICs of BEH-TEBP and its photodegradation products P1 (tribrominated), P2 (dibrominated) and P3 (monobrominated) in methanol after 9 h of outdoor solar exposure.....	140
Figure 5-10. BEH-TEBP and its debromination products in methanol at different UV-C irradiation times.....	140
Figure 5-11. Proposed degradation pathway of BEH-TEBP through hydrolysis of the ester groups and formation of an anhydride, adapted from [247].....	141
Figure 5-12. XICs of BTBPE (peak at 7.8 marked in bold) and its photodegradation products P1 (1-(2,4,6-tribromophenoxy)-2-(2,4-dibromophenoxy)ethane), P2/3 (1,2-bis(2,4-dibromo-phenoxy) ethane / 1-(2,4,6-tribromophenoxy)-2-(4-bromophenoxy)ethane and P4 (1-(2,4-dibromo-phenoxy)-2-(4-bromophenoxy)ethane) in methanol after 48 h of UV-C irradiation.....	142
Figure 5-13. XICs of further BTBPE photodegradation products P5 (2-ethanol-2,4,6-tribromophenoxy ether), P6 (2-ethenol-2,4,6-tribromophenoxy ether), P7 (2-ethenol-2,4-dibromophenoxy ether), P9 (2,4,6-tribromophenol) and P12 (2,4-dibromophenol) in methanol after 48 h of UV-C irradiation, for P7 (RT 5.26), P9 (RT 5.74) and P12 (5.14) the described compounds are marked in bold.....	143
Figure 5-14. Relative amount debromination products of BTBPE in methanol at different UV-C irradiation times.....	144
Figure 5-15. Proposed degradation pathway of BTBPE, bold arrows mark the main pathway, adapted from [250].....	145
Figure 5-16. XICs of DBDPE and its photodegradation products P1-P7 (nona- to tri-BDPE) in methanol after 9 h (for DBDPE, P1 and P2) and 130 h (P3-P7) of outdoor solar irradiation.....	146
Figure 5-17. Relative amounts of DBDPE and its debromination products in methanol at different UV-C irradiation times.....	147
Figure 5-18. XICs of DBDPE and further photodegradation products nona- to hexa-BDPE) in methanol after 9 h of outdoor solar irradiation.....	148
Figure 5-19. XICs of DBDPE and further photodegradation products nona- to hexa-BDPE) in methanol after 22 h of UV-C irradiation.....	148
Chapter VI - <i>In vitro</i> biotransformation of NBRs by trout liver microsomes	
Figure 6-1. Formation of 2,3,4,5 tetrabromobenzoic acid (TBBA) from EH-TBB through cleavage of the 2-ethylhexyl chain.....	155
Figure 6-2. Selected UPLC–Orbitrap–MS XIC of EH-TBB (APCI) and its metabolite TBBA (ESI) formed by TLM exposure to 10 µM EH-TBB for 60 min., including Br ion trace from all ion fragmentation (AIF).....	156
Figure 6-3. Selected UPLC–Orbitrap–MS XIC of BEH-TEBP after TLM exposure to 10 µM BEH-TEBP for 60 min, including Br ion trace from all ion fragmentation (AIF).....	157
Figure 6-4. Temperature dependent formation of metabolite TBBA from the parent compound EH-TBB exposed to trout liver microsomes for 60 min.....	160

Figure 6-5. Selected UPLC–Orbitrap–MS XIC of DBE-DBCH and its metabolites formed by TLM exposure to 10 μ M of technical DBE-DBCH (panels b, d and f) and β -DBE-DBCH (panels c and e) for 60 min. Parent compounds (panel b and c) are measured in APCI, metabolites and Br trace (panels a and d-f) in ESI..... 162

Figure 6-6. Kinetic study of technical DBE-DBCH metabolite formation fit to a Michaelis–Menten model following 60 min incubation with TLM at various substrate concentrations. Data are means \pm SD (n = 3) 164

Figure 6-7. Kinetic study of β -DBE-DBCH metabolite formation fit to a Michaelis–Menten model following 60 min incubation with TLM at various substrate concentrations. Data are means \pm SD (n = 3)..... 164

Annex III

Figure 11-1. The concentration of EH-TBB at different irradiation times (top) during indoor exposure, including first order kinetic degradation rates in toluene, hexane and methanol (bottom)..... 205

Figure 11-2. The concentration of BEH-TEBP at different irradiation times (top) during indoor exposure, including first order kinetic degradation rates in toluene, hexane and methanol (bottom)..... 206

Figure 11-3. The concentration of BTBPE different irradiation times (top) during indoor exposure, including first order kinetic degradation rates in toluene, hexane and methanol (bottom)..... 207

Figure 11-4. The concentration of DBDPE different irradiation times (top) during indoor exposure, including first order kinetic degradation rates in toluene, hexane and methanol (bottom)..... 208

Figure 11-5. The concentration of EH-TBB different irradiation times (top) during outdoor exposure, including first order kinetic degradation rates in toluene, hexane and methanol (bottom)..... 209

Figure 11-6. The concentration of BEH-TEBP different irradiation times (top) during outdoor exposure, including first order kinetic degradation rates in toluene, hexane and methanol (bottom)..... 210

Figure 11-7. The concentration of BTBPE different irradiation times (top) during outdoor exposure, including first order kinetic degradation rates in toluene, hexane and methanol (bottom)..... 211

Figure 11-8. The concentration of DBDPE different irradiation times (top) during outdoor exposure, including first order kinetic degradation rates in toluene, hexane and methanol (bottom)..... 212

Figure 11-9. The concentration of EH-TBB, BEH-TEBP, BTBPE and DBDPE different irradiation times (top) during UV-B exposure, including first order kinetic degradation rates in methanol (bottom)..... 213

Figure 11-10. The concentration of EH-TBB, BEH-TEBP, BTBPE and DBDPE different irradiation times (top) during UV-C exposure, including first order kinetic degradation rates in methanol (bottom)..... 214

List of Tables

Chapter I - Introduction

Table 1-1. Physical and chemical properties of legacy BFRs ¹ and novel BFRs ² (adapted from ^a [14], ^b [24])	6
Table 1-2. Summary of mean concentrations (min.-max. in parentheses) as indicated in each study of legacy BFRs and NBFRs in environmental samples around the world.....	15
Table 1-3. Halogen isotope abundances of brominated, chlorinated and mixed-halogenated compounds, adapted from Vetter <i>et al.</i> [163]	32

Chapter II - Materials and Methods

Table 2-1. Experimental set-up for the <i>in vitro</i> screening study	44
Table 2-2. Experimental set-up for the <i>in vitro</i> kinetic experiment series with DBE-DBCH (equimolar mixture of α - and β -DBE-DBCH, as well as single β - DBE-DBCH)	44
Table 2-3. Experimental set-up for the <i>in vitro</i> temperature study with EH-TBB	44
Table 2-4. HPLC elution programme for sediment/dust analysis and master mix measurements.....	52
Table 2-5. HPLC elution programme for <i>in vitro</i> and photodegradation samples	52
Table 2-6. Ion generated in the APCI / ESI source from injection of standards and exact mass of the most abundant isotope in the pattern for LC-HRMS analysis.....	53
Table 2-7. Calibration ions for mass accuracy in positive and negative ESI mode	61
Table 2-8. Calibration curves.....	65
Table 2-9. Comparison of UPLC-HRMS data for BFRs with NIST SRM 1944 certified values..	66
Table 2-10. Instrument LOD and LOQ (pg/ μ l), linearity and relative standard deviation (n=10) of target compounds.....	67
Table 2-11. Sample LOD and LOQ (pg/g) for sediment analysis and internal standards used for quantification	68
Table 2-12. Compound Discoverer workflow nodes and settings.....	74

Chapter III - A Comparison of Two High Mass Resolution Mass Spectrometric Methods for Screening for Halogenated Compounds in Complex Mixtures

Table 3-1. Compounds tentatively identified in the dust sample	85
Table 3-2. Compounds tentatively identified in the sediment sample	89
Table 3-3. Selected compounds measured on GCxGC-TOF at 12 and 70 eV, relative abundance (%) of molecular ion in the mass spectrum	96

Chapter IV - Legacy PBDEs and NBFRs in Sediment Samples of the River Thames

Table 4-1. Summary of the concentrations in both μ g kg ⁻¹ dry weight and μ g kg ⁻¹ organic carbon of selected BFRs in surficial sediments from the River Thames.....	103
---	-----

Chapter V - Photochemical transformation reactions of NBFRs

Table 5-1. Photodegradation kinetics for indoor exposure experiments for EH-TBB, BEH-TEBP, BTBPE and DBDPE, including half-lives $t_{1/2}$ and linearity of the decay R^2	132
---	-----

Table 5-2. Photodegradation kinetics for outdoor sunlight exposure experiments for EH-TBB, BEH-TEBP, BTBPE and DBDPE, including half-lives $t_{1/2}$ and linearity of the decay R^2 ...	133
Table 5-3. Photodegradation kinetics (rate constant k and half-life $t_{1/2}$) for UV-B / UV-C exposure experiments calculated for EH-TBB, BEH-TEBP, BTBPE and DBDPE in methanol, including degradation rate constant k , half-lives $t_{1/2}$ and linearity of the decay R^2	134
Table 5-4. Identified EH-TBB ($C_{15}H_{18}Br_4O_2$) degradation products, including measured accurate mass-to-charge and mass deviation; tentative formula and measured ion ..	135
Table 5-5. Identified BEH-TEBP ($C_{24}H_{34}Br_4O_4$) degradation products, including measured accurate mass-to-charge and mass deviation; tentative formula and measured ion ..	138
Table 5-6. Identified BTBPE ($C_{14}H_8Br_6O_2$) degradation products, including measured accurate mass-to-charge and mass deviation; tentative formula and measured ion.....	142
Table 5-7. Identified DBDPE ($C_{14}H_4Br_{10}$) degradation products, including measured accurate mass-to-charge and mass deviation; tentative formula and measured ion.....	146

Chapter VI - *In vitro* biotransformation of NBRs by trout liver microsome

Table 6-1. Metabolic enzymes in different liver subcellular fractions (adapted from ¹):.....	152
Table 6-2. Selection of <i>in vitro</i> / <i>in vivo</i> studies of trout (rainbow and juvenile brown)	159
Table 6-3. List of identified DBE-DBCH metabolites produced after incubation of technical DBE-DBCH with TLM for 60 min.	163
Table 6-4. Kinetic parameters derived from Michaelis–Menten model for the formation of DBE-DBCH metabolites following incubation of technical DBE-DBCH and β -DBE-DBCH with TLM for 60 Min.	165

Annex II

Table 10-1. Distance from Teddington Lock, TOC and site name for Thames Estuary surface sediments	197
Table 10-2. Calibration standards CS1 to CS5, with native compounds, internal standards (IS) and syringe standard (SS – recovery determination standard)	198
Table 10-3. Summary of the concentrations ($\mu\text{g kg}^{-1}$ dry weight / organic carbon) of PBDE congeners in sediments from the River Thames	200
Table 10-4. Summary of concentrations in ng g^{-1} dry weight for all PBDE congeners analysed in all 45 sediment samples	201
Table 10-5. Summary of concentrations in ng g^{-1} dry weight for (N)BFRs analysed in all 45 sediment samples.....	203

Abbreviations

aCl10DP	Cl10 Dechlorane Plus
aCl11DP	Cl11 Dechlorane Plus
aDP	anti Dechlorane Plus
AGC	automatic gain control
AICc	Akaike Information Criterion corrected
AIF	all ion fragmentation
amu	atomic mass unit
ANOVA	analysis of variance
AO	aldehyde oxidase
APCI	atmospheric pressure chemical ionization
APPI	atmospheric pressure photoionisation
ASE	accelerated solvent extraction
ATE	2,4,6-tribromophenylallylether (TBP-AE)
BAF	bioaccumulative factor
BATE	2-bromoallyl-2,4,6-tribromophenylether (TBP-BAE)
BB153	2,2',4,4',5,5'-hexabromobiphenyl
BEH-TEBP	bis(2-ethylhexyl)tetrabromophthalate
BFR	brominated flame retardant
BTBPE	1,2-bis-(2,4,6-tribromophenoxy)ethane
CYP	cytochrome P450
DBDPE	decabromodiphenylethane
DBE-DBCH	1,2-dibromo-4-(1,2 dibromoethyl)cyclohexane (TBECH)
DCM	dichloromethane
DDT	dichlorodiphenyltrichloroethane
Dec 602	Dechlorane 602
Dec 603	Dechlorane 603
Dec 604	Dechlorane 604
decaBDE	decabromo diphenyl ether
DEHP	bis(2-ethylhexyl)phthalate
DNA	deoxyribonucleic acid
DPTE	2,4,6-Tribromophenyl 2,3-dibromopropyl ether (TBP-DBPE)
EC	European Commission
ECOSAR	Ecological Structure Activity Relationships
EFSA	European Food Safety Authority
eFT	enhanced Fourier Transformation
EH-TBB	2-ethylhexyl-2,3,4,5-tetrabromobenzoate
EPA	Environmental Protection Agency
EPS	expanded polystyrene
ESI	electrospray ionisation
EU	European Union
FMO	flavin monooxygenase
FS	full scan
FWHM	full width at half-maximum
GC	gas chromatography

GCxGC	two dimensional gas chromatography
GST	glutathione transferase
HBB	hexabromobenzene
HCD	higher energy collisional dissociation
HCDBCO	hexachlorocyclopentadienyl-dibromocyclooctane
HESI	Heated electrospray ionisation
HLM	human liver microsome
HPLC	high-performance liquid chromatography
HPVC	high production volume chemical
HRMS	high resolution mass spectrometry
IS	internal standard
IT	injection time
K _{ow}	octanol-water partition coefficient
LBFR	legacy brominated flame retardants
LOD	limit of detection
LOQ	limit of quantification
LTQ	Linear Trap Quadrupole
LPVC	low production volume chemical
LRAT	long range atmospheric transport
m/z	mass to charge ratio
MAO	monoamine oxidase
max.	maximum
MCPD	monochloro-propanediol
MDF	mass defect filter
MEHP	mono(2-ethylhexyl)phthalate
min.	minimum
MRM	multiple reaction monitoring
MS	mass spectrometry
NADPH	nicotinamide adenine dinucleotide phosphate
NBFR	novel brominated flame retardant
OBTMPI/OBIND	octabromotrimethyl-phenylindane
OC	organic carbon
octaBDE	octabromo diphenyl ether
OPFR	organo phosphate flame retardant
OSPAR	Oslo-Paris Commission
PBB	polybrominated biphenyl
PBDD	polybrominated dibenzo-p-dioxin
PBDE	polybrominated diphenyl ether
PBDF	polybrominated dibenzo furan
PBEB	pentabromoethylbenzene
PBP	pentabromophenol
PBP-Acr	pentabromobenzyl acrylate
PCA	principal component analysis
PCB	polychlorinated biphenyls
PCDD/Fs	polychlorinated dibenzo-p-dioxins/furans
PCDPEs	polychlorinated diphenyl ethers
PCN	polychlorinated naphthalene

pentaBDE	pentabromo diphenyl ether
POP	persistent organic pollutant
ppm	parts per million
PTV	programmed temperature vaporizer
QA/QC	quality assurance/quality control
RDS	Recovery Determination Standard
REACH	Registration, Evaluation, Authorisation and Restriction of Chemicals
RIA	relative isotopic abundances
RLM	rat liver microsome
rms	root mean square
RRF	relative response factor
RSD	relative standard deviation
RT	retention time
SD	standard deviation
sDP	syn Dechlorane Plus
SULT	sulfurtransferase
Sy.x	standard deviation of the residuals
TBA	2,4,6-tribromoanisol
TBBA	2,3,4,5-tetrabromobenzoic acid
TBBPA	tetrabromo bisphenol A
TBBPA-DAE	tetrabromo-bisphenoldiallylether
TBBPA-DBPE	tetrabromobisphenol-bis(2,3-dibromopropylether)
TBECH	1,2-dibromo-4-(1,2 dibromoethyl)cyclohexane
TBMB	2,3,4,5-tetrabromobenzoate
TBMEHP	mono(2-ethylhexyl)tetrabromophtalate
TBOEP	tris(2-butoxyethyl) phosphate
TBP	tribromophenol
TBP-AE	2,4,6-tribromophenylallylether (ATE)
TBP-BAE	2-bromoallyl-2,4,6-tribromophenylether (BATE)
TBP-DBPE	2,4,6-Tribromophenyl 2,3-dibromopropyl ether (DPTE)
TBX	2,3,5,6,-tetrabromo-p-xylene
TCEP	tris(2-chlorethyl)phosphate
TCiPP	tris(2-chlorisopropyl)phosphate
TDBPP	tris(2,3-dibromopropyl) phosphate
TDCiPP	tris(1,3-dichloroisopropyl)phosphate
TIC	total ion current
TLM	trout liver microsome
TOF	time of flight
TPHP	Triphenylphosphate
UGT	uridine glucuronide transferae
UNEP	United Nations Environment Programme
UPLC	ultra-performance liquid chromatography
US EPA	United States Environmental Protection Agency
WHO	World Health Organisation
XIC	extracted ion chromatogram
XPS	extruded polystyrene

Chapter I - Introduction

1.1. General background on PBDEs and NBRs

Large numbers of organic flame retardants have been produced to date. They are a diverse set of chemicals applied to textiles, furniture, electronic equipment, building materials and polymers, with the aim of reducing or preventing their flammability and thereby decreasing the spread of fire. These chemicals can both be incorporated as additives (blended with the used material) or reactives (chemically bonded) into the manufactured material [1]. Further, they can be divided into organohalogen (organochlorine, organobromine) and organophosphorus compounds. This review will focus on the first of these classes, with a special emphasis on emerging organobrominated chemicals.

While there are indications that the use of flame retardants saves lives and reduces economic loss [1], consumer safety benefits against possible risks is still debated [2]. Potential risks include adverse effects on animals and humans, which are compounded by environmental persistence [3].

The mechanism of action of brominated flame retardants (BFRs) relies on their ability to quench the radical oxidation reactions that occur during combustion, by reacting with H and HO radicals. In these reactions bromine is released [1]. Hence it is assumed that similar debromination reactions or the release of radicals take place also in the environment [4].

Chemical stability and persistence, bioaccumulative characteristics, semi-volatility and observed ubiquity through the ability to circulate globally via the atmosphere, a phenomenon also described as long range atmospheric transport (LRAT) are all properties of persistent organic pollutants (POPs), some BFRs being part of this group. These properties are underlined

by the numerous notable signees of the 'San Antonio Statement' [5] of various fields within environmental sciences and emphasizes why BFRs are a topic of major concern to today's global society.

1.2. Legislative regulation on brominated flame retardants

Since the 1960s a wide variety of BFRs has been introduced to various products in general use. The most extensively used BFRs include: tetrabromobisphenol A (TBBPA), hexabromocyclododecane (HBCDD) and three commercial technical mixtures of polybrominated diphenyl ethers (PBDEs), namely pentabromo diphenyl ether (pentaBDE), octabromo diphenyl ether (octaBDE) and decabromodiphenyl ether (decaBDE) [3]. Within the European Union, manufacture and new use of pentaBDE and octaBDE formulations were prohibited in 2004, and these formulations were listed under the UNEP Stockholm Convention on persistent organic pollutants (POPs) in 2009 [6]. Restrictions on the manufacture and use of decaBDE have followed, and it was listed in 2017 under Annex A of the Stockholm Convention [7]. A key consideration with respect to its possible listing under the Stockholm Convention, is the potential of decaBDE to form lower BDEs by various debromination processes [4]. Further, HBCDD was listed under Annex I of the POP regulation in 2013 [8]. Although TBBPA is not considered for inclusion in the POPs list, since it does not fulfil the persistence criteria, it has been classified as Class 2A carcinogenic to humans by the International Agency for Research on Cancer (IARC) and has known toxic implications for aquatic organisms [9].

Some countries or states, such as the UK, Ireland and California have set requirements for furniture and electrical equipment to meet precise flammability tests [10]. However there is growing evidence that these requirements may not always meet their intended use and that the fire safety standards do not always have measurable benefits [11].

The European Union (EU) has set a regulation concerning the registration, evaluation, authorization and restriction of chemicals (REACH). It came into effect on the 1st of June 2007 and is intended to protect human health and the environment from potential risks posed by chemicals. Through the implementation of REACH, industries will be in charge to assess the risks of their chemicals and provide adequate safety information [12].

1.3. Novel brominated flame retardants (NBFRs)

Due to these legislative restrictions on manufacture and use of mentioned BFRs, several new variants of such chemicals have been developed and their overall production is continuously rising [13]. Concurrently, some of these new chemicals have already been in production for several years and are now finding an increase in production due to use as replacement products. These chemicals are commonly referred to as novel brominated flame retardants (NBFRs), with the word “novel” relating to their new presence on the market, as well as their recent observation in environmental samples [4]. In addition, terms such as: “alternate”, “new”, “emerging”, and “non-PBDE” have been used to describe these compounds [14]. Global NBFR production has an estimated volume between 10,000 and 18,000 tons per year, although for most NBFRs detailed information on their production levels and use is not yet available [15].

Recent publications have focused on the analysis, presence and environmental fate and behaviour of NBFRs [14, 16, 17], as well as their bioaccumulative behaviour and presence in the Arctic environment as an indicator of long range atmospheric transport (LRAT) [18]. However, the literature to date still contains data gaps. Early studies focused on the analysis and occurrence of BTBPE and DBDPE in the Great Lakes region and China. Stepwise more data is available in other Asian regions and Europe, as well an extended interest to other NBFRs. A recent review concluded that DBDPE, acting as replacement for decaBDE, is now present in

the environment at concentrations comparable to PBDEs in surficial sediments in Asia [19]. The presence of other NBRs, such as EH-TBB, BEH-TEBP and BTBPE is also reported more consistently, but at lower detection frequencies compared to DBDPE in sediments and soil [19]. The replacement of legacy PBDEs by NBRs is not yet evident in all environmental compartments. A correlation analysis in the atmospheric environment for example did not indicate the replacement of decaBDE by DBDPE or the penta-BDE technical mixture by Firemaster 550 [20]. Therefore, more studies on NBRs are needed to better explain their geographic distribution and bioavailability, as well as possible time trends and spatial variations [17].

Further, there is a general lack of information on how many NBRs are currently in use. It is not within the scope of this chapter to attempt to give an extensive list of all NBRs mentioned in literature at present. Hence, based on de Wit *et al.* [21] and assessment of relevant scientific papers and reports the best studied NBRs to date are BTBPE, DBDPE, EH-TBB, BEH-TEBP, PBEB, PBT, DBE-DBCH and TBP-DBPE with other NBRs also found in various environmental compartments.

With an increase of produced and discovered chemicals in the field of flame retardants (FR), the amount of used abbreviations in literature has also risen over the last years. Various short forms for the same chemical compound may lead to confusion, can make literature searches more time-intensive and call for a harmonized nomenclature amongst scientist and others for addressing these chemicals. To approach this issue and implement a common vocabulary, Bergman *et al.* proposed a standardized abbreviation list for flame retardants, as well as for other halogenated chemicals [10]. It was suggested to use practical abbreviations (PRABs), rather than structural abbreviations (STABs), which are often long and complicated. Therefore, in this thesis, this suggested nomenclature will be applied.

In terms of analysis techniques, high resolution mass spectrometry (HRMS) is becoming a popular and relevant method for the detection of small molecules including emerging environmental pollutants and their possible transformation products. Other fields such as metabolomics, drug discovery and forensics also benefit from the potential of this approach [22]. Employed techniques, based on traditional approaches and non-target analysis will be discussed in more detail towards the end of this chapter.

1.3.1. Environmental fate

The environmental behaviour of legacy BFR (LBFRs) such as PBDEs has been described by Watanabe *et al.* [23]. In the absence as yet of sufficient information for NBFRs, these observations can reasonably be extrapolated to provide an initial understanding of the environmental fate and behaviour of NBFRs. Higher brominated compounds are less mobile in the environment and therefore are more likely to be found in sediments and soils in the vicinity of sources rather than in biota samples. In contrast, lower brominated compounds, including degradation products, have a higher volatility, water solubility and bioaccumulation behaviour and are consequently widespread in various environmental compartments. Physical and chemical properties of LBFRs (Table 1-1 p. 6), compared to selected NBFRs (Table 1-1 p. 7-8) are summarised in Table 1-1 .

Table 1-1. Physical and chemical properties of legacy BFRs¹ and novel BFRs² (adapted from ^a[14], ^b[24])

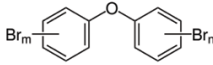
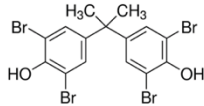
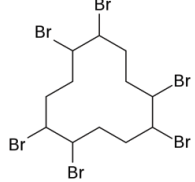
(N)BFR name	Acronym	Molecular Formula	Chemical structure	Mol. Weight	Boiling point (°C)	Water Solubility (g/L, 25°C, pH=7)	Vapour Pressure (Pa, 25 °C, * 21°C)	Octanol-water coefficient Log K _{ow}
2,4,4'-TriBDE ^{1, b}	BDE-28	C ₁₂ H ₇ Br ₃ O		406.89441	371	7.0 × 10 ⁻⁸	1.6 × 10 ⁻⁵	5.9
2,2',4,4'-TetraBDE ^{1, b}	BDE-47	C ₁₂ H ₆ Br ₄ O		485.78999	395	1.1 × 10 ⁻⁸	2.5 × 10 ⁻⁴	6.8
2,2',4,4',5-PentaBDE ^{1, b}	BDE-99	C ₁₂ H ₅ Br ₅ O		564.68558	decomp. at > 300	2.4 × 10 ⁻⁹	5.0 × 10 ⁻⁵	6.7
2,2',4,4',6-PentaBDE ^{1, b}	BDE-100	C ₁₂ H ₅ Br ₅ O		564.68558	416	4.0 × 10 ⁻⁸	2.1 × 10 ⁻⁷	7.2
2,2',4,4',5,5'-HexaBDE ^{1, b}	BDE-153	C ₁₂ H ₄ Br ₆ O		643.58117	471	9 × 10 ⁻¹⁰	5.8 × 10 ⁻⁶	7.9
2,2',4,4',5,6'-HexaBDE ^{1, b}	BDE-154	C ₁₂ H ₄ Br ₆ O		643.58117	453	1 × 10 ⁻⁹	2.8 × 10 ⁻⁸	7.8
2,2',3,4,4',5',6-HeptaBDE ^{1, b}	BDE-183	C ₁₂ H ₃ Br ₇ O		722.47675	491	2 × 10 ⁻⁹	3.5 × 10 ⁻⁹	8.3
Decabromodiphenylether ^{1, b}	BDE-209	C ₁₂ Br ₁₀ O		959.16352	decomp. at > 320	< 1 × 10 ⁻¹⁰	4.6 × 10 ⁻⁶ *	6.3 – 10.0
Tetrabromo-bisphenol-A ^{1, b}	TBBPA	C ₁₅ H ₁₂ Br ₄ O ₂		543.86925	decomp. at >250	4.2 × 10 ⁻¹¹	1.8 × 10 ⁻¹¹	4.5
1,2,5,6,9,10-hexabromocyclo-dodecane ^{1, b}	HBCDD	C ₁₂ H ₁₈ Br ₆		641.69293	decomp. at >190	α 4.9 × 10 ⁻⁸ β 1.5 × 10 ⁻⁸ γ 2.1 × 10 ⁻⁹	6.3 × 10 ⁻⁵	5.6

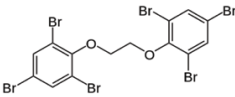
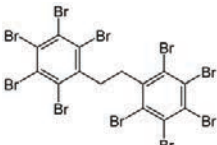
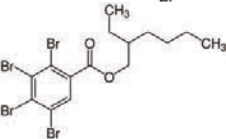
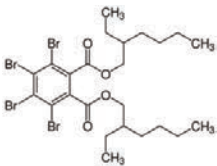
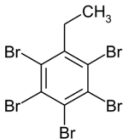
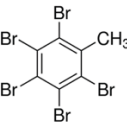
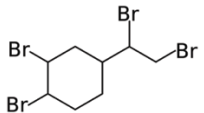
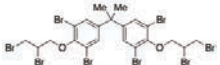
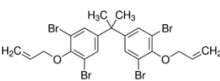
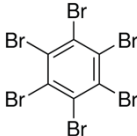
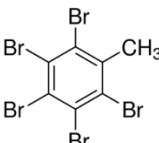
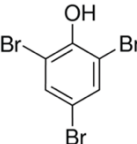
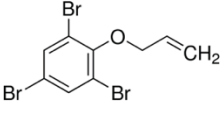
Table 1-1 continued	Acronym	Formula	Chemical structure	MW	BP	Solubility	VP	Log K _{ow}
1,2 bis (2,4,6-tribromophenoxy) ethane ^{2, a}	BTBPE	C ₁₄ H ₈ Br ₆ O ₂		687.63381	566 ± 50	2 x 10 ⁻⁵	3.9 x 10 ⁻¹⁰	7.9 ± 0.9
Decabromo-diphenyl-ethane ^{2, a}	DBDPE	C ₁₄ H ₄ Br ₁₀		971.21735	676 ± 50	2.1 x 10 ⁻⁷	6.0 x 10 ⁻¹⁵	11.1
2-ethylhexyl 2,3,4,5-tetrabromo-benzoate ^{2, b}	EH-TBB	C ₁₅ H ₁₈ Br ₄ O ₂		549.91689	477	1.1 x 10 ⁻¹¹	-	7.3 - 8.8
Bis (2-ethyl-1-hexyl) tetrabromophthalate ^{2, a}	BEH-TEBP	C ₂₄ H ₃₄ Br ₄ O ₄		706.13938	585 ± 45	1.6 x 10 ⁻⁶	1.6 x 10 ⁻¹¹	10.1 ± 0.9
Pentabromoethyl-benzene ^{2, a}	PBEB	C ₈ H ₅ Br ₅		500.64323	413 ± 40	3.5 x 10 ⁻⁴	3.2 x 10 ⁻⁴	6.4 ± 0.6
Pentabromotoluene ^{2, a}	PBT	C ₇ H ₃ Br ₅		486.61661	394 ± 37	7.8 x 10 ⁻⁴	1.2 x 10 ⁻³	5.9 ± 0.6
1,2-Dibromo-4-(1,2-dibromoethyl)cyclohexane ^{2, b}	DBE-DBCH (TBECH)	C ₈ H ₁₂ Br ₄		427.79529	371	7.0 x 10 ⁻¹¹	1.4 x 10 ⁻²	5.2

Table 1-1 continued	Acronym	Formula	Chemical structure	MW	BP	Solubility	VP	Log K _{ow}
Tetrabromobis-phenol A-bis(2,3-dibromopropyl-ether) ^{2, a}	TBBPA-DBPE	C ₂₁ H ₂₀ Br ₈ O ₂		943.61130	677 ± 55	1.6 x 10 ⁻⁷	1.6 x 10 ⁻⁷	10.4 ± 0.7
Tetrabromobis-phenol A diallyl-ether ^{2, a}	TBBPA-DAE	C ₂₁ H ₂₀ Br ₄ O ₂		623.99720	525 ± 55	1.6 x 10 ⁻⁵	1.8 x 10 ⁻⁸	8.5 ± 0.6
Hexabromobenzene ^{2, a}	HBB	C ₆ Br ₆		551.48558	418 ± 40	7.7 x 10 ⁻⁴	1.1 x 10 ⁻⁴	5.9 ± 0.7
Pentabromotoluene ^{2, a}	PBT	C ₇ H ₃ Br ₅		486.61661	394 ± 37	7.8 x 10 ⁻⁴	1.2 x 10 ⁻³	5.9 ± 0.6
2,4,6-tribromophenol ^{2, a}	TBP	C ₆ H ₃ Br ₃ O		330.79823	287	1.3	0.41	4.3 ± 0.5
2,4,6-tribromophenyl allyl ether ^{2, a}	TBP-AE (ATE)	C ₉ H ₇ Br ₃ O		370.86220	340 ± 37	2.0 x 10 ⁻²	4.9 x 10 ⁻²	5.0 ± 0.6

Moreover, Wu *et al.* reported that current-use NBRs have comparable or sometimes even greater bioaccumulative characteristics compared to legacy PBDEs, based on bioaccumulative factor (BAF) determination in aquatic species from a natural pond in an electronic waste recycling site in South China. Therefore further investigations based on their potential bioaccumulation and toxic effects on wildlife are warranted [25].

In the outdoor environment, soil and sediment can be regarded as sinks for flame retardants and therefore have the potential to disclose which emerging BFRs are persistent and might lead to environmental concern in the future [19]. Soil plays a central role in the environmental fate of flame retardants e.g. via its role in air/soil exchange. Concentrations of flame retardants are generally higher in soils of urban and suburban areas compared to rural and background areas [26]. This is possibly due to the elevated production, use and disposal of these chemicals in urban and suburban areas, as well as the presence of treated products in general. Factors affecting the concentration and distribution of these compounds in sediment samples include organic matter content, actual source and transportation pathways, such as atmospheric wet/dry disposition and direct input from sewage outlets [27]. Sewage treatment plants have been reported as one of the major sources of BFR pollution through the discharge of wastewater effluents and subsequent usage of sewage sludge. Therefore, sewage sludge represents another early indicator for leakage of these emerging chemicals in the environment [28].

In the indoor environment, flame-retarded products have the potential to outgas PBDEs to the indoor air leading to high indoor concentrations [29]. A further indicator for the presence of both legacy and emerging flame retardant indoors is dust. This presence leads to human exposure and studies have indicated that positive correlations exist between levels of PBDEs in dust and blood [30, 31], as well as human milk [31, 32].

Indoor air levels have been shown to contain higher concentrations of PBDEs compared to outdoor levels [33, 34]. Regarding transportation mechanisms from the indoor to the outdoor environment, studies in the UK [35], Sweden [36] and Canada [37] indicate that PBDEs contained in indoor airborne air, vapour and particulate matter are a source to the outdoor environment. Indoor air can travel unaltered through ventilation systems to the outdoors. Through these processes the wider environment is affected, with possible contamination of food webs and human food sources [29]. PBDEs in air especially originate from urban and industrialised areas, with a concentration gradient from urban to rural areas and possible long-range atmospheric transportation processes. Further, flame retardants contained in settled floor dust are directly released to the ambient environment [38].

The following section will give an overview over the most widely used NBRs and explore their production, usage and environmental occurrence. Table 1-2 summarises the presence and environmental concentrations with a special focus on NBRs, but also highlighting how these compare to the presence of legacy BRs.

1.3.2. 1,2-Bis(2,4,6-tribromophenoxy)ethane (BTBPE)

BTBPE, referred to as TBE in older studies, is an additive flame retardant and marketed as FF-680 by the Great Lakes Chemical Corporation in Arkansas, USA [39]. It is a part of tribromophenoxy flame retardants, a group of structurally similar compounds which include also 2,3-dibromopropyl-2,4,6-tribromophenyl ether (TBP-DBPE, previously DPTE), 2-allyl-2,4,6-tribromophenyl ether (TBP-AE, previously ATE), 2-bromoallyl 2,4,6-tribromophenyl ether (TBP-BAE, previously BATE), as well as 2,4,6-tribromoanisole (TBA) which are all derived from 2,4,6-Tribromophenol (TBP) [19]. Hoh *et al.* reported the presence of BTBPE in sediments of Lake Michigan, which first appeared around 1973 according to their sediment core dating.

Others state its first observation in the environment was in 1977, but more increased attention to its occurrence only started from around 2005 [40]. BTBPE levels increased until 1985 and stayed constant thereafter. Reports on production volume stated that between 1986 and 1994, an estimated 4,500-22,500 t of BTBPE was produced per year, declining to 450-4,500 t per year after 1998 [39]. However, since around 2004 BTBPE was employed as a replacement product for octaBDE there might be an increase in production and hence elevated concentrations in the environment are expected [39, 40].

Levels of BTBPE found in a Lake Michigan sediment core were lower than those of decaBDE, but much higher than those of BDE-47, -99, and -100, the main constituents of the pentaBDE mixture [39]. Hoh *et al.* reported high concentrations in air (particle phase) in a rural Arkansas site with 0.30 pg/m³, in relative proximity to Great Lakes Chemical and Albemarle BFR manufacturers. Further high BTBPE levels correlated with high levels of decaBDE, possibly indicating similar sources [41]. The occurrence of BTBPE in the Great Lakes region further shows that it is prone to atmospheric transport and deposition [40].

BTBPE has been reported in various abiotic samples such as landfill leachate [42], sediments [39, 40, 43, 44], sewage sludge [45, 46], dust [47, 48], indoor [49] and outdoor air [39], as well as in biota samples, including fish [43, 50], mussels [51], birds [43] and bird eggs [52].

1.3.3. Decabromodiphenyl Ethane (DBDPE)

DBDPE has been marketed as a possible replacement of decaBDE and is mainly produced in higher volumes in China and the US. DBDPE was introduced on the market in the mid-1980s and is available under the trade names Saytex 8010 (Albemarle, USA) and Firemaster 2100 (Chemtura) [21]. With the proposed debromination behaviour of decaBDE to lower BDEs, the production of DBDPE has further increased [4]. There is evidence for long-range atmospheric

transport and deposition based on the fact that lakes around Sweden studied to date have no proven point of entry for BFRs [53].

Amongst NBRs, there are more studies available on the occurrence and environmental fate of DBDPE. Its presence has been reported in surface sediments and sediment cores in South China [54] and the UK [55], lake and marine sediments in Sweden [53] and China [56], sewage sludge samples from Sweden [28, 57], Spain [58] and Canada [59]. In the UK it has further been detected in outdoor air and soil samples [60]. DBDPE has also frequently been detected in dust samples in the UK [48, 49, 61], Belgium [62], USA [63] and China [43]. Further it was reported in fish [51, 52, 64], birds [65] and mammals [66], as well in food products in the UK [67]. The bioavailability of DBDPE is still unclear; specifically, while Wang *et al.* reported the accumulation of DBDPE in rat tissue and biota [68], Hardy *et al.* regarded DBDPE as a chemical with low bioavailability due to its large molecular weight and high log K_{OW} , therefore with little risk to aquatic and sediment organisms [69].

1.3.4. Bis(2-ethylhexyl)tetrabromophthalate (BEH-TEBP) and 2-ethylhexyltetrabromobenzoate (EH-TBB)

BEH-TEBP (or TBPH) and EH-TBB (or TBB) are two of the main constituents of the technical flame retardant mixture Firemaster 550, with an approximate ratio of EH-TBB:BEH-TEBP of 4:1 [63]. These ratios however vary in measured samples, i.e. blubber samples 0.03 – 3 [70], while in house dust from 0.05 – 50 [63]. BEH-TEBP has a wider range of applications and is also applied on its own outside the Firemaster 550 mixture. This might lead to an enrichment of BEH-TEBP compared to EH-TBB in environmental and biota samples, compared to their ratio in the technical mixture [55]. BEH-TEBP, but no EH-TBB was detected in outdoor air samples, while both compounds were absent in soil samples of the UK [60]. In human breast milk samples, levels of BEH-TEBP were lower compared to EH-TBB, possibly due to the higher

bioaccessibility of the latter compound [67]. Both compounds were detected in house dust, firstly reported in the USA in 2008 [63], followed by a study in Europe in 2011 [62], and also in recent studies in the UK [49, 61, 71]. Levels in house dust in Boston households were found to be at comparable levels to HBCDDs [63]. Further BEH-TEBP and EH-TBB were detected in sewage sludge from a wastewater treatment plants (WWTP) in the area of the San Francisco Bay [72], as well as sewage sludge from various WWTP in the Mid-Atlantic US [46]. Berr et al. has highlighted the accumulation, metabolism and genotoxicity of both compounds in fish and their possible adverse effects to aquatic species [73]. The Firemaster mixture further contains triphenyl phosphate (TPHP), which recently has been reported to act as an endocrine disruptor and affect sperm concentration [74]. EH-TBB and BEH-TEBP have also been reported in marine mammals, which is especially of concern, since they were found in top-trophic-level marine organisms [75].

1.3.5. 2,3,4,5,6-pentabromoethylbenzene (PBEB)

Pentabromobenzene is a low production chemical with an estimated yearly production of 10-1,000 tons until 2002 [16], but does not appear to have subsequently been produced or used by any of the Oslo-Paris Commission (OSPAR) signatory countries [76]. The presence of PBEB was reported by Hoh *et al.* in Chicago ambient air in 2002-2003 at concentrations up to 550 pg/m³, which was 10 times higher than the levels of total PBDEs in the same sample. In general however, levels of PBEB in air samples in the US were in the lower detectable region and lower than PBDEs [39]. Vorkamp and Rigét have reviewed the presence of PBEB in the Arctic environment [18], while Wu *et al.* reported its bioaccumulation potential [25], which is further underlined by studies in both North America and Europe [77-79]. Furthermore, Ismail *et al.* highlighted concentrations of PBEB in fish tissue remained constant over the period 1979–2004 [50]. This indicates the need to monitor this chemical in the environment and investigate

its potential toxicity in aquatic organisms [80]. PBEB has been also reported in sediments [27] and sewage sludge [81], indoor air [49] and dust [49, 61], as well as wildlife like harbour seal [78] and fish [80, 82].

1.3.6. 2,3,4,5,6-pentabromotoluene (PBT)

Pentabromotoluene is a constituent of the commercial mixture Flammex 5-BT [76] and marketed under the trade name FR-105 in the United States. It is used as an additive flame retardant [16] and has a rough annual production volume of 5,000 t worldwide. Further it has been reported to be a possible degradation product of DBDPE and TBBPA [18, 83]. PBT has been reported in sediment and suspended particulate matter [84], in Arctic biota samples [76] and in the atmosphere of the European Arctic [85].

1.3.7. 1,2-dibromo-4-(1,2-dibromoethyl)cyclohexane (DBE-DBCH)

DBE-DBCH (or TBECH) is used as an additive flame retardant, with a low production volume of 4-225 t in the United States in 2002, but is not reported as a low or high production volume chemical (LPVC / HPVC) in the European Union [45]. The chemical is constituted of four diastereomers of which α and β are the principal components in roughly equal proportions within the technical mixture. The formation through isomerization of the other isomers, γ and δ , can occur at elevated temperatures greater than 120 °C. All of these four isomers are reported as endocrine disruptors [18]. With respect to environmental contamination, Nyholm *et al.* report the presence of DBE-DBCH at low levels in sewage water, waste water and sewage sludge [45], with its presence also reported in herring gull eggs [52]. DBE-DBCH has been reported to be the predominant NBRF in UK indoor air [49] and dust [49, 61], outdoor air [60], as well as UK human milk and diet samples [67]. In European sediment it has been reported in sediment of German rivers [86]. Outside of Europe, DBE-DBCH was reported in sediments of the Great Lakes [87] for the first time in 2012, as well Chinese river and marine sediments

[88] [89]. However, it was shown that DBE-DBCH degrades quickly in soil, both aerobically and anaerobically [90].

1.3.8. 2,3-dibromopropyl-2,4,6-tribromophenyl ether (TBP-DBPE)

TBP-DBPE, also abbreviated with DPTE, is a flame retardant of the Bromkal group [18]. The chemical has been reported to be produced in Germany until 1985 [91], but data on more recent usage is lacking [18]. Its presence has been reported in ringed seals from Greenland [92] and seal blubber [91].

Table 1-2. Summary of mean concentrations (min.-max. in parentheses) as indicated in each study of legacy BFRs and NBFRs in environmental samples around the world

Sample	Target compounds	Mean (Conc. Range)	Region	Ref.
Ambient Air pg/m³	∑tetra-hepta PBDEs	1.4 (0.8-5.4)	Sweden	[93]
	∑tri-hepta PBDEs	nr (6.8-66)	UK	[60]
	∑tri-hepta PBDEs	129 (44-232)	China	[43]
	BDE-209	0.1 (0.03-0.6)	Sweden	[93]
	BDE-209	nr (92-370)	UK	[60]
	BDE-209	2,772 (196-9,261)	China	[43]
	∑HBCDDs	0.1 (<0.03-0.6)	Sweden	[93]
	∑HBCDDs	1.6 (0.2-11)	USA	[41]
	∑HBCDDs	nr (64-130)	UK	[60]
	BTBPE	0.1 (<0.03-0.5)	Sweden	[93]
	BTBPE	3.4 (0.06-70)	USA	[41]
	BTBPE	31 (3.8-67)	China	[43]
	DBDPE	0.2 (<0.1-0.3)	Sweden	[93]
	DBDPE	1,916 (402-3,578)	China	[43]
	BEH-TEBP	0.1 (<0.03-0.5)	Sweden	[93]
PBT	0.2 (0.1-0.5)	Sweden	[93]	
DBE-DBCH	nr (2.5-9.3)	UK	[60]	
DBE-DBCH	0.5 (0.2-2.4)	Sweden	[93]	
Indoor air pg/m³	∑tri-hepta PBDEs	357 (2.4-4,682)	UK	[49]
	∑tetra-hepta PBDEs	62 (<13-107)	Sweden	[93]
	BDE-209	660 (23-3,800)	UK	[49]
	BDE-209	48 (<31-130)	Sweden	[93]
	∑HBCDDs	320 (19-1,500)	UK	[49]
	∑HBCDDs	3.1 (<1.3-19)	Sweden	[93]
	BTBPE	11 (<1.0-50)	UK	[49]

Table 1-2 continued

	DBDPE	26 (<10-97)	UK	[49]
	DBDPE	79 (<90-250)	Sweden	[93]
	BEH-TEBP	10 (<0.1-130)	UK	[49]
	BEH-TEBP	42 (<35-150)	Sweden	[93]
	EH-TBB	4.8 (0.05-44)	UK	[49]
	PBEB	1.6 (0.4-5.4)	UK	[49]
	PBT	17 (2.3-63)	UK	[49]
	PBT	10 (2.6-29)	Sweden	[93]
	DBE-DBCH	173 (30-600)	UK	[49]
	DBE-DBCH	43 (7-130)	Sweden	[93]
	TBP-DBPE	3.5 (<0.4-14)	UK	[49]
dust	Σ tri-hepta PBDEs	60 (18-116)	UK	[61]
ng/g dw	Σ tri-hepta PBDEs	65 (6-257)	UK	[49]
	Σ tri-hexa PBDEs	77 (7.1-250)	UK	[48]
	Σ tetra-octa PBDEs	73 (1.7-1,370)	Belgium	[62]
	Σ tetra-hepta PBDEs	345 (<5.4-436)	Sweden	[93]
	Σ tetra-hepta PBDEs	nr (65-1,288)	China	[43]
	BDE-209	2,986 (1,637-4,035)	UK	[61]
	BDE-209	34,000 (160-370,000)	UK	[49]
	BDE-209	260,000 (<dl-2,200,000)	UK	[48]
	BDE-209	604 (15-5,295)	Belgium	[62]
	BDE-209	nr (1,736-4,408)	China	[43]
	BDE-209	90 (<1.3-2,600)	Sweden	[93]
	Σ HBCDDs	190 (17-2,900)	Sweden	[93]
	Σ HBCDDs	8,300 (50-110,000)	UK	[49]
	Σ HBCDDs	138 (<10-11,070)	USA	[63]
	BTBPE	19 (<2.8-61)	UK	[61]
	BTBPE	14 (0.01-110)	UK	[49]
	BTBPE	120 (<dl-1,900)	UK	[48]
	BTBPE	303 (55-2,126)	Belgium	[62]
	BTBPE	48 (4.7-651)	USA	[63]
	BTBPE	nr (15-232)	China	[43]
	BTBPE	13 (<0.8-150)	Sweden	[93]
	DBDPE	195 (11-700)	UK	[61]
	DBDPE	240 (<1.2-2,300)	UK	[49]
	DBDPE	270 (<dl-3,400)	UK	[48]
	DBDPE	303 (55-2,126)	Belgium	[62]
	DBDPE	354 (4.5-130,200)	USA	[63]
	DBDPE	nr (<2.5-139)	China	[43]
	DBDPE	21 (<0.4-2,220)	Sweden	[93]

Table 1-2 continued

	BEH-TEBP	746 (80-3,187)	UK	[61]
	BEH-TEBP	240 (<1.2-2,300)	UK	[49]
	BEH-TEBP	212 (<2-436)	Belgium	[62]
	BEH-TEBP	234 (3-10,630)	USA	[63]
	BEH-TEBP	160 (<33-1,500)	Sweden	[93]
	EH-TBB	11 (<2.5-65)	Sweden	[93]
	EH-TBB	9 (4-23)	UK	[61]
	EH-TBB	21 (<0.01-85)	UK	[49]
	EH-TBB	20 (<2-436)	Belgium	[62]
	EH-TBB	322 (<6.6-15,030)	USA	[63]
	PBEB	2.3 (<0.01-21)	UK	[49]
	PBT	0.9 (<0.07-5.5)	Sweden	[93]
	PBT	7.1 (<0.01-300)	UK	[49]
	DBE-DBCH	0.9 (<0.07-3.8)	Sweden	[93]
	DBE-DBCH	21 (2.9-131)	UK	[49]
	TBP-DBDPE	6.6 (<0.05-47)	UK	[49]
Sewage	∑tri-hepta PBDEs	nr (12-69)	China	[43]
sludge	∑tri-hepta PBDEs	nr (4.1-135)	Greenland	[45]
ng/g dw	∑tri-hepta PBDEs	527 (21-2326)	Spain	[81]
	BDE-209	30,000 (1,227-64,559)	China	[43]
	BDE-209	nr (88-326)	Greenland	[45]
	BDE-209	nr (32-292)	Spain	[58]
	BDE-209	nr (466-1,860)	Canada	[59]
	BDE-209	539 (nd-2,303)	Spain	[81]
	BTBPE	nr (0.7-1.4)	Greenland	[45]
	BTBPE	nr (0.3-17)	China	[43]
	BTBPE	10,200 (nr)	USA	[46]
	DBDPE	nr (1.9-6.3)	Greenland	[45]
	DBDPE	nr (1,690-4,820)	USA	[46]
	DBDPE	nr (0.2-15)	Spain	[58]
	DBDPE	nr (5.6-32)	Canada	[59]
	DBDPE	81 (nd-257)	Spain	[81]
	DBDPE	220 (nr)	Germany	[28]
	DBDPE	1183 (266-1,995)	China	[43]
	BEH-TEBP	33,500 (nr)	USA	[46]
	EH-TBB	89,900 (nr)	USA	[46]
	PBEB	0.3 (nd-2.3)	Spain	[81]
	DBE-DBCH	nr (0.6-1.4)	Greenland	[45]

Table 1-2 continued

Sediments	Σ tri-hepta PBDEs	nr (2.9-133)	China	[43]
ng/g dw	Σ hepta-deca PBDEs	nr (2.2-219)	Italy	[94]
	Σ tri-hepta PBDEs	2.8 (nr)	Canada	[40]
	Σ tri-hepta PBDEs	nr (0.7-7.6)	China	[95]
	Σ tri-hepta PBDEs	0.3 (0.02-1.3)	China	[27]
	Σ tetra-hepta PBDEs	12 (2.7-32)	China	[89]
	BDE-209	nr (33-2015)	China	[43]
	BDE-209	nr (77-5700)	China	[95]
	BDE-209	25 (3.9-103)	China	[27]
	BDE-209	nr (0.5-4.7)	Sweden	[53]
	BDE-209	nr (1.0-88)	Sweden	[53]
	BDE-209	14 (nr)	Canada	[40]
	BDE-209	nr (4.7-260)	Netherlands	[84]
	BDE-209	nr (0.9-106)	USA	[87]
	BDE-209	4.6 (1.4-11)	China	[89]
	Σ HBCDDs	nr (<dl-24)	Italy	[94]
	Σ HBCDDs	33 (<dl-186)	Africa	[42]
	Σ HBCDDs	nr (0.04-3.1)	USA	[87]
	Σ HBCDDs	0.2 (0.1-0.4)	China	[89]
	BTBPE	nr (0.05-22)	China	[43]
	BTBPE	6.7 (nr)	Canada	[40]
	BTBPE	nr (<dl-2.3)	Italy	[94]
	BTBPE	6.7 (nr)	Canada	[40]
	BTBPE	51 (<dl-310)	Africa	[42]
	BTBPE	nr (0.2-0.3)	Netherlands	[84]
	BTBPE	nr (0.1-8.3)	USA	[87]
	BTBPE	0.02 (<0.02-0.08)	China	[89]
	DBDPE	247 (39-364)	China	[43]
	DBDPE	nr (19-430)	China	[95]
	DBDPE	6.4 (2.4-19)	China	[89]
	DBDPE	nr (3.3-280)	Italy	[94]
	DBDPE	nr (0.2-2.1)	Sweden	[53]
	DBDPE	nr (0.2-11)	Sweden	[53]
	DBDPE	nr (0.7-10)	Netherlands	[84]
	DBDPE	nr (0.1-2.8)	USA	[87]
	BEH-TEBP	11 (<dl-60)	Africa	[42]
	BEH-TEBP	1.0 (0.5-3.1)	China	[89]
	EH-TBB	10 (<dl-56)	Africa	[42]
	EH-TBB	0.4 (<0.2-1.1)	China	[89]
	DBE-DBCH	nr (0.05-1.4)	USA	[87]

Table 1-2 continued

	DBE-DBCH	3.7 (0.9-8.5)	China	[89]
	PBEB	0.3 (<0.07-1.9)	China	[27]
	PBT	nr (0.01-0.7)	Netherlands	[84]
Soil	Σ tri-hepta PBDEs	nr (1.4-5.8)	UK	[60]
ng/g dw	Σ tri-hepta PBDEs	nr (3.7-6.7)	China	[43]
	Σ tetra-hepta PBDEs	1.4 (0.5-3.5)	Sweden	[93]
	BDE-209	nr (1.0-45)	UK	[60]
	BDE-209	nr (22-179)	China	[43]
	BDE-209	2.7 (0.3-31)	Sweden	[93]
	BTBPE	nr (0.1-6.2)	China	[43]
	DBDPE	nr (0.15-1.0)	UK	[60]
	DBDPE	nr (4.56)	China	[43]
	DBDPE	2.7 (0.2-160)	Sweden	[93]
	PBT	0.01 (<0.009-0.02)	Sweden	[93]
Arctic biota	BTBPE	0.7 (<0.005-1.1)	Norway	[18]
ng/g ww	DBDPE	0.6 (<0.002-0.6)	Norway	[18]
	BEH-TEBP	1.7 (<0.1-3.8)	Norway	[18]
	EH-TBB	0.9 (0.2-4.3)	Norway	[18]
	DBE-DBCH	0.06 (nr)	Norway	[18]
Fish	Σ tri-hepta PBDEs	nr (43-212)	China	[43]
ng/g ww	Σ tri-hepta PBDEs	91 (40-560)	China	[64]
	Σ tri-deca PBDEs	240 (128-427)	Canada	[51]
	Σ tri-deca PBDEs	nr (42-420)	Italy	[82]
	Σ tri-deca PBDEs	2876 (nr)	Canada	[80]
	BDE-209	nr (9.6-212)	China	[43]
	BDE-209	7.8 (0.9-260)	China	[64]
	Σ HBCDDs	65 (37-84)	Canada	[51]
	Σ HBCDDs	nr (27-1232)	Italy	[82]
	BTBPE	nr (0.01-0.2)	China	[43]
	BTBPE	0.8 (<dl-1.5)	Canada	[51]
	BTBPE	nr (<dl-23)	Italy	[82]
	DBDPE	0.7 (<dl-3.3)	Canada	[51]
	DBDPE	68 (nd-230)	China	[64]
	DBDPE	27	Canada	[80]
	BEH-TEBP	5.4	Canada	[80]
	PBEB	nr (<dl-0.9)	Italy	[82]
Birds	Σ tri-deca PBDEs	nr (150-14,000)	China	[96]
ng/g lw	BTBPE	nr (0.07-241)	China	[43]
	DBDPE	nr (nd-220)	China	[96]

Table 1-2 continued

	DBDPE	nr (9.6-124)	China	[43]
Bird eggs	Σ tri-hepta PBDEs	nr (288-1,140)	USA	[52]
ng/g ww	BDE-209	nr (4.5-20)	USA	[52]
	BTBPE	nr (<0.06-0.2)	USA	[52]
	DBDPE	nr (9.3-44)	USA	[52]
	DBE-DBCH	nr (0.1-0.5)	USA	[52]

dl = detection limit; nd = not detected; dw = dry weight; ww = wet weigh; lw = lipid weight; nr = not reported

1.4. Behaviour and fate of NBFRs and their transformation products

While research efforts over the last two decades have enhanced greatly our understanding of the environmental sources, fate, and behaviour of BFRs like PBDEs, HBCDDs, and TBBPA; comparatively little is known about their longer-term environmental fate. In particular, the identity of the degradation and metabolic products of such LBFRs and the extent to which they are present in the environment is relatively little understood. Moreover, recent restrictions on the use of LBFRs like PBDEs are widely thought to have led to increased use of alternative flame retardants including NBFRs. This creates a further research gap, namely our knowledge of the degradation and metabolic products of these NBFRs. Enhanced knowledge of such degradation and metabolic products of both LBFRs and NBFRs will help direct future monitoring of the extent and distribution of such environmental contamination, and inform the development of legislation to limit their adverse effects.

This thesis will mainly focus on the presence and levels of target NBFRs in various environmental compartments, along with their possible transformation products. In the following for easier legibility; degradation and metabolic transformation products will be referred to collectively as “transformation products” (TPs).

It is suggested that although NBFRs are different chemical molecules compared to traditional BFRs, most of their physical and chemical properties, such as lipophilic character, aromatic groups and halogen substitution are comparable in both groups (Table 1-1) [2]. Therefore, it

can be assumed that the environmental fate of NBFRs is potentially comparable to their banned BFR counterparts. Further, some NBFRs are found in the Arctic, thus indicating their capacity for long range atmospheric transport [16].

To better explain the environmental fate and behaviour of NBFRs and their TPs in various environmental compartments general considerations have to be taken into account: 1. Flame retardants can enter the environment through various pathways [3] - release during product manufacturing, utilisation and during end-of-life phase activities such as waste combustion, leaching and volatilisation from land filled waste materials. 2. Biotransformation in the environment can be based on multiple processes, following photolytic, chemical, as well as biological pathways as will be described later; and 3. TPs can possibly have higher toxicity and diverse chemical properties compared to their parent compounds due to the undergone structural change.

While the presence and pathways of TPs of PBDEs, HBCDDs and TBBPA have been well studied and processes such as their debromination and oxidative metabolism have been reported [4]; extensive reports on TPs of NBFRs are not yet available. Dirtu *et al.* reviewed the TPs of BFRs, mainly focusing on PBDEs, HBCDDs and TBBPA, while also listing NBFRs such as DBDPE, BTBPE, EH-TBB and BEH-TEBP [4].

1.5. Transformation products of NBFRs

TPs in the environment can originate both from biotic as well as abiotic factors. While abiotic factors refer to non-living physical and chemical elements in the ecosystem, such as water, air, soil, sunlight, and minerals, biotic factors on the other hand are living or once-living organisms in the ecosystem, such as animals, birds, plants, fish and other similar organisms. Research on transformation processes of BFRs has mainly focused on legacy compounds, like PBDEs and HBCDDs, so far. However due to the occurrence of other BFRs, the focus of studies

has been expanded to better understand their transformation mechanisms. Dirtu *et al.* and Weijs *et al.* give an overview of the different pathways of BFRs and their TPs, with a special focus on PBDEs, HBCDDs, TBBPA and NBFRs such as DBDPE, BTBPE, EH-TBB BEH-TEBP in both biotic and abiotic samples [4, 97]. Degradation of BFRs [98], photochemical reactions being the most studied and reported in literature. These degradation processes may lead to a change of structure, together with a change in the characteristics and properties of these contaminants. Degradation can occur via chemical, biological and photolytic processes. In these processes degradation rates can be affected by temperature, light, humidity and the microorganism flora, these factors need to be considered when conducting respective studies [90].

1.5.1. Abiotic transformation processes

Photodegradation

Photochemical degradation of PBDEs has been studied by Fang *et al.* [99] and Shih and Wang [100]. Both groups suggest that PBDEs are degraded under UV light through a sequential dehalogenation mechanism and undergo reductive debromination. Experiments with HBCDDs in dust after indoor light exposure revealed a rapid photolytically-mediated shift from γ -HBCDD to α -HBCDD, as well as slower degradative loss of HBCDDs via elimination of HBr [101]. While no debromination or isomerization was observed for HBCDDs in textiles exposed to natural sunlight, photolysis of BDE-209 in textiles resulted in the formation of polybrominated dibenzofurans (PBDFs), as well as the formation of di- to hexa-BDF congener [102]. Similarly, due to the structural similarities, photodegradation can be expected to occur in NBFRs. Davis *et al.* was the first group to observe the photodegradation of EH-TBB and BEH-TEBP via debromination reactions and identified some of their photodegradation products. Photolytic degradation rates were slower compared to nona- and deca-BDE [103].

Thermal degradation

Thermal degradation is another abiotic pathway for degradation. Thermal decomposition behaviour was described for BTBPE [104] and DPDPE [4]. While BTBPE generally forms TBP and vinyl 2,4,6-tribromophenyl ether, DBDPE is prone to debromination or intermolecular ring closure, but also generates bromotoluenes.

1.5.2. Biological transformation processes

Stiborova *et al.* reported [105] the biodegradation potential of microorganisms under anaerobic conditions for PBDEs and HBCDDs, which can be found in landfill sites and sewage sludge. It is shown that BDE-209 is degraded in sewage sludge to octa- and nonabromodiphenyl ether congeners under anaerobic conditions [106]. Degradation through anaerobic bacterial mixed cultures extracted from river sediment was investigated for BDE-47, BDE-99, BDE-100, BDE-153 and BDE-154 [107]. Also mixed bacterial cultures extracted from soils demonstrated a rapid breakdown of a technical penta-mixture DE-71 and were able of utilizing this as a carbon source [108]. However, results of degradation profiles differ with the selection of certain of microbial species (*Sulfurospirillum multivorans* and *Dehalococcoides*) when exposing them to PBDEs [109].

Hakk and Letcher reviewed the metabolism and toxicokinetics of several BFRs, including PBDEs, TBBPA, HBCDDs and BTBPE [110]. They report that these BFRs are prone to form metabolites through various transformations, including oxidative and reductive debromination, oxidative cytochrome P450 enzyme-mediated processes and Phase II conjugation through glucuronidation and sulfation. Most studies are available on the metabolism of polybrominated biphenyls (PBBs), followed by PBDEs.

A study reports on the soil-plant interaction of TBBPA and HBCDDs, which reduces their concentrations in the ground due to strong sorption to soil particles, but at the same time

might lead to increased exposure risk by uptake of these compounds into plants and thus enhances their bioavailability [111].

BDE-209 has been reported to metabolize to lower brominated congeners, ranging from hexa to nonaBDE by various fish species, including rainbow trout, common carp and lake trout. However, extent of the assimilation and metabolites formed varies among the species [112, 113]. It was further shown that accumulation and debromination of decaBDE in juvenile fathead minnows negatively affects thyroid hormone regulation [114]. Debromination for DBDPE can tentatively be expected to occur in a comparative way in aquatic organisms.

Bearr et al. studied the *in vitro* metabolism of both BEH-TEBP and EH-TBB using hepatic subcellular fractions of fathead minnow, common carp, mouse and snapping turtle and observed metabolite formation for EH-TBB after incubation with the exception of the snapping turtle. The main metabolite was identified as 2,3,4,5-tetrabromomethylbenzoate (TBMB) with 2,3,4,5-tetrabromobenzoic acid (TBBA) as an intermediate product. For BEH-TEBP significant loss of the parent compound after incubation was observed, but no metabolites could be identified [115]. This indicates the capability of various species to metabolize these chemicals, but further research is needed to confirm these findings, identify metabolites formed and understand their fate.

Unlike PBDEs, hydroxylated BDEs (OH-BDEs) have not been produced industrially or are by-products of technical brominated products [116, 117]. However OH-BDEs have been reported in biotic and abiotic samples of the aquatic and marine environment, such as salmon [116], mussels [118], algae [119] as well as sediments [120], surface waters [121] and sewage treatment plant effluents [122]. Studies suggest that they are natural products of marine environments, as well as a result of metabolic products from anthropogenic PBDEs [119, 121], however exact natural formation is not thoroughly understood yet [117]. The position of the

hydroxyl group (OH-) seems to be an indicator of whether OH-BDE congeners are formed through oxidation or metabolic reactions [116, 118, 120]. Possible sources and transformations found in literature include microbial aerobic degradation [123, 124], photochemical reactions of bromophenols [125] and PBDEs [126], transformation of bromophenol by marine bacteria [127] and a red algae enzyme [117], reactions of PBDEs with atmospheric OH radicals [121], as well as in sewage treatment plants through oxidative reactions and excretion from human and animal metabolism [121]. A study suggests that OH-BDEs found in marine animals could originate from demethylation of methoxylated BDEs, which have been reported as occurring naturally in the environment [128]. To conclude, OH-BDEs have been reported to exhibit similar or even higher toxic [129] and estrogenic [130] effects on both human [131] and wildlife [132, 133] compared to PBDEs, their presence and relevance need to be further investigated.

1.6. Analysis of NBFRs using high resolution mass spectrometry and mass defect filtering

High resolution mass spectrometry is becoming an increasingly available and popular technique in environmental chemical analysis of small molecules. In recent years, around 200 research papers have been published in the field of environmental research each year based on this technique [22].

1.6.1. Types of Mass Spectrometer scans

Mass spectrometric application in the field of environmental analysis can be divided into qualitative screening and quantitative determination.

Quantitative selective determination techniques include single ion monitoring (SIM), multiple reaction monitoring (MRM), also sometimes referred to as selected reaction monitoring (SRM) and full scan (FS) high resolution accurate mass (HR/AM) quantitation. The latter one relies on

accurate quantitation and identification of targeted compounds through the use of high resolution (up to 280,000 on the Thermo Fisher Scientific Q-Exactive Plus) and accurate mass (< 1 ppm internal, < 3 ppm external calibration), as well allows for non-targeted compounds to be detected retrospectively.

Qualitative approaches include low resolution (LR) full scan measurements. Precursor ion scan, whereby only those compounds which give the predefined specific fragment ion are detected. Bromine containing precursor ions can be selectively picked out by scanning for fragments m/z 79 or 81 and then obtain structural information on the parent compounds via full scan analysis. This type of scan clearly can only detect compounds that are formed in the chosen ionization mode [134]. Neutral loss scan is another screening technique, where only those compounds forming a specific fragment and thereby losing a defined part of the molecule are detected. This can be exploited for the detection of metabolite formation whereby certain conjugates are formed [135].

1.6.2. Hyphenated chromatography/mass spectrometry analytical approaches

Classically, BFRs are determined by gas chromatography (GC) methods coupled to mass spectrometry. The instruments are operated in either electron impact ionization (EI) or electron capture negative ionization (ECNI) coupled to various types of mass analysers (single or triple quadrupole, ion trap, time-of-flight and magnetic sector). Drawbacks of using GC and the need for high temperatures include the possibility of decomposition, either during the injection step or on-column degradation, especially when analysing thermally labile higher brominated congeners like BDE-209 or DBDPE. This can be solved by cold on-column injection or the use of a programmed temperature vaporizer (PTV) to minimise the thermal stress on the compound, as well as the use of columns with higher isothermal temperature limits, shorter lengths, and higher phase ratios [136]. Further, for the analysis of more polar

compounds a derivatization step is often required in GC-MS. Besides, when analysing isomeric compounds such as HBCDDs, high temperatures above 160 °C lead to isomeric interconversion and render separation of the isomers impossible [137]. New developments however have been made to analyse higher brominated FRs such as DBDPE and BTBPE using atmospheric pressure chemical ionization (APCI) coupled to a triple quadrupole mass analyser [138] or high resolution TOF mass spectrometer [139, 140].

In recent years, liquid chromatography (LC)-based methods coupled to LR mass spectrometers have also been developed [141]. Advances in coupling LC to HR-MS have been made to facilitate accurate measurements and identification of target compounds, possible transformation products and unknowns. Following LC separation, commonly used techniques for the detection of PBDEs and other BFRs are atmospheric pressure chemical ionization (APCI) [141, 142] and atmospheric pressure photoionization (APPI) [136, 143-146], which allow for the ionisation of semi-polar and non-polar substances [142]. Electrospray ionization (ESI) on the other hand is chosen for the detection of HBCDDs [147] or TBBPA [148], as well as more polar transformation products (hydroxylated congeners). Several papers have compared these three ionization techniques against each other [146, 149] and a comparison in regard to analyte polarity and molecular weight working range of each technique is shown in Figure 1-1. Depending on the ionisation technique used, different pseudo-molecular ions are formed and have to be targeted. While in ESI depending on the polarity either $[M-H]^-$ or $[M+H]^+$ are formed, in APCI and APPI generally more complex ions are observed $[M-Br]^-$, $[M-Br+O]^-$ or $[M+O_2]^-$ for brominated compounds, with comparable mechanisms for chlorinated species [141].

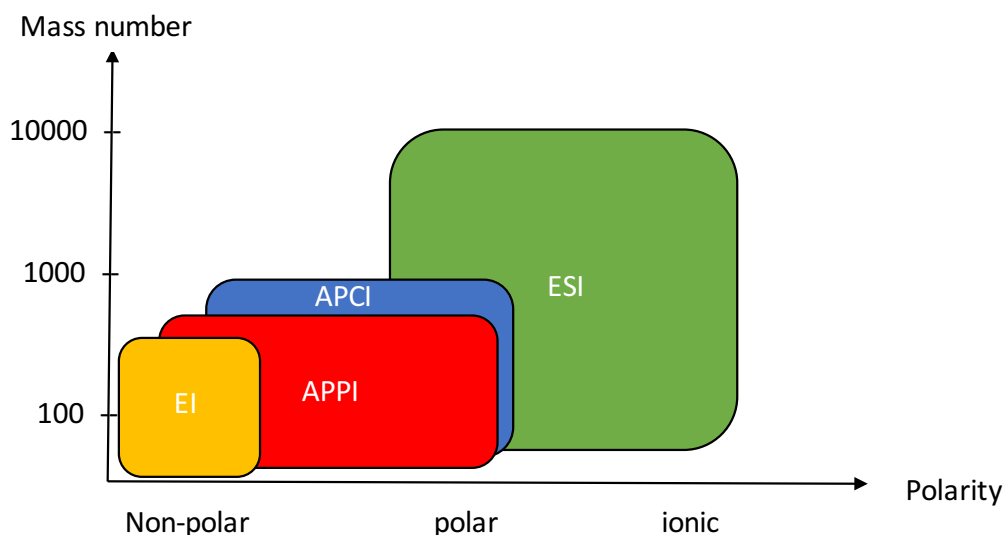


Figure 1-1. Comparison of ionization modes (APCI, APPI and ESI) for LC-MS systems, based on molecular weight and compound polarity, adapted from [150]

To better understand the environmental fate of NBFRs, analytical instrumentation with enhanced sensitivity needs to be employed for the analysis. Especially high recovery extraction and analysis methods focusing on higher brominated flame retardants like DBDPE [17].

To date most employed analytical methods do not solely focus on NBFRs analysis, but rather legacy BFRs such as PBDEs and HBCDDs, with data on some NBFRs included as collateral information. Papachlimitzou *et al.* reviewed the analysis of NBFRs to allow for comparable and qualitative analysis methods for NBFRs. As with any other analytical approach, they suggest following these aspects: Inter-laboratory comparison in order to reduce the variability between methods, use of certified reference materials and labelled standards to obtain more accurate results, use of validated and fit-for purpose analytical methods, identification of sources of contamination in blank materials, appropriate clean-up and extraction methods. Further degradation of target compounds can occur through strong acids or bases, light, as well as reaction with solvents used [151].

Generally, the incorporation of standard reference materials (SRMs) must be considered when analysing complex samples. In dust analysis, most commonly the SRM 2585 (Organic Contaminants in House Dust) is used. Although not certified in SRM2585, values for HBCDDs, BTBPE, EH-TBB and BEH-TEBP are usually compared between studies where values are reported [63, 152-156]. For sediment analysis, the SRM 1944 (New York/New Jersey Waterway Sediment) is available with certified values for PBDEs and HBCDDs, as well as other organic contaminants such as PAHs and PCBs. There are not many reports in literature on the use of sediment SRM 1944 to date [149, 157].

1.6.3. Mass defect and transformation products

The term 'mass defect' is defined as the difference between a compound's nominal mass and its exact mass. The nominal mass, sometimes referred to as integer mass, is calculated as the simple addition of the number of neutrons and protons of an elemental formula or isotope. The difference of the nominal mass and the exact mass originates from the fact that upon formation and stabilization of the nucleus of a monoisotopic element a minimal amount of energy is released, also referred to as the nuclear binding energy. Monoisotopic ^{12}C by convention has been defined as the element with zero mass defect and thus its exact mass is 12.0000 zero atomic mass units (amu). Depending on the relative nuclear binding energy of other isotopes in comparison to ^{12}C , the mass defect can either be positive (larger than the nominal mass, i.e. 0.0031 amu for ^{14}N ; 0.0078 amu for ^1H) or negative (smaller than the nominal mass, i.e. -0.0051 amu for ^{16}O ; -0.0279 amu for ^{32}S) [158]. Stable isotopes with mass numbers from approximately 80 (Br) to 150 (Eu) have the largest mass defect values of all the elements, differing by about -0.1 amu from ^{12}C [159]. The use of mass defect analysis in modern mass spectrometry has been extensively reviewed elsewhere [160].

Most commonly occurring elements (C, H, N, O) have negligible mass defects relative to ^{12}C , while elements of the halogen group such as bromine and chlorine have a unique negative mass defect (-0.0817 for ^{79}Br ; -0.0311 for ^{35}Cl), which can be used for distinction. Furthermore, halogens have a distinctive isotopic pattern which distinguishes them from other non-halogenated compounds in a complex full scan mass spectrum [161, 162]. The natural abundance of isotopes for Br is around 1:1 (^{79}Br : ^{81}Br) and roughly 3:1 for Cl (^{35}Cl : ^{37}Cl), leading to different intensity ratios in the isotope patterns. Figure 1-2 displays examples for Br_3 , Cl_3 and Br_2Cl_2 isotope pattern, including the molecular ion peak M and its isotope peaks M+2, +4, +6 etc. depending on the number of halogens.

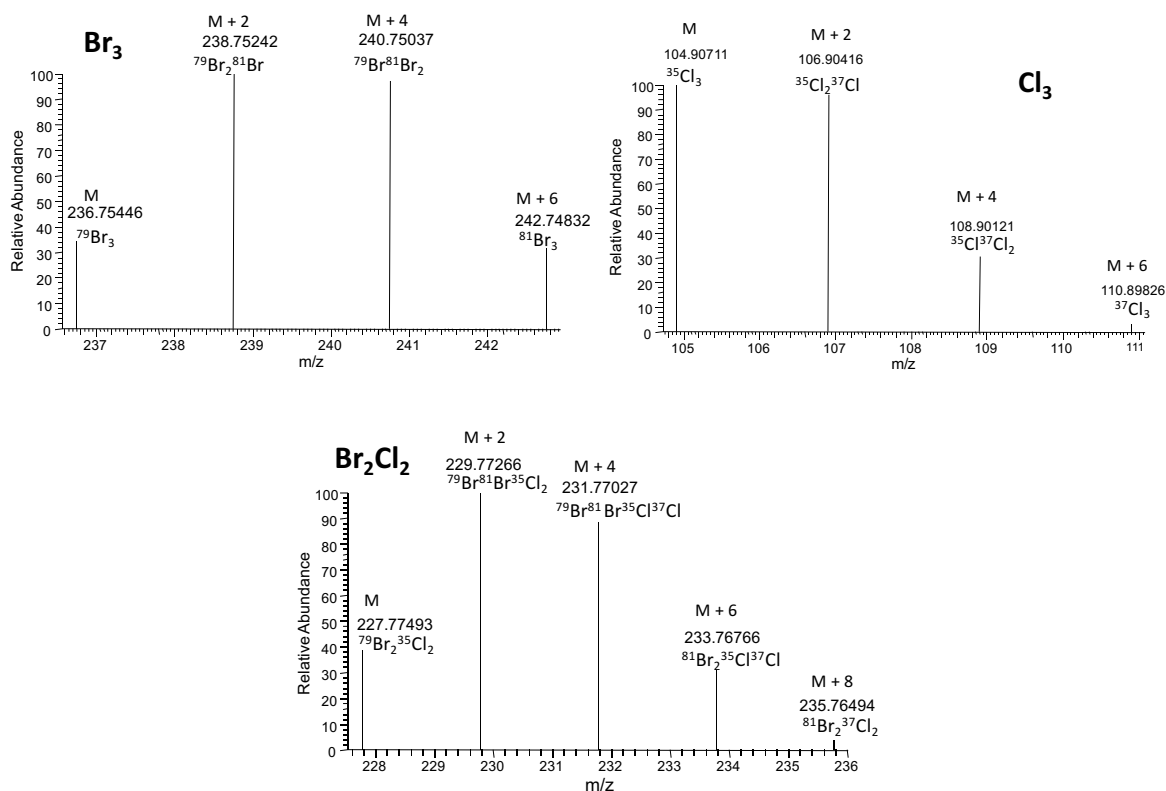


Figure 1-2. Halogen isotope patterns of Br_3 , Cl_3 and Br_2Cl_2 , M = molecular ion peak, M+2, +4, +6, +8 = isotope peaks

Figure 1-3 further gives an overview for brominated, chlorinated and mixed halogenated isotopic patterns of compounds, with the values for the isotopic abundance listed in Table 1-3. Although these patterns are very distinct, Vetter *et al.* mentions the similarity between selected patterns (i.e. heptachloro-, pentabromo and tetrabromodichloro isotope pattern), which makes identification challenging and may lead to misinterpretations. Special attention should be paid to low-abundance peaks, where the difference between these pattern often lies, to avoid erroneous assignments. Correct interpretation also requires the acquisition of high quality mass spectra with little isotope abundance variation compared to the theoretical isotope pattern values [163].

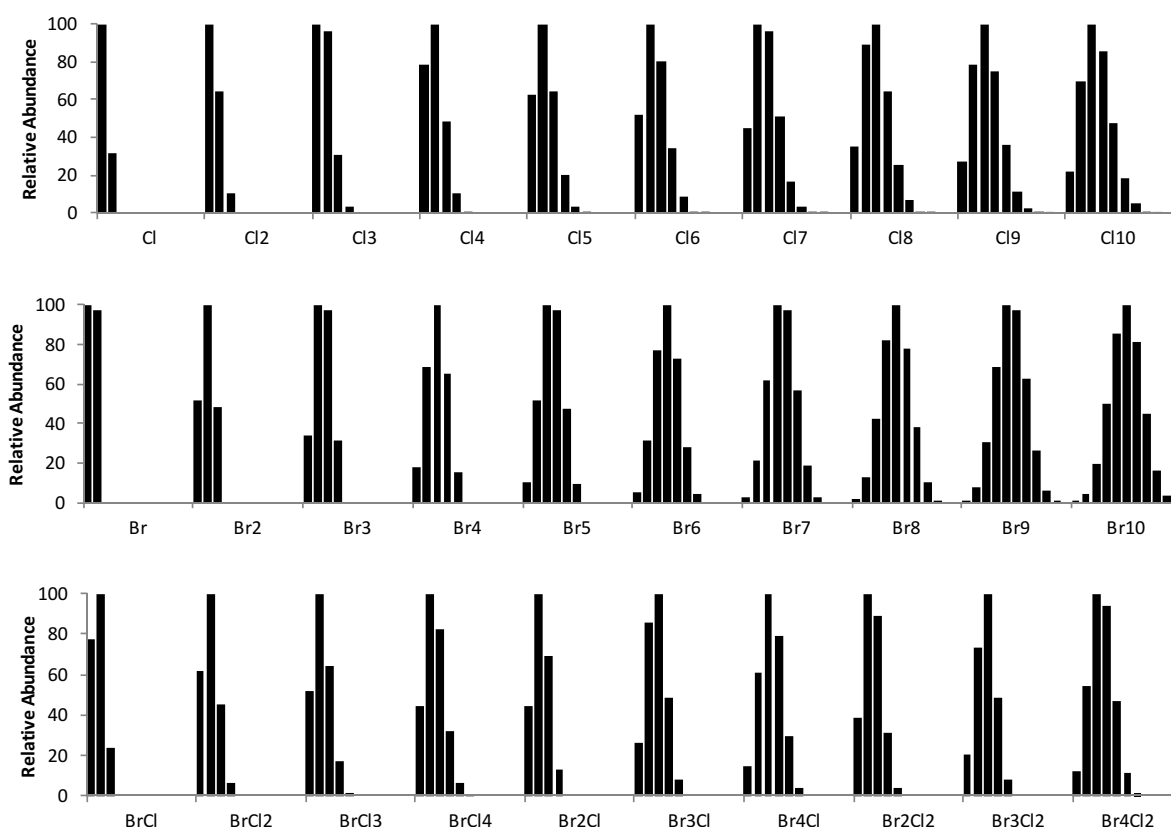


Figure 1-3. Halogen isotope patterns of chlorinated, brominated and mixed-halogenated compounds, adapted from Vetter *et al.* [163]

Table 1-3. Halogen isotope abundances of brominated, chlorinated and mixed-halogenated compounds, adapted from Vetter *et al.* [163]

	M	M + 2	M + 4	M + 6	M + 8	M + 10	M + 12	M + 14	M + 16	M + 18	M + 20
Cl	100	32.0									
Cl₂	100	63.9	10.2								
Cl₃	100	95.9	30.7	3.3							
Cl₄	78.2	100	47.9	10.2	0.8						
Cl₅	62.6	100	63.9	20.4	3.3	0.2					
Cl₆	52.2	100	79.9	34.1	8.2	1.0	<0.1				
Cl₇	44.7	100	95.9	51.1	16.3	3.1	0.3	<0.1			
Cl₈	35.0	89.4	100	63.9	25.5	6.5	1.0	0.1	<0.1		
Cl₉	27.2	78.2	100	74.6	35.8	11.4	2.4	0.3	<0.1	<0.1	
Cl₁₀	21.8	69.5	100	85.2	47.7	18.3	4.9	0.9	0.1	<0.1	<0.1
Br	100	97.3									
Br₂	51.4	100	48.6								
Br₃	34.3	100	97.3	31.5							
Br₄	17.6	68.5	100	64.9	15.8						
Br₅	10.6	51.4	100	97.3	47.3	9.2					
Br₆	5.4	31.7	77.1	100	73.0	28.4	4.6				
Br₇	3.1	21.1	61.7	100	97.3	56.8	18.4	2.6			
Br₈	1.6	12.4	42.3	82.2	100	77.8	37.9	10.5	1.3		
Br₉	0.9	7.8	30.2	68.5	100	97.3	63.1	26.3	6.4	0.7	
Br₁₀	0.5	4.4	19.4	50.3	85.7	100	81.1	45.1	16.4	3.6	0.4
BrCl	77.4	100.0	24.1								
BrCl₂	62.0	100.0	44.9	6.2							
BrCl₃	51.8	100.0	64.2	17.1	1.6						
BrCl₄	44.4	100.0	82.5	32.3	6.1	0.5					
Br₂Cl	44.2	100.0	69.2	13.4							
Br₃Cl	26.5	85.9	100.0	48.5	7.8						
Br₄Cl	14.5	60.8	100.0	79.4	29.9	4.1					
Br₂Cl₂	38.7	100.0	88.7	31.1	3.7						
Br₃Cl₂	20.6	73.7	100.0	48.7	7.9						
Br₄Cl₂	12.0	54.6	100.0	93.7	46.8	11.7	1.1				

Mass defect plots have been used to visualise these differences in a complex mixtures of compounds and for better visualisation the mass defect is plotted against the exact mass [162-165] This can be exploited to screen and identify characteristic halogenated isotopic patterns in various samples [166-168]. Recently, Peng *et al.* described a non-target screening method for halogenated substances based on data-independent precursor isolation and characteristic Br fragment identification [169, 170].

Kendrick introduced the idea of plotting a large set of data, by grouping compounds with similar mass defect [171]. The aim was to visualize homologous hydrocarbon molecules, which contain different numbers of CH₂ groups. The Kendrick factor therefore is $(CH_2) = 14 / 14.01565$, whereby the factor is calculated by the division of the nominal mass by its exact mass. Other factors reported in literature to identify halogenated compounds (Br, Cl, F) in the environment are often referred to as transformed or non-traditional mass scales. They rely on the fact that homologous group of compounds can be represented by a hydrogen for halogen substitution, $-H / +Cl$ ($34 / 33.96102$) [164] or $-H / Br$ ($78 / 77.91051$) [164, 165, 172]. Figure 1-4 shows an example for a H/Cl transformed mass scale for the detection of chlorinated compounds in an extracted trout sample [164]. Other examples include the detection of perfluorinated compounds CF₂ ($50 / 49.99681$) and fluorine for chlorine substitution $+F / -Cl$ ($16 / 15.97045$) [173], where mass defect plots were applied for the identification of fluoropolymer thermal decomposition products.

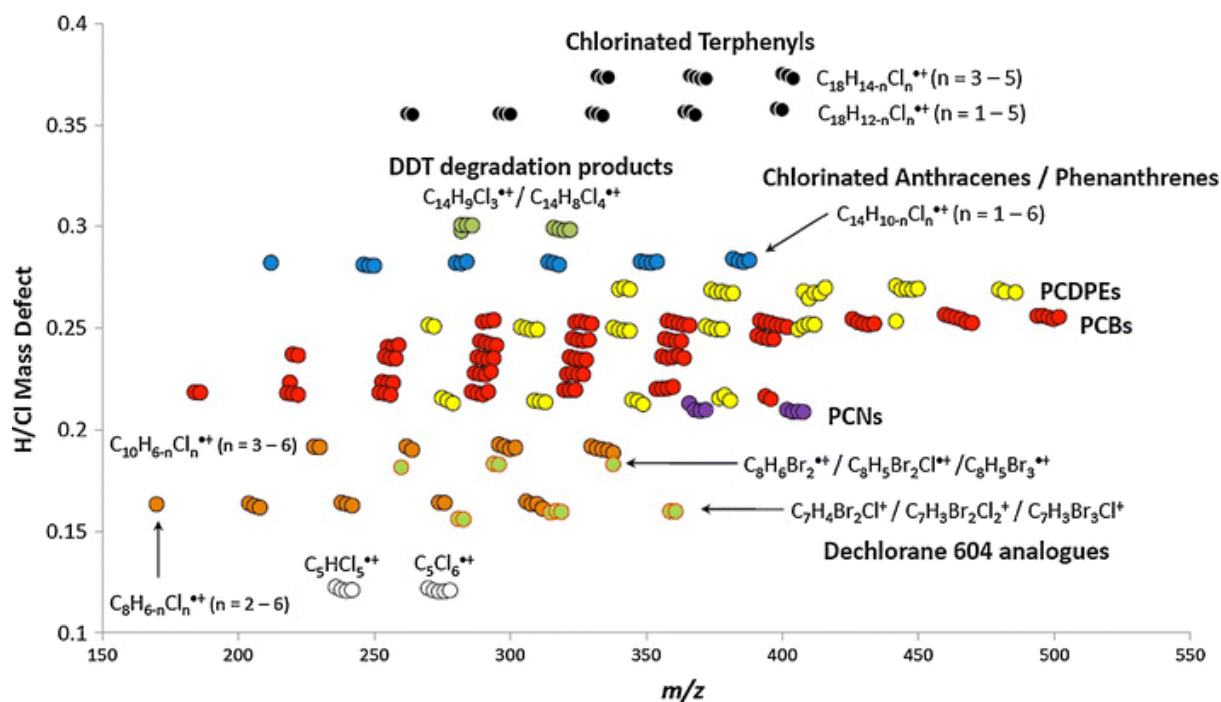


Figure 1-4. Mass defect plot using the H/Cl transformed Kendrick mass scale of an extract of Lake Ontario lake trout, adapted from Jobst *et al.* [164] DDT= dichlorodiphenyltrichloroethane; PCN = polychlorinated naphthalene; PCBs = polychlorinated biphenyls; PCDPEs = polychlorinated diphenyl ethers

Ballesteros *et al.* analysed plastic samples from electric and electronic devices containing TBBPA using an in-house script for the recognition of halogenated compounds based on isotope pattern and mass defect cluster analysis. Results indicate the presence of impurities, by-products or degradation products of TBBPA and TBBPA derivatives in the samples [161].

Other applications where the principle of mass defect is exploited are various. They range from the identification of black carbon derived structures in volcanic ash soil [174], molecular characterization of natural organic matter [175], over analysing organic mixtures such as petroleum crude oil in the field of petroleomics [176], through to employing bromine as mass defect tag for protein sequencing applications [159] and identification for metabolites in biological matrices [177] and *in vitro* / *in vivo* studies [178]. In the food industry samples can be tested at various stages of the processing workflow for the presence of halogenated

contaminants and their possible precursors. Nagy *et al.* describe the use of this technique for the detection and identification of chlorinated substances, which may act as a chlorine donor and thus a precursor for the formation of toxic monochloro-propanediol (MCPD) esters [179]. Other uses of this mass defect filtering technique are employed in the pharmaceutical sector when it comes to applications related to drug metabolite discovery and identification. This would go beyond the scope of this thesis and can be read elsewhere [180].

Mass defect filtering (MDF) or multiple mass defect filtering (MMDF) are post acquisition data filtering techniques that allows the analyst to identify parent molecules and their metabolites, degradation or transformation products, based on their common mass defect. Since bromine and chlorine have the afore mentioned characteristic negative mass defect value, these elements can be used for tagging other molecules of interest, which can then be shifted into less noisy regions of complex mass defect spectra, a technique known as mass defect labelling. One of the prerequisites for using the MDF approach is the employment of high resolution accurate mass instruments, since they have sufficient resolving power to accurately resolve and distinguish the mass defect of measured compounds. With the increased development of these instruments during the last decade, analysis based on MDF in drug metabolite discovery for example, has become more widely used. The mass defect filtering approach however works better for conjugative metabolites than for oxidative ones, since elements with a greater mass defect value are introduced into the molecule in the latter case. Selectivity of the approach depends on structural similarity of parent drug and metabolites, as well as interference from endogenous biological matrix. In some cases MDF alone might not be effective enough to filter out possible interferences, but other processing techniques, such as neutral loss, use of control samples, extracted ion chromatographic analysis and product ion

analysis, might have to be used in combination [181]. Cuyckens *et al.* indeed suggested that the combination of techniques such as mass defect, neutral loss and isotope filtration is more powerful for *in vivo* and *in vitro* metabolite detection, compared to using these techniques separately on their own [182].

1.6.4. Unknown screening approaches

As summarized in Figure 1-6 unknown screening is a technique recently gaining popularity in non-target HR-MS. This approach is used where no prior information is available about the compounds/metabolites detected and several steps have to be completed before coming to a conclusion, including: 1. measurement of the accurate mass-to-charge ratio (m/z) of molecular, fragment and adduct ions; 2. determination of relative isotopic abundances (RIA) of molecular and fragment ions; 3. fragmentation experiments to obtain dissociation patterns for chemical structures of the target compounds and 4. comparison of experimental data to databases containing physico-chemical data (i.e. monoisotopic masses and molecular formulas) or experimental derived data (i.e. retention times and fragmentation mass spectra), as well as the use of *in-silico* prediction software [183]. This sets itself apart from target screening approaches, where authentic chemical reference standards are employed and the chemical properties of target compounds are known prior to data acquisition, combined with the availability of developed analytical methods, with high accuracy, precision and selectivity [183]. In suspect screening on the other hand, no reference standards are obtainable, but prior information on the compounds such as exact mass, isotopes and formed adducts is available [184]. With more and more studies based on HR-MS, Schymanski *et al.* proposed a system to compare and better communicate the level of confidence between different studies and compounds detected (see Figure 1-5) [22]. This approach should be used as a

recommendation next to the already existing EU Guideline 2002/657/EC, dealing with the performance of analytical methods and the interpretation of obtained results.

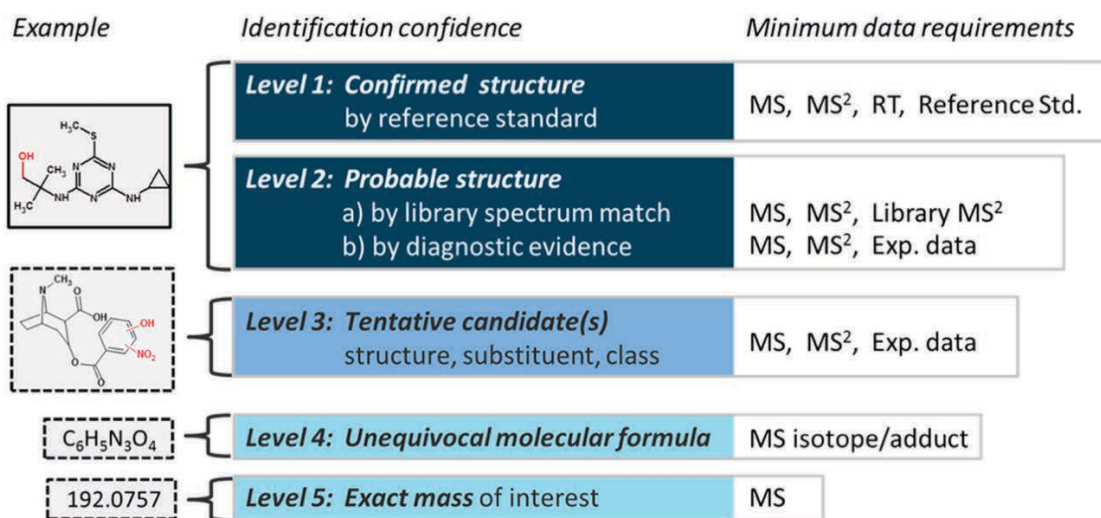


Figure 1-5. Different levels of confidence in the identification process of compounds by high resolution mass spectrometry, adapted from Schymanski et al. [22]

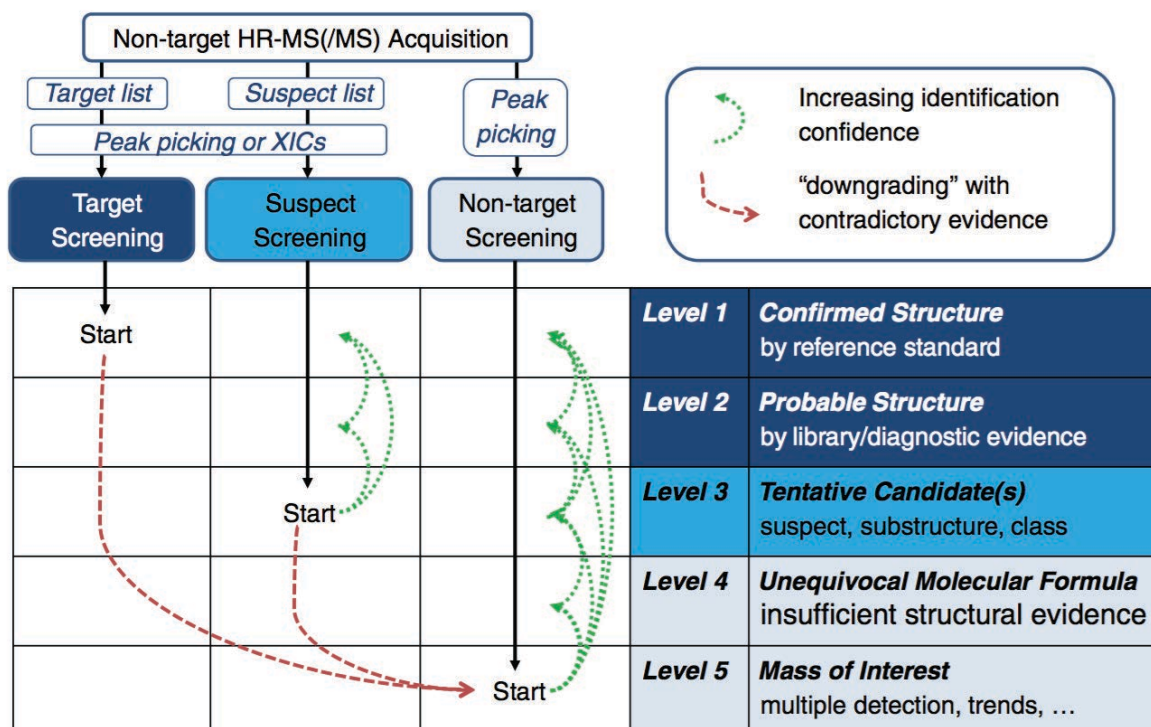


Figure 1-6. Different approaches for identification of compounds and levels of confidence, adapted from Schymanski et al. [184]

1.7. Aims and Objectives

It is clear from the above that there are several research gaps with respect to the environmental presence, fate and behaviour of NBFRs in the environment. In order to try and address these gaps, this project will test the hypothesis that degradation/metabolic products of legacy and novel BFRs are measurable and ubiquitous throughout various compartments of the ambient environment. Moreover, it is hypothesised that LC-HRMS techniques provide a viable method for identifying and quantifying such transformation products in the environment. We also evaluated the hypothesis that concentrations of NBFRs in the environment are approaching those of LBFRs, as a result of restrictions on manufacture and use of the latter.

These hypotheses will be tested by:

1. Developing an instrumental method for the detection of BFRs and NBFRs based on a HPLC-HRMS system, and subsequently testing its suitability for the intended purpose.
2. Using software tools in order to extract relevant information on the presence of halogenated compounds in a complex data set, by exploiting their characteristic mass defect.
3. Establishing protocols for the extraction and clean-up of various sample types with the aim of detecting both parent and possible transformation products.
4. Measuring the levels of NBFRs in selected environmental matrices and comparing these with concentrations of legacy BFRs in the same samples.
5. Conducting controlled experiments to gain an insight into the mechanisms of transformation processes of target compounds in aquatic biota (through *in-vitro* trout liver microsome exposure studies) and sun exposed samples (through forced indoor and outdoor photodegradation studies of chemical standards in solution).

Chapter II - Materials and Methods

Within this work the determination of PBDEs and NBRs was required in several different sample matrices, with varying degrees of complexity and matrix interferences. These matrices comprised: simple solvents, *in vitro* cell media, dust and sediments. Generally, the analysis was conducted based on four main steps: sampling, extraction, clean-up and instrumental analysis. For most samples, the developed multi-residue instrumental analytical method was used, whilst the extraction and clean-up procedure varied. Where possible, methods were validated against stringent QA/QC measures that are outlined in this chapter.

2.1. Chemicals

All solvents (acetone, toluene, hexane, dichloromethane) used were purchased from Fisher Scientific (Loughborough, UK) and were of HPLC grade or higher. Mobile phase water and methanol used for the UPLC separation were of Optima™ LC-MS grade and were also acquired from Fisher Scientific (Loughborough, UK).

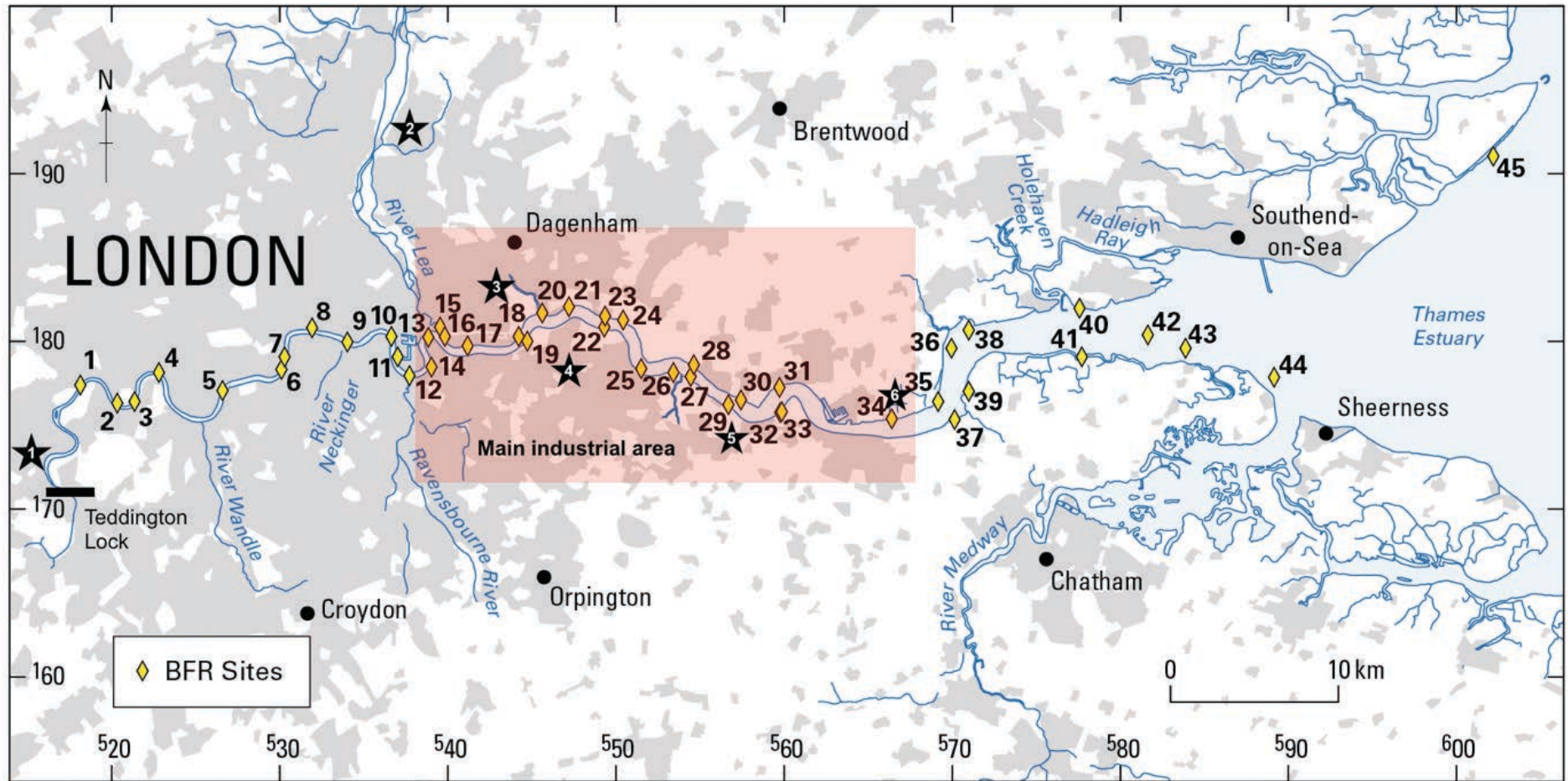
2.1.1. Sediment analysis

Target compounds were the following: PBDEs (BDE-17, BDE-28, BDE-47, BDE-99, BDE-100, BDE-153, BDE-154, BDE-183, BDE-196, BDE-197, BDE-206, BDE-207 and BDE-209), HBB, TBP, α -, β and γ -HBCDDs, TBBPA and the emerging flame retardants EH-TBB, BEH-TEBP, BTBPE, DBDPE, PBEB, a/s-DP, BB153 α - and β -DBE-DBCH and were all purchased from Wellington Laboratories Inc. (Guelph, Canada). The standard reference material (SRM 1944, “New York/New Jersey Waterway Sediment” certified for PCBs, PAHs and PBDEs) was obtained from the National Institute of Standards and Technology - NIST (Gaithersburg, MD, USA).

2.2. Sampling

2.2.1. Sediment Sampling

Sampling of sediments from the River Thames was carried out in October 2011 at the locations shown in Figure 2-1. The sampling campaign was conducted by Dr. Christopher Vane and his collaborators from the British Geological Survey. All sites were accessed via a jet boat using predetermined GPS coordinates to accurately locate each position to ± 3 m [185, 186]. At each location, surface sediments (0-5 cm) were collected from four corners of a square of ca. 2 m² area, using either a stainless steel trowel or a polycarbonate tube fitted with a core catcher manually driven into the surface [187]. The four corner samples and one central sample were combined and transported to shore in a polyethylene zip-lock bag. Sediments were immediately frozen at -18 °C in the dark to avoid post collection chemical changes and physical movement, then transported frozen to the laboratory within 3 days. Each sample was then freeze-dried, sieved through a 2 mm brass mesh and ground to a fine powder using an agate ball-mill and stored in sealed polyethylene bags in a desiccator in the dark [188].



Contains Ordnance Survey data © Crown Copyright and database rights 2017

Figure 2-1. Sampling locations (yellow diamonds) of surface sediments along the Thames Estuary. Stars represent the main discharge locations of sewage effluents; 1. Mogden; 2. Abbey Mills; 3. Beckton STP; 4. Crossness STP; 5. Long Reach STP; 6. Tilbury STP. Red shaded area shows the main industrial discharge area on the Thames (samples 13-34). The Teddington Lock on the left divides the river Thames in to a tidal and non-tidal part. Adapted from Lopes dos Santos and Vane [185]. STP – sewage treatment plants

2.2.2. Total organic carbon (TOC) determination

TOC was measured using the method described by Lopes dos Santos and Vane [185]. Briefly, samples were treated with 1 M HCl, left overnight, washed with deionised water, and oven dried at 60 °C. Analysis was performed with a Europa Scientific Elemental Analyser.

2.2.3. Dust sampling

Dust samples were collected according to an established protocol [189] in offices, laboratories and instrument assembly rooms of the Thermo Fisher Scientific building in Bremen, Germany in August and September 2016. In summary, in carpeted rooms, 1 m² of carpet was vacuumed for 2 min and in rooms with bare floors, 4 m² was vacuumed for 4 min. Samples were collected using nylon sample socks (25 µm pore size) that were mounted in the furniture attachment tube of the vacuum cleaner. The socks were then removed and closed with a twist-tie. The dust was then sieved through a 250 µm mesh sieve and placed in clearly labelled zip-seal plastic bags and stored at -20 °C until analysis.

2.2.4. Master standard-mixture for multi-residue analysis

A mixture of 60 various brominated, chlorinated and other toxic organic compounds was used to assess and compare instrumental capabilities. For this master mixture, five pre-mixtures were prepared in toluene, each containing the listed compounds at a concentration of 1 ng µL⁻¹. Most compounds were purchased dissolved in toluene, if different, they were solvent exchanged into toluene. Concentrations in general for acquired compounds were 50 ng µL⁻¹, while for a few they ranged from 10 - 1000 ng µL⁻¹ and dilutions were made accordingly.

Group 1: 10 PBDEs (BDE-28, BDE-47, BDE-99, BDE-100, BDE-153, BDE-154, BDE-183, BDE-196, BDE-207 and BDE-209), α-,β and γ-HBCDDs and TBBPA.

Group 2: 8 PCBs (PCB-28, PCB-52, PCB-101, PCB-105, PCB-118, PCB-138, PCB-153, PCB-180).

Group 3: 16 PAHs (Naphthalene, Acenaphthylene, Acenaphthene, Fluorene, Phenanthrene, Anthracene, Fluoranthene, Pyrene, Benz[*a*]anthracene, Chrysene, Benzo[*b*]fluoranthene, Benzo[*k*]fluoranthene, Benzo[*a*]pyrene, Dibenz[*a,h*]anthracene, Benzo[*ghi*]perylene, Indeno[1,2,3-*cd*]pyrene).

Group 4: 21 emerging brominated and chlorinated flame retardants ATE, BATE, TBP, DPTE, β -DBE-DBCH, PBEB, HBB, BB153, BTBPE, EH-TBB, BEH-TEBP, HCDBCO, DBDPE, aCl10DP, aCl11DP, Dec 602, Dec 603 and Dec 604.

Group 5: 3 phosphorus flame retardants TCEP, TCiPP and TDCiPP.

The final master mix was obtained by adding equivalent volumes (40 μ L) of each of the pre-mixes into a vial, which resulted in a final concentration of 200 $\text{pg } \mu\text{L}^{-1}$. For GC measurements the master mix in toluene was used, while for LC a part of the mix was solvent exchanged into methanol.

2.2.5. *In vitro* biotransformation of NBRs by trout liver microsomes

Various experiments were conducted, initial screening to assess the formation of metabolites (EH-TBB, BTBPE, BEH-TEBP and DBE-DBCH - Table 2-1), as well as kinetic (equimolar mixture of α - and β -DBE-DBCH and single β -DBE-DBCH - Table 2-2) and temperature (EH-TBB - Table 2-3) dependent studies. The overall workflow was adapted from previous work within the group [190]. Technical BTBPE, EH-TBB, BEH-TEBP and DBE-DBCH were obtained as neat standard from Accustandard, Inc. (New Haven, CT, USA). A 1000 μ M dosing solution was prepared by dissolving each compound in dimethyl sulfoxide (DMSO) or toluene in the case of BTBPE (due to incomplete solubility in DMSO). High purity standards of β -DBE-DBCH, α - and β -DBE-DBCH mixture (equimolar concentrations), BTBPE, ^{13}C -BTBPE, EH-TBB, ^{13}C -EH-TBB, TBBA, TBP, BEH-TEBP, ^{13}C -BEH-TEBP, BDE-77, and ^{13}C -BDE-100 were purchased from Wellington Laboratories (Guelph, ON, Canada).

0.5 mg of female trout liver microsomes (Thermo Fisher Scientific, UK) were exposed to 10 μM (varied from 1-15 μM in kinetic study) of selected NBFRs (dissolved in 10 μL of either DMSO or toluene). Incubation was conducted in a William's E Medium (Thermo Fisher Scientific, UK) at 15 $^{\circ}\text{C}$ for 1 hour (varied from 10-30 $^{\circ}\text{C}$ for temperature study). The reaction was initiated through the addition of 100 μL XenoTech RapidStart™ NADPH regenerating system (XenoTech, USA) at a final concentration: 2.0 mM nicotinamide adenine dinucleotide phosphate, 10.0 mM glucose-6-phosphate and 2 units/mL glucose-6-phosphate dehydrogenase) to make a final volume of 1 mL. At the end of the incubation, 1 mL of ice-cold methanol was added to stop the reaction prior to sample extraction. Where available 20 ng of isotopically-labelled standards were used as internal standard, where unavailable samples were spiked with 20 ng of ^{13}C -BDE-100 instead.

Table 2-1. Experimental set-up for the *in vitro* screening study

NBFR	μM	μL NBFR stock	μL William's E Medium
EH-TBB	10	10	880
BEH-TEBP	10	10	880
BTBPE	10	10	880
DBE-DBCH	10	10	880

Table 2-2. Experimental set-up for the *in vitro* kinetic experiment series with DBE-DBCH (equimolar mixture of α - and β -DBE-DBCH, as well as single β - DBE-DBCH)

μM	μL stock	μL William's E Medium
1	1	889
2	2	888
5	5	885
10	10	880
15	15	875

Table 2-3. Experimental set-up for the *in vitro* temperature study with EH-TBB

Temp. $^{\circ}\text{C}$	μM	μL stock	μL William's E Medium
10	10	10	880
15	10	10	880
20	10	10	880
30	10	10	880

2.2.6. Photodegradation experiments

Photodegradation experiments were conducted under several conditions: indoor exposure, natural sunlight and exposure to an UV A/B or UV C lamp. High purity standards of BTBPE, EH-TBB, BEH-TEBP and DBDPE (Wellington Laboratories, Canada) were prepared in methanol, hexane or toluene at a concentration of $0.5 \text{ ng } \mu\text{L}^{-1}$ for BTBPE, EH-TBB, BEH-TEBP and DBDPE. Plastic cuvettes used in this study for standards dissolved in methanol were small 2.5 mL chambers (Sigma Aldrich, UK), which were rated by the producer to transmit throughout the UV/visible range of 230 to 900 nm. The cuvette was sealed with a small strip of Parafilm. For all other solvents, sealable glass vials (Sigma Aldrich, UK) were used, due to the unavailability of quartz cuvettes and the incompatibility of the solvents with the plastic cuvettes used. The set-up was kept wrapped in aluminium foil inside the laboratory until the exposure began. The set-up was exposed on a styrofoam box lined with aluminium foil. As a dark control, three cuvettes of each solvent were kept sealed in aluminium foil in the laboratory at room temperature for the duration of the experiment. Similarly, for outdoor exposure three cuvettes of each solvent were placed inside the box for the duration of the experiment as a dark control.

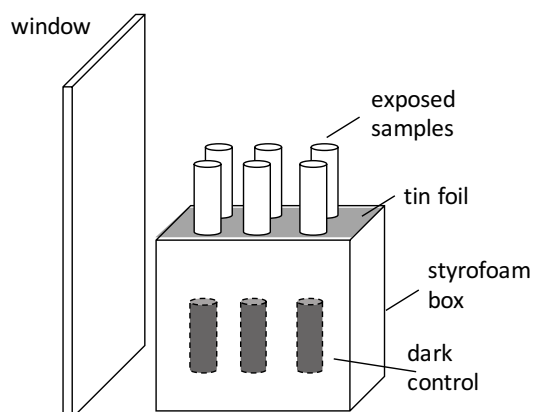


Figure 2-2. Schematic of indoor exposure experiment

Indoor exposure

The box (experimental setup – Figure 2-2) was placed indoors behind a glass window and exposed to indoor light for a cumulative period of 245 h. The room was located on the University of Birmingham campus in Birmingham, UK (located at N 52° 27' 3" latitude and W 1° 55' 50" longitude at an altitude of 144.0 m above mean sea level). The study began on July, 5th 2017 and ended on August, 29th 2017. Temperature was measured next to the experimental set-up using a TinyTag™ temperature logger with measurements recorded every 30 min. Exposed and non-exposed temperature measurements were recorded separately.

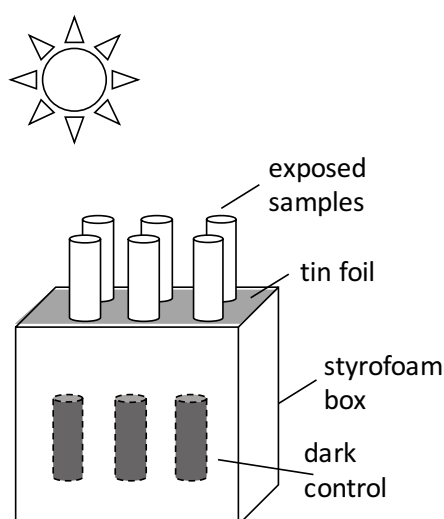


Figure 2-3. Schematic of outdoor exposure experiment

Outdoor exposure

The box (experimental setup –Figure 2-3) was placed outdoors at the parking lot of the Public Health Building on the University of Birmingham campus in Birmingham, UK (Figure 2-4) (located at N 52° 27' 3" latitude and W 1° 55' 50" longitude at an altitude of 144.0 m above mean sea level). As long as there was no precipitation in the forecast, the set-up was placed outside every day, including weekends from approximately 9:00 AM to 6:00 PM until a cumulative period of 130 h exposure was achieved. At the beginning of the day the sample

was briefly shaken. When not exposed to sunlight, the set-up was sealed in aluminum foil and stored in the laboratory. The present study began on July, 8th 2017 and ended on August, 29th 2017. Hourly radiation measures were taken from a UK MetOffice weather station close to the University of Birmingham (located at N 52° 28' 57" latitude and W 1° 41' 46" longitude at an altitude of 96.0 m above mean sea level), which measures the hourly radiation with a pyranometer. Temperature was measured next to the experimental set-up using a TinyTag™ temperature logger with measurements recorded every 30 min. Exposed and non-exposed temperature measurements were recorded separately.



Figure 2-4. Location of the outdoor exposure experiment (red circle) on the University of Birmingham campus

UV-light exposure

UV exposure was conducted inside an incubator (experimental setup - Figure 2-5) at a constant temperature of 20 °C. Solvents were placed at a distance of 10 cm from a UV-C light (6 W) or a UV-A/B light (30 % UVA + 10 % UVB, 15W) and exposed for 48 h with regular sampling intervals. Solvent samples wrapped aluminum foil were placed next to the exposed samples for the duration of the exposure as dark control.

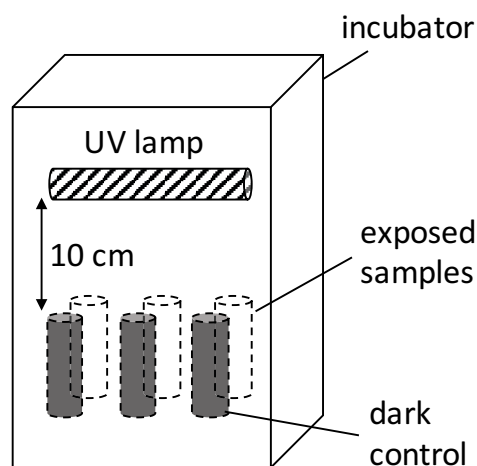


Figure 2-5. Schematic of UV exposure experiment

2.3. Extraction and Clean-up

2.3.1. Sediment

2 g of freeze-dried sediment, NIST SRM 1944 (New York/New Jersey Waterway Sediment) or sodium sulfate as blanks were weighed into a pre-cleaned glass extraction tube and spiked with 20 μL of the internal standard mixture (concentration of 1 $\text{ng } \mu\text{L}^{-1}$ for ^{13}C -BDE28, BDE77, BDE128, ^{13}C -TBBPA and ^{13}C - α -, β -, and γ -HBCDDs, 2 $\text{ng } \mu\text{L}^{-1}$ for ^{13}C -BDE209, ^{13}C -EH-TBB, ^{13}C -BEH-TEBP and ^{13}C -BTBPE). Individual standards were purchased from Wellington Laboratories (Guelph, ON, Canada). The exact chemical composition of internal standards, including ^{13}C -labeled and deuterated standards is listed in Table 2-6. 2 g of copper was added for sulfur removal. Samples were then extracted using 4 mL of hexane:acetone (3:1 v/v), vortexing for 5 min, followed by ultrasonication (20 min) and centrifugation (5 min at 4000 r.p.m.). This procedure was repeated twice. The combined extract was then evaporated to dryness under a gentle stream of N_2 and reconstituted in 2 mL of hexane. This was followed by a sulfuric acid wash of the extract, with the layers allowed to separate overnight. The organic phase was collected and the acid layer washed twice with 2 mL of hexane. The

combined extracts were then reduced to ~1 mL under a gentle stream of N₂ and loaded onto a conditioned HyperSep™ 1 g Florisil SPE cartridge (Thermo Fisher Scientific, UK), on top of which 1 g of sodium sulfate (dried over night at 120 °C) was added. Subsequent elution was performed with 20 mL of hexane:dichloromethane (1:1 v/v), with TBBPA eluted in a second fraction with 15 mL of methanol. Both fractions were combined, concentrated to dryness under a N₂ flow using a Turbovap™ and reconstituted in 200 µL methanol:toluene (1:1 v/v) containing 200 pg µL⁻¹ of ¹³C-BDE100 as a recovery determination standard.

2.3.2. Dust

0.5 g of dust was weighed and mixed with diatomaceous earth as dispersant. Extraction was conducted using a Thermo Scientific™ Dionex™ ASE™ 350 accelerated solvent extractor based on an established method developed in the group [191]. 33 mL stainless steel extraction cells were used with 100 mL in total of different solvent mixtures. The extraction was conducted in 3 static cycles at a temperature of 100 °C at 1500 psi, with a heating time of 5 min, a static extraction time of 5 min, purged for 100 sec and rinsed with 60% of the cell volume in between cycles.

A solvent mixtures of hexane:dichloromethane (3:1 v/v) was used for extraction. Further in-cell cleanup using layers of 5 g silica and Florisil™ each in the ASE cell was performed to reduce possible matrix interferences. Samples were evaporated to dryness using a Thermo Scientific Rocket™ Evaporator system and then reconstituted in 200 µL methanol:toluene (1:1).

2.3.3. *In vitro* biotransformation of BFRs by trout liver microsomes (TLM).

Post-incubation, samples were extracted using 2 mL of hexane:dichloromethane mixture (1:1 v/v) and three cycles of vortex (1 min), ultrasonication (10 min) and centrifugation steps (10 min at 4000 r.p.m.). The organic layer was collected in each step, while the cell pellet was

initially discarded. The combined extracts were concentrated under a gentle stream of N₂ before reconstitution in 100 µL methanol. Where quantitation was conducted the final solution contained 20 ng of BDE-77 as a syringe standard for QA/QC purposes. For further quality control purposes, three negative control blanks were included for each study, a solvent blank (no NBFR), a heat inactivated blank (heat treated TLM – 10 min at 100 °C), as well as a non-enzymatic metabolism blank (whereby no NADPH regenerating system solution was added).

2.3.4. Photodegradation

At predetermined time intervals, aliquots were taken from each solvent, blown down under a gentle stream of N₂, reconstituted in methanol, wrapped in aluminum foil, and stored in a freezer at -20 °C until analysis.

2.4. Instrumental Analysis

Brominated flame retardants are generally analysed using GC methods. Recently LC based methods coupled to low resolution mass spectrometers have been used for their detection. In this work, proving the potential of employing a LC-HRMS for the detection of these compounds was one of the main aims. Therefore, a suitable LC method had to be developed, together with optimized values for the HR mass spectrometric detection.

2.4.1. Analytical method description

Samples were analysed on a UPLC-Orbitrap-HRMS instrument (Thermo Fisher Scientific, Bremen, Germany) composed of an UltiMate® 3000 high performance liquid chromatography system equipped with a HPG-3400RS dual pump, a TCC-3000 column oven and a WPS-3000 auto sampler. The UPLC system was coupled to a Q-Exactive™ Plus Orbitrap mass spectrometer. Chromatographic separation was performed on a Thermo Scientific Accucore™

RP-MS column (100 x 2.1 mm, 2.6 μm) with water (mobile phase A) and methanol (mobile phase B). Gradient elution programmes at a flow rate of 400-500 $\mu\text{L min}^{-1}$ were applied as shown in Table 2-4 for sediment analysis, while Table 2-5 for *in-vitro* and photodegradation samples.

Most compounds were measured in negative atmospheric pressure chemical ionization (APCI) mode. The general parameters of the Orbitrap were set as follows: (-) APCI full scan mode at 70 000 resolution (full width at half maximum – FWHM at 200 m/z), automatic gain control (AGC) target 1e^6 , maximum injection time 100 ms, scan range 250 to 1000 m/z, profile spectrum data type, sheath gas flow rate 25 AU (arbitrary units), aux gas flow rate 5 AU, discharge current 30 μA , capillary temperature 250 $^{\circ}\text{C}$, S-lens RF level 50 AU and aux gas heater temperature 320 $^{\circ}\text{C}$.

For screening, identification of possible degradation products and confirmation purposes, samples were also analysed using the more universal, softer electrospray ionization (ESI) in negative mode. In this case the general parameters were as follows: (-) heated ESI (HESI) full scan mode at 70 000 FWHM resolution, AGC target 1e^6 , maximum injection time 100 ms, scan range 250 to 1000 m/z, profile spectrum data type, sheath gas flow rate 50 AU (arbitrary units), aux gas flow rate 13 AU, spray discharge voltage 2.5 kV, capillary temp 265 $^{\circ}\text{C}$, S-lens RF level 50 AU and aux gas heater temperature 425 $^{\circ}\text{C}$.

Both the HPLC gradient programme and ionization values were optimized based on the measurement of reference standard solutions. Screening for brominated compounds was conducted using an All Ion Fragmentation Scan (AIF) in parallel to the Full Scan measurement. AIF is a data independent analysis whereby all ionised molecules are fragmented without mass filtering of the quadrupole. This aids in the identification of bromine containing molecules,

which through fragmentation lose their bromine molecules and hence show a distinct peak in the bromine mass trace ($m/z = 78.918336 / 80.916290$) in the final data raw files.

Table 2-4. HPLC elution programme for sediment/dust analysis and master mix measurements

Time [min.]	% A (Water)	% B (Methanol)	Flow rate [$\mu\text{L min}^{-1}$]
0	35	65	400
3	35	65	400
4	15	85	400
6	15	85	400
7	0	100	500
10	0	100	500
11	15	85	400
13	15	85	400
14	35	65	400
17	35	65	400

Table 2-5. HPLC elution programme for in vitro and photodegradation samples

Time [min.]	% A (Water)	% B (Methanol)	Flow rate [$\mu\text{L min}^{-1}$]
0	80	20	400
9	0	100	400
12	0	100	400
12.1	80	20	400
15	80	20	400

High resolution accurate mass was used for the detection of all compounds. Table 6 indicates the masses detected, considering the formation of the most abundant pseudo-molecular ions within the APCI / HESI source. Formation of multiple ions per compound has been reported in literature [141]. Therefore, individual standards were measured and the principal formed ion selected.

Table 2-6. Ion generated in the APCI / ESI source from injection of standards and exact mass of the most abundant isotope in the pattern for LC-HRMS analysis

Compound	Formula	Principal Ion formed in APCI	Principal Ion formed in HESI	Exact mass of most abundant isotope
ATE (TBP-AE)	C ₉ H ₇ Br ₃ O	[M-Br+O] ⁻	-	306.87923
TBP	C ₆ H ₃ Br ₃ O	[M-Br+O] ⁻	-	328.76408
BATE (TBP-BAE)	C ₉ H ₆ Br ₄ O	[M-Br+O] ⁻	-	384.78975
DPTE (TBP-DBPE)	C ₉ H ₇ Br ₅ O	[M-Br+O] ⁻	-	466.71386
DBE-DBCH	C ₈ H ₁₂ Br ₄	[M+O ₂] ⁻	-	459.75354
PBEB	C ₈ H ₅ Br ₅	[M-Br+O] ⁻	-	436.70330
HBB	C ₆ Br ₆	[M-Br+O] ⁻	-	486.58251
BB153	C ₁₂ H ₄ Br ₆	[M-Br+O] ⁻	-	562.61436
BTBPE	C ₁₄ H ₈ Br ₆ O ₂	C ₆ Br ₃ H ₂ O ⁻	-	328.76408
		[M-HBr+O ₂] ⁻	-	637.62109
EH-TBB	C ₁₅ H ₁₈ Br ₄ O ₂	[M-Br+O] ⁻	-	484.87911
BEH-TEBP	C ₂₄ H ₃₄ Br ₄ O ₄	[M-Br+O] ⁻	-	640.99414
HCDBCO	C ₁₃ H ₁₂ Br ₂ Cl ₆	[M+O ₂] ⁻	-	571.72852
DBDPE	C ₁₄ H ₄ Br ₁₀	[M-Br+O] ⁻	-	906.28307
aCL10DP	C ₁₈ H ₁₄ Cl ₁₀	[M-Cl+O] ⁻	-	564.81824
aC11DP	C ₁₈ H ₁₃ Cl ₁₁	[M-Cl+O] ⁻	-	598.77927
anti/syn-DP	C ₁₈ H ₁₂ Cl ₁₂	[M-Cl+O] ⁻	-	632.74084
Dec 602	C ₁₄ H ₄ Cl ₁₂ O	[M-Cl+O] ⁻	-	592.67261
Dec 603	C ₁₇ H ₈ Cl ₁₂	[M-H] ⁻	-	638.68781
Dec 604	C ₁₃ H ₄ Br ₄ Cl ₆	[M-Br+O] ⁻	-	626.58935
triBDE ¹	C ₁₂ H ₇ Br ₃ O	[M-Br+O] ⁻	-	342.87978
tetraBDE ²	C ₁₂ H ₆ Br ₄ O	[M-Br+O] ⁻	-	420.78975
pentaBDE ³	C ₁₂ H ₅ Br ₅ O	[M-Br+O] ⁻	-	500.69876
hexaBDE ⁴	C ₁₂ H ₄ Br ₆ O	[M-Br+O] ⁻	-	578.60927
heptaBDE ⁵	C ₁₂ H ₃ Br ₇ O	[M-Br+O] ⁻	-	658.51719
octaBDE ⁶	C ₁₂ H ₂ Br ₈ O	[M-Br+O] ⁻	-	736.42825
nonaBDE ⁷	C ₁₂ HBr ₉ O	[M-Br+O] ⁻	-	816.33672
decaBDE ⁸	C ₁₂ Br ₁₀ O	C ₆ Br ₅ O ⁻	-	486.58306
4-OH-BDE17	C ₁₂ H ₇ Br ₃ O ₂	[M-H] ⁻	[M-H] ⁻	420.78975
2-OH-BDE-28	C ₁₂ H ₇ Br ₃ O ₂	[M-H] ⁻	[M-H] ⁻	420.78975
6-OH-BDE-47	C ₁₂ H ₆ Br ₄ O ₂	[M-H] ⁻	[M-H] ⁻	500.69876
HBCDDs	C ₁₂ H ₁₈ Br ₆	[M-H] ⁻	[M-H] ⁻	640.63746
TBBPA	C ₁₅ H ₁₂ Br ₄ O ₂	[M-H] ⁻	[M-H] ⁻	542.74571
triPCB ⁹	C ₁₂ H ₇ Cl ₃	[M-Cl+O] ⁻	-	236.98794
tetraPCB ¹⁰	C ₁₂ H ₆ Cl ₄	[M-Cl+O] ⁻	-	270.94897
pentaPCB ¹¹	C ₁₂ H ₅ Cl ₅	[M-Cl+O] ⁻	-	306.90705
hexaPCB ¹²	C ₁₂ H ₄ Cl ₆	[M-Cl+O] ⁻	-	340.86808
heptaPCB ¹³	C ₁₂ H ₃ Cl ₇	[M-Cl+O] ⁻	-	374.82910
TCEP	C ₆ H ₁₂ Cl ₃ O ₄ P	-	[M+H] ⁺	284.96115

Table 2-6 continued

TCiPP	C ₉ H ₁₈ Cl ₃ O ₄ P	-	[M+H] ⁺	327.00811
TDCiPP	C ₉ H ₁₅ Cl ₆ O ₄ P	-	[M+H] ⁺	430.88824
TBBA	C ₇ H ₂ Br ₄ O ₂	[M-H] ⁻	[M-H] ⁻	436.66746
¹³ C-TBBA	¹³ C ₆ CH ₂ Br ₄ O ₂	[M-H] ⁻	[M-H] ⁻	442.68759
¹³ C-BDE209	¹³ C ₁₂ Br ₁₀ O	¹³ C ₆ Br ₅ O ⁻	-	492.60319
¹³ C-EH-TBB	¹³ C ₆ C ₉ D ₁₇ HBr ₄ O ₂	[M-Br+O] ⁻	-	508.00594
¹³ C-BEH-TEBP	¹³ C ₆ C ₁₈ D ₃₄ Br ₄ O ₄	[M-Br+O] ⁻	-	681.22736
¹³ C-BTBPE	¹³ C ₆ C ₈ H ₈ Br ₆ O ₂	¹³ C ₆ Br ₃ H ₂ O ⁻	-	334.78421
¹³ C-HBCDDs	¹³ C ₁₂ H ₁₈ Br ₆	[M-H] ⁻	[M-H] ⁻	652.67772
¹³ C-TBBPA	¹³ C ₁₂ C ₃ H ₁₂ Br ₄ O ₂	[M-H] ⁻	[M-H] ⁻	554.78591
¹³ C-BDE-28	¹³ C ₁₂ H ₇ Br ₃ O	[M-Br+O] ⁻	-	354.92004
¹³ C-BDE-100	¹³ C ₁₂ H ₅ Br ₅ O	[M-Br+O] ⁻	-	512.73902

¹ BDE-17, BDE-28⁵ BDE-183⁹ PCB-28² BDE-47, BDE-77⁶ BDE-196, BDE197¹⁰ PCB-52³ BDE-99, BDE-100⁷ BDE-206, BDE-207¹¹ PCB-101, PCB-105, PCB-118⁴ BDE-128, BDE-153, BDE-154⁸ BDE-209¹² PCB-138, PCB-153¹³ PCB-180

Example of extracted ion chromatograms for PBDEs, HBCDDs, TBBPA, NBRs, Dechloranes, OPFRs and PCBs based on the exact masses listed in Table 2-6 are shown in Figure 2-7 to Figure 2-11 in standard solutions.

Figure 2-7 shows additional minor peaks for BATE, DPTE and BTBPE, which have the same exact mass as TBP (328.76408), which elutes earlier. This is caused by the fact that these compounds are structurally similar and through inadvertent in-source fragmentation break down to form TBP. As listed in Table 2-6, BTBPE can be detected both as [M-HBr+O₂]⁻ at 637.62109, as well as C₆Br₃H₂O⁻ at 328.76408 (which is the same mass of TBP). Therefore, retention time is a necessary parameter for identification and distinction between compound and breakdown products formed during measurement.

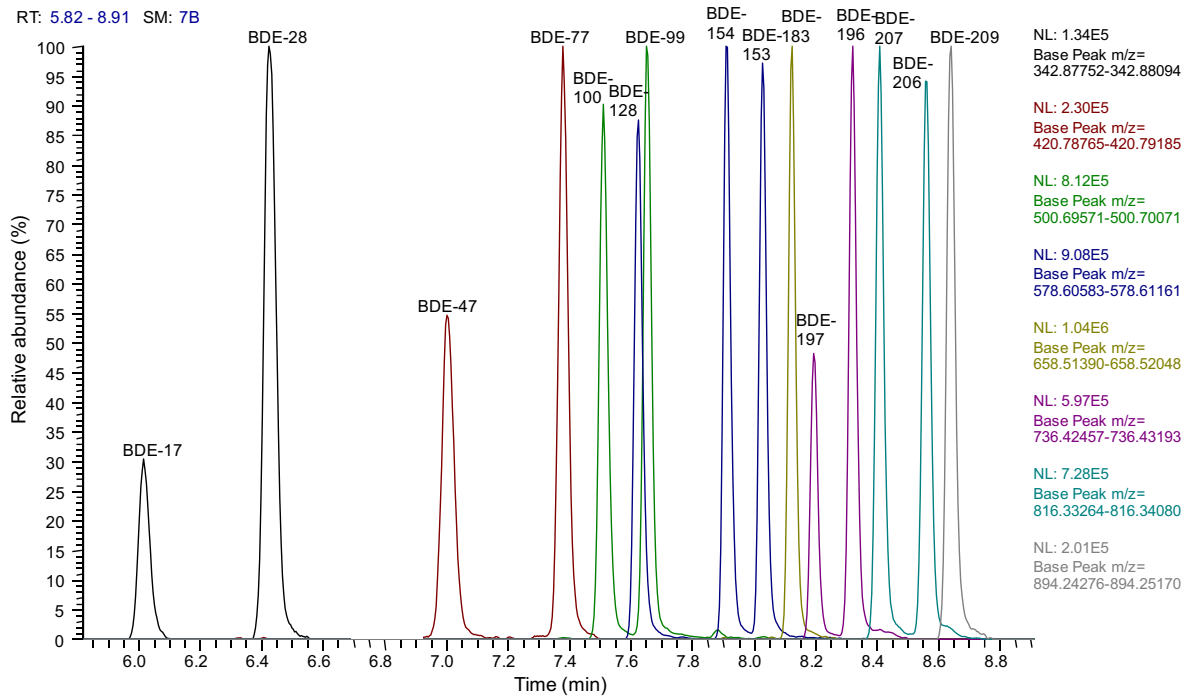


Figure 2-6. Excerpt from an extracted ion chromatogram for selected PBDEs measured in APCI in a 200 $\mu\text{g } \mu\text{L}^{-1}$ standard solution

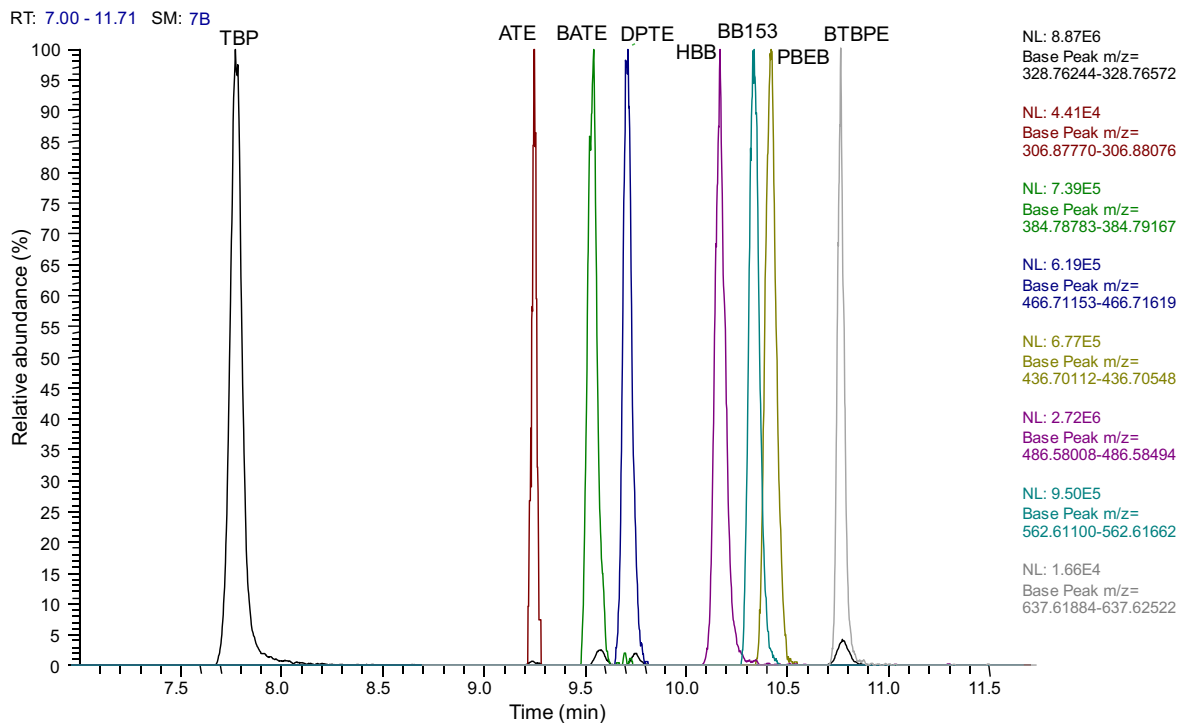


Figure 2-7. Excerpt from an extracted ion chromatogram for selected NBRs measured in APCI in a 200 $\mu\text{g } \mu\text{L}^{-1}$ standard solution

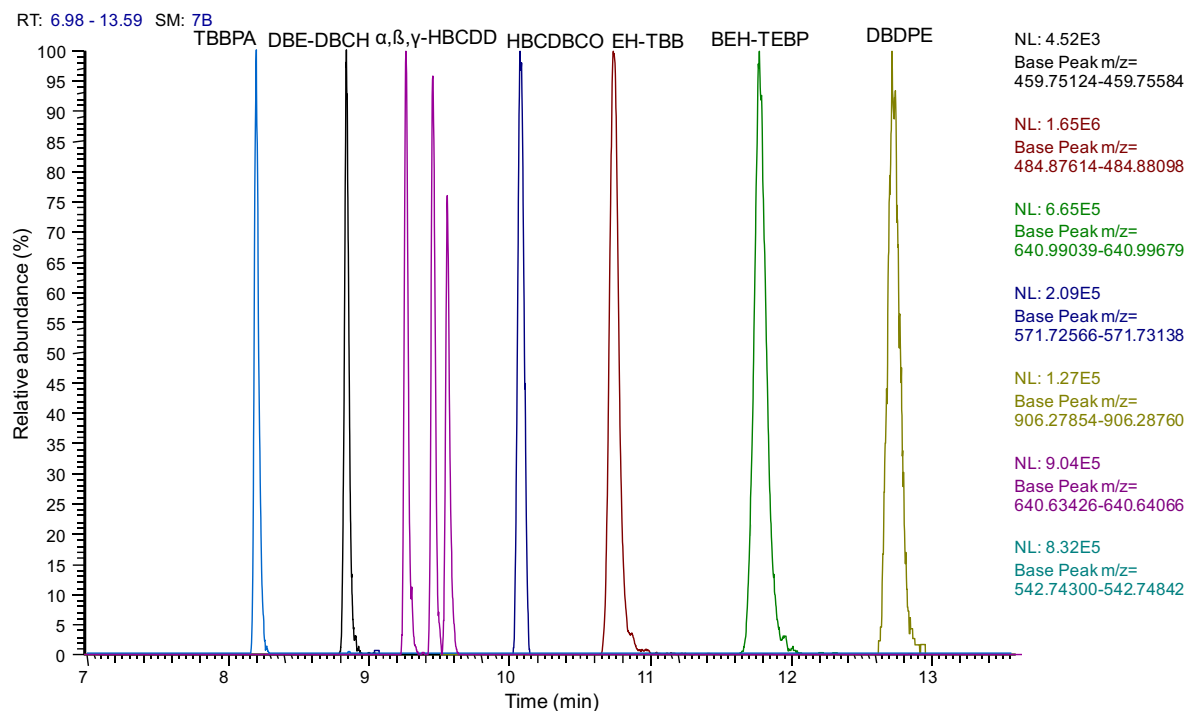


Figure 2-8. Excerpt from an extracted ion chromatogram for selected BFRs measured in APCI in a $200 \text{ pg } \mu\text{L}^{-1}$ standard solution

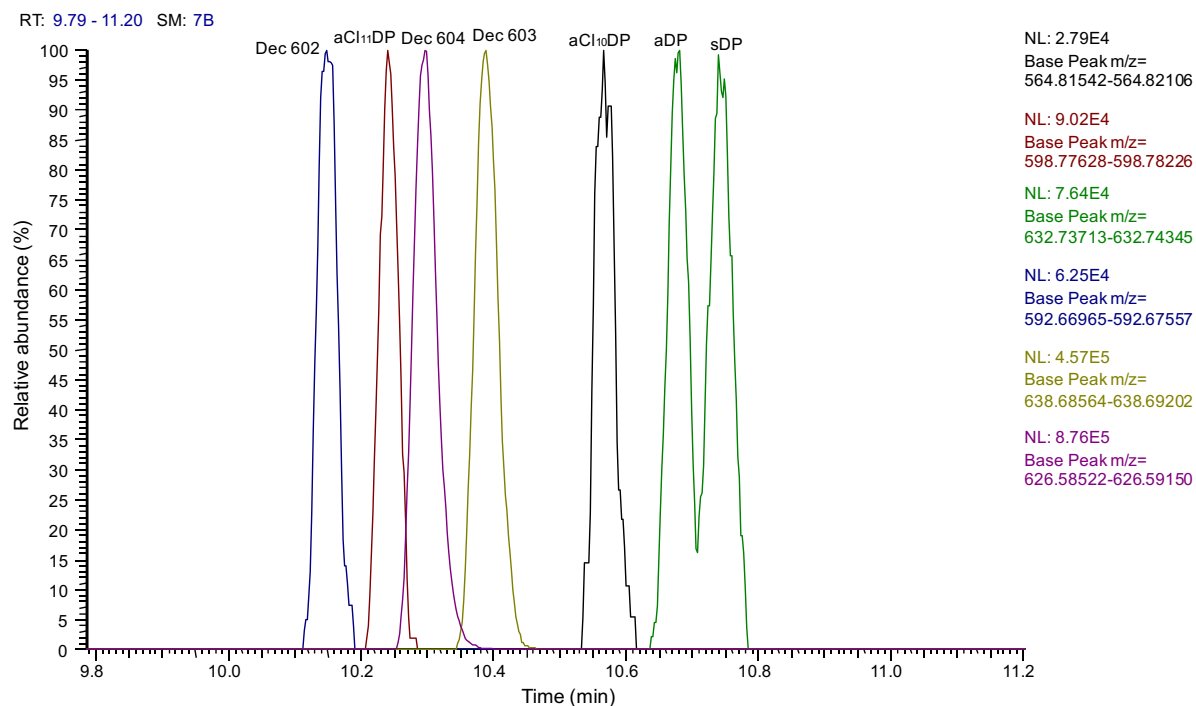


Figure 2-9. Excerpt from an extracted ion chromatogram for Dechloranes measured in APCI in a $200 \text{ pg } \mu\text{L}^{-1}$ standard solution

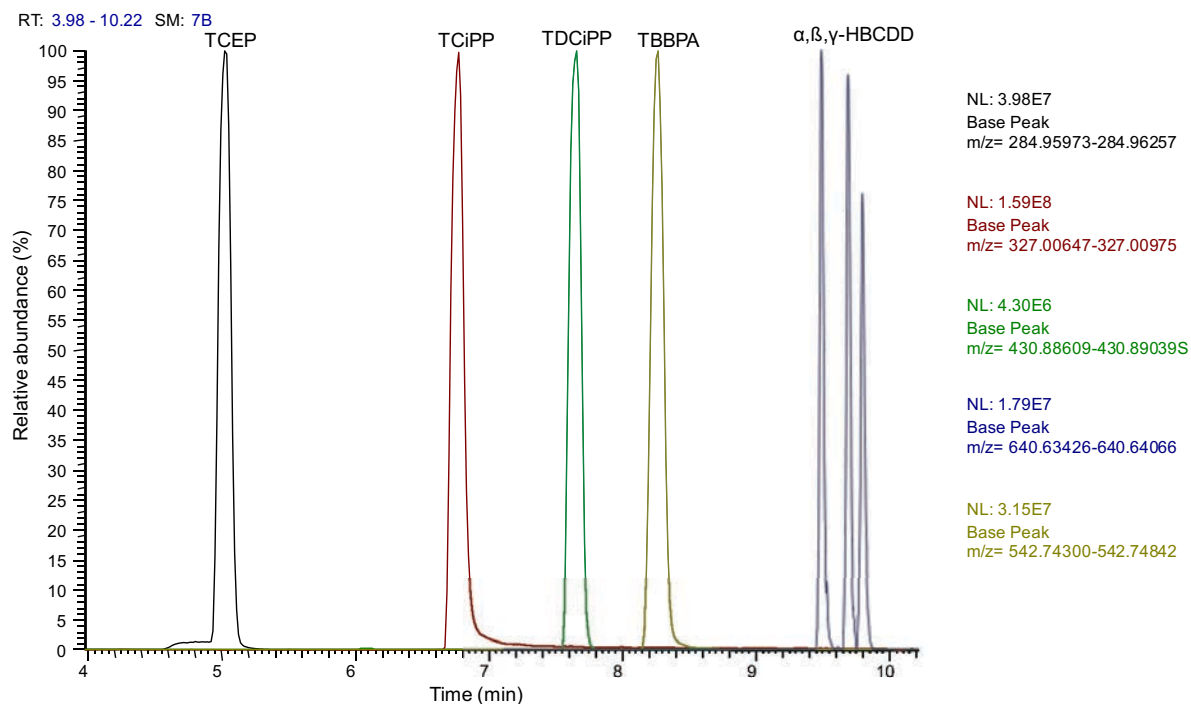


Figure 2-10. Excerpt from an extracted ion chromatogram for OPFRs (pos.), HBCDDs (neg.) and TBBPA (neg.) measured in HESI in pos./neg. switching mode in a 200 pg μL^{-1} standard solution

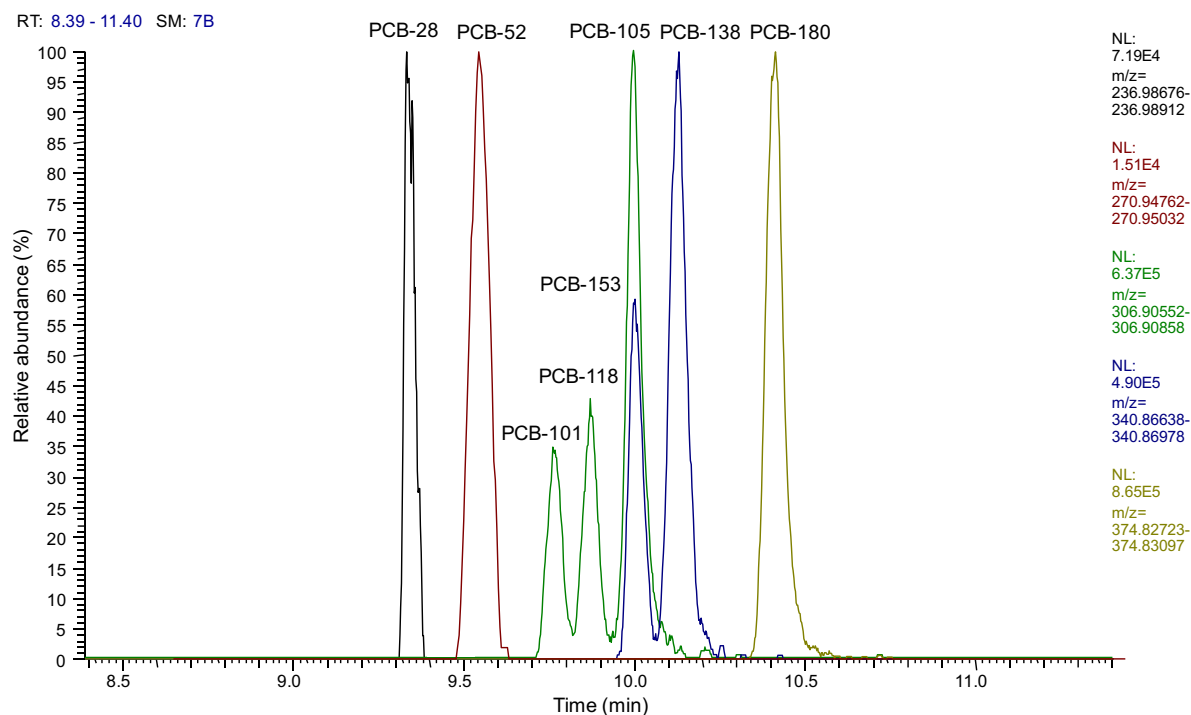


Figure 2-11. Excerpt from an extracted ion chromatogram for PCBs measured in APCI in a 200 pg μL^{-1} standard solution

Additionally, extracted ion chromatograms for PBDEs and selected NBRFRs are shown for a dust sample (Figure 2-12 and Figure 2-13) and a sediment standard reference material (Figure 2-14 and Figure 2-15).

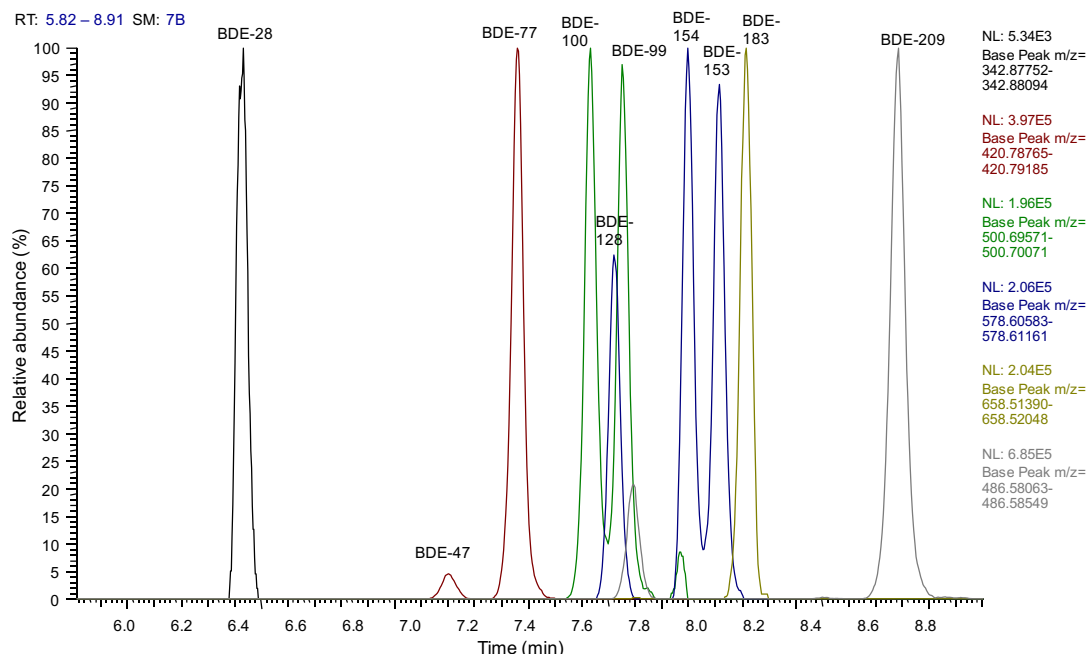


Figure 2-12. Excerpt from an extracted ion chromatogram for selected PBDEs measured in APCI in an extracted dust sample

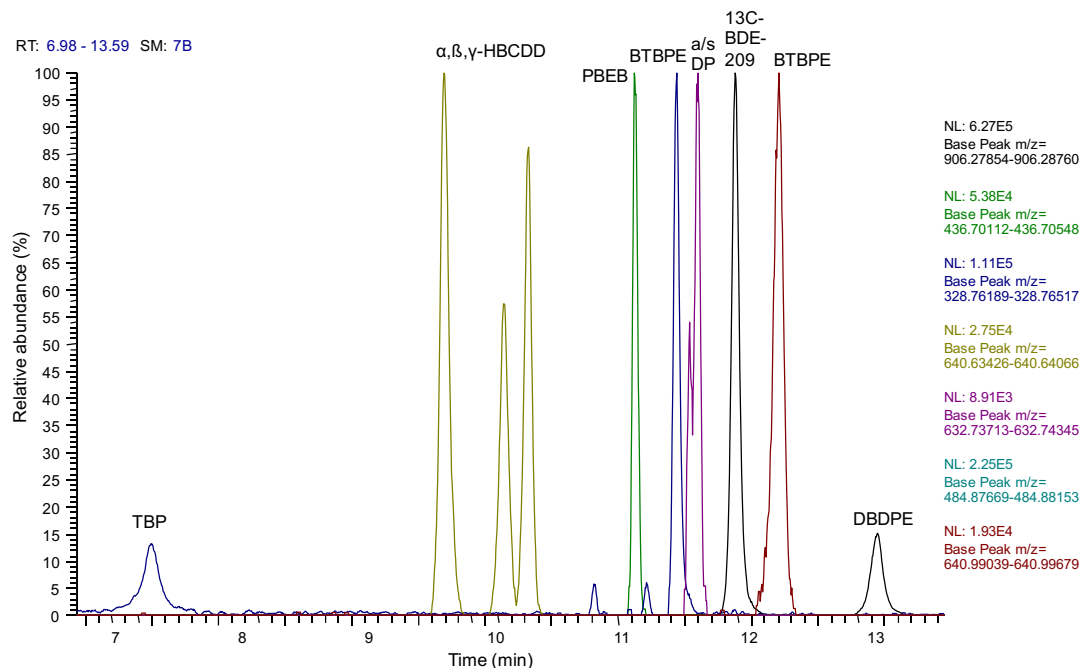


Figure 2-13. Excerpt from an extracted ion chromatogram for HBCDD and selected NBRFRs measured in APCI in an extracted dust sample

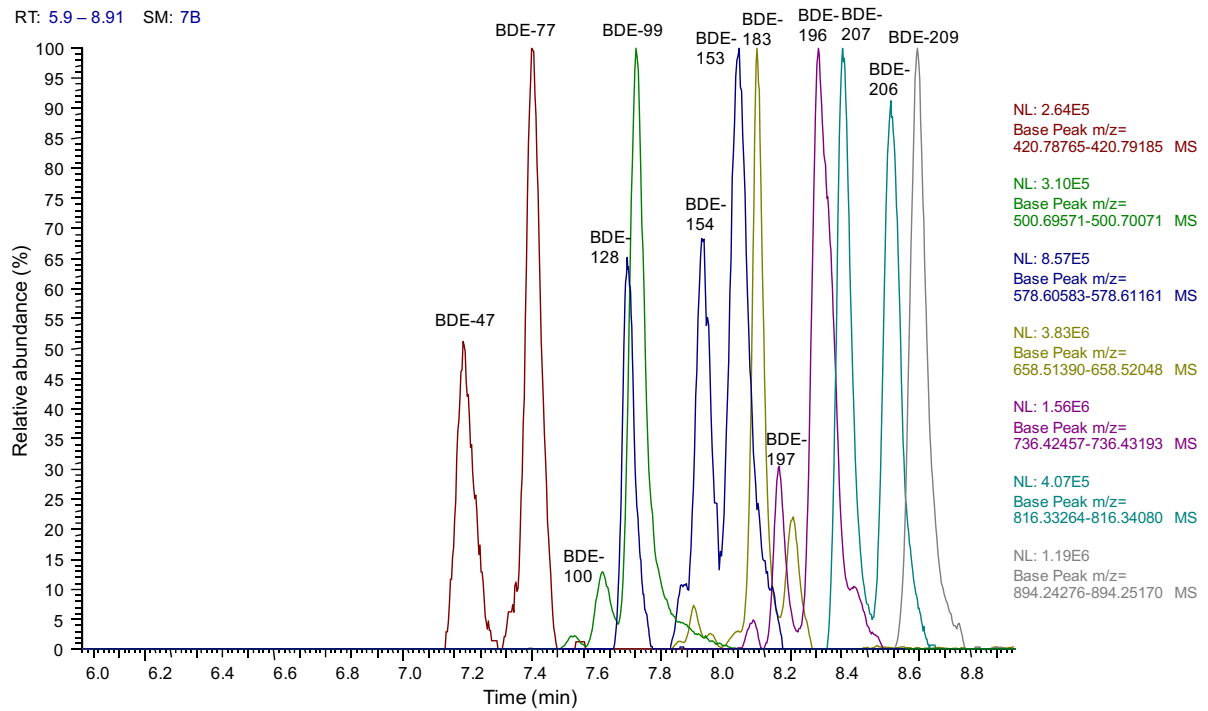


Figure 2-14. Excerpt from an extracted ion chromatogram for selected PBDEs measured in APCI in the sediment SRM 1944

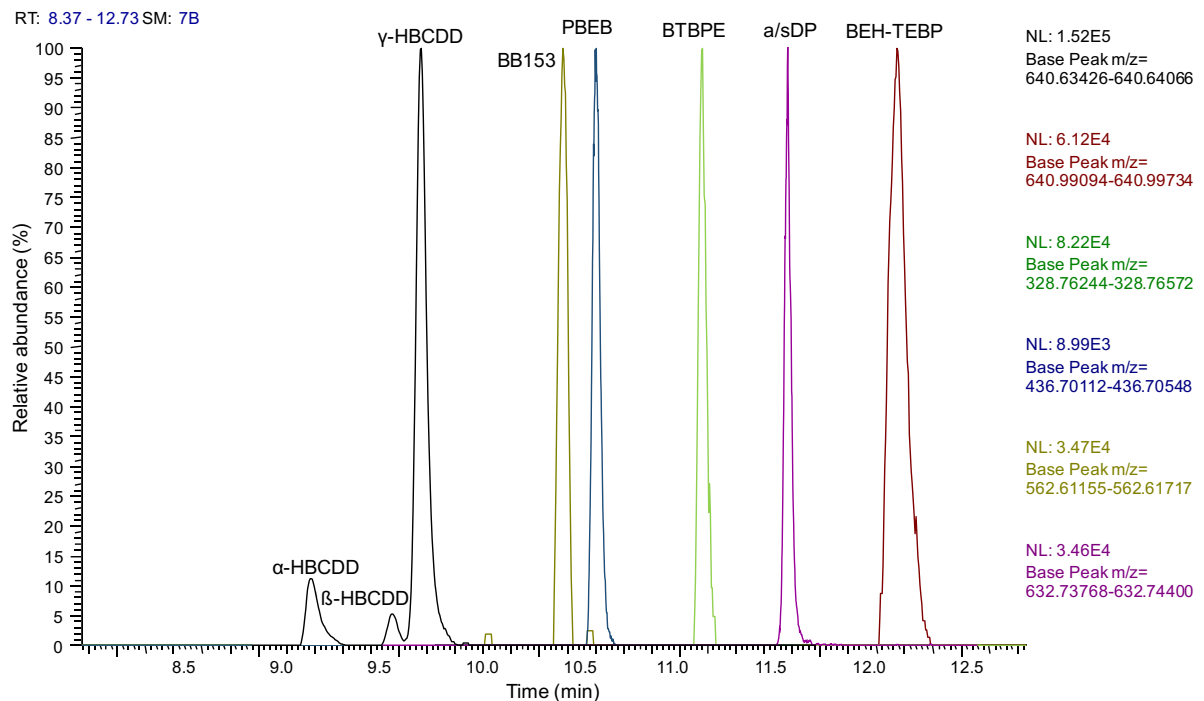


Figure 2-15. Excerpt from an extracted ion chromatogram for HBCDD and selected NBFs measured in APCI in the sediment SRM 1944

2.4.2. Maintenance of the instrument

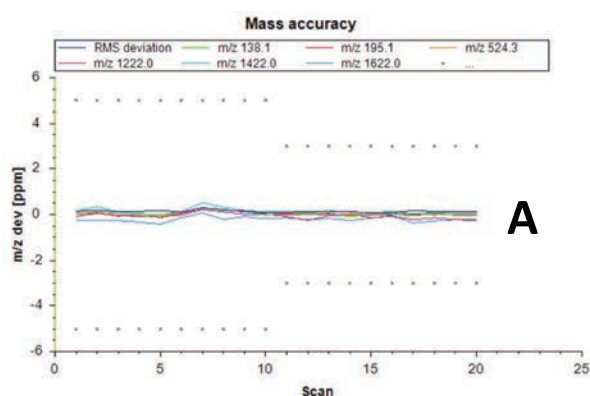
The Q-Exactive Plus Orbitrap mass spectrometer was regularly checked for its performance in order to ensure highest sensitivity and accuracy of all measurements. Calibration solutions for both positive (Pierce LTQ Velos ESI Positive Ion Calibration Solution) and negative (ESI Negative Ion Calibration Solution) ionisation were used as recommended by the manufacturer. Calibration solutions were directly infused into the system by a syringe pump at 5 $\mu\text{L}/\text{min}$. Before starting the evaluation/calibration, satisfactory sensitivity and good spray stability were achieved by optimising the probe position and ESI related parameters, such as spray voltage, gas flow rates and capillary temperature. As a rule, a total ion current (TIC) above 10^8 , with a TIC variation of less than 10 % and an ion injection time (IT) of 5 ms or less are needed prior to starting the evaluation/calibration procedure.

Mass calibration was conducted on a regular basis in ESI, using the above mentioned calibration solution. Mass calibration is based on the ions listed in Table 2-7 and results in a spectrum as shown in Figure 2-17 and Figure 2-18 for both positive and negative mode respectively. During mass calibration, the instrument performs 10 scan using external calibration and 10 scan using internal calibration. The mass deviation for all the calibrators is plotted and the results shown as $\text{rms} = \text{internal} / \text{external ppm}$ as shown in Figure 2-16 A and Figure 2-16 B for positive and negative calibration respectively. Only when the mass accuracy was below 1 ppm root mean square (rms) for internal calibration and 3 ppm rms for external calibration measurements were conducted on the instrument. Next to the mass calibration, the system was also evaluated before a set of measurements was conducted. In cases where evaluation procedures failed, calibration of the respective parameters was conducted. This includes values for the ion transfer, quadrupole mass isolation and resolution, analyser accuracy and eFT (enhanced Fourier Transformation).

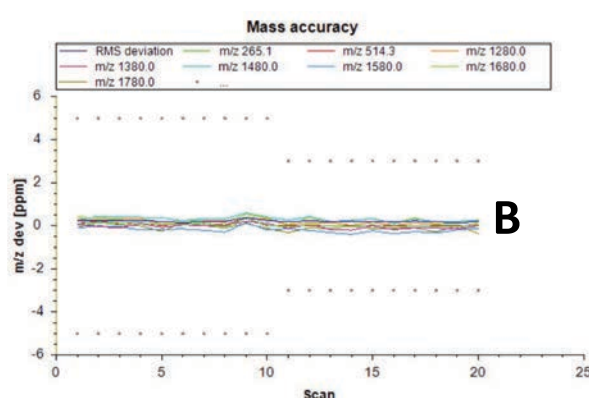
The calibration of the instrument was always conducted in ESI as mentioned, since the calibration solutions only qualify for this ionisation mode. However, most samples were measured in APCI mode. To ensure data integrity, after calibration and change to the APCI probe, standards with our target compounds were run before a set of samples to test that mass accuracy and mass deviation were within a specified range (for mass deviation, retention time and intensity).

Table 2-7. Calibration ions for mass accuracy in positive and negative ESI mode

Component	Positive Ion (m/z)	Negative Ion (m/z)
Caffeine	138.06619	
	195.08765	
MRFA	524.26496	
Ultramark 1621	1221.99064	
	1421.97786	
	1621.96509	
Sodium Dodecyl Sulfate		265.14790
Sodium Taurocholate		514.28444
Ultramark 1621		1279.99721
		1379.99083
		1479.98444
		1579.97805
		1679.97166
		1779.96528



Procedure result: **passed** (rms = 0.13/0.17 ppm)



Procedure result: **passed** (rms = 0.18/0.23 ppm)

Figure 2-16. Results of an acceptable mass accuracy calibration in positive (A) and negative (B) ESI mode, with rms = (internal- / external ppm)

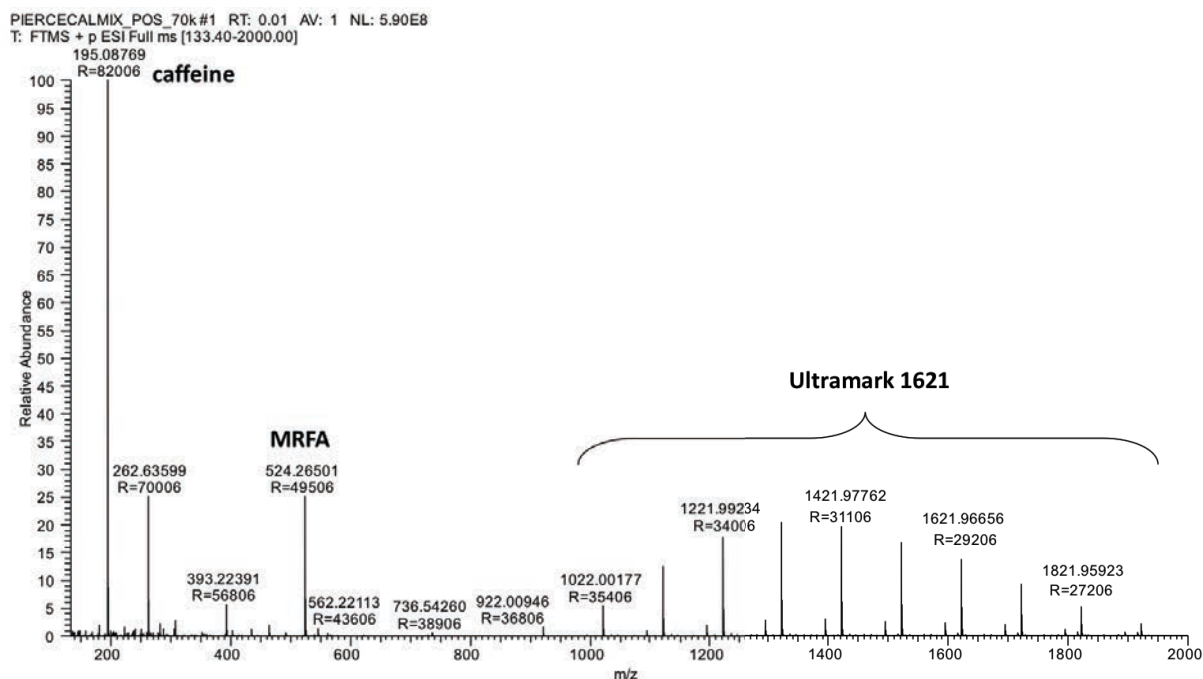


Figure 2-17. ESI Positive Ion Calibration Solution Spectra - Formulation: caffeine ($20 \mu\text{g mL}^{-1}$), MRFA ($1 \mu\text{g mL}^{-1}$) and Ultramark 1621 (0.001 %) in an aqueous solution of acetonitrile (50 %), methanol (25 %) and acetic acid (1 %). Caffeine @195, MRFA @524, Ultramark @1222, 1422, 1622

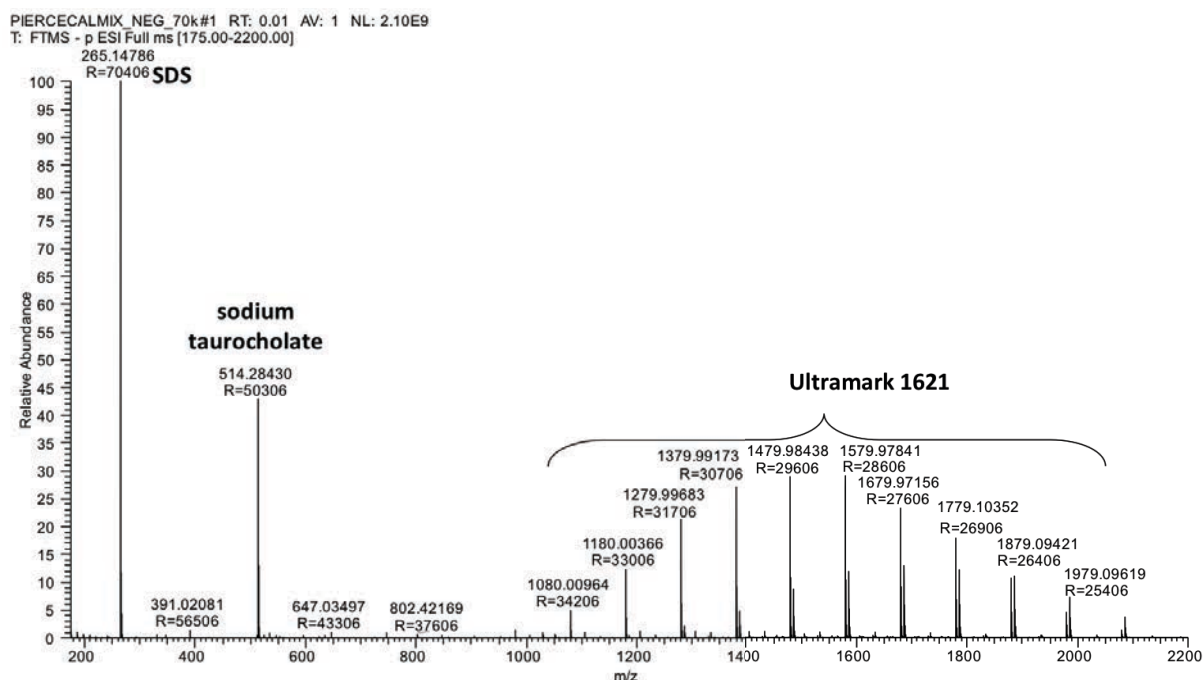


Figure 2-18. ESI Negative Calibration Solution Spectra - Formulation: sodium dodecyl sulfate (SDS) ($2.9 \mu\text{g mL}^{-1}$), sodium taurocholate ($5.4 \mu\text{g mL}^{-1}$) and Ultramark 1621 (0.001 %) in an aqueous solution of acetonitrile (50 %), methanol (25 %) and acetic acid (1 %). SDS @265, sodium taurocholate @514, Ultramark @1280, 1380, 1480, 1580, 1680, 1780

2.4.3. GCxGC-TOF mass spectrometer

For a comparative multiresidue method for screening of halogenated compounds, samples were also analysed on a GCxGC-TOF instrument. This consisted of an Agilent 7890B GC equipped with a Zoex ZX2 cryogenic modulator. The 1st column was a SGE BPX5, non-polar capillary column (30 m, 0.25 mm ID, 0.25 μm – 5% phenyl polysilphenylene-siloxane), followed by a shorter more polar SGE BPX50 column (4.0 m, 0.1 mm ID, 0.1 μm – 50% phenyl polysilphenylene-siloxane) in the 2nd dimension. This system was interfaced to a Markes BenchTOF-Select platform, with an acquisition rate of 50 Hz and covering the mass range of 40 up to 1000 m/z, with a mass resolution of >1200 FWHM at 70 eV and >800 FWHM at 14 eV over 100–1000 m/z (as indicated by the manufacturer) [192]. Electron impact ionization energies were set at 12 eV or 70 eV, to either retain molecular ions (12 eV) or cause extensive fragmentation in order to compare with standard library spectra (70 eV). 1 μL of sample was injected in a splitless mode at 300 °C. The initial temperature of the oven (120 °C) was held for 4 min, heated at 2.5 °C min⁻¹ to 210 °C and further to 325 °C at 2 °C min⁻¹ and held for 2 min. The modulation period was 4 s. The transfer line temperature was 325 °C and the ion source temperature was 320 °C. Helium was used as the carrier gas at a constant flow rate of 1.0 mL min⁻¹. Data files were processed using GC Image™ v 2.1.

2.5. Qualification/Quantification

2.5.1. Qualification

For screening purposes on the HPLC-Orbitrap, the exact mass of each target compound was calculated (with a mass accuracy of 5 ppm and for the most abundant isotopic species of the isotope cluster) and this value employed within the software programme used. Isotope pattern were simulated using Xcalibur software, as shown in Figure 2-19 for EH-TBB, comparing the measured standard against the simulation, with mass accuracy values below

1 ppm. MS/MS fragmentation studies were conducted in the identification process of possible transformation products.

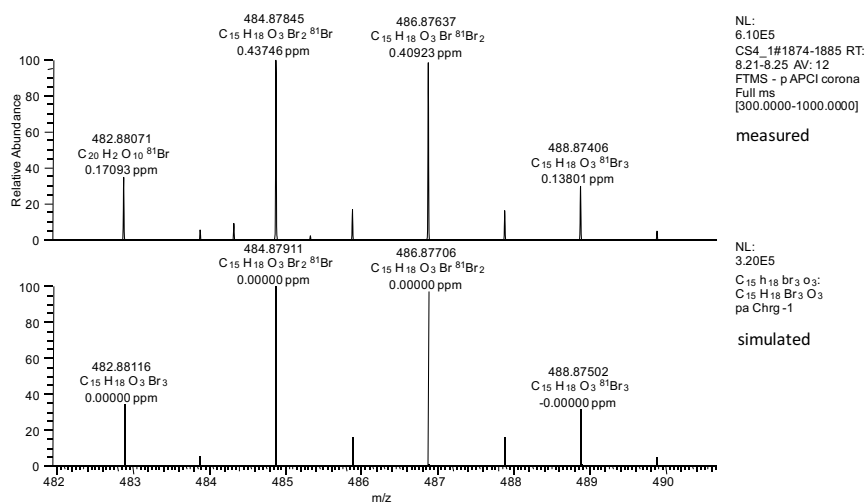


Figure 2-19. Isotope pattern of EH-TBB standard (80 pg), measured (top) and simulated with Xcalibur (bottom)

2.5.2. Quantification

Internal standard method

Quantification was performed by the internal standard method, as described in more detail in the QA/QC procedures in Appendix I. An internal standard mix containing 1 ng μL^{-1} of ^{13}C -BDE-28, BDE-77, BDE-128, ^{13}C - α -, β -, and γ -HBCDDs, ^{13}C -TBBPA and 2 ng μL^{-1} of ^{13}C -BDE-209, ^{13}C -EH-TBB, ^{13}C -BEH-TEBP and ^{13}C -BTBPE was used to spike samples prior to extraction. The recovery determination standard contained 200 pg μL^{-1} of ^{13}C -BDE-100. A five-point calibration curve was prepared from a series of standards, containing native, labelled and recovery standards. In some cases internal standards were used for the quantification of several native compounds (Table 2-10).

External calibration

For photodegradation experiments parent compounds were quantified using external calibration. Therefore a 5-point calibration curve was analysed with each set of experiments, as shown in Table 2-8 and exemplified for EH-TBB in Figure 2-20.

Table 2-8. Calibration curves

Compound	Linearity	equation
BEH-TEBP	0.9985	$y = 28800 * x - 2800$
BTBPE	0.9965	$y = 6512 * x + 85400$
DBDPE	0.9987	$y = 2222 * x - 1756$
EH-TBB	0.9979	$y = 28810 * x - 2803$

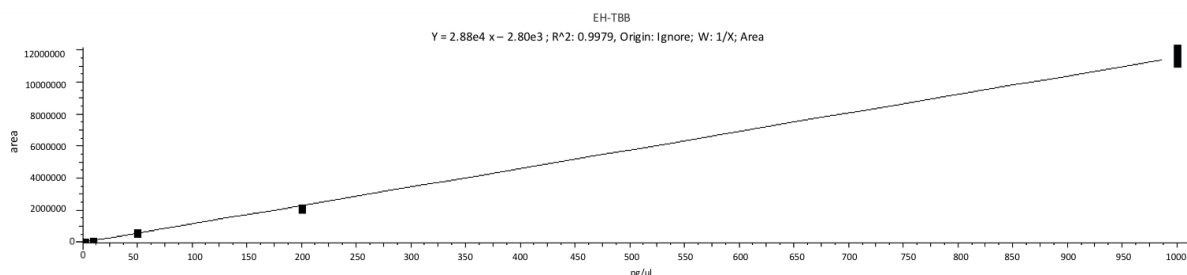


Figure 2-20. Five-point calibration curve for EH-TBB.

2.5.3. QA/QC Criteria

General practices

All glassware was cleaned by soaking in a detergent solution overnight, before rinsing with deionized water. This was followed by washing with acetone, hexane, toluene and dichloromethane and subsequent baking at 120 °C overnight. To assess any possible contamination during sample preparation, method blanks (sodium sulfate replacing the sediment) were analysed with every set of 6 samples. Instrumental blanks (10 µL methanol) were injected in regular intervals during analysis. In none of the method and instrumental blanks target were compounds detected, hence there was no need for blank correction of the data.

Standard reference material (SRM)

The standard reference material SRM 1944 (NIST) for sediment samples was used to evaluate the accuracy of the method for PBDEs and HBCDDs. An SRM sample was included for every 15 sediment samples, resulting in 4 replicates as indicated in Table 2-9. Values obtained for the

SRM 1944 were generally in good accordance with the certified levels. In addition, non-certified compounds including BTBPE, BEH-TEBP, PBEB, TBP, BB153 and DP were detected in the SRM 1944, but concentrations varied between replicates. It has to be noted that the SRM sediment showed to be a relatively complex matrix. Our measurements on the UPLC-HRMS resulted in wider repeatability values, compared to the reproducibility factor stated for the SRM, which was measured by several laboratories. Possible explanations, include the use of different extraction and clean-up procedures, as well other analytical approaches employed (targeted GC-MS).

Table 2-9. Comparison of UPLC-HRMS data for BFRs with NIST SRM 1944 certified values

Compound	UPLC-HRMS $\mu\text{g}/\text{kg}$ (n=4)	Reference value SRM $\mu\text{g}/\text{kg}$
BDE-47	1.80 \pm 0.6	1.72 \pm 0.28
BDE-99	1.65 \pm 0.7	1.98 \pm 0.26
BDE-100	0.48 \pm 0.1	0.447 \pm 0.027
BDE-153	6.57 \pm 1.9	6.44 \pm 0.37
BDE-154	1.05 \pm 0.7	1.06 \pm 0.08
BDE-183	31.82 \pm 4.5	31.8 \pm 0.1
BDE-206	6.96 \pm 1.5	6.2 \pm 1.0
BDE-209	87.43 \pm 10.2	93.5 \pm 4.4
ΣHBCDDs	13.09 \pm 2.5	21.2
BDE-196	52.0 \pm 7.9	-
BDE-197	25.74 \pm 5.0	-
BDE-207	12.71 \pm 3.2	-
BTBPE	4.72 \pm 2.2	-
BEH-TEBP	0.99 \pm 0.1	-
PBEB	0.73 \pm 0.3	-
BB153	1.99 \pm 0.8	-
TBP	0.18 \pm 0.1	-
DP	27.41 \pm 17.0	-

Instrumental and sample LOD and LOQ

Instruments limits of detection (LOD) and limits of quantification (LOQ) were estimated based on method described by Taylor [193] and listed in Table 2-10. This method is a statistical approach to estimate the LOD and LOQ. Each calibration standard CS1 to CS5 (concentrations

listed in Appendix II) was measured 10 times. The standard deviation of each measured concentration is estimated as the concentration approaches zero (s_0). The s_0 is determined by regressing the standard deviation of measured concentration versus the specified concentration. The intercept of the resulting regression line corresponds to s_0 . The LOD is defined as $3 \times s_0$, while the LOQ is defined as $10 \times s_0$. Sample LOD and LOQs were then calculated as described in the QA/QC protocol in the Appendix I, using the values from the sediment analysis and are listed in Table 2-11.

Table 2-10. Instrument LOD and LOQ (pg/ μ l), linearity and relative standard deviation (n=10) of target compounds

Compound	LOD pg/μl	LOQ pg/μl	Linearity	RSD n=10
BDE-17	9.0	30	0.9923	5.8
BDE-28	5.8	19	0.9952	4.5
BDE-47	0.7	2.4	0.9991	3.3
BDE-100	0.2	0.6	0.9983	2.9
BDE-99	0.9	3.1	0.9979	2.1
BDE-154	0.5	1.7	0.9974	2.1
BDE-153	0.2	0.7	0.9983	2.1
BDE-183	0.2	0.7	0.9980	2.4
BDE-197	0.9	3.0	0.9981	3.8
BDE-196	0.04	0.1	0.9989	2.3
BDE-207	0.03	0.1	0.9986	2.9
BDE-206	0.3	1.0	0.9994	2.6
BDE-209	0.03	0.1	0.9983	5.3
HBCDDs	02	0.01	0.9984	1.6
TBBPA	0.2	0.6	0.9973	2.6
HBB	0.5	1.6	0.9980	2.4
TBP	0.3	1.1	0.9943	5.0
BB153	0.2	0.6	0.9971	2.7
PBEB	1.2	3.9	0.9981	2.2
abTBECH	27	91	0.9932	5.7
asDP	1.0	3.5	0.9994	2.7
BEH-TEBP	0.6	1.9	0.9985	1.8
BTBPE	0.5	1.5	0.9965	4.1
DBDPE	11	36	0.9987	3.3
EH-TBB	0.8	2.6	0.9979	2.5

Table 2-11. Sample LOD and LOQ (pg/g) for sediment analysis and internal standards used for quantification

Compound	LOD pg/g	LOQ pg/g	IS used
BDE17	365	1217	MBDE-28
BDE28	237	789	MBDE-28
BDE47	29	97	MBDE-28
BDE100	8.9	30	BDE-77
BDE99	45	151	BDE-77
BDE154	29	97	BDE-128
BDE153	11	36	BDE-128
BDE183	8.6	29	MBDE-209
BDE197	37	122	MBDE-209
BDE196	1.5	5.0	MBDE-209
BDE207	1.3	4.5	MBDE-209
BDE206	12	41	MBDE-209
BDE209	1.1	3.7	MBDE-209
HBCDDs	0.1	0.4	MHBCDDs
TBBPA	17	57	MTBBPA
HBB	27	91	BDE-128
TBP	13	43	MBDE-28
BB153	10	33	BDE-128
PBEB	64	215	BDE-128
abTBECH	1102	3675	MBDE-28
asDP	43	142	MBDE-209
BEH-TEBP	22	74	MBEH-TEBP
BTBPE	20	66	MTBPE
DBDPE	446	1485	MBDE-209
EH-TBB	34	112	MEH-TBB

Target compounds were positively identified and quantified if they fulfilled all the following parameters within Trace Finder:

1. The signal to noise ratio must exceed 5:1
2. The retention time of the compound must be within a window of ± 5 sec compared to the calibration standards ran that day
3. m/z of the molecular ion peak must be within 5 ppm of its theoretical value at resolution power 70,000 FWHM
4. Br Isotope pattern must match within 80 % of the theoretical values

Concerning the Br isotope pattern in point 4, the accurateness of the relative isotopic abundances (RIA) compared to theoretical values was not practically tested on the Orbitrap, however a study has shown that RIA errors generally were below 20 % of their theoretical value, with mean errors of 16 % in positive-ion and 12 % in negative-ion mode on a Linear Trap Quadrupole (LTQ) Orbitrap [194], which has a different setup to the Q-Exactive Orbitrap employed in our work. A more detailed accuracy analysis of RIA values with the employed instrument appears warranted.

2.6. Data analysis

2.6.1. Mass defect plots

Mass defect plots were created using Microsoft® Excel to visualize the presence of halogenated compounds. For this, all masses detected in a retention time window of interest were extracted using Thermo Scientific Xcalibur™ software. A threshold was set to exclude peaks below a certain absolute intensity value. The underlying principle of mass defect conversion was first described by Kendrick [171]. He realized that by changing the International Union of Pure and Applied Chemistry (IUPAC) mass scale (C = 12.000 Da) to one in which CH₂ = 14.000 Da (Equation 2-1) organic ions belonging to a homologous series can be identified in a complex mixture due to their common mass defect [164].

$$\text{Kendrick mass} = \text{IUPAC mass} * (14 / 14.01565) \quad \text{(Equation 2-1)}$$

The conversion used in this work is based on a transformed Kendrick mass defect, whereby a hydrogen atom is substituted by a bromine atom, thus resulting in the transformed factor 78 / 77.91051 (- 1 + 79 = 78 / -1.00783 +78.91834 = 77.91051). This allows to elegantly visualize and recognize classes of homologous compounds that differ by a selected group or atom, such as a bromine (or halogen atom) compounds [161, 164] and arranges them in a horizontal line within the plot (due to the same mass defect).

The mass defect plot was obtained by multiplication of each mass peak of the chosen mass spectrum by the transformed factor and plotting the nominal mass vs. the transformed mass defect on the x- and y-axes, respectively. Values were calculated as follows:

1. transformation factor (-H / +Br) = nominal mass / exact mass (78 / 77.91051)
2. exact transformed mass = accurate measured mass (IUPAC) * transformation factor
3. nominal transformed mass = exact transformed mass (rounded down)
4. transformed mass defect = exact transformed mass - nominal transformed mass (rounded down)

2.6.2. Statistical analysis

Statistical analysis of the data was performed using IBM SPSS statistics software version 23. A one-way ANOVA was used for testing significant differences between arithmetic means. For statistical purposes, non-detects were replaced with zero, while detects with a concentration below the LOQ were assigned a value of LOQ/2 or in cases of a detection frequency below 50 % the LOQ was multiplied by the detection frequency factor. I.e. for DPDBPE the LOQ was calculated as $1.49 \mu\text{g kg}^{-1}$ (1485 pg g^{-1}), while the LOD was $0.45 \mu\text{g kg}^{-1}$ (446 pg g^{-1}). In our sediment samples study the detection frequency of DBDPE was 20% and therefore samples which detected values below the LOQ, but above the LOD, were multiplied by the factor 0.2. P values < 0.05 were taken to indicate statistical significance.

Reproducibility of the method was calculated out of 3 sets with five samples (spiked blanks) each, which were extracted during 3 different days and parameters, such as batch of chemicals/solvents used, were varied. RSD values for the within-laboratory reproducibility resulted in a range of 9-26% for our target compounds and were within the acceptance criteria as stated in the QA/QC section in Appendix I.

2.6.3. Enzymatic kinetics

SigmaPlot v13 and its Enzyme Kinetics Module v1.1 (Systat Software Inc., Richmond, CA) were used for modeling enzyme kinetics for *in vitro* metabolism studies. Different non-linear regression models (Michaelis–Menten, Hill and substrate-inhibition) were tested. To evaluate the goodness of fit, the model with the lowest values for the two statistical criteria AICc (Akaike Information Criterion corrected for small sample size) and Sy.x (standard deviation of the residuals) was chosen.

2.6.4. Qualification and Quantitation using XCalibur and Trace Finder

XCalibur™ version 4.0 software and Trace Finder™ version 3.3 software (Thermo Fisher Scientific, Bremen, Germany) were used to process raw data files and integrate peaks, while calculations for quantification of the compounds of interest was conducted using Microsoft Excel 2010.

2.6.5. Unknown Screening using Compound Discoverer

Compound Discoverer version 2.0 software (Thermo Fisher Scientific, Bremen, Germany) was used to process raw files and screen for unknown halogenated compounds, as well as for possible degradation and metabolic transformation products of native target compounds. Workflows can be adapted and implemented according to the specific analysis using different nodes as shown in Figure 2-21. Generally, treated/exposed samples are measured against a control group (negative control). The shown workflow detects unknown compounds with elemental composition prediction, automatically hides background compounds (detected in blanks), performs ChemSpider library searching and scores the compounds based on user defined isotope patterns. Each of the nodes used and its general settings are described in Table 2-12.

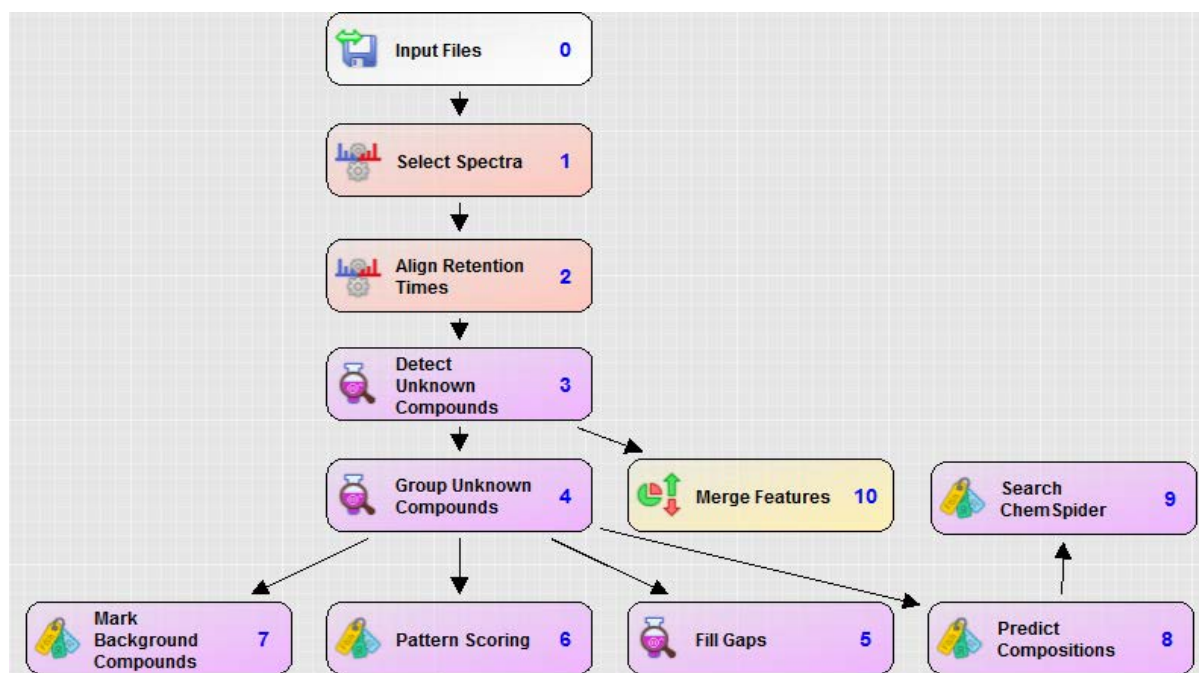
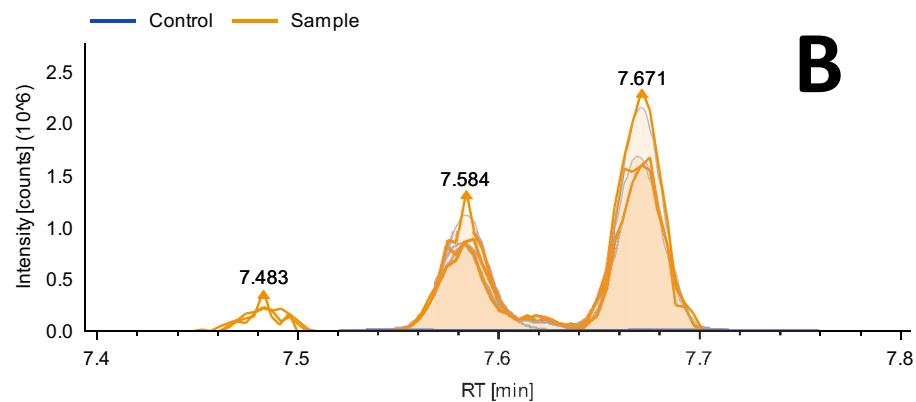


Figure 2-21. Workflow of Compound Discoverer to screen for unknown compounds.

Figure 2-22 shows an example of a metabolite screening workflow result, for an experiment where trout liver microsomes were exposed to DBE-DBCH (as described in 2.2.5). Part A in the figure is an excerpt of the list of hits, indicating the predicted formula, molecular weight, retention time and area of the identified compound (monohydroxy-DBE-DBCH). Further, the isotopic pattern matches the one of a Br₄ containing compound, as also appears in the mass spectrum in part C for the [M-H]⁻ ion (the boxes represent the 5 ppm position and 20% intensity tolerance of the pattern). Part B displays the identified peak in an extracted ion chromatogram at RT = 7.6 min (the other peaks indicate the possible presence of other isomers). Since samples were measured in triplicates, different peaks are visible at the same retention time, while the identified compound is not present in the control (blank, negative controls), as also shown in part A for the ratio, log₂ fold change and statistical significance (p < 0.05) of the sample vs. the control (negative control). More details of the results of this experiment are described in 6.2.4.

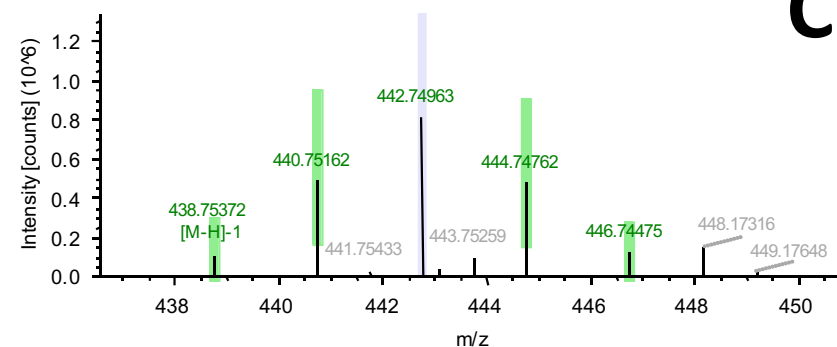
A

	Predicted Formula	Molecular Weight	RT [min]	Area (Max.)	Pattern Matches	Group Areas	Ratio	Log2 Fold Change	P-value
					Br4* Br3 Br2	Sample* Control	(Sample) / (Control) *	(Sample) / (Control) *	(Sample) / (Control) *
1	C8 H12 Br4 O	439.76147	7.639	88734	<input checked="" type="checkbox"/> <input type="checkbox"/> <input type="checkbox"/>	7.35e4 6.48e2	113.519	6.83	1.4e-4



B

20b_ESI, #1752, RT=7.676 min, FTMS (-)
C8 H12 Br4 O as [M-H]⁻1



C

Figure 2-22. Example for a result from a Compound Discoverer workflow to screen for DBE-DBCH metabolites in a trout liver microsomes *in-vitro* study, A: list of hits and identified parameters, B: extracted ion chromatogram of sample vs. control measurement, C: mass spectrum of the identified compound (monohydroxy-DBE-DBCH) together with isotope pattern matching (green boxes)

Table 2-12. Compound Discoverer workflow nodes and settings

# Node	Description	Parameters
0 Input Files	LC-MS data file input	NA
1 Select Spectra	Select and retrieve the spectra for further processing	Min. Precursor Mass: 77 Da Max. Precursor Mass: 1000 Da Polarity Mode: negative S/N Threshold: 1.5
2 Align Retention Times	Align retention times of multiple data files	Alignment Model: Adaptive curve Mass Tolerance: 5 ppm Maximum shift: 0.5 min
3 Detect Unknown Compounds	Detect compounds in a file by Compound Elucidator algorithm	Mass Tolerance: 5 ppm Intensity tolerance: 20% S/N threshold: 1.5 Min. Peak Intensity: 1000 Ion: [M-H] ⁻ , [M-Br+O] ⁻ Min. Element Counts: C _x H _y Br _z O _a Max. Element Counts: C _x H _y Br _z O _a Min. # Scans per Peak: 5
4 Group Unknown Compounds	Group all detected compounds by molecular weight and retention time across all files	Mass Tolerance: 5 ppm Retention Time Tolerance: 0.1 min
5 Fill Gaps	Fill the gaps for missing peaks in detected compounds	Mass tolerance: 5 ppm S/N Threshold: 1.5 Retention Time Tolerance: 0.1 min
6 Pattern Scoring	Score detected compounds by user-defined isotope patterns	Isotope Pattern: Br _x , Cl _y , Br _x Cl _y Mass Tolerance: 5 ppm Intensity Tolerance: 20%
7 Mark Background Compounds	Annotate and filter background compounds (compared to blank samples)	Max. Sample/Blank: 3 Hide Background = True
8 Predict Composition	Predict elemental compositions for detected compounds	Mass tolerance: 5 ppm Max. Element Counts: C _x H _y Br _z O _a Max. RDBE: 20 Max. # Candidates: 10
9 Search ChemSpider	Provide ChemSpider results for detected compounds	Databases: KEGG Mass tolerance: 5 ppm
10 Merge Features	Merge all detected features and provide the links for available explanations	Mass tolerance: 5 ppm Retention time tolerance: 0.1 min.
Differential Analysis	Provide simple differential statistics for detected compounds (such as PCA and ANOVA)	Log ₁₀ Transform Values: True p < 0.05

Chapter III - A Comparison of Two High Mass Resolution Mass Spectrometric Methods for Screening for Halogenated Compounds in Complex Mixtures

3.1. General overview

Advances in high resolution mass spectrometry facilitate accurate measurements and identification of unknowns, as well as possible degradation and transformation products. Full scan experiments allow for the analysis of target and non-target compounds in the same sample. Moreover, bromine and chlorine isotopic pattern analysis and the use of mass defect plots help identify relevant substances, with such techniques starting to be more commonly used in environmental science [164]. Mass analyser types that allow samples to be measured with the necessary resolving power and acquisition frequency include: time-of-flight high resolution mass spectrometry (TOF-HRMS), Orbitrap and Fourier transform ion cyclotron resonance (FT-ICR) mass spectrometers [195]. For each of these, studies have been published using mass defect plots for screening of halogenated compounds. Dust from an electronic recycling facility [165], soil [172] and sediments [168] were measured by GCxGC-TOF, trout muscle extracts [164] and fluoro thermal decomposition products [173] were injected on an FT-ICR-MS system, while for the Orbitrap only a study analysing eel samples was found [195]. Multidimensional gas chromatography coupled to time-of-flight mass spectrometry (GCxGC-TOF-MS) on the other hand offers enhanced chromatographic separation to enable resolution of complex chemical mixtures and to improve the ability to interpret mass spectra for identification of unknown compounds. To harness these advantages, a fast mass detector such as a TOF-MS is needed for this purpose, as it is able to acquire data at a fast acquisition rate and allows searching spectra from even the narrowest peaks.

In this chapter the potential of two advanced chromatography/mass spectrometry hyphenated platforms for multi-residue analysis of a complex mixture of environmental relevant organic contaminants was evaluated, including 60 compounds (10 PBDEs, HBCDDs, TBBPA, 15 NBRs, 6 Dechloranes, 3 OPFRs, as well as 8 PCBs and 16 PAHs). Selected PAHs could only be detected by means of GCxGC-TOF (see 3.5), but not under our UPLC-Orbitrap conditions (see 3.2.6). The first instrument is the high-resolution accurate mass (HRAM) quadrupole Orbitrap mass spectrometer, connected to a UPLC system, while the second is a two-dimensional gas chromatography system (GCxGC) coupled to a time-of-flight mass spectrometer (TOF-MS). Mass defect plots were constructed for samples measured on the Orbitrap, which allowed for visual discrimination of halogenated contaminants in a very complex dataset.

3.2. Mass defect measurements

Full scan experiments were conducted both in APCI and HESI modes and from the obtained data, a mass defect plot was constructed to estimate the number of brominated and chlorinated compounds within a sample. Halogenated compounds have a unique negative mass defect, which readily distinguishes them from other molecules in a complex mass spectrum [164]. Furthermore, homologous series of compounds can be easily visualized [171]. One mass scale applicable to environmental analytical chemistry is defined by the substitution of a hydrogen atom by a bromine atom (+H / -Br), as well as by a chlorine atom (+H / -Cl). Both the +H / -Br (78 / 77.91051) and the +H / -Cl (34 / 33.96013) transformation factors are very close (1.001149 / 1.001148, respectively) and thus can be used interchangeably for the construction of a transformed mass defect plot to visualize brominated and chlorinated compounds [161, 165, 195]. Mass defect plots shown in this chapter were drawn in Microsoft Excel and calculated as described in 2.6.1.

3.2.1. Workflow

A workflow of how compounds were tentatively identified is provided in Figure 3-1. Once the mass defect plot was created, exact masses could be deduced manually by selecting the isotope cluster of interest. Such manual review of clusters is quite time consuming and requires much effort, and thus the automation of this process has been described [161, 168, 195]. Xcalibur software was used to compare extracted ion chromatograms (XICs) of selected exact masses of isotope patterns to each other. The same software was also employed to estimate the number of bromine and chlorine atoms within a compound and calculate the elemental composition. This was based considering the following elements: C, H, O, Br and Cl, as well as a mass accuracy of 5 ppm and single negative/positive m/z charge depending on the ionization mode used during measurement. Where possible, hypotheses on structural composition were suggested and evaluated using simulated isotopic patterns. Regularly, several elemental compositions were obtained from an entered exact mass (see Figure 3-1) and the best fitting pattern was chosen, considering the presence of all the ions in the pattern, the number of lighter/heavier isotopes suggested compared to the $M + x$ position in the pattern, as well the isotopic abundance ratio (as described in 1.6.3). Chemspider was employed as a final step to obtain a tentative compound from the formula found. Identification of compounds, especially in APCI mode, can be challenging, since formed pseudo molecular ions formed are numerous and sometimes differ from $[M-H]^-$ or $[M-Br/Cl+O]^-$. Moreover, formation of adducts has to be considered. Structural isomers, where present, were separated by chromatographic means. Pseudo-molecular ions and possible adduct formation were assumed and tested in the prediction workflow, based on information found in other studies on these compounds.

4. Elemental composition

Elemental composition

Single mass

Mass: 284.81454

Max. results 3

Calculate

Id	Formula	RDB	Delta ppm
1	C ₆ H ₂ OBr ⁷⁹ BrCl	4.5	-0.191
2	C ₇ H ₂ ⁷⁹ Br ₂ ⁷⁹ Cl	5.5	-0.502
3	C ₆ H ₂ OBr ₂ ⁷⁹ Cl	4.5	2.981

File... List Simulate

Limits

Charge: -1

Nitrogen-Rule: Do not use

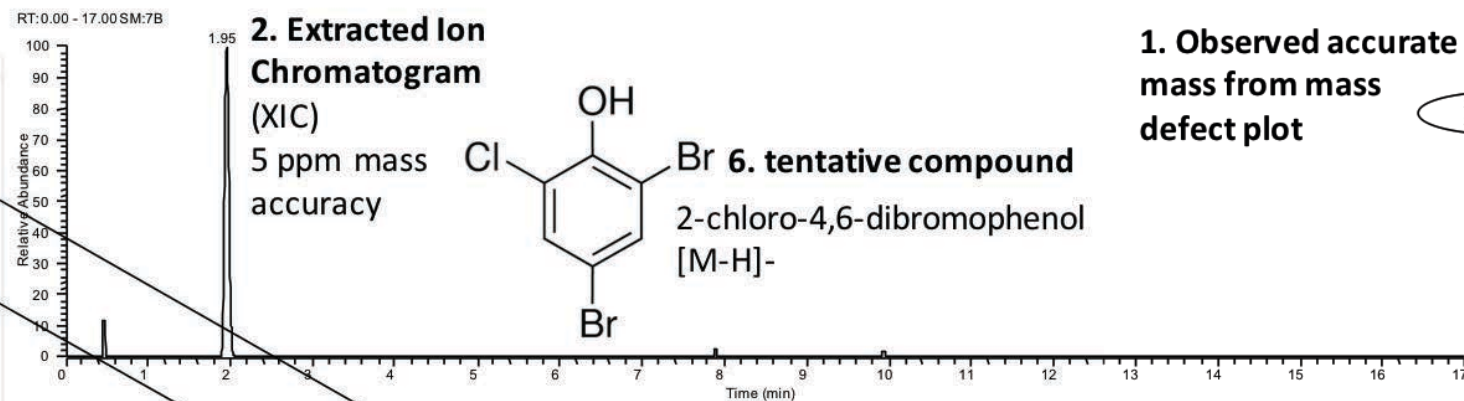
Mass tolerance: 5.00 ppm

RDB equiv: -1.0-100.0

Elements in use

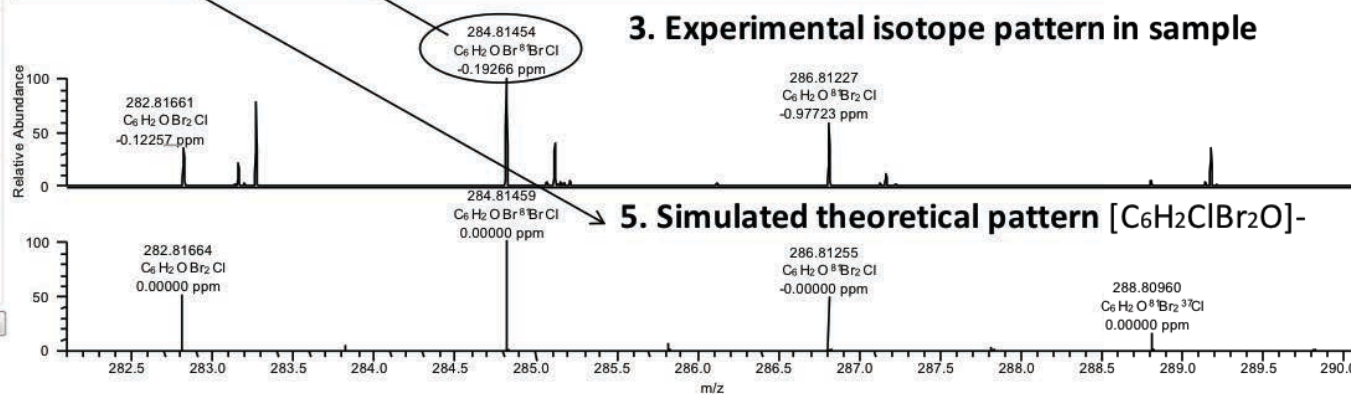
Isotope	Min	Max	DB eq.	Mass
16 O	0	15	0.0	15.995
12 C	0	30	1.0	12.000
1 H	0	60	-0.5	1.008
79 Br	0	10	-0.5	78.918
81 Br	0	10	-0.5	80.916

Load... Save as... Apply Help



1. Observed accurate mass from mass defect plot

NL: 1.20E5
Base Peak m/z= 284.81157-284.81727
MS
Dust_ASE



NL: 5.38E4
Dust_ASE#835-893 RT: 1.89-2.02 AV: 59 T: FTMS - p APCI corona Full ms [70.0000-1050.0000]

NL: 3.54E5
c, h, clbr, o
C₆H₂ClBr₂O₁
pa Chrg -1

Figure 3-1. Screen capture from Xcalibur workflow for the identification of compounds, including the observed accurate mass taken from the mass defect plot (1), the extracted ion chromatogram (2), the experimental isotope pattern and mass-to-charge value (3), the predicted elemental composition (4) based on the employed settings, the simulated theoretical isotope pattern and mass-to-charge value (5), with a subsequent calculated mass deviation value in ppm (3) and the resulting tentative compound identification (6), after conducting a ChemSpider database search.

As described in Chapter 2, initially a mixture of target standard compounds was measured. This consisted of 10 PBDEs, HBCDDs, TBBPA, 15 NBRFs, 6 Dechloranes, 3 OPFRs, as well as 8 PCBs and 16 PAHs which were injected on the UPLC-Orbitrap system. The resulting mass defect plot is shown in Figure 3-2 containing 44 identified compounds (isomeric compounds such as PCBs and PBDEs can only be separated chromatographically and visualised in an XIC, while the 16 PAHs were not detected). Results from the UPLC-HRAM Orbitrap platform show the potential for determination of various contaminants using both APCI (e.g. for PBDEs) and HESI (e.g. HBCDDs, TBBPA and OPFRs), which covers the range from non-polar to more polar compounds respectively, as well as switching between positive (e.g. OPFRs) and negative (e.g. for HBCDDs and TBBPA) HESI ionization modes in a single run. While the ionization and detection of PAHs was not possible with our UPLC-Orbitrap system, higher brominated compounds like BDE-209 and DBDPE are easily detectable.

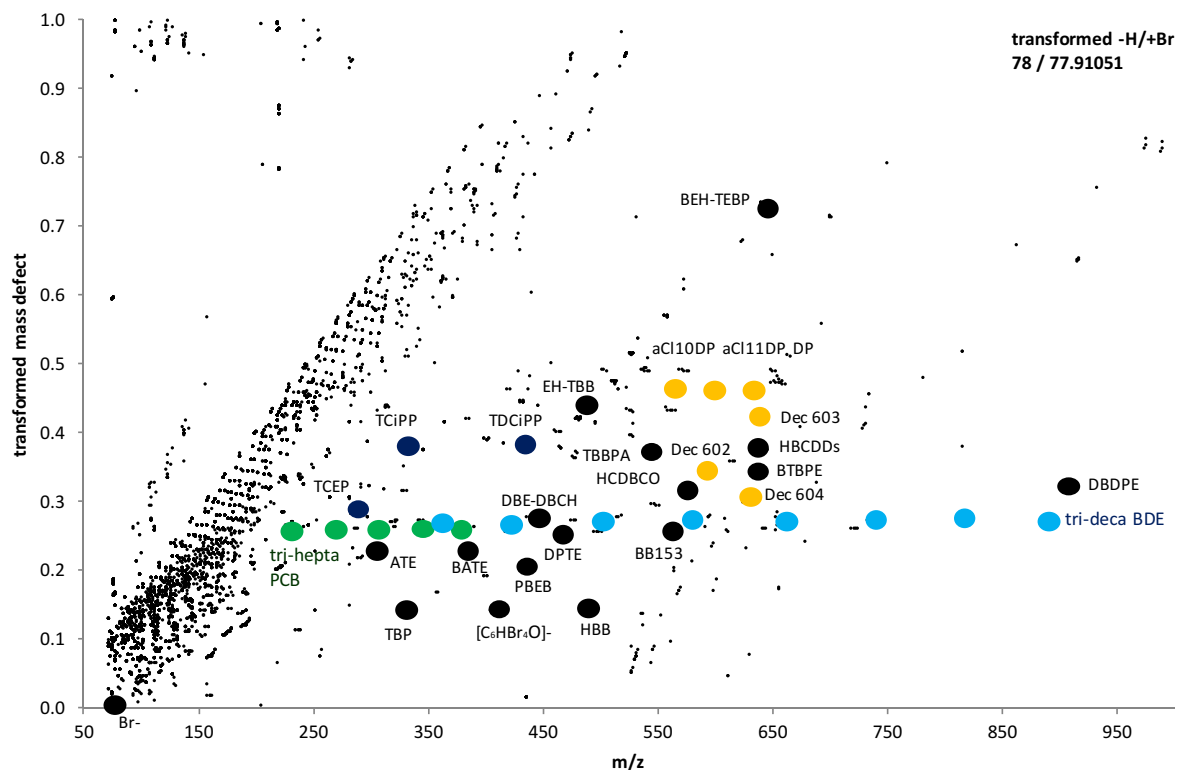


Figure 3-2. Mass defect plot of master mix containing 200 $\mu\text{g } \mu\text{l}^{-1}$ of PBDEs, HBCDDs, TBBPA, NBRFs, Dechloranes, OPFRs and PCBs

3.2.2. PBDEs and PCBs

Individual plots present the results for selected group of compounds. Figure 3-3 shows the results for PBDEs and PCBs. In both cases a series of homologues can be observed. The distance between two patterns is 77.91051 Da for bromine and 33.96013 Da for chlorine respectively and represents the sequential replacement of hydrogen by bromine/chlorine atoms with increasing m/z. Furthermore, a three bromine pattern with $[C_6H_nOBr_x]^-$ ions ($n+x=5$) was detected. By comparing their retention time to PBDEs, it could be concluded that these are fragmentation products of higher brominated compounds. $[C_6Br_5O]^-$ derived from decaBDE and nonaBDEs, $[C_6HOBr_4]^-$ stems from nonaBDEs and octaBDEs, while $[C_6H_2OBr_3]^-$ is formed from pentaBDEs. However, $[C_6OBr_5]^-$ is also the fragment used for the detection of HBB and $[C_6H_2OBr_3]^-$ for TBP, both of which were present in the standard mixture. This shows the limitation of these plots as a screening method only and the need to employ standards and retention time checks for confirmation purposes.

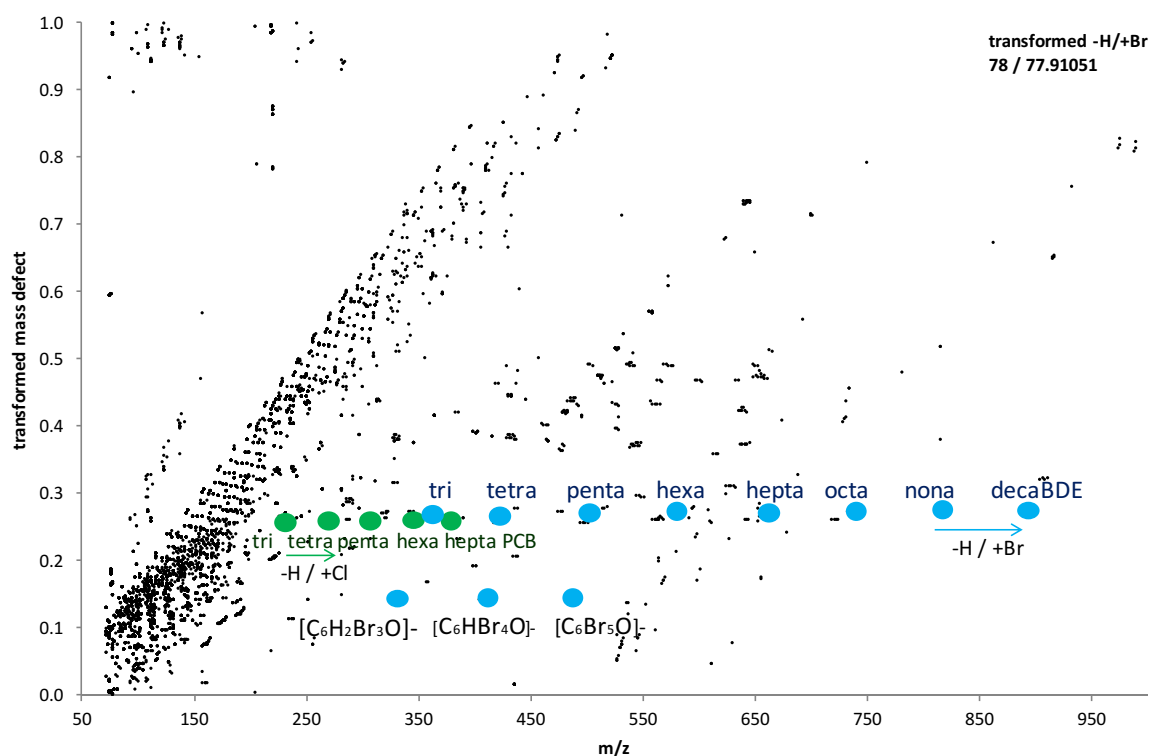


Figure 3-3. Mass defect plot of master mix only showing PBDEs and PCBs

3.2.3. NBFRs, HBCDDs and TBBPA

Figure 3-4 displays the mass defect plot for NBFRs, HBCDDs and TBBPA. There are no evident homologue groups, but selected compounds share the same transformed mass defect. This is the case for the structurally related compounds TBP-AE (ATE) ($C_9H_7Br_3O$) and TBPA-BAE (BATE) ($C_9H_6Br_4O$), as well as TBP ($C_6H_3Br_3O$) and HBB (C_6Br_6), but also for non-structurally related chemicals like TBBPA ($C_{15}H_{12}Br_4O_2$) and HBCDDs ($C_{12}H_{18}Br_6$). The latter compound consists of three isomers (α , β and γ), which appear as single compound in the plot due to their identical mass. Similarly to PBDE and PCB congeners, these can be separated chromatographically and visualized individually in an XIC, which has to be considered when interpreting these plots.

3.2.4. OPFRs and Dechloranes

Figure 3-5 shows the mass defect plot for selected OPFRs and Dechloranes. Since the latter compounds are measured in APCI, while OPFRs are measured in ESI, the mass defect plot shows the combined result of two separate runs. There are numerous other OPFRs of current interest, however these are not halogenated and thus their location in the mass defect plot is not well defined and missing the characteristic isotope pattern which facilitates their identification. Due to their structural similarity aCl10DP ($C_{18}H_{14}Cl_{10}$), aCl11DP ($C_{18}H_{13}Cl_{11}$) and a/sDP ($C_{18}H_{12}Cl_{12}$) have the same transformed mass defect and are separated by the addition of a chlorine and loss of a hydrogen atom.

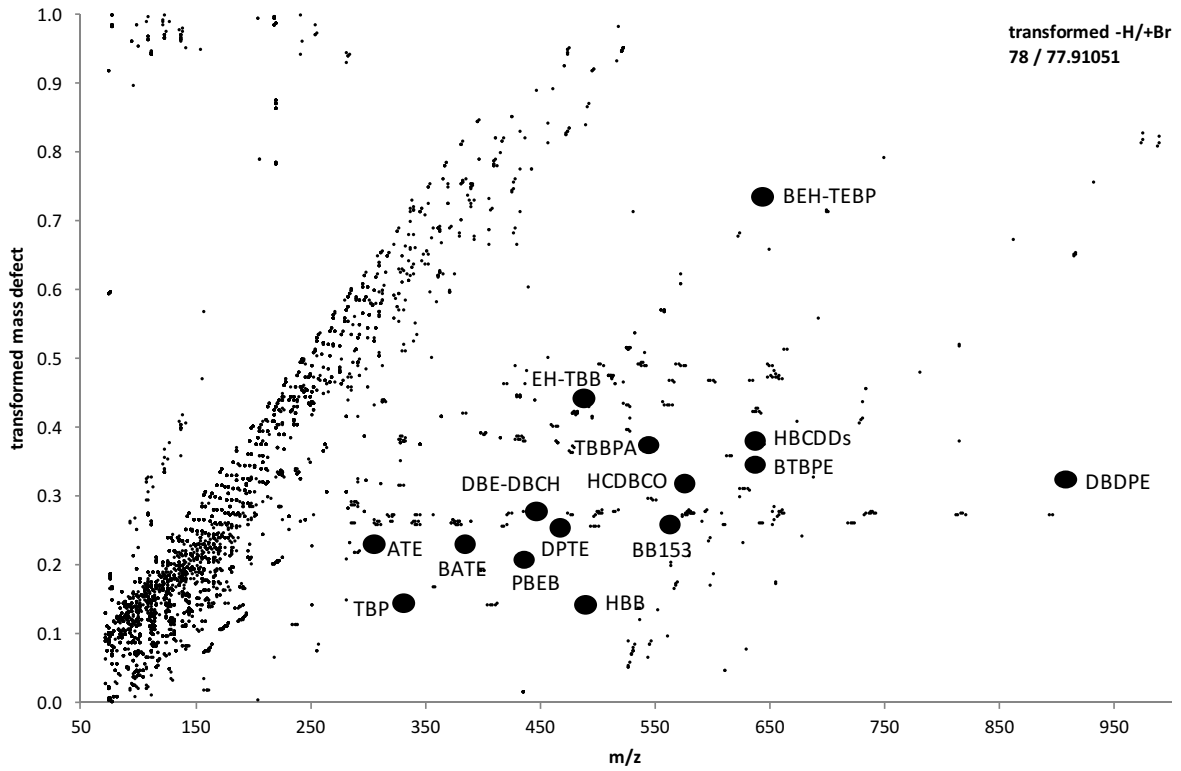


Figure 3-4. Mass defect plot of master mix only showing NBRs, HBCDDs and TBBPA

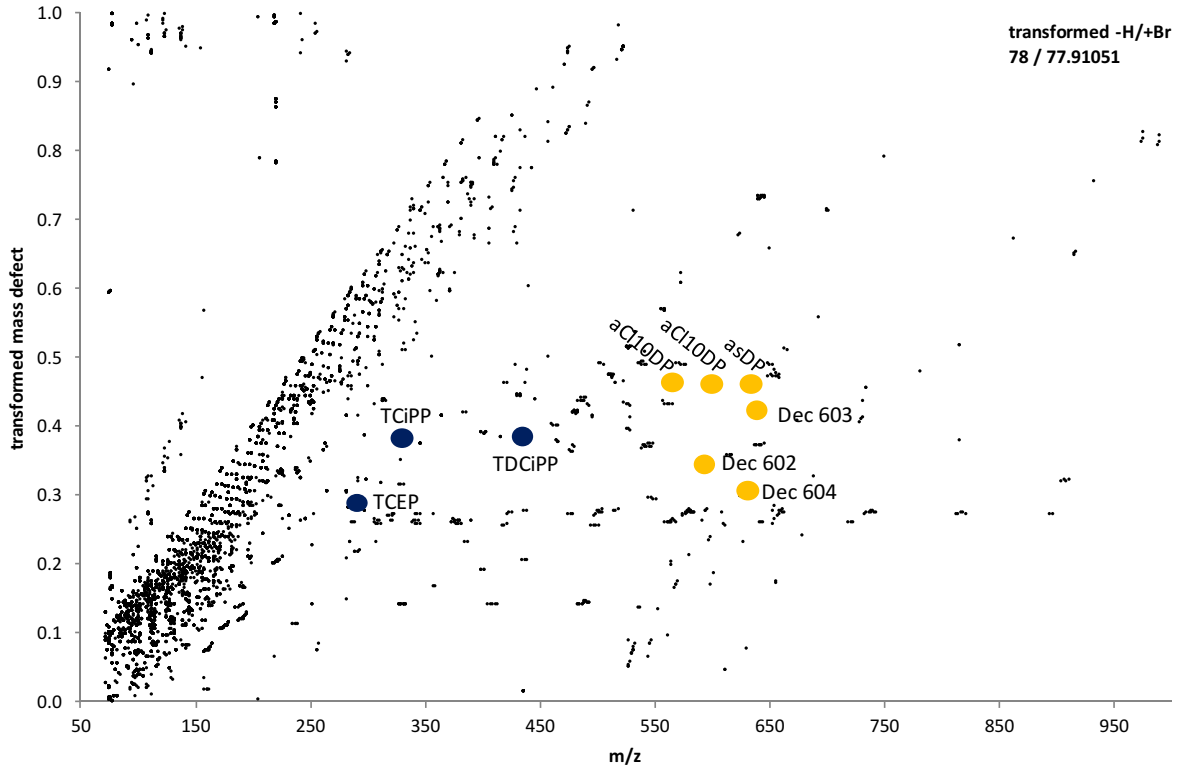


Figure 3-5. Mass defect plot of master mix only showing OPFRs and Dechloranes

3.2.5. Remarks

Additional information can be deduced from the mass defect plot by observing the orientation of an simulated isotopic cluster as illustrated in Figure 3-6. For brominated clusters (i.e. hexaBDE), the slope is slightly positive, caused by the marginally higher $-H / +Br$ -scale transformed mass defect of ^{81}Br compared to ^{79}Br . In contrast, for chlorinated clusters (i.e. Dec 602), the slope is slightly negative [195]. For mixed bromo-chloro clusters the slope depends on the number of bromines compared to chlorines within a compound, for example slightly negative for Dec 604 due to more chlorines than bromines, and presumably zero where a molecule contains equal numbers of bromine and chlorine atoms.

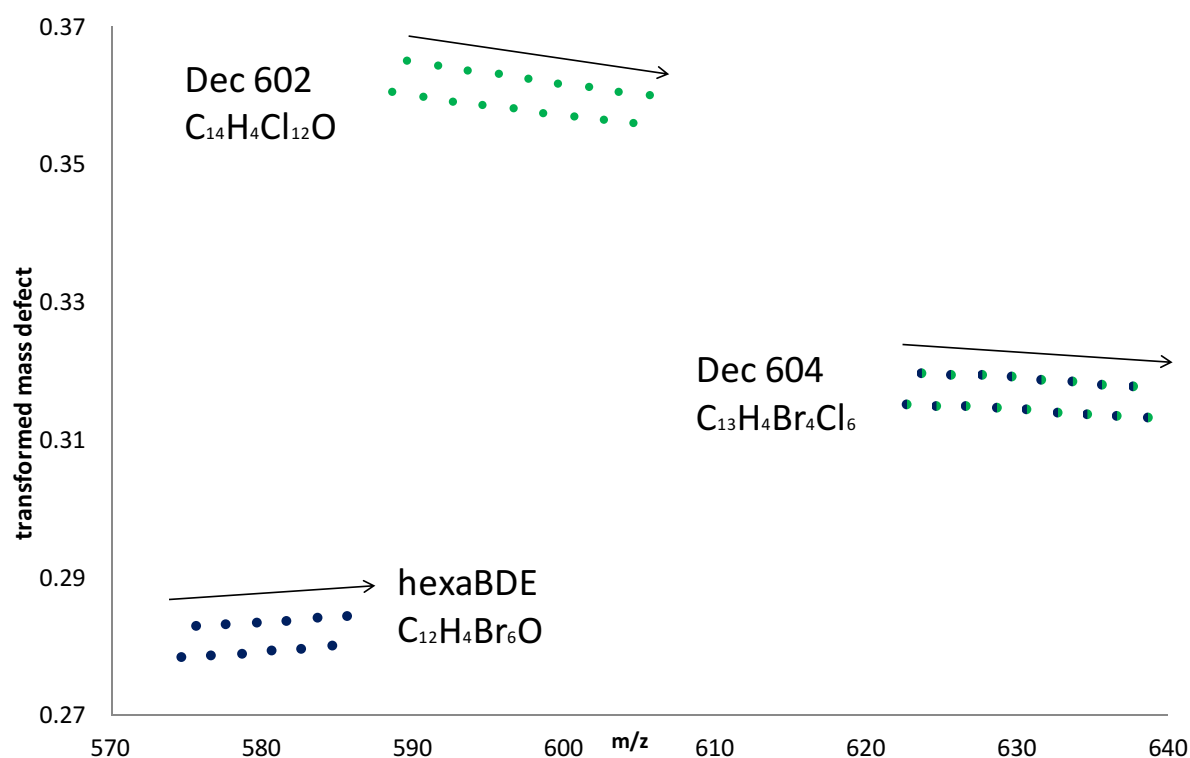


Figure 3-6. Mass defect plot of simulated isotopic patterns of brominated (hexaBDE), chlorinated (Dec 602) and mixed compounds (Dec 604) to visualise the slope of the isotopic cluster

3.2.6. PAHs

16 PAHs, belonging to the group of priority pollutants as defined by the US EPA due to their toxicity, potential for human exposure and frequency of occurrence [196], were included in the master mixture as important representative of environmental relevant contaminants to be measured by GCxGC-TOF. It was not intended to measure them by means of HPLC, neither include them in the mass defect plot as they are non-halogenated. GC is the method of choice for the analysis of PAHs, but limited studies have reported detection methods using LC. Atmospheric pressure photoionization (APPI) is more efficient in ionizing non-polar compounds like PAHs, compared to atmospheric pressure chemical ionization (APCI), with sensitivities of up to eight times higher for naphthalene [197, 198]. Nevertheless, APCI has been used for the detection of PAHs in LC-MS/MS systems [199, 200]. The ionization mechanism has been described to be based on proton transfer from water clusters forming $[M+H]^+$ ions, as well as charge exchange from N_2^+ and O_2^+ , resulting in $[M]^+$ species [199, 201]. However, ionization in APCI is not easy and parameters have to be optimized accordingly [200], which was not further pursued in this work.

3.3. Mass defect plot of dust sample

A dust sample from an instrument assembly room was extracted as described in Chapter 2 and measured in Full Scan in APCI mode. The resulting mass defect plot is presented in Figure 3-7, showing the presence of confirmed and tentatively identified compounds. The latter ones are listed in Table 3-1 and include information on exact mass, possible ions formed, as well mass accuracy. It can be noted that ppm deviations in the table seem to decrease significantly at low m/z , outside the desired ± 5 ppm window. This is caused by the fact that during calibration caffeine with a m/z of 195 and its fragment at 136 m/z are the lowest masses

available. To calibrate at lower m/z and thereby improve the mass deviation, further specific fragments have to be included, which was not further investigated in this study.

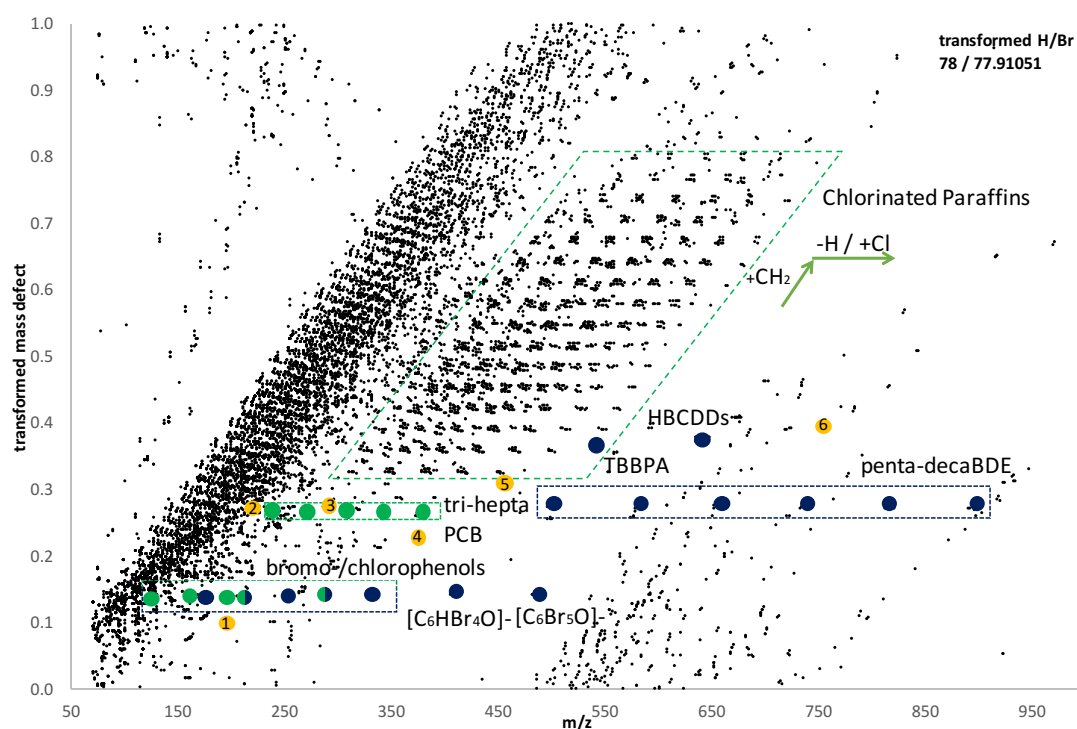


Figure 3-7. Mass defect plot of extracted dust sample transformed with H/Br scale 78/77.91051.

Table 3-1. Compounds tentatively identified in the dust sample

nr	m/z	tentative compound	measured ion	ion formed	ppm	Transf. MD
	126.99422	monochlorophenol	$[C_6H_4ClO]^-$	$[M-H]^-$	-10.99	0.14
	160.95535	dichlorophenol	$[C_6H_3Cl_2O]^-$	$[M-H]^-$	-8.22	0.14
	170.94393	monobromophenol	$[C_6H_4BrO]^-$	$[M-H]^-$	-7.2	0.14
	196.91371	trichlorophenol	$[C_6H_2Cl_3O]^-$	$[M-H]^-$	-5.03	0.14
	206.90294	chlorobromophenol	$[C_6H_3ClBrO]^-$	$[M-H]^-$	-3.56	0.14
	250.85324	dibromophenol	$[C_6H_3Br_2O]^-$	$[M-H]^-$	-1.38	0.14
	284.81442	chlorodibromophenol	$[C_6H_3ClBr_2O]^-$	$[M-H]^-$	-0.36	0.14
	328.76427	tribromophenol	$[C_6H_2Br_3O]^-$	$[M-H]^-$	0.38	0.14
1	194.87476	1,1,3,3-Tetrachloroacetone / 1,1,2,3,3-pentachloropropene	$[C_3HCl_4O]^-$	$[M-H]^- / [M-Cl+O]^-$	-5.23	0.10
2	217.01860	$C_{10}H_{12}Cl_2O / C_{10}H_{11}Cl_3$	$[C_{10}H_{11}Cl_2O]^-$	$[M-H]^- / [M-Cl+O]^-$	-2.74	0.27
3	286.94392	Triclosan / 1,2-Dichloro-4-(2,4-dichlorophenoxy)benzene	$[C_{12}H_6Cl_3O_2]^-$	$[M-H]^- / [M-Cl+O]^-$	0.61	0.27
4	374.80024	1,1,1,3,3,5,5,7-Octachloroheptane	$[C_7H_7Cl_8]^-$	$[M-H]^-$	-0.61	0.23
5	455.78493	n/a – tribrominated?	$[C_{12}H_7Br_3O_4]^-$	n/a	-1.58	0.31
6	753.53042	n/a – hexabrominated?	$[C_{17}H_6Br_6O_4]^-$	n/a	-0.45	0.40

3.3.1. PBDEs, HBCDDs and TBBPA

PBDEs were present in the analysed dust sample, ranging from penta to deca BDE. $[M-Br+O]^-$ ions were formed and found in a homologue series at a common transformed mass defect of 0.27. Targeted XICs showed the presence of pentaBDEs (1 isomer), hexaBDEs (3 isomers), heptaBDEs (3 isomers), octaBDEs (3 isomers), nonaBDEs (2 isomers) and decaBDE.

HBCDDs and TBBPA were detected in the dust sample, both with a transformed mass defect of 0.37. Similar to the standard measurements, the dust derived mass defect plot showed fragmentation products of PBDEs with $[C_6H_nOBr_x]^-$ ions ($n+x=5$) at a transformed mass defect of 0.14.

3.3.2. PCBs

A chlorinated homologue series at a transformed mass defect of 0.26 corresponds to PCBs when assuming that they ionise as $[M-Cl+O]^-$ ions as shown by standard measurements. It includes, triPCB as $[C_{12}H_7OCl_2]^-$, tetraCB as $[C_{12}H_6OCl_3]^-$, pentaCB as $[C_{12}H_5OCl_4]^-$, hexaCB as $[C_{12}H_4OCl_5]^-$, as well as heptaCB as $[C_{12}H_3OCl_6]^-$.

3.3.3. Bromophenols, chlorophenols and mixed bromo-chloro phenols

A series of homologue isotope patterns was identified at a transformed mass defect of 0.14. Further investigation showed that these could tentatively originate from bromo- and chlorophenols and ionize as $[M-H]^-$, when comparing the results to the TBP standard measured. XICs of selected masses exhibited peaks at early retention times, possibly from mono-, di- and tribromophenol, with identified clusters of $[C_6H_2OBr_3]^-$, $[C_6H_3OBr_2]^-$ and $[C_6H_4OBr]^-$ respectively. Further, three clusters of $[C_6H_nOCl_x]^-$ ions ($n+x=5$, $1 \leq x \leq 3$) were identified as mono-, di- and trichlorophenol. Finally, a further two clusters shown to originate

from mixed halogenated compounds with $[C_6H_nOCIBr_x]^-$ ions and were identified as chlorobromophenol and chlorodibromophenol. XICs of all these phenols are shown in Figure 3-8. The double peak with an m/z of 250 (dibromophenol) at RT 1.9-2.2, is likely a result of in-source fragmentation of chlorodibromo- and tribromophenol, since it is eluting at the same time and is a part of the structure of both compounds.

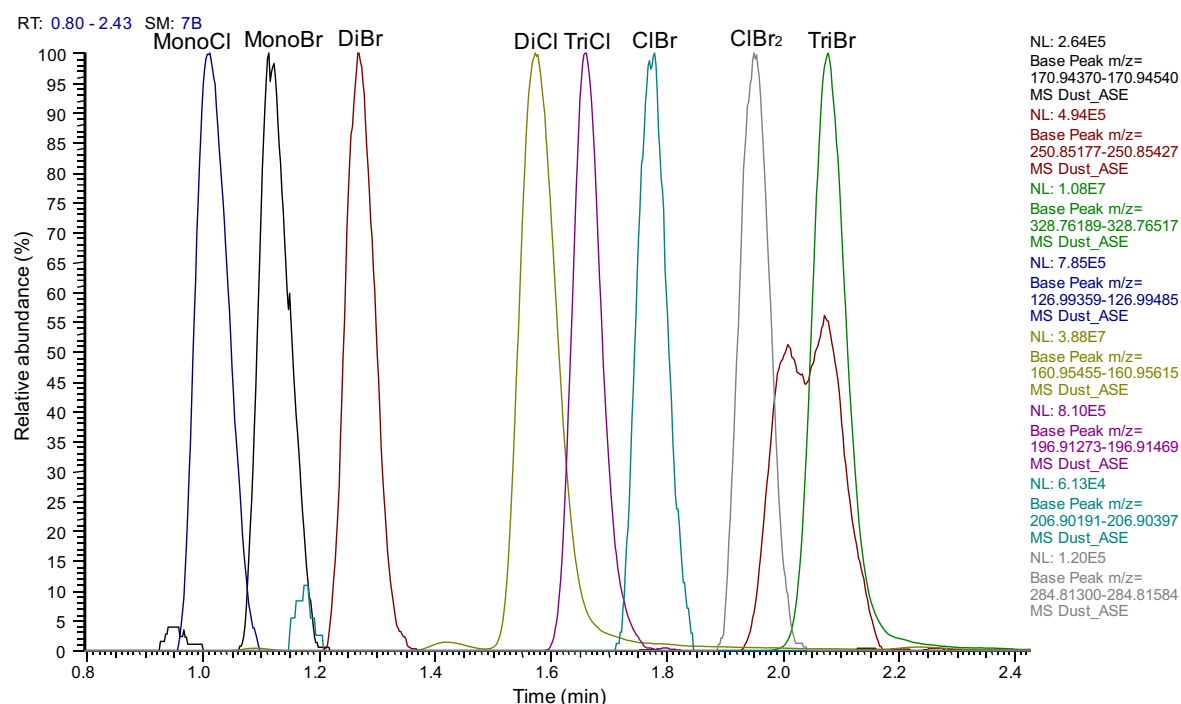


Figure 3-8. XICs of bromophenols (mono-, di- and tri-), chlorophenols (mono-, di- and tri-) and mixed phenols (chlorobromo and chlorodibromo) in an extracted dust sample

3.3.4. Chlorinated paraffins (CPs)

The mass defect plot showed a sizeable area of homologue peaks. Further investigation showed that these could likely be chlorinated paraffins, forming $[M+Acetate]^-$ ions as reported in the literature [195]. CPs, also referred to as polychloroalkanes are a complex isomer group of chlorinated products of n-alkane mixtures. They can be divided into groups, depending on their carbon chain length, short chain SCCPs (C_{10} - C_{12}), medium chain MCCPs (C_{14} - C_{19}) and long

chain LCCPs (C₂₀-C₃₀), as well as according to their degree of chlorination ranging from 30-70 %. CPs are used as flame retardants, plasticizers, as well as additives in metal-working fluids, paints and sealants [202]. In the literature, only a few studies exist reporting the occurrence of CPs in indoor dust [203]. XICs showed that peak widths of selected masses were in the range of 30 to 90 sec, confirming the presence of unresolved isomer mixtures. Due to the lack of information and standards available, characterization of the CPs fraction within the dust sample was not further investigated. However, this demonstrates again the potential of this mass defect technique, as an elegant way in identifying single substances or homologue groups of brominated or chlorinated compounds in environmental samples. Given the reported difficulties in measuring individual CPs in the environment [204-206], further exploration of the mass defect approach for this application appears warranted.

3.3.5. Other tentative compounds

As listed in Table 3-1 other brominated and chlorinated compounds were tentatively identified, which are marked with yellow dots and nr. 1-6 in Figure 3-7. However, exact formulae and compounds could not always be elucidated. Isotopic pattern of these compounds often missed the low-abundance peaks of the pattern needed for a correct identification (as described in 1.6.3). Where possible, the pattern was compared to theoretical values (relative isotopic abundance) and an elemental composition provided. Fragmentation studies could aid in the further identification, but intensity threshold need to be met.

3.4. Mass defect plots of a sediment sample

A sediment sample from the River Thames (Figure 2-1 location nr. 21) taken in the industrial area of London was extracted (as described 2.3.1) and measured in Full Scan in APCI mode. The resulting mass defect plot is visualized in Figure 3-9 with confirmed compounds and internal standards identified, while tentatively assigned compounds are listed in Table 3-2.

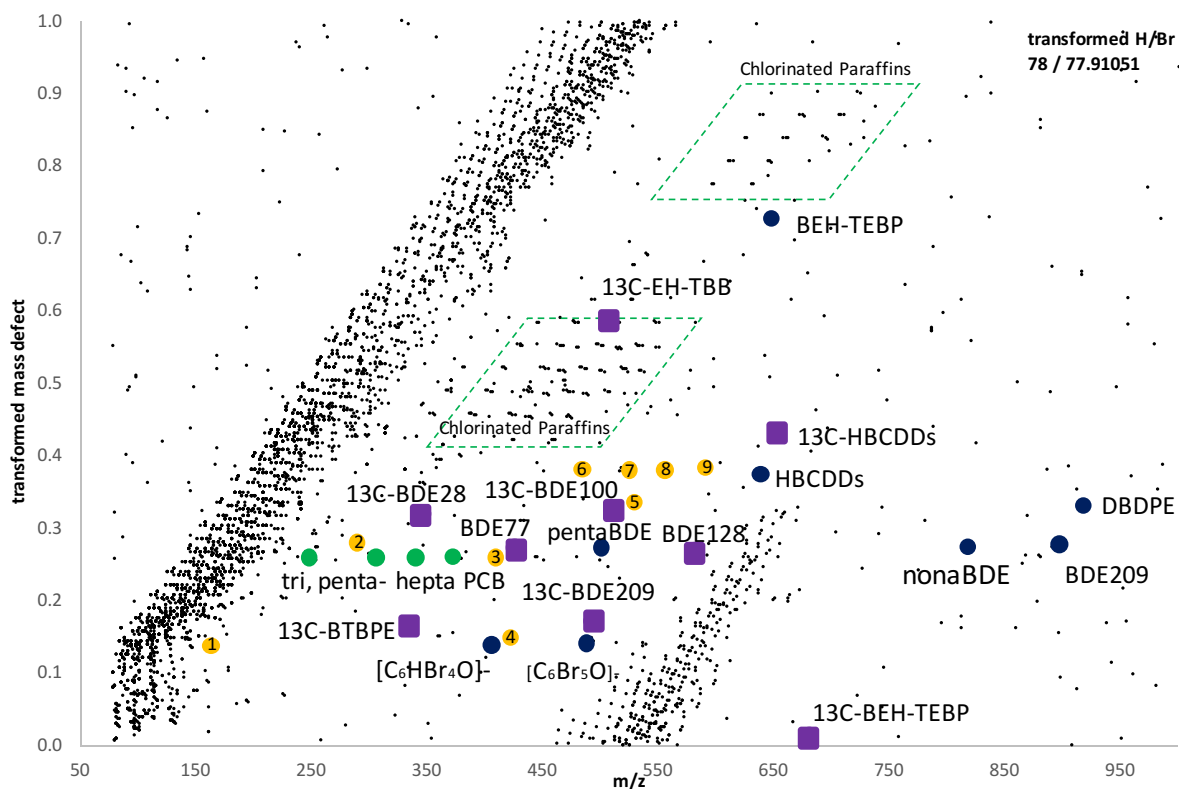


Figure 3-9. Mass defect plot of extracted sediment sample transformed with H/Br scale 78/77.91051

Table 3-2. Compounds tentatively identified in the sediment sample

nr	m/z	tentative compound	measured ion	ion formed	ppm	Transf. MD
1	160.95528	dichlorophenol	$[C_6H_3Cl_2O]^-$	$[M-H]^-$	-8.22	0.14
2	286.94392	Triclosan / 1,2-Dichloro-4-(2,4-dichlorophenoxy)benzene	$[C_{12}H_6Cl_3O_2]^-$	$[M-H]^- / [M-Cl+O]^-$	0.61	0.27
3	408.79013	n/a - tribrominated?	$[C_{11}H_6Br_3O_2]^-$	n/a	-0.25	0.26
4	421.66190	n/a - tribrominated?	n/a	n/a	n/a	0.14
5	525.72801	n/a - tetrabrominated?	n/a	n/a	n/a	0.33
6	486.81629	octachloroterphenyl	$[C_{18}H_6Cl_7O]^-$	$[M-Cl+O]^-$	-0.58	0.38
7	520.77732	nonachloroterphenyl	$[C_{18}H_5Cl_8O]^-$	$[M-Cl+O]^-$	-0.51	0.38
8	554.73834	decachloroterphenyl	$[C_{18}H_4Cl_9O]^-$	$[M-Cl+O]^-$	-0.41	0.38
9	588.69937	undecachloroterphenyl	$[C_{18}H_3Cl_{10}O]^-$	$[M-Cl+O]^-$	-0.37	0.38

3.4.1. Internal standards

All internal standards, added prior to extraction of the sediment sample for quantification purposes, were identified in the mass defect plot. These are marked with purple squares in Figure 3-9 and include ^{13}C -BDE-28, BDE-77, BDE-128, ^{13}C -BDE-209, ^{13}C -BTBPE, ^{13}C -EH-TBB, ^{13}C -BEH-TEBP and ^{13}C -HBCDDs, as well as ^{13}C -BDE-100 added as recovery determination standard. During extraction and cleanup of the sediment sample, TBBPA and ^{13}C -TBBPA were eluted in a different fraction and thus measured separately.

3.4.2. PBDEs, HBCDDs and NBFRs

Some native BDE homologues were paired at a transformed mass defect of 0.27. It includes decaBDE, as the most intense halogenated cluster in the data file, but also pentaBDE and nonaBDE, together with fragmentation products $[\text{C}_6\text{Br}_5\text{O}]^-$ and $[\text{C}_6\text{HBr}_4\text{O}]^-$, as described for the standard mixture and dust sample. HBCDDs were detected as well, while TBBPA was measured separately as explained above. NBFRs detected included BEH-TEBP and DBDPE.

3.4.3. PCBs

A chlorinated homologue series at a transformed mass defect of 0.26 corresponds to PCBs forming $[\text{M}-\text{Cl}+\text{O}]^-$ ions. Results indicate the presence of triCB as $[\text{C}_{12}\text{H}_7\text{OCl}_2]^-$, pentaCB $[\text{C}_{12}\text{H}_5\text{OCl}_4]^-$, hexaCB as $[\text{C}_{12}\text{H}_4\text{OCl}_5]^-$, as well as heptaCB as $[\text{C}_{12}\text{H}_3\text{OCl}_6]^-$.

3.4.4. Chlorinated paraffins

Similar to the dust sample, also the mass defect plot of the sediment sample indicates the possible presence of CPs, however as a much smaller fraction. XICs of selected masses showed peak widths in the range of 30 to 60 sec, again confirming the occurrence of unresolved isomer mixtures, which need to be further explored.

3.4.5. Other tentative compounds

As listed in Table 3-2 other brominated and chlorinated compounds were tentatively identified, which are marked with yellow dots and nr. 1-9 in Figure 3-9. Interestingly the same exact mass 286.94392 with a transformed mass defect of 0.27 was detected as in the dust sample, however at different RT (5.28 in sediment and 5.13 in dust extract). Further, a homologue series was observed at a transformed mass defect of 0.38, with a distance of 33.96103 Da between clusters (corresponding to $-H / +Cl$). XICs showed unresolved isomer mixtures, which were identified as chlorinated terphenyls with a general formula of $C_{18}H_{14-n}Cl_n$. Assuming that these ionize as $[M-Cl+O]^-$, the four identified clusters are octa- $[C_{18}H_6Cl_7O]^-$, nona- $[C_{18}H_5Cl_8O]^-$, deca- $[C_{18}H_4Cl_9O]^-$ and undecachloro terphenyl $[C_{18}H_3Cl_{10}O]^-$. Their presence has been reported in aquatic biota, sediment [207] and electronic waste [165].

3.4.6. Conclusion

In the dust sample 34 halogenated compounds were detected (excluding a major fraction of chlorinated paraffins), of which 28 were positively identified. Instead, for the sediment sample 18 compounds (apart from the 9 spiked internal standards and a smaller fraction of chlorinated paraffins) could be detected and 14 thereof identified. Compared to the dust sample, it appears that the sediment fingerprint is less complex. However, since two different extraction and clean-up protocols were followed and the samples are not related to each other, a direct comparison is not possible. Extensive purification/clean-up steps (copper, acid wash, Florisil) used in the sediment extraction very likely reduced the organic compounds and allowed to investigate a limited fraction only. Differences between samples could also be caused by compounds present at low concentrations, which then fall below the threshold applied when calculating the plots and are thus not visualised.

3.5. GCxGC-TOF/MS measurements

The same standard mixture injected on the UPLC-Orbitrap system was also injected on the GCxGC-TOF instrument, but compounds were dissolved in toluene rather than methanol. The results of this measurement are shown in Figure 3-10. No mass defect plots could be calculated for the TOF measurements, since the employed instrument was only able to acquire data in low resolution. This gives insufficient resolving power to measure the mass defect and distinguish halogenated compounds from other organic substances in a measured sample.

However, the GCxGC-TOF-MS demonstrated enhanced chromatographic separation of most compounds (including PAHs and PCBs) and can easily perform database searches based on fragmentation spectra for confirmation purposes. Challenges with this technique include the inherent lack of sensitivity for relatively polar compounds (e.g. TBBPA), as well as higher brominated species (BDE-209 and DBDPE) and chlorinated compounds (a/sDP and Dec 604), as well as stereoisomers of HBCDD due to thermal degradation and isomeric-interconversion, respectively. Thus, of the 60 compounds injected, 50 were detected and positively identified at 70 eV. Some higher brominated (BEH-TEBP, BTBPE) and chlorinated species (a/sDP, Dec 604) could be further detected and identified when measuring at 12 eV as described in 3.5.1.

The high chromatographic throughput of the GCxGC system requires a rapid acquisition rate (50 Hz or above) to reliably detect all the compounds in a complex mixture. As mentioned above for the generation of mass defect plots a high resolution instrument is needed. However, when using a HR-TOF, these instruments can generally only acquire the data at 10 Hz [162] or 25 Hz [208]. Further, the dynamic range of the detector at times is insufficient for the detection of environmental pollutants distributed at various concentrations [209].

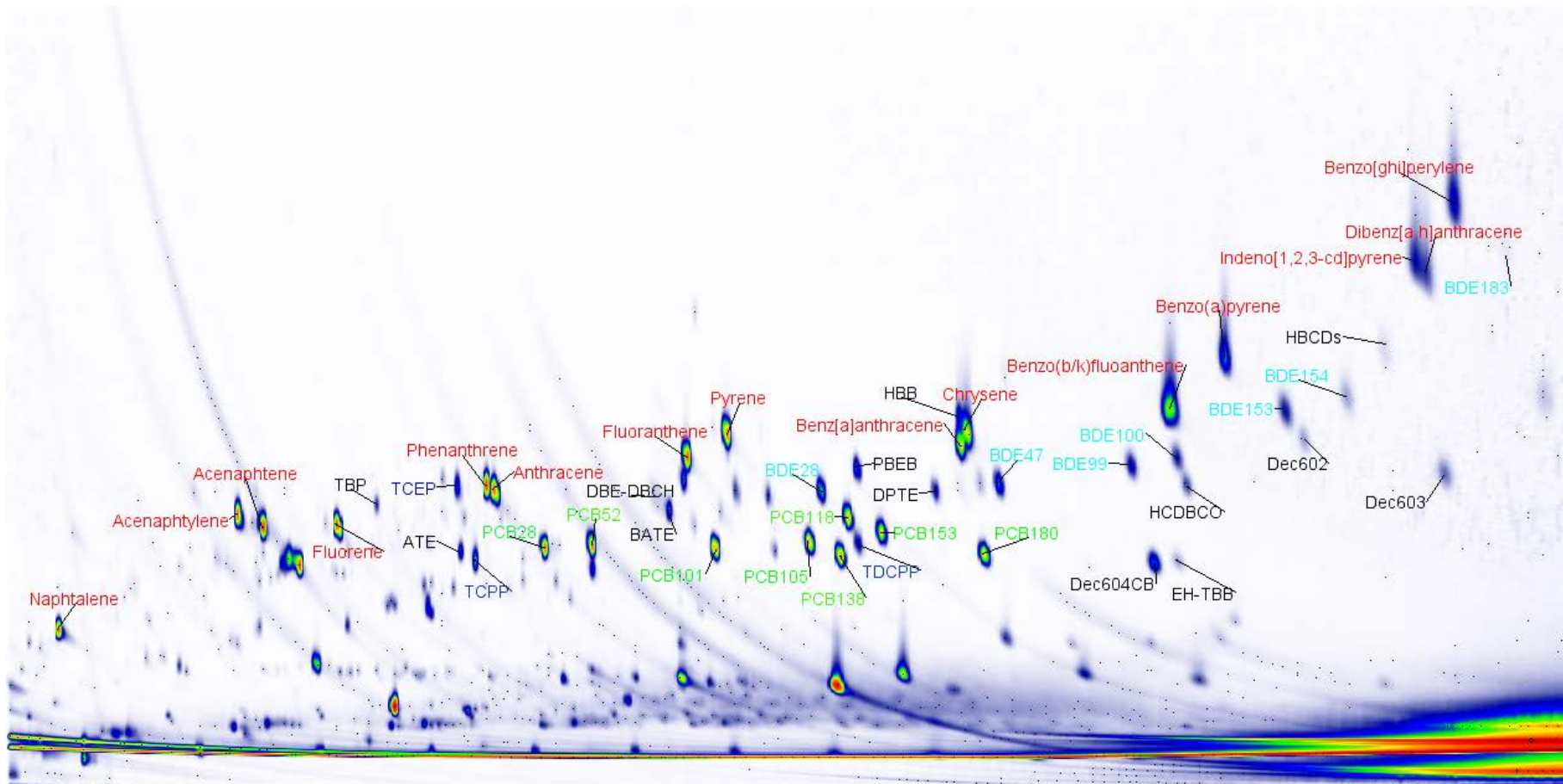


Figure 3-10. GCxGC-TOF results for master mixture standard measured at 70 eV containing 200 $\mu\text{g } \mu\text{L}^{-1}$ of PBDEs, HBCDDs, TBBPA, NBRs, Dechloranes, OPFRs, PCBs and PAHs

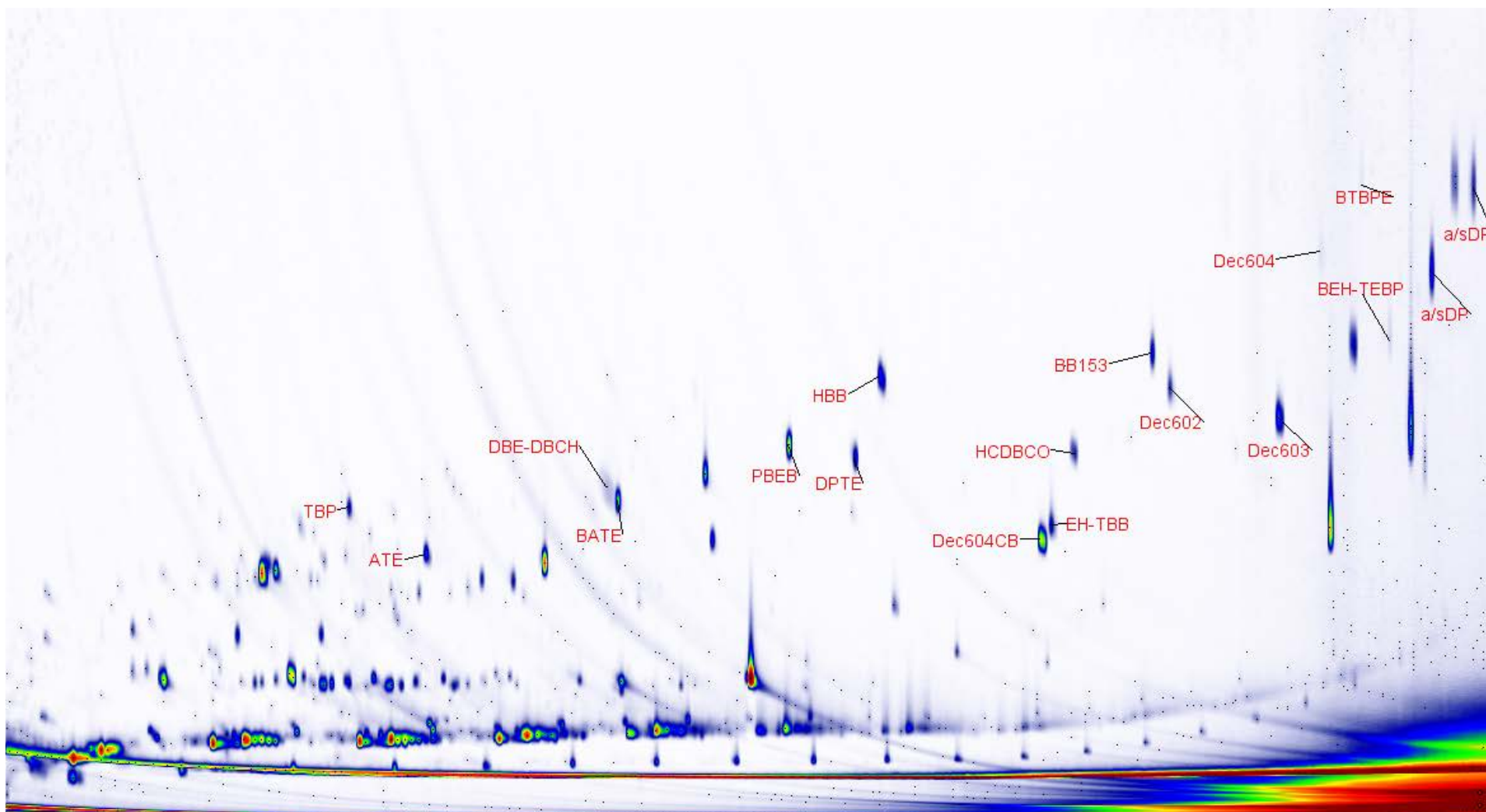


Figure 3-11. GCxGC-TOF results measured at 12 eV for standard containing $200 \mu\text{L}^{-1}$ of only NBFRs

3.5.1. Variable ionization energies

To address the issue of extensive in-source fragmentation of higher brominated and chlorinated species, we investigated the application of variable energy electron ionization switching to 12 eV, instead of 70 eV (SELECT eV[®] source technique). A resulting measurement for a NBFR standard is presented in Figure 3-11. When comparing Figure 3-10 and Figure 3-11 it becomes visible that at 12 eV higher brominated (BEH-TEBP and BTBPE) and chlorinated (a/sDP and Dec 604) compounds become detectable, which were not detected when using 70 eV ionization energy, due to their weak molecular ions and the strong fragmentation yielding inconclusive spectra. Figure 3-12 illustrates the larger fraction of retained molecular ion at 12 eV compared to 70 eV for HCDBCO, whilst retaining a useful degree of fragmentation. An EI ion source normally uses a potential difference of 70 eV to accelerate electrons from a negatively charged filament to a positively charged ion chamber. In soft ionization this potential is reduced, resulting in a significant loss of sensitivity due to the inefficiency of drawing electrons into the ion chamber, as well as losing sample as neutrals in the source. However, when using a variable ionization source, like in our study, datasets can be acquired with variable ionization energies to be tuned between 10 and 70 eV. Due to special ion optics, a high potential difference is always maintained for accelerating electrons and only reduced prior to arriving at the ion chamber [192, 210].

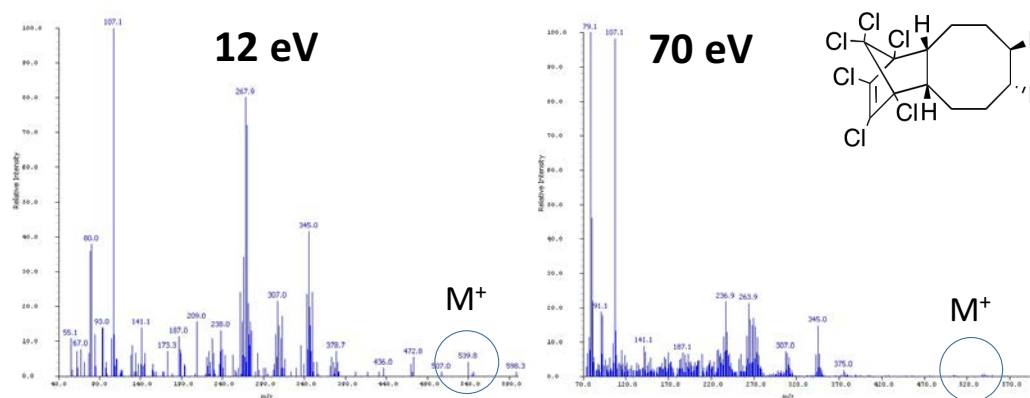


Figure 3-12. GCxGC-TOF spectrum for HCDBCO measured at 12 and 70 eV, M⁺=molecular ion

The larger relative abundance of the molecular ion retained at 12 eV compared to 70 eV ionization energy is listed in Table 3-3 for selected compounds.

Table 3-3. Selected compounds measured on GCxGC-TOF at 12 and 70 eV, relative abundance (%) of molecular ion in the mass spectrum

Compound	molecular Ion m/z	% of molecular ion at 12 eV	% of molecular ion at 70 eV
ATE	371.8	9.86	3.42
BATE	449.8	3.86	1.70
HCDBCO	539.8	0.35	0.08
PBEB	499.7	18.8	6.57
TDCPP	430.6	0.12	0.08
BDE153	643.5	8.23	3.17
EH-TBB	550.1	0.17	0.04
2,4,6-TBP	329.8	34.6	19.4
BDE99	563.7	20.3	8.29
PCB180	393.9	29.1	9.66

3.6. Impact of collision energy and fragmentation in the HRAM Orbitrap

On the Orbitrap systems, fragmentation studies using the higher energy collisional dissociation (HCD) cell can be run next to the full scan experiment for structural confirmation purposes. While for proteins the collision energy (CE) needed to achieve optimum fragmentation efficiency follows a linear correlation with m/z, this is not the case for chemical compounds in general. The Orbitrap uses a normalized collision energy (NCE), which automatically compensates for the mass dependency and adapts the collision energy depending on the m/z, i.e. higher energies for ions at higher m/z. NCE is a dimensionless number, but can be regarded as CE (in eV) for a reference m/z of 500, while the actual value is calculated based on the m/z of ions. Figure 3-13 shows fragmentation spectra of a BDE-209 standard at stepped collision energies (SCE) 10, 20 and 30 and the occurrence of debrominated fragments. While at 10 most of the molecular ion (m/z 894) is not fragmented and smaller fragments are not formed, at 20, the molecular ion peak is already fully fragmented and at 30 most of the compound fragments to bromine (m/z 79).

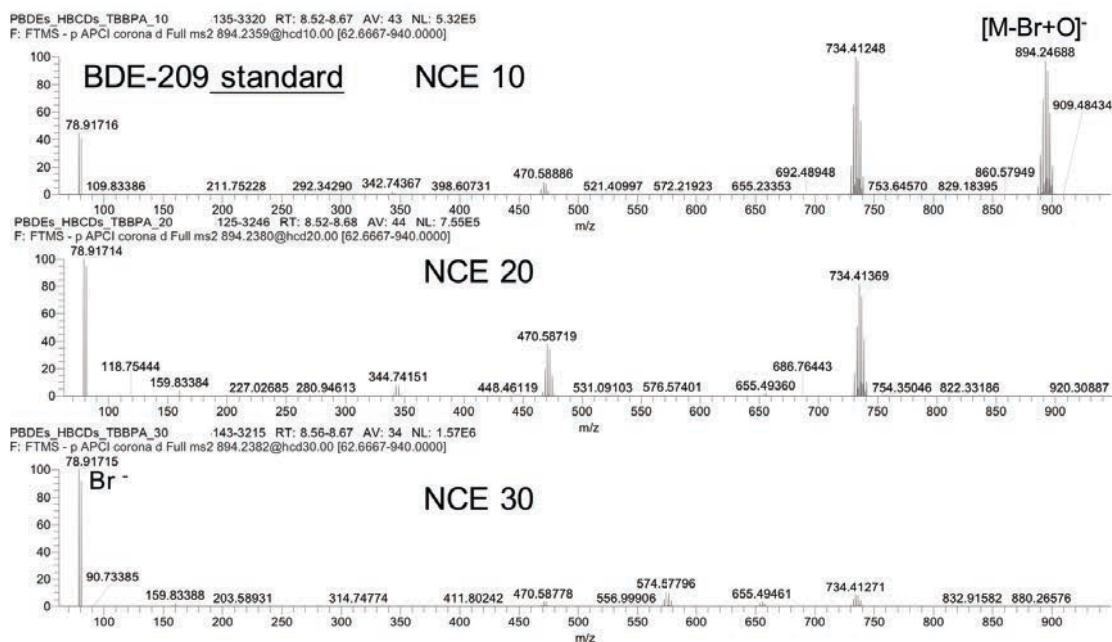


Figure 3-13. Fragmentation of decaBDE standard in different measurements on LC-orbitrap employing selected normalized collision energies (10, 20 and 30)

For this purpose, as shown in Figure 3-14, the user can decide to fragment the compound at selected energies (stepped collision energy - SCE), which are then combined to a single spectrum. This results in both smaller and larger fragments and aids compound identification.

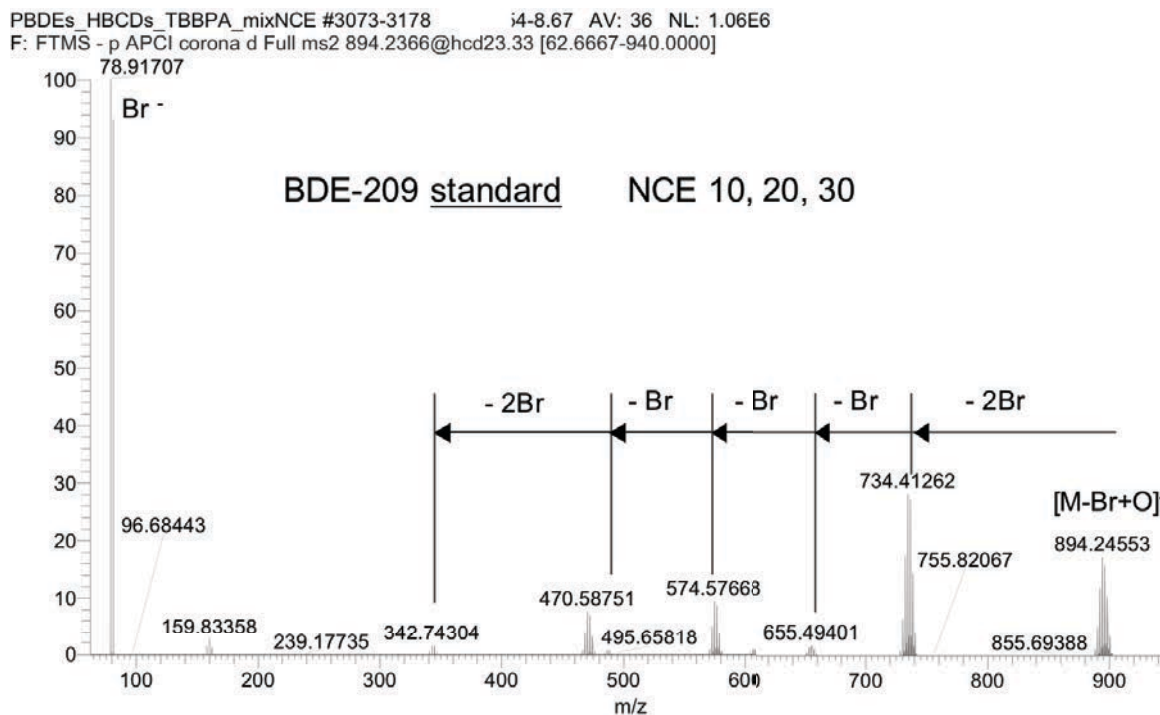


Figure 3-14. Fragmentation of decaBDE standard in a single measurement on LC-Orbitrap at stepped collision energies (SCE) of 10, 20 and 30

3.7. Conclusions

A multi-residue analysis method for the detection of 60 environmental relevant contaminants, including 10 PBDEs, HBCDDs, TBBPA, 15 NBRs, 6 Dechloranes, 3 OPFRs, as well as 8 PCBs and 16 PAHs, was successfully tested on both a UPLC-HRMS Orbitrap platform and a GCxGC-TOF system using standard solutions.

The UPLC-Orbitrap positively identified 44 compounds, with the exception of PAHs which cannot be detected on the present instrument. Its potential relies on the use of both positive and negative ionization in APCI and HESI mode, thereby covering a range from non-polar to more polar compounds respectively and easily detecting higher brominated and chlorinated compounds. GCxGC-TOF on the other side, positively identified 50 compounds within the mixture at 70 eV ionization energy, with the option of also detecting higher brominated and chlorinated compounds when using soft ionization at 12 eV (variable ionization energy). The instruments advantages are based on the enhanced chromatographic separation in two dimensions and the ease of use of database searches based on fragmentation spectra for confirmation purposes.

Further, with the use of high resolution accurate mass measurements on the Orbitrap, transformed (+H/-Br) mass defect plots were constructed in order to screen for halogenated compounds in a complex data set of organic contaminants. Since a single m/z measurement in such a complex mass spectrum cannot be assigned to a defined molecular formula based on accurate measurements of m/z only [211], further parameters, such as isotope patterns and relative isotope abundances were taken into account for identification purposes, where no standard was available for confirmation.

MD plots revealed the presence of several halogenated classes of compounds within an extracted dust and sediment sample. Of the 34 halogenated compounds detected in the dust

sample, 28 were identified, while the sediment sample revealed 18 halogenated compounds detected, with 14 identifications. With different extraction and clean-up procedures used for dust and sediment, a direct comparison is not feasible.

The results of this MD approach can serve to draw attention to halogenated ions that do not correspond to targeted compounds and would otherwise be very challenging to discover. Especially, when series of related compounds have been identified, such as chlorinated paraffins and -terphenyls in the investigated samples. In the case of our study, the MD plot revealed the presence of both brominated contaminants (including LBFRs, NBFRS, bromophenols) and chlorinated compounds (like PCBs, chlorinated paraffins, chlorinated terphenyls, chlorophenols), as well as mixed halogenated bromochloro phenols. The plot also led to the detection of further halogenated contaminants whose elemental composition has to be further investigated.

Transformed mass defect plots cannot be used to discriminate between legacy BFRs and novel BFRs and are not the right tool to separate isomers, but can readily visualize the presence of potentially novel persistent and bioaccumulative halogenated chemicals in a complex mass spectrum. This approach shows promising results for the screening and untargeted analysis of environmental samples, especially when combined with automated scripts for data extraction. Examples include, identification of novel classes of environmental contaminants that have not previously been detected in fish [164], detection of brominated impurities, byproducts and degradation products of TBBPA in plastics, leading to possible mitigation in to the environment and call for the necessity of appropriate exposure assessment [161], as well as the identification of chlorinated Dechlorane analogs in sediments [168].

Chapter IV - Legacy PBDEs and NBFRs in Sediment Samples of the River Thames

4.1. General overview

BFRs generally have limited biodegradability, are persistent and tend to accumulate in the environment [212]. Due to their chemical properties, BFRs tend to partition to organic carbon rich matter and have been detected in samples of sediment, dust and sewage sludge around the world [14]. Since most NBFRs have similar physicochemical properties (i.e. low water solubility and high K_{ow} values) to PBDEs, we hypothesize that sediments represent important sinks for NBFRs. Studies on BFRs in sediments in the UK have been conducted on samples from lakes [213-215], rivers and estuaries [216-219], coastal [217, 220] and marine regions [217, 221]. However, apart from one study in the UK [217], which analysed a broad range of halogenated flame retardants in both marine and fresh water sediments, other studies in the UK have mainly focused on PBDEs and HBCDDs. Given this lack of information on the levels and profiles of NBFRs in freshwater sediments, the aim of this study was to compare concentrations of 13 PBDEs, HBCDDs, TBBPA and 10 selected (N)BFRs in samples of surficial sediments taken at 45 locations along the River Thames in the UK. In addition, spatial variations in (N)BFR concentrations were examined relative to the location of activities such as sewage outfalls, in an effort to identify potential sources of these BFRs to the river. The Thames was chosen as it is one of the major rivers in Europe and spatial trends relative to various points and diffuse sources in such an industry rich area permit assessment of the relative importance of such sources. Moreover, the potential of high resolution Orbitrap mass spectrometry was exploited for multi-residue analysis of a broad range of BFRs and NBFRs in

a single run with sensitive, rapid and reliable measurement of target analytes, as well as their potential degradation products.

4.2. Sediment analysis

4.2.1. Levels and trends of PBDEs and NFRs in sediments

Mean, median and concentration ranges of our target BFRs in surface sediments from the River Thames are summarized in Table 4-1, while an overview of individual PBDE congeners is illustrated in Figure 4-2 (a table with concentrations of all PBDE congeners can be found in Appendix II). To account for potential variability of concentrations due to organic carbon content, organic carbon normalisation was conducted on all sample concentrations using the measured total organic carbon (TOC) for each sample, as described in 4.2.2. No correlation between BFR concentrations and TOC values was observed in the studied samples. This is likely explained by the fact that samples were taken from different locations with diverse source input strengths. If samples originate from the same location (such as sediment cores) with the same source input strength, a positive linear correlation between TOC and BFR dry weight concentration would be expected. Similarly, for the composition of the sediment, no correlation between the BFR concentration and its geological composition (clay, silt or sand content) was observed in our samples.

4.2.2. TOC

The TOC determination was conducted by Dr. Christopher Vane and his collaborators from the British Geological Survey as described in [185], which also sampled and provided the sediments for this study. The TOC content of the surface sediments varied from < 1% to 6.35 % and decreased towards the sea (Figure 4-1). This can be explained by dilution of organic rich river sediment with organic poor marine sand from the southern North Sea. The systematic decrease from land to sea was disrupted by lower TOC values at sites in central London and higher values at a few sites located towards the sea. The low and high values may be explained by dilution of man-made sediment. A detailed list of all sampling locations , including TOC content, distance from Teddington lock and name of the site can be found in Appendix II.

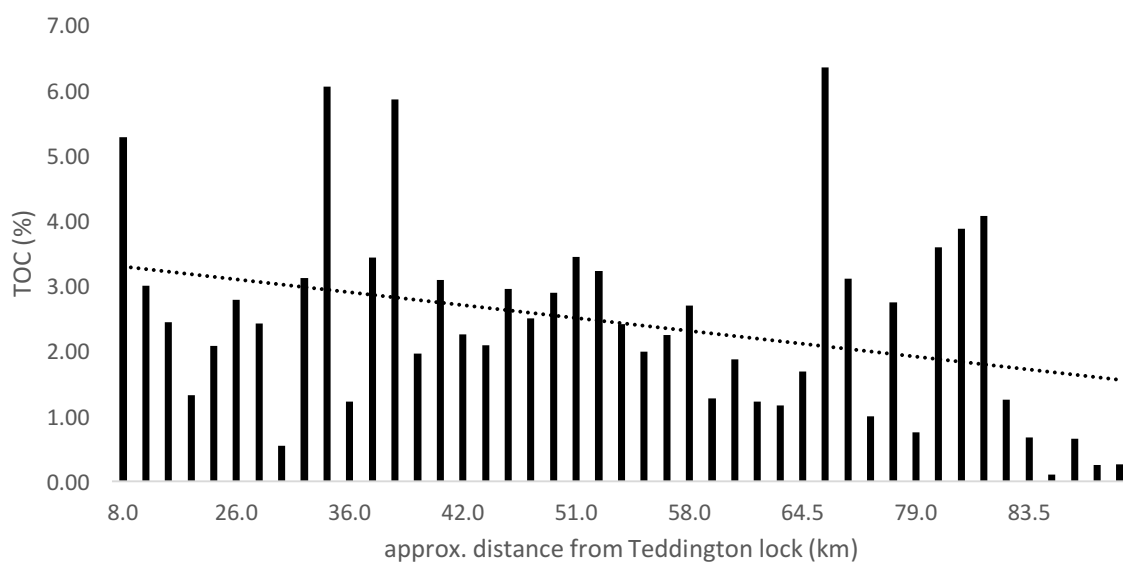


Figure 4-1. TOC content from surface sediments of the Thames Estuary

Table 4-1. Summary of the concentrations in both $\mu\text{g kg}^{-1}$ dry weight and $\mu\text{g kg}^{-1}$ organic carbon of selected BFRs in surficial sediments from the River Thames

Compound	DF (%)	Median	Average	Range	Median	Average	Range
		$\mu\text{g kg}^{-1}$ dry weight			$\mu\text{g kg}^{-1}$ organic carbon		
Σ_{12} BDEs	16-100	3.8	5.9	n.d. – 29	182	228	n.d. – 672
BDE-28	27	<0.2	0.4	n.d. – 4.0	<0.2	12	n.d. – 116
BDE-47	53	<0.03	0.2	n.d. – 2.5	<0.03	6.7	n.d. – 48
BDE-99	71	0.5	0.8	n.d. – 4.4	15	28	n.d. – 130
BDE-153	16	<0.01	0.03	n.d. – 0.6	<0.01	1.2	n.d. – 33
BDE-183	71	0.05	0.1	n.d. – 0.7	0.4	3.3	n.d. – 23
BDE-206	96	2.6	3.3	n.d. – 11.7	115	135	n.d. – 389
BDE-209	100	148	174	0.03 - 535	6969	7673	0.03 - 20762
Σ HBCDDs	91	1.9	3.7	n.d. – 38	67	157	n.d. – 1357
TBBPA	98	0.6	0.6	n.d. – 2.6	21	34	n.d. – 476
EH-TBB	0	<0.03			<0.03		
BEH-TEBP	76	2.1	3.5	n.d. – 14	100	134	n.d. – 445
BTBPE	51	<0.02	0.4	n.d. – 3.8	0.7	15	n.d. – 142
TBP	69	0.1	0.1	n.d. – 0.4	3.5	4.6	n.d. – 34
asDP	11	<0.04	2.0	n.d. – 66	<0.04	51	n.d. – 1249
PBEB	7	<0.06	1.7	n.d. – 48	<0.06	53	n.d. – 1385
DBDPE	20	<0.45	1.3	n.d. – 24	<0.45	42	n.d. – 1154
α/β -DBE-DBCH	0	<1.1			<1.1		
HBB	0	<0.03			<0.03		
BB153	0	<0.01			<0.01		

* Σ_{12} BDEs does not include BDE-209

* n.d. - not detected

* < indicates the value of the LOD

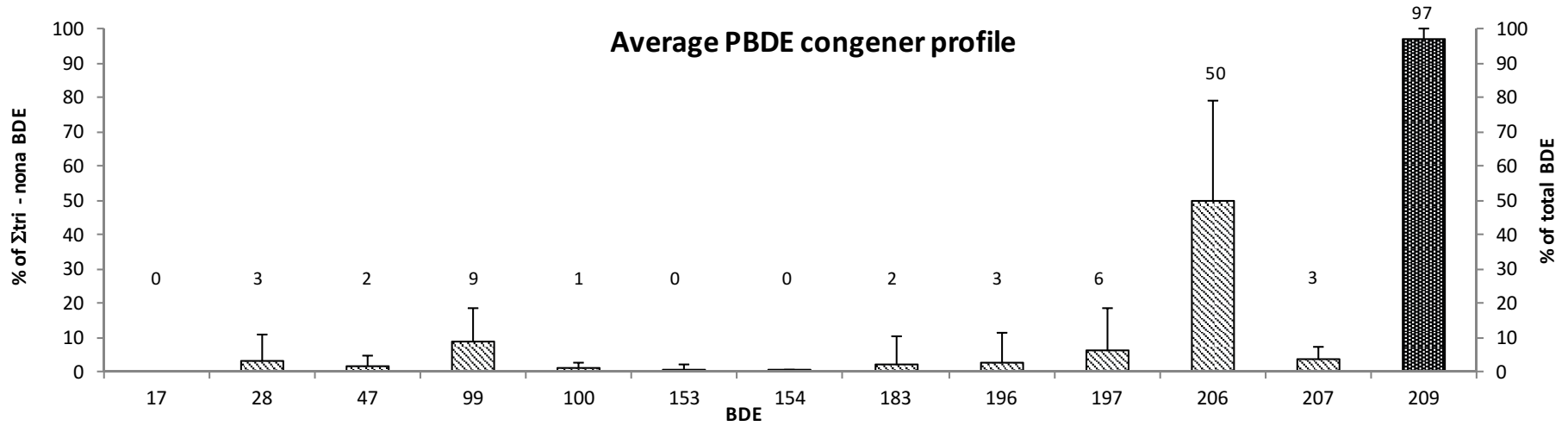


Figure 4-2. Average PBDE congener profile in all sediment samples. BDE-209 is on a different scale. Average percent contributions are indicated above each congener with error bars representing the standard deviation.

4.2.3. PBDEs

PBDE levels showed wide variability in sediments at the 45 sites sampled along the River Thames. Our data indicates BDE-209 to be the predominant congener in all samples, accounting for ~ 95 % of total PBDEs detected (Figure 4-2). Vane *et al.* reported BDE-209 to represent 80% of total PBDEs in sediments collected from the Clyde Estuary around Glasgow [222]. This indicates a greater presence of the DecaBDE formulation in our samples, further supported by high concentrations of BDE-206. Similarly, other studies reported nona-brominated PBDE congeners as the second most abundant after BDE-209 in river sediment samples of the UK (inner Clyde estuary) [222] and China (industrial area of Dongjiang river) [95], possibly indicating degradation of BDE-209 to form lower brominated congeners. This finding is especially of interest with the recent listing of Deca-BDE under the Stockholm Convention and underlines its future environmental concern. A comparison of our data to the technical Deca-BDE formulation will be discussed further on in this chapter.

Concentrations of BDE-209 ranged from <0.1 to $540 \mu\text{g kg}^{-1} \text{ dw}$ (<0.1 to $20762 \mu\text{g kg}^{-1} \text{ OC}$) in our study. Other PBDEs were detected in our samples at lower levels, with prominent congeners being BDE-206, followed by BDE-99 and BDE-28. Sediments from several UK lakes [55] contained BDE-209 at concentrations ranging from 1.63 to $116 \mu\text{g kg}^{-1} \text{ dw}$. Meanwhile, river and marine sediments from various locations around the UK [217] were reported between $0.3 - 1333 \mu\text{g kg}^{-1} \text{ dw}$, $1 - 2337 \mu\text{g kg}^{-1} \text{ dw}$ for sediments of the river Clyde [222] and $2 - 98125 \mu\text{g kg}^{-1} \text{ dw}$ for Scottish sediment cores [223]. This sets our results at the lower end of previously detected concentrations of BDE-209 in UK sediments, possibly indicating that there is less input (leachates from consumer products or emissions from manufacturer) in the Thames. However, since only a limited sample size at localised points was analysed, further more recent and detailed sampling campaigns are needed to confirm this finding, study of

time trends, along with the possible analysis of suitable marker substances (i.e. related industrial contaminants, plasticizers, etc.), to better understand whether BDE-209 originates mainly from consumer products or industry emissions in the London outdoor environment.

Harrad recently reviewed the levels of legacy BFRs in UK environmental samples [224]. Where BFR levels in UK river and lake sediments were reported, BDE-209 was the prevailing congener, followed by BDE-99 and BDE-47. Interestingly in our study, levels for BDE-28 were higher than those found for BDE-47, suggesting a potential degradation of PentaBDE congeners to form BDE-28.

A recent study analysed contamination levels of PBDEs in sediments from the Thames estuary. They reported a concentration range for Σ_6 BDEs (congeners 28, 47, 99, 100, 153 and 154) of <MDL to $14.4 \mu\text{g kg}^{-1} \text{ dw}$ [219]. This is in good accordance with our results, with a values ranging from n.d. to $12.8 \mu\text{g kg}^{-1} \text{ dw}$, when only accounting for those congeners. Barber *et al.* reported a range for river and marine sediments around the UK for Σ_{11} BDEs of n.d. to $32.15 \mu\text{g kg}^{-1} \text{ dw}$ [217], which is comparable to our range of Σ_{12} BDEs with n.d. to $29 \mu\text{g kg}^{-1} \text{ dw}$.

4.2.4. HBCDDs and TBBPA

HBCDDs (sum of α -, β -, and γ HBCDD) in our study were detected in most samples (91% detection frequency) at an average concentration of $3.7 \mu\text{g kg}^{-1} \text{ dw}$, which is comparable to the average concentrations of Σ_{12} BDEs (excluding BDE-209) we report with $5.9 \mu\text{g kg}^{-1} \text{ dw}$. Concentrations of Σ HBCDDs in our samples ranged from n.d. to $38 \mu\text{g kg}^{-1} \text{ dw}$. A study on estuarine and marine sediments around the UK reported a comparable range from <MDL to $47.2 \mu\text{g kg}^{-1} \text{ dw}$ [217]. Values for lake sediments in the UK ranged from 0.4 to $7.9 \mu\text{g kg}^{-1} \text{ dw}$

[55]. Higher values were detected in the River Skerne in northeast England with concentrations from <2.4 up to 1680 $\mu\text{g kg}^{-1}$ dw [218], possibly originating from the vicinity of a former BFR manufacturing site. HBCDDs values for marine sediments in coastal regions tend to be lower with maximum values up to 1.6 and 1.8 $\mu\text{g kg}^{-1}$ dw for southern and northern UK respectively [86].

TBBPA was found in all but one sample, with concentration of up to 2.6 $\mu\text{g kg}^{-1}$ dw and average value of 0.6 $\mu\text{g kg}^{-1}$ dw, in which is an order of magnitude lower than found in this study for HBCDDs and Σ_{12} BDEs. Comparatively few studies have reported TBBPA concentrations in European sediment samples. Sediments from the southern and northern UK coast were reported with values up to 6.4 $\mu\text{g kg}^{-1}$ dw for TBBPA and an average of 1.7 and 2.7 $\mu\text{g kg}^{-1}$ dw respectively [86]. TBBPA interestingly was the predominant compound with a detection frequency of 87 % in these coast sediments. Morris *et al.* [218] analysed riverine and estuarine sediments from various rivers (Tees, Tyne, Humber, Clyde and Mersey) in the UK and found higher average values of 451 $\mu\text{g kg}^{-1}$ dw and up to 9750 $\mu\text{g kg}^{-1}$ dw in the River Skerne. For the latter case, this was attributed to the vicinity of sampling sites to a former BFR manufacturing site. TBBPA levels detected in our study are more comparable to those reported in sediment samples from rivers in The Netherlands and Germany with average values of 2.2 $\mu\text{g kg}^{-1}$ dw [218] and 0.3 $\mu\text{g kg}^{-1}$ dw [86] respectively.

4.2.5. NBFRs

NBFRs were quantified in most samples at varying concentrations (Table 4-1) in the following order (detection frequency): BEH-TEBP (76%) > TBP (69%) > BTBPE (51%), with DBDPE (20%), DP (11%) and PBEB (7%) identified only in a few samples. Where detected, concentrations of

NBFRs were comparable to those of BDEs (excluding BDE-209). Target compounds like EH-TBB, HBB, BB153 and α/β -DBE-DBCH were not detected in any of the studied samples.

Consistent with our study, Barber *et al.* [217] did not detect HBB, BB153 and DBE-DBCH in 42 marine and river sediments samples from around the UK, while EH-TBB was detected in one sample at a concentration of $0.29 \mu\text{g kg}^{-1} \text{ dw}$. In addition, EH-TBB has been reported in sediment samples from UK lakes [55] and southern and northern coastal locations [86].

As far as we know, this is the first time BEH-TEBP was detected in UK sediments (Table 4-1), although this FR has already been reported in sediments from South Africa [42, 225] and China [88, 89]. BEH-TEBP was detected in 76 % of our samples with an average of $3.5 \mu\text{g kg}^{-1} \text{ dw}$ ($134 \mu\text{g kg}^{-1} \text{ OC}$) and maximum values of up to $14 \mu\text{g kg}^{-1} \text{ dw}$ ($445 \mu\text{g kg}^{-1} \text{ OC}$). This comparable to values of La Guardia *et al.* in South Africa (average of $96 \text{ ng g}^{-1} \text{ OC}$, 60% detection rate) and Zhu *et al.* in China (average of $1.01 \text{ ng g}^{-1} \text{ dw}$).

BEH-TEBP and EH-TBB are two of the main constituents of the technical flame retardant mixture Firemaster 550. In the present study, interestingly only BEH-TEBP was detected, possibly reflecting the infrequent use of Firemaster 550 in the UK. BEH-TEBP is applied on its own as a plasticizer, while EH-TBB mainly as a flame retardant [226] and thus might explain our findings. Several studies in the UK have targeted both EH-TBB and BEH-TEBP in the indoor and outdoor environment. These studies focused on indoor dust [61], indoor [49] and outdoor air [60], food and human milk [67], as well soil samples [60]. In general, where reported, BEH-TEBP was detected at concentrations 1-2 orders of magnitude higher than what was found for EH-TBB. Furthermore, EH-TBB was not detected in outdoor air or soil [60], consistent with the absence of the compound in our sediments.

Concentrations of BTBPE in our sediments reached up to $3.8 \mu\text{g kg}^{-1} \text{ dw}$ with a detection frequency of 51 %, which accords well with what Barber *et al.* reported at a maximum of

1.8 $\mu\text{g kg}^{-1}$ dw and detection frequency of 48 % [217]. The presence of BTBPE was also reported in lake sediment in the UK [55].

TBP was detected in 69% of our sediments at relatively low concentrations up to 0.4 $\mu\text{g kg}^{-1}$ dw. To our best knowledge, TBP has not been reported in UK sediments so far. DBDPE, DP and PBEB in our study were only detected in localised points at low detection frequencies. DBDPE has been reported in sediments throughout Europe, including lake sediments in the UK (up to 6.4 $\mu\text{g kg}^{-1}$ TOC) [55] and Italy (up to 280 $\mu\text{g kg}^{-1}$ dw) [94], as well as river sediments in The Netherlands [57] and Spain (equally up to 24 $\mu\text{g kg}^{-1}$ dw) [227]. PBEB has been reported both in UK and German sediments [86, 217], while the same goes for DP [86, 228]. HBB and BB153 were not detected in this study, but their presence has been previously reported in surface and tributary sediments of Lake Ontario [229], with HBB also detected in river sediments in Germany [86]. An extensive review on emerging brominated flame retardants in sediments around the world can be found elsewhere [19].

The non-appearance of DBE-DBCH from our sediment samples is perhaps surprising as DBE-DBCH has been reported to be the predominant NBR in UK indoor air and dust [49], outdoor air [60], as well as UK human milk and diet samples [67]. This may be attributable to the physico-chemical properties of DBE-DBCH, namely its relatively high volatility and low K_{ow} compared to lower brominated BDEs. This is likely to minimise its partitioning to sediment. Benthic degradation processes are a further possible cause and have been reported for DBE-DBCH in aerobic and anaerobic soil [90]. In European sediment it has been reported in sediment of German rivers [86]. Outside of Europe, DBE-DBCH was reported in sediments of the Great Lakes [87] for the first time in 2012, as well Chinese river and marine sediments [88, 89].

4.3. Spatial trends in concentrations of PBDEs and NBFs

Spatial variation in BFR concentrations in sediments from the River Thames is shown in Figure 4-5 for Σ_{12} BDEs, HBCDDs and TBBPA (top), as well as Σ_{12} BDEs, BEH-TEBP, BTBPE and TBP (bottom). As shown, samples from the industrial area (numbers 13-34) showed substantially higher concentrations compared to both: (a) samples from the inner (numbers 1-12) and (b) outer (numbers 35-45) Thames. These differences were shown to be significant ($p < 0.05$) via an ANOVA test of samples from the 3 groups. The bottom image reveals that the Σ_{12} BDEs and BEH-TEBP show a similar concentration pattern along the river, possibly indicating a similar source input. BTBPE and TBP on the other hand only show few localized input hotspots.

HBCDDs in the industrial area showed three distinct locations with very high concentrations, around Gallions Reach (site nr. 18), St Clement's Reach (nr. 31) and Tilbury (nr. 34). A possible explanation could be the vicinity to sewage discharge locations, in close vicinity of sites nr. 30-33 (Long Reach STP) and sites nr 34-35 (Tilbury STP). Other sources impacting the sediments in this area could be manufacturer utilizing HBCDDs in their products, such as building and construction facilities, as well the textile manufacturing industries. Inspection of HBCDD diastereomer profiles at the three locations above, revealed the profile to resemble that of the technical mixture, with γ -HBCDD predominant (85-92 %), followed by α -HBCDD (6-12 %) and β -HBCDD (2-3 %) only present in small quantities, as shown in Figure 4-4. This could indicate fresh input sources at the locations of the analysed sediments, as the diastereomer profile in these samples differs markedly from that in other samples (Figure 4-3). In average, the diastereomer profile in the industrial area prevailed in γ -HBCDD, followed by α -HBCDD and only minor amounts of β -HBCDD, while in the non-industrial area the ratio between the three stereoisomers was more equilibrated (Figure 4-3).

Whether these fresh input sources of HBCDD derive from a certain industry (i.e. the building industry manufacturing thermal insulation, where HBCDD is primary applied in extruded (XPS) and expanded (EPS) polystyrene foam) has to be investigated through investigation on the presence of related industries at and around the three distinct locations mentioned above. Especially, when considering that HBCDD has been included in 2013 in the Stockholm Convention's Annex A for elimination (with exemptions for EPS and XPS in buildings) [8]. Similar to BDE-209, more recent sampling campaigns are needed and time trends need to be studied to see how concentrations and HBCDD profiles behave over time.

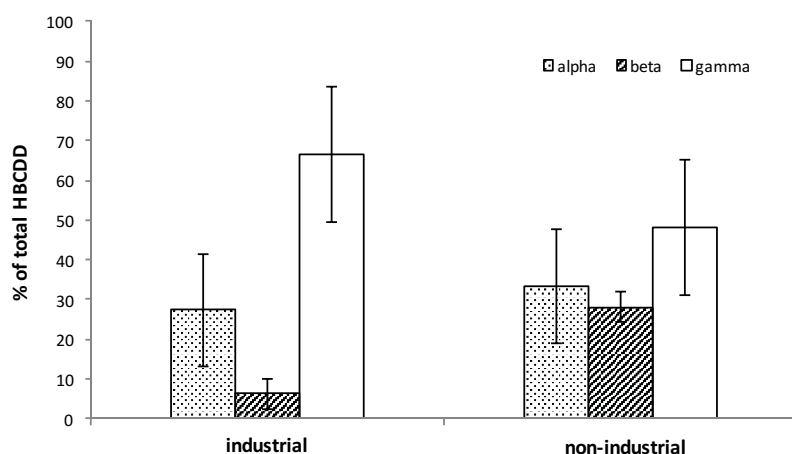


Figure 4-3. Average HBCDD diastereomer profile in industrial and non-industrial area

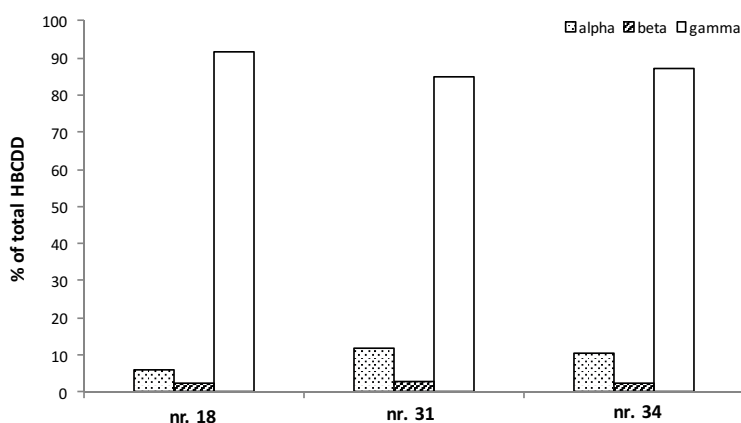


Figure 4-4. HBCDD diastereomer profile of 3 sampling sites (location nr. 18, 31 and 34) with comparatively high HBCDDs concentrations.

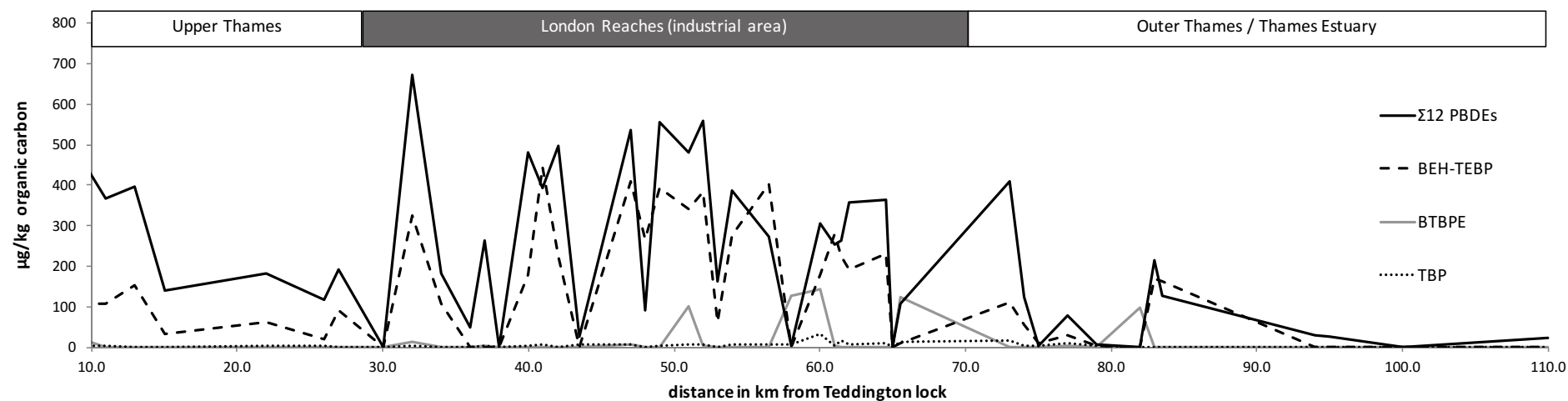
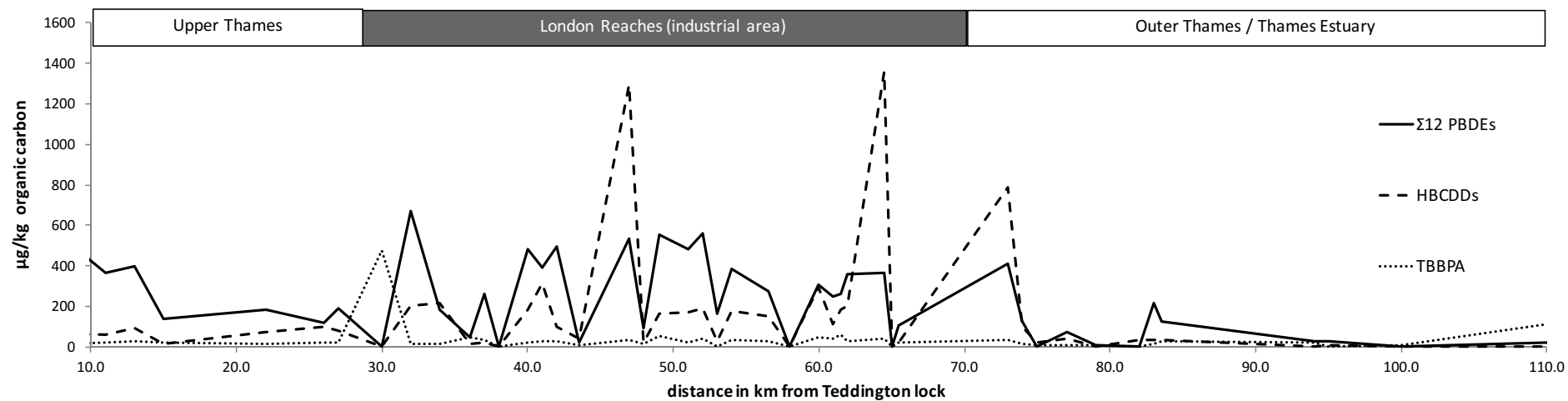


Figure 4-5. Spatial trends for Σ_{12} BDEs, HBCDDs and TBBPA (top) and Σ_{12} BDEs, BEH-TEBP, BTBPE and TBP (bottom) measured (in $\mu\text{g kg}^{-1}$ organic carbon) along the river Thames, with an approximate distance from Teddington Lock.

Figure 4-6 and Figure 4-7 illustrate the spatial variation in organic carbon-normalised concentrations of Σ_{12} BDEs and BDE-209 respectively. There is a general high-high-medium-low concentration profile from west to east for Σ_{12} BDEs (with average concentration values for the 4 zones 290, 309, 219 and 51 $\mu\text{g kg}^{-1}$ OC), while for BDE-209 a medium-high-high-very low profile (7291, 9299, 9834 and 3255 $\mu\text{g kg}^{-1}$ OC) can be observed. This could be a possible indication for different sources of the two groups of compounds. The general decline from west to east in both cases is probably driven by London as a major source of pollution, as well as flocculation-deposition of sediment controlled by salinity (salting-out). The four salinity zones indicated were adapted from the study of Pope *et al.* [230]. The fact that the BDE transect data is rather variable can be explained by the fact that the suspended particles can travel up and downstream by 10 - 20 km on one tide. The Thames sediments are subject to regular capital and maintenance dredging which has the potential to mobilise and redistribute sediments or requires disposal at sea or on-land. Recent evaluation of historical sediment profiles of mercury (Hg) [186] as well as surface distributions of phosphorus (P) [231] and natural tetraether lipids [185] confirm that contamination originates from both diffuse and point sources. Nevertheless, sites like Bow Creek (site nr. 15) which receive contamination discharged from the Lea Valley due to industrial activity, Barking (nr. 21), a site situated close to major sewage outfall Beckton STP and Tilbury (nr. 34) with its docks, power station and the STP show higher concentrations related to the intensive land-river-use.

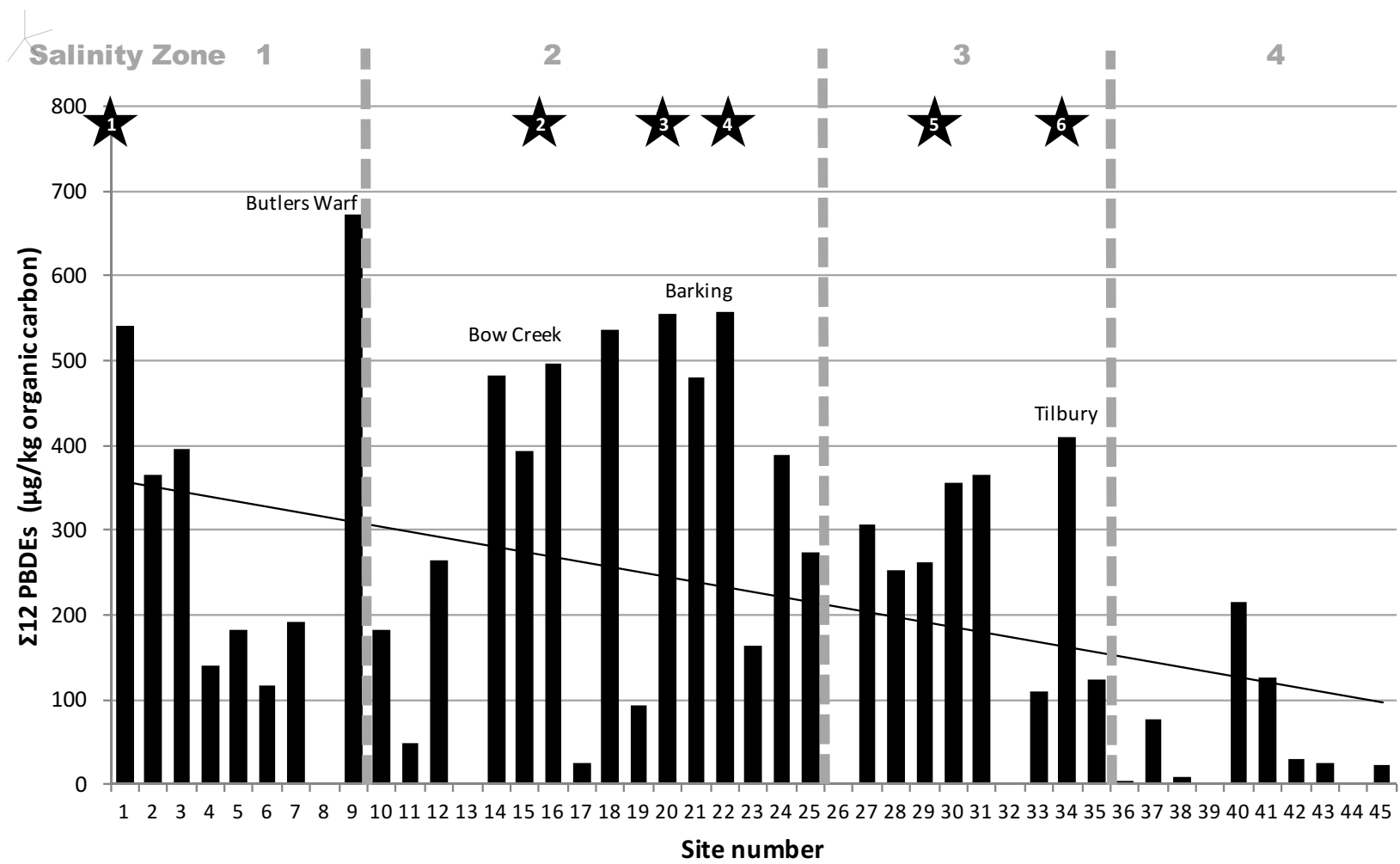


Figure 4-6. Concentrations ($\mu\text{g kg}^{-1}$ organic carbon) of Σ_{12} PBDEs in River Thames sediments at each sampling location. Stars represent the main discharge locations of sewage effluents; 1. Mogden; 2. Abbey Mills; 3. Beckton STP; 4. Crossness STP; 5. Long Reach STP; 6. Tilbury STP. Adapted from Lopes dos Santos and Vane [185]. STP – sewage treatment plants

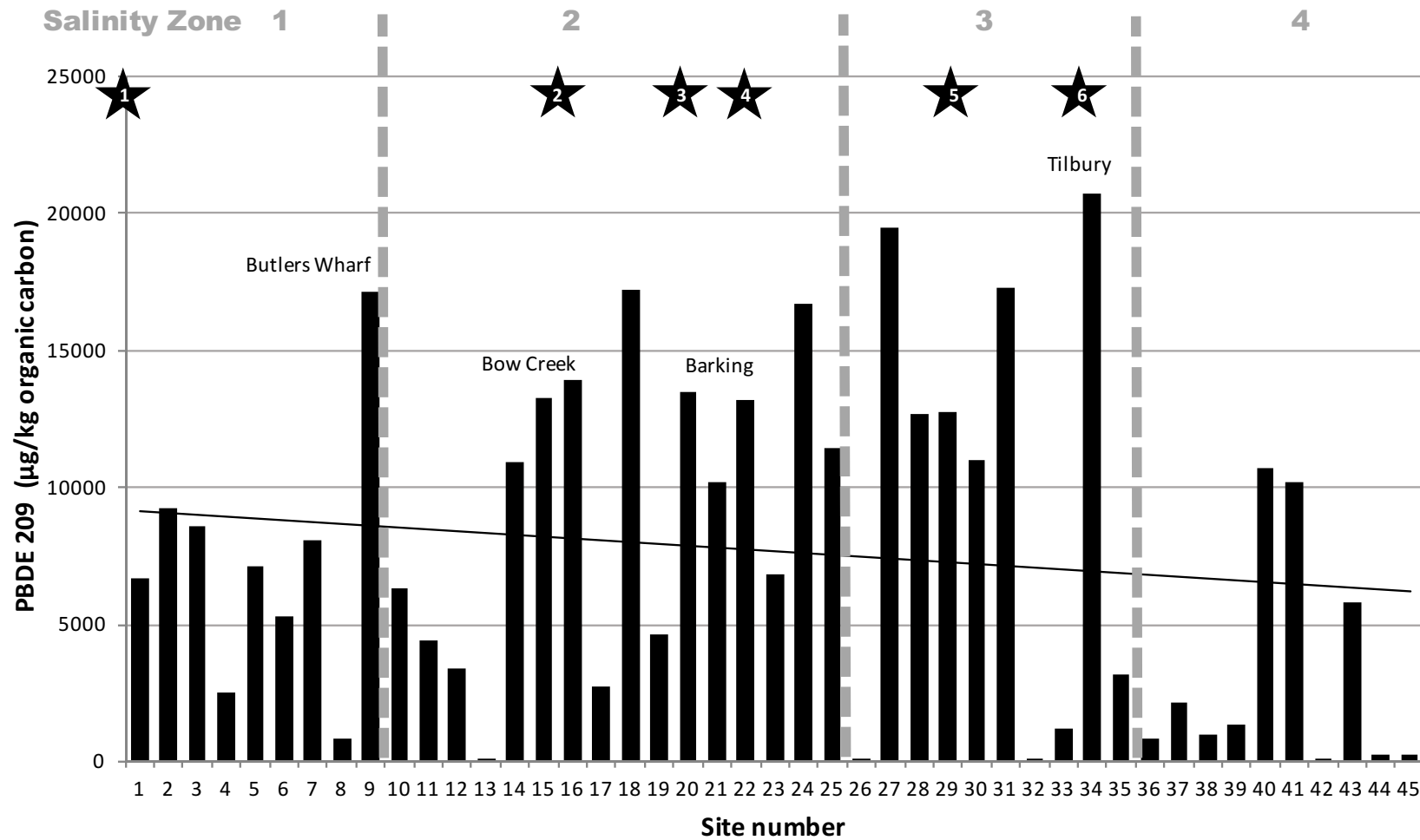


Figure 4-7. Concentrations ($\mu\text{g kg}^{-1}$ organic carbon) of BDE-209 in River Thames sediments at each sampling location. Stars represent the main discharge locations of sewage effluents; 1. Mogden; 2. Abbey Mills; 3. Beckton STP; 4. Crossness STP; 5. Long Reach STP; 6. Tilbury STP. Adapted from Lopes dos Santos and Vane [185]. STP – sewage treatment plants

4.4. PBDE / NBFR patterns

Figure 4-8 compares the average PBDE profile of the industrial area and the non-industrial one against the penta, octa and deca technical PBDE mix. While caution must be exercised when comparing congener profiles in environmental samples with those in the commercial formulations, as congener-specific differences in physicochemical properties will modify the congener profile between source and receptor. In general, no significant differences can be observed between the pattern of PBDEs between the industrial and non-industrial area. Compared to the technical Penta-BDE mixture, the PBDE profile pattern in our sediment samples is shifted towards lower brominated congeners such as BDE-28, possibly indicating debromination reactions. The figure further shows that even though the ratio between BDE-47 and 99 is shifted towards the latter congener, most likely due the stronger partition of BDE 99 to sediments, even though BDE-99 is also present at higher concentrations in the Penta-BDE mixture. For the Octa-BDE technical mixture, the higher contribution of BDE-206 than BDE-207 is indicative of a shift from the commercial formulations of both the octa and deca mix. This likely indicates debromination of BDE-209 as the source of the elevated BDE-206 levels [232], but might also underline that the octa mixture has not heavily been used. The technical Deca-BDE however, showed no deviation from the pattern in our sediment samples and possible debromination reactions in sediment samples need to be further investigated.

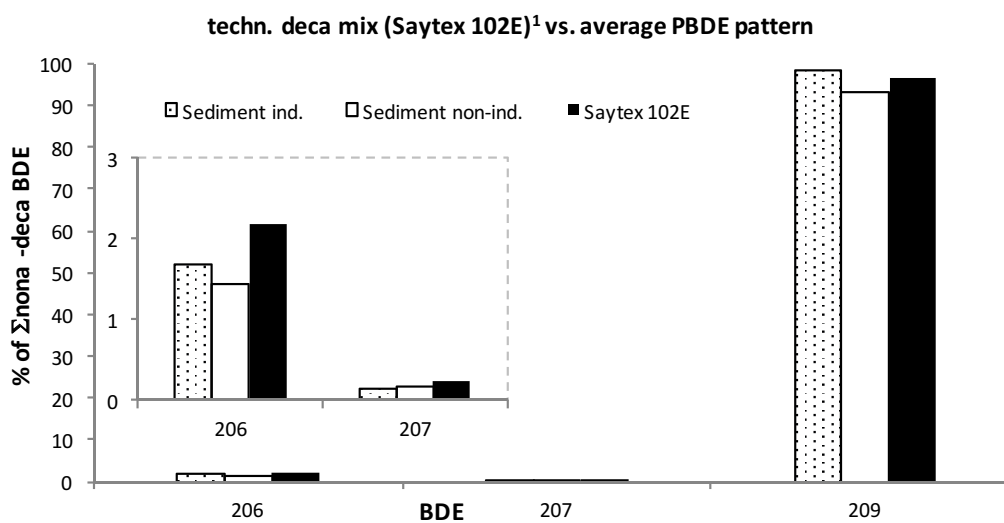
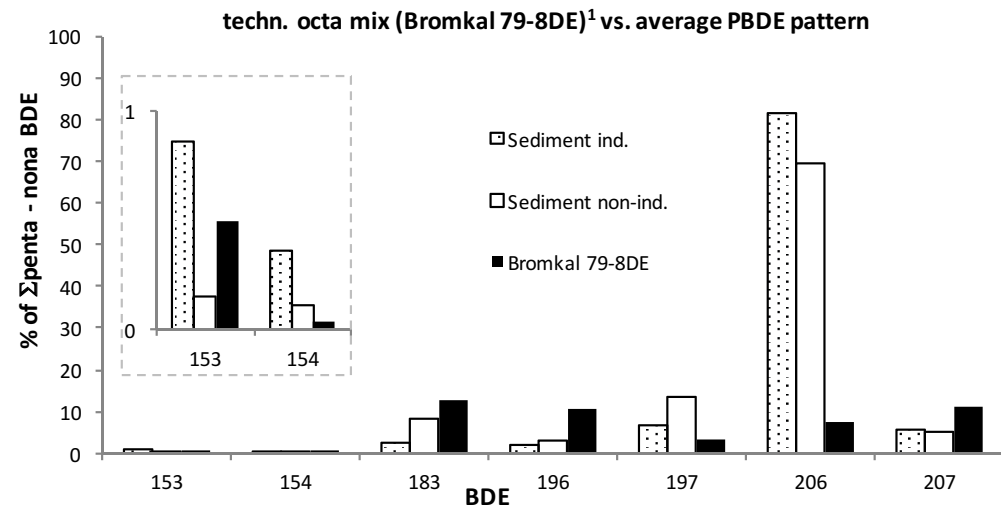
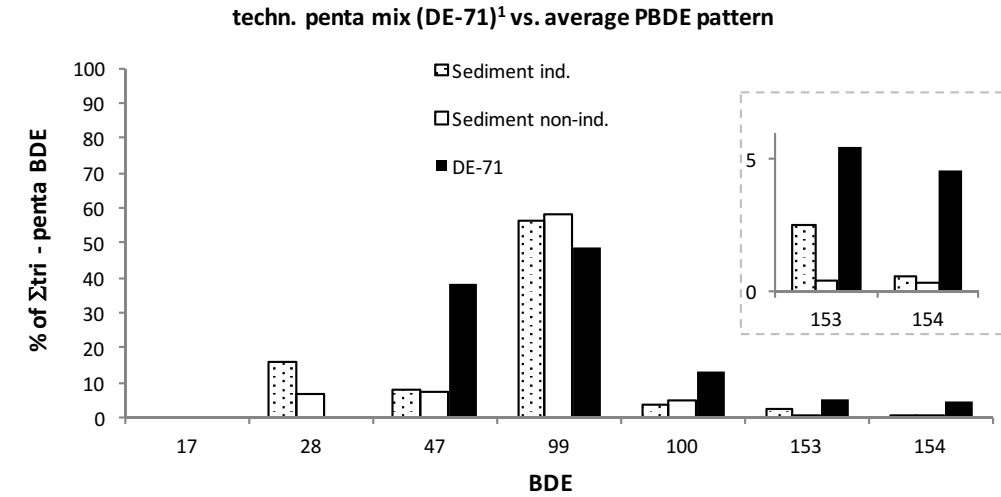


Figure 4-8. Comparison of an average PBDE profile in the industrial area (dotted) and outside the industrial area (white) to a technical penta / octa / deca BDE mix (black) – technical mixture values adapted from La Guardia et al. [233]

4.5. Screening for degradation products and other low production volume NBFRs

The UPLC-HRMS used in this study proved to be an excellent platform for the identification and quantification of PBDEs and NBFRs. Moreover, rapid HRMS analysis in full scan mode allows post-acquisition data analysis for further identification of compounds/transformation products of interest (e.g. potential degradation products, other NBFRs).

To screen for further brominated compounds in the sample set, a Br trace ($m/z = 78.918336 / 80.916290$) was queried from the full scan - all ion fragmentation (AIF) acquisition using Xcalibur software. This revealed the presence of brominated compounds with shorter retention times than brominated PBDEs. Further investigation of the accurate mass, isotope patterns and comparison to the high resolution mass spectrum of hydroxylated PBDE (OH-BDEs) standards revealed the identified peaks as OH-BDEs (further details are provided in 4.5.1). Unlike PBDEs, OH-BDEs have not been produced industrially or are by-products of technical brominated products [116, 117]. However OH-BDEs have been reported in biotic and abiotic samples of the aquatic and marine environment, such as salmon [116], mussels [118], algae [119] as well as sediments [120], surface waters [121] and sewage treatment plant effluents [122]. Studies suggest that they are natural products of marine environments, as well as a result of metabolic products from anthropogenic PBDEs [119, 121], however exact natural formation is not thoroughly understood yet [117]. The position of the hydroxyl group (OH-) seems to be an indicator of whether OH-BDE congeners are formed through oxidation or metabolic reactions [116, 118, 120]. Possible sources and transformation found in literature include microbial aerobic degradation [123, 124], photochemical reactions of bromophenols [125] and PBDEs [126], transformation of bromophenol by marine bacteria [127] and a red algae enzyme [117], reactions of PBDEs with atmospheric OH radicals [121], as well as in sewage treatment plants through oxidative reactions and excretion from human and animal

metabolism [121]. Whether the OH-BDEs detected in the sediment samples of this study are of environmental and/or biological origin is beyond the initial scope of this work and was not further investigated. However, since OH-BDEs have been reported to exhibit similar or even enhanced toxic [129] and estrogenic [130] effects on both human [131] and wildlife [132, 133] compared to PBDEs, their presence and relevance needs to be further investigated.

Barber *et al.* [217] reported on the presence of NBRs in UK sediments. However, screening of our sediment samples for those such as: 2,3,5,6,-tetrabromo-p-xylene (TBX), tris(2,3-dibromopropyl) phosphate (TDBPP), tetrabromo-bisphenoldiallylether (TBBPA-DAE), tetrabromobisphenol-bis(2,3-dibromopropylether) (TBBPA-DBPE), octabromotrimethylphenylindane (OBTMPI/OBIND), pentabromophenol (PBP) and pentabromobenzyl acrylate (PBB-Acr) did not reveal them to be present in our study.

4.5.1. Hydroxylated BDEs

Measurements of hydroxylated HO-BDE standards (2-HO-BDE-28 and 6-HO-BDE-47) in HESI mode revealed the presence of impurities (i.e. HO-BDE-28 standard contain traces of a HO-di-BDE as shown in

Figure 4-9, while the 6-HO-BDE-47 standard contains several impurities of HO-tri-BDE as illustrated in Figure 4-14, of which likely HO-BDE-28 at retention time 5.66). While in sediment sample nr. 22 HO-BDE-28 was identified due to comparative fragmentation measurements of the standard (Figure 4-11) and sediment sample (Figure 4-10), sediment sample nr. 21 revealed the presence of 6-HO-BDE-47, based again on comparable retention time, accurate mass and MS² profile (MS² of peak in sediment sample as shown in Figure 4-16 compared to standard measurement presented in Figure 4-15). Further, the impurity contained in HO-BDE-28 standard at retention time 5.23, was also detected in sediment sample nr. 21 and

supported by similar fragmentation spectra (standard in Figure 4-12 compared to sample in Figure 4-13).

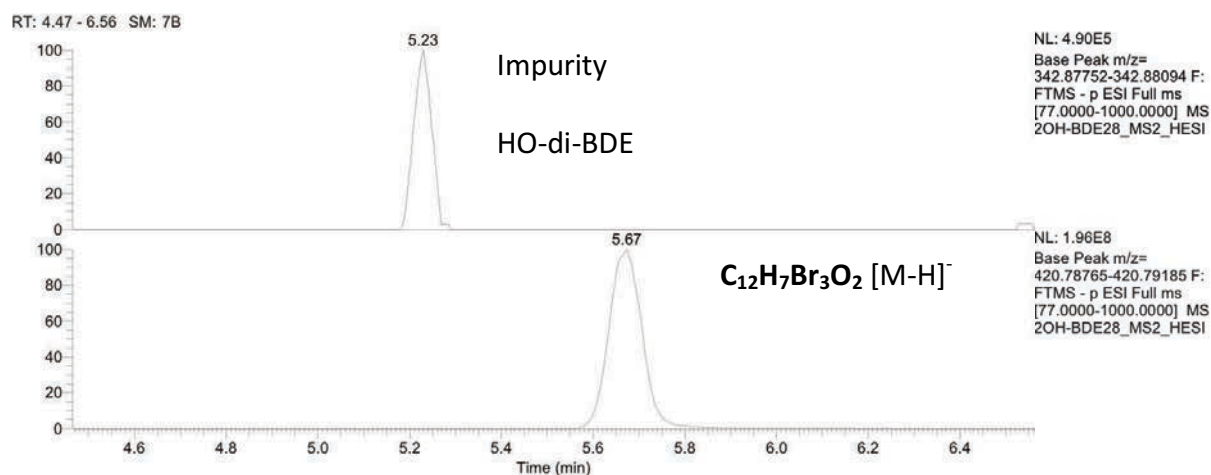


Figure 4-9. XICs of 2-HO-BDE28 ($C_{12}H_7Br_3O_2$) standard (bottom) measured in HESI, including the trace of a dibrominated impurity (top)

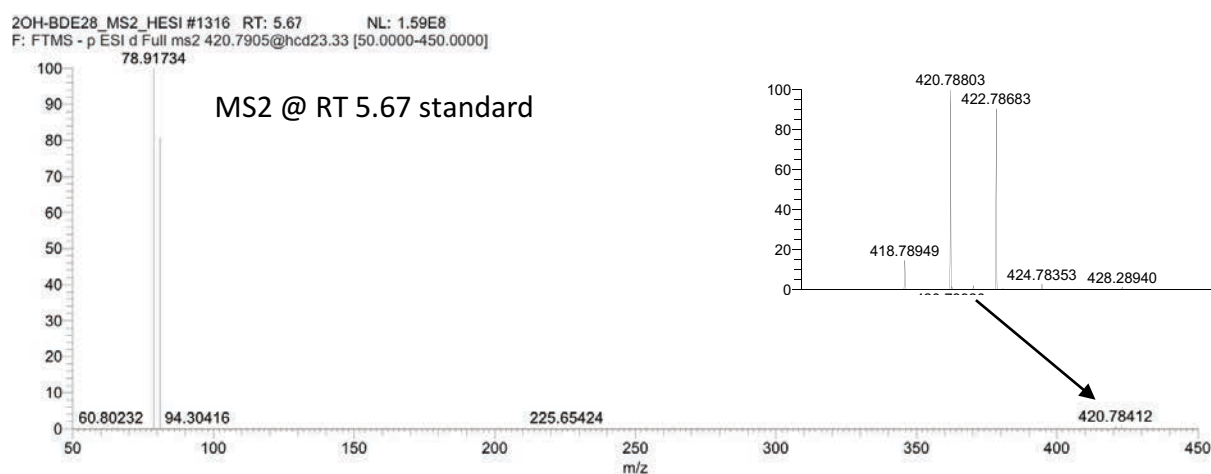


Figure 4-10. MS² fragmentation spectra of a 2-HO-BDE28 standard at retention time 5.67

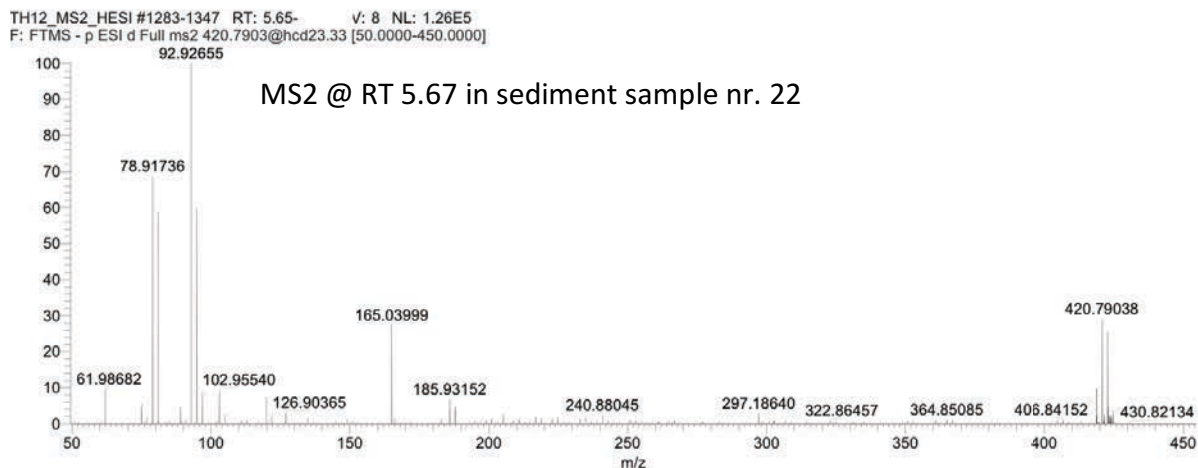


Figure 4-11. MS² fragmentation spectra of a sediment sample (nr. 22) at retention time 5.67

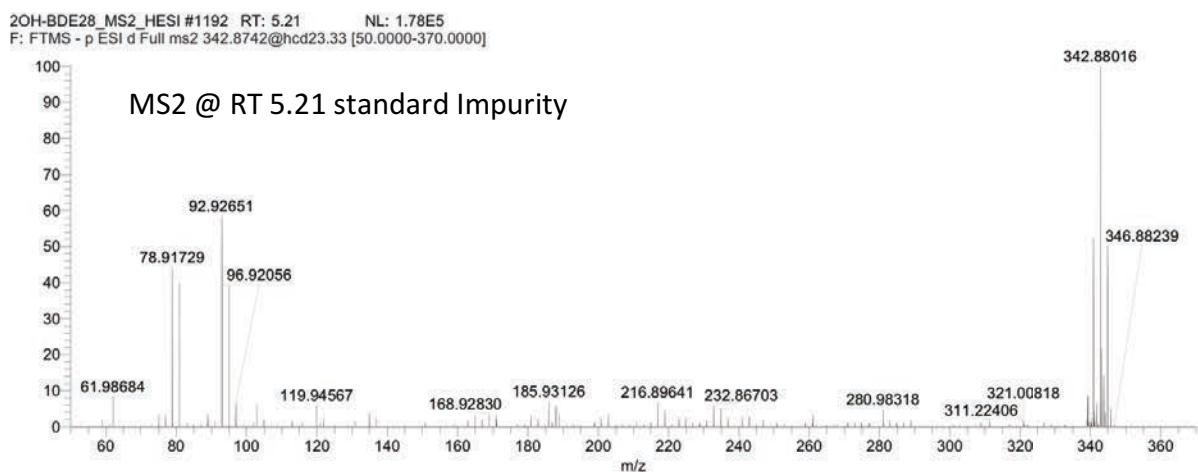


Figure 4-12. MS² fragmentation spectra of impurity in the 2-HO-BDE28 standard at retention time 5.21

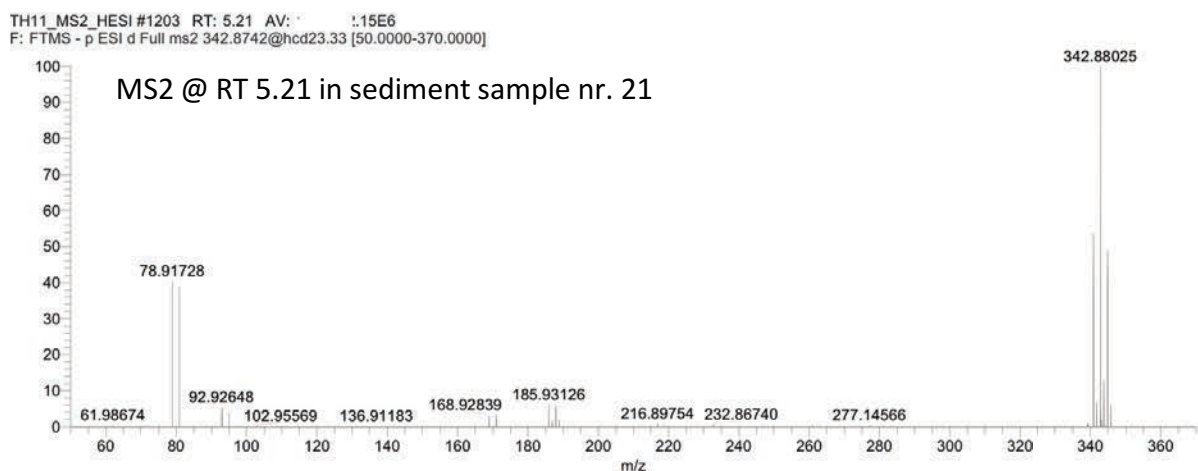


Figure 4-13. MS² fragmentation spectra of a sediment sample (nr. 21) at retention time 5.21

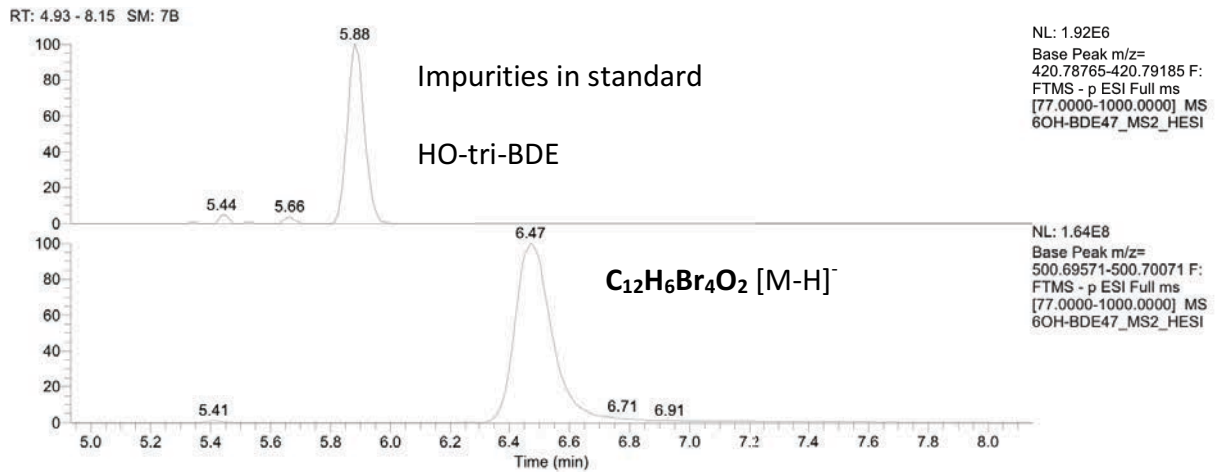


Figure 4-14. XICs of 6-HO-BDE47 ($C_{12}H_6Br_4O_2$) standard (bottom) measured in HESI, including the trace of 3 different dibrominated impurities (top)

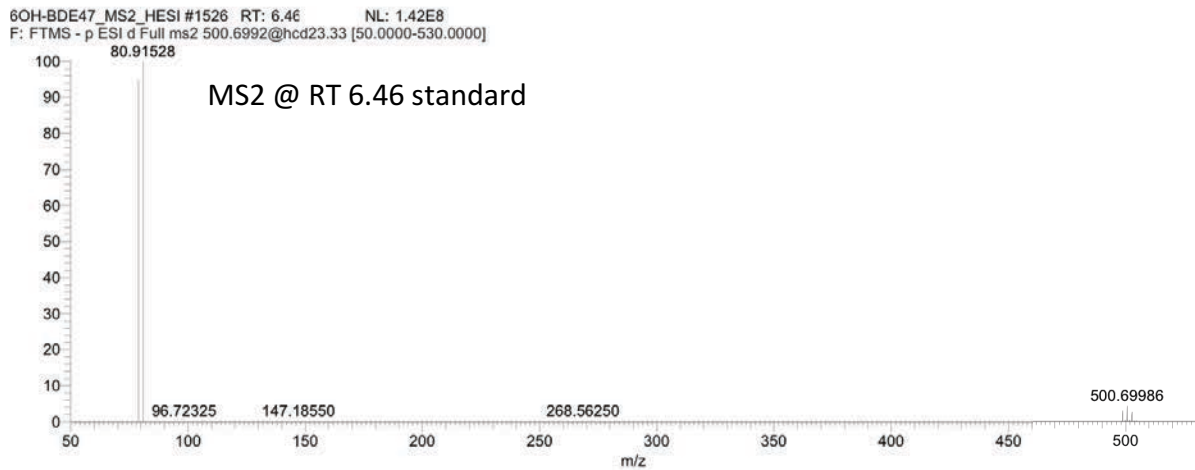


Figure 4-15. MS² fragmentation spectra of a 6-OH-BDE47 standard at retention time 6.46

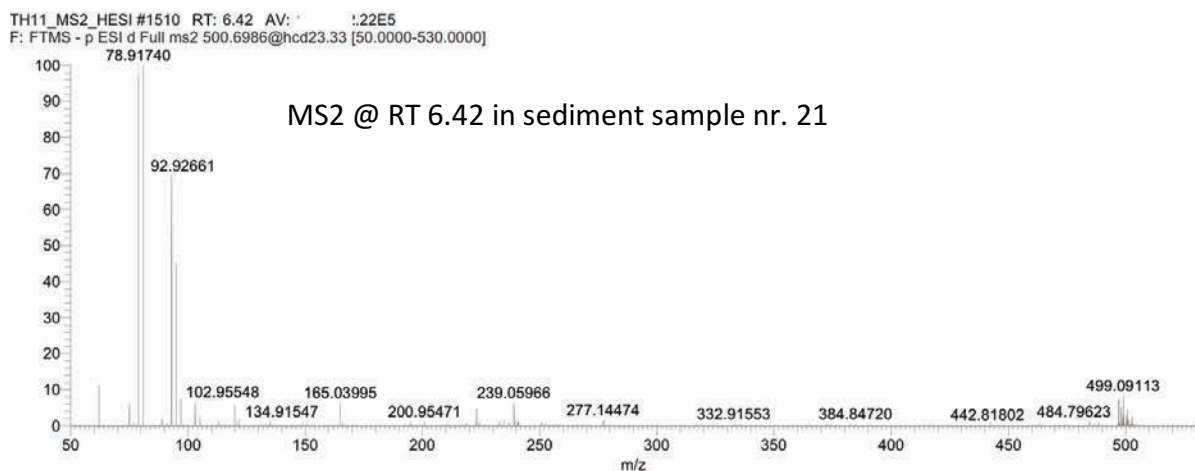


Figure 4-16. MS² fragmentation spectra of a sediment sample (nr. 21) at retention time 6.42

For hydroxylated HO-BDE there are several potential congeners for each depending on the position of the lost Br so retention times may vary, but accurate mass and MS² profile confirm the number of Br and not their positions. Finally, the fact they were separated on the column with different retention times precludes their formation within the source. Standards were not infused in to the mass spectrometer, but injected onto the UPLC column to make sure chromatographic separation was seen and confirm it is not an in-source fragmentation pattern. The presence of mono- and dibromophenols in these and other selected sediment samples further supports the occurrence of OH-BDEs in our samples through possible transformation reactions (i.e. bromophenol as a source for marine bacteria and some red algae enzymes) as earlier explained.

4.6. Conclusion

Flame retardants are mainly applied in consumer products and building materials. Populated areas such as London with its industrial area can act as a possible emission source. Since the river Thames passes through this area, it can act as an indicator for recent emissions such as NBFRs, but also show which of the legacy BFRs are still in use or reach the river through leachates. The spatial distributions indicate that the input and presence of industrial activity and sewage treatment plants is a major source of (N)BFRs to the river. Whether these compounds in the investigated area originate from leachates from consumer products on landfill sites, sewage treatment plants or are emissions from industry cannot be confirmed at this point. A study on the industries employing BFR in their products in the investigated area is necessary. Follow-up sampling campaigns, studies of time trends and investigation of suitable marker compounds appear warranted to obtain information on specific sources and take regulatory actions where necessary.

Results indicate that BDE-209 is the predominant congener in all samples, accounting for ~ 95 % of total PBDEs detected, with a concentration range of <math><0.1</math> to \Sigma_{12}BDEs in this study, as well as showing a similar concentration pattern along the river, possibly indicating a similar source input. Spatial variation analysis of the sediment samples further revealed that locations within the industrial area of London had significantly higher concentrations of Σ_{12} BDEs, HBCDDs, TBBPA, as well as BEH-TEBP, BTBPE and TBP. Therefore, it is suggested to especially track the latter three compounds as NBFrs candidates in future environmental studies. Analysis of HBCDD diastereomer patterns revealed samples from three locations within the industrial area possessed comparatively high concentrations and diastereomer profiles matching those of the technical mixture. This could possibly indicate fresh input sources at these locations at the time of sampling in 2011, but more recent samples are needed to understand time and concentration trends, if these sources persist, together with an investigation of the presence of industries and their industrial discharges to this region.

The presence of hydroxylated PBDEs suggests the presence of transformation products in the sediments. Sources, formation reactions and impact on the environment and human health of these compounds have to be further investigated, along with the presence of other possible transformation products.

More studies are needed to understand NBFRs and which ones might be the ones to target, with a special focus on compounds like BEH-TEBP (together with EH-TBB) and BTBPE, which act as a replacement of currently banned technical mixtures, PentaBDE and OctaBDE respectively. In this regard, sediment analysis can contribute to reveal which emerging BFRs are persistent and thus might pose an environmental problem in the long run. It has to be noted however that levels and pattern of NBFRs vary in different countries and factors like location and land-use have to be taken into account.

Chapter V – Photochemical transformation reactions of NBFRs

5.1. Overview

In this chapter the photochemical transformation of selected NBFRs was studied in various solvents under experimental and natural conditions, both indoors and outdoors. BFRs have been reported to be susceptible to various types of transformation reactions, including photochemical reactions [4]. These have been extensively studied, especially for PBDEs, with a particular focus on BDE-209, leading to an insight into degradation mechanisms and pathways. In general, degradation processes may alter the structure of compounds, leading to potential differences in characteristics and properties. Through dehalogenation and other transformation reactions there is the potential formation of more persistent, bioaccumulative and toxic halogenated species [98, 234]. *In vitro* studies for example showed that sunlight generated by-products of BDE-209 affected the expression of genes in chicken embryonic hepatocytes [235]. Therefore, it is essential to study and understand the formation of degradation products, their environmental fate, toxicological behaviour and ultimately, their presence in the environment and evaluate their potential adverse health effects.

5.1.1. PBDEs, HBCDDs and TBBPA

Photochemical transformation reactions have been reported to be caused by direct photolysis under the action of solar irradiation [98]. Several studies have investigated the photodegradation behaviour of PBDEs in various matrices, including organic solvents and aqueous phases, as well as gas and solid phases [236], both under experimental UV irradiation [99, 100] and natural sunlight conditions [232, 237]. The photodegradation mechanisms of

PBDEs are based either on reductive debromination or intramolecular elimination of HBr as the two major paths for the production of lower brominated BDEs [103, 238] and polybrominated dibenzofurans (PBDFs) [102, 236, 239], respectively.

Other derivatives formed from PBDEs include hydroxylated PBDEs (OH-PBDEs) [126] and bromophenols [240], as a result of the reaction of PBDEs with OH radicals originating from aqueous and atmospheric systems [236]. Additionally, OH-PBDEs have been reported to produce polybrominated dibenzo-p-dioxins (PBDDs) through photochemical ring closure [241]. It was further shown that dibromophenols have the potential to form OH-PBDEs through photoformation involving 2,6-bromophenoxy radicals [242].

Studies indicate that the reaction rate decreases with declining number of bromine atoms present in the compound for PBDEs. Hence, it is assumed that flame retardants with a higher degree of halogenation are likely to be subject to a faster photodegradation rate [234, 243]. Santos *et al.* reviewed different photochemical degradation mechanisms as a technique for the elimination of PBDEs in liquid systems [244].

There is little information on the photodegradation of HBCDDs. Two studies on dust samples reported the change in diastereomer pattern and reductive debromination of HBCDDs through the loss of HBr to form tetra- and pentabrominated derivatives (TBCDDs/PBCDDs) [101, 245]. However, no debromination or isomerization of HBCDD diastereomers was observed in textiles under natural sunlight exposure [102]. Also studies on photodegradation of TBBPA are scarce. Major degradation products of TBBPA include isopropylphenol derivatives [246].

5.1.2. NBFRs

To date, only a limited number of studies have focused on the photolytic degradation of NBFRs. While some data is available on controlled exposure experiments, field-based fate studies are lacking. The first study to report the photodegradation of EH-TBB and BEH-TEBP, alongside nonaBDE congeners, was in 2009 in three different solvents (methanol, toluene and THF) which were exposed to natural sunlight. The authors reported the degradation rate constant of EH-TBB and BEH-TEBP to be an order of magnitude lower compared to nonaBDEs and identified debrominated products as result of the degradation [103]. The photochemical transformation of EH-TBB and BEH-TEBP was also investigated in a mesocosm with the formation of similar debrominated products [247]. Further this group also analysed the photodegradation of BTBPE and TBBPA-DBPE using the same experimental set-up, identifying degradation products, 2,4,6-TBP through possible ether cleavage for BTBPE, while TBBPA was likely formed through hydrolysis from TBBPA-DBPE.

The photolytic degradation of DBDPE was studied in a variety of matrixes (hexane, THF, methanol/water, humic acid/water and silica gel) under UV irradiation and in hexane under natural light exposure [248]. Results indicate that initially nona-BDPE is formed with subsequent degradation to produce lower brominated congeners (octa- and hepta-BDPEs) in all matrices at different degradation rates. However, no debromination products were formed in plastic samples containing DBDPE exposed to natural sunlight [249].

Photodegradation of other NBFRs, including TBP-AE (ATE), TBP-BAE (BATE), TBP-DBPE (DPTE), BTBPE and TTBP-TAZ was also investigated. Several photoproducts and pathways were identified for DPTE and BTBPE, DPTE was transformed through debromination on the phenyl, while debromination and ether bond cleavage were the main photo transformation pathways for BTBPE [250].

There are various procedures for measuring degradation reactions and differing results for the same compound might be obtained, due to the choice of solvent/matrix, instrumentation and selection of wavelengths [98]. The effect of different solvents in photochemical transformations for selected PBDEs has been investigated [28] and their mechanisms and predicting descriptors studied [251]. A mesocosm study revealed that selected NBRs are persistent in sediment samples and photodegradation occurs to a higher extent in the water column compared to the sediment compartment [247].

5.1.3. Calculations and QA/QC

Calculations of photodegradation rate constants and half-lives was fitted to a first-order kinetic model based on Equation 5-1:

$$C_t = C_0 e^{-k t} \quad \text{(Equation 5-1)}$$

where C_t represents the concentration at a selected time t , C_0 is the initial concentration and k is the degradation rate constant. To check for 1st order kinetics the natural logarithm (\ln) of the concentration was plotted against time. The fitness of the model was based on linearity (R^2) of the correlation. The negative slope of the equation equals to the rate constant k .

For exposure experiments following a 1st order kinetic model, half-lives were calculated according to equation 5-4, which was derived from 5-1 through equations 5-2 and 5-3.

$$\frac{\ln C_0}{C_t} = k \times t \quad \text{(Equation 5-2)}$$

$$\frac{\ln C_0}{C_0/2} = \ln 2 = k \times t_{\frac{1}{2}} \quad \text{with } \ln 2 \approx 0.693 \quad \text{(Equation 5-3)}$$

$$t_{\frac{1}{2}} = \frac{0.693}{k} \quad \text{(Equation 5-4)}$$

Dark control samples were employed to control for any reactions occurring in the absence of light. Dark control samples, for both indoor and outdoor exposure experiment did not show any reduction in concentration and no presence of degradation products.

Temperature measurements over the time of experiment for indoor experiments (Figure 5-1) showed mean values of $22.9\text{ }^{\circ}\text{C} \pm 3.1\text{ }^{\circ}\text{C}$ (light-exposed) and $23.3\text{ }^{\circ}\text{C} \pm 3.3\text{ }^{\circ}\text{C}$ (dark control), while for outdoor exposure experiments (Figure 5-2) mean values were $21.7\text{ }^{\circ}\text{C} \pm 3.2\text{ }^{\circ}\text{C}$ (light-exposed) and $21.5\text{ }^{\circ}\text{C} \pm 3.3\text{ }^{\circ}\text{C}$ (dark control). Therefore, it was assumed that due to comparable values the temperature is unlikely to affect the degradation between light-exposed and dark control samples both indoors and outdoors. For UV-B/C measurements the temperature within the incubator was kept constant at $20\text{ }^{\circ}\text{C} \pm 0.1\text{ }^{\circ}\text{C}$ for both the light-exposed and dark control samples.

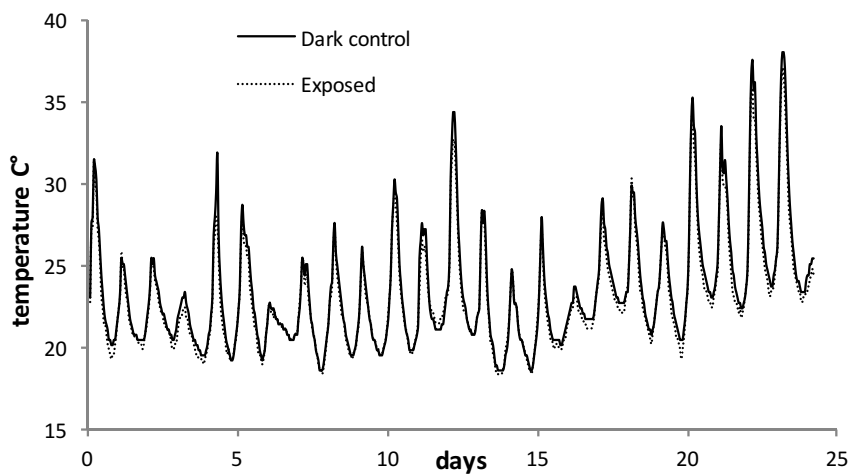


Figure 5-1. Temperature profile for indoor exposure experiment (05.08.-29.08.2017), solid line: dark control, dotted line: exposed samples

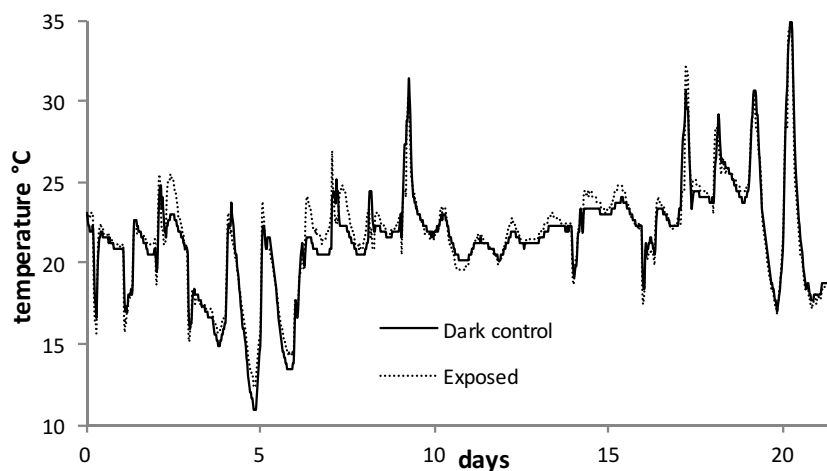


Figure 5-2. Temperature profile for outdoor exposure experiment (08.08.-29.08.2017), located at N 52° 27' 3" latitude and W 1° 55' 50" longitude; solid line: dark control, dotted line: exposed samples

To obtain an estimate of the sunlight irradiation during outdoor exposure global hourly radiation values in KJ/m^2 were obtained from a close-by weather station in Coleshill, converted to W/m^2 (KJ/m^2 divided by 3.6) and plotted as shown in Figure 5-3. Five sets of samples were taken during the total exposure period at different time points as indicated by the black arrows. Further, as illustrated in Figure 5-4 cumulative irradiation values were calculate for each of the five sample collection points (2761, 28036, 34999, 45949 and 58022 W/m^2 accordingly), by addition of all the radiation values from the beginning of the exposure period until respective sample collection time. These irradiation levels can be used as a mean to normalize the data and compensate for the fluctuation of solar radiation intensity during different sampling times (day times, weeks etc.) and locations, also when comparing studies.

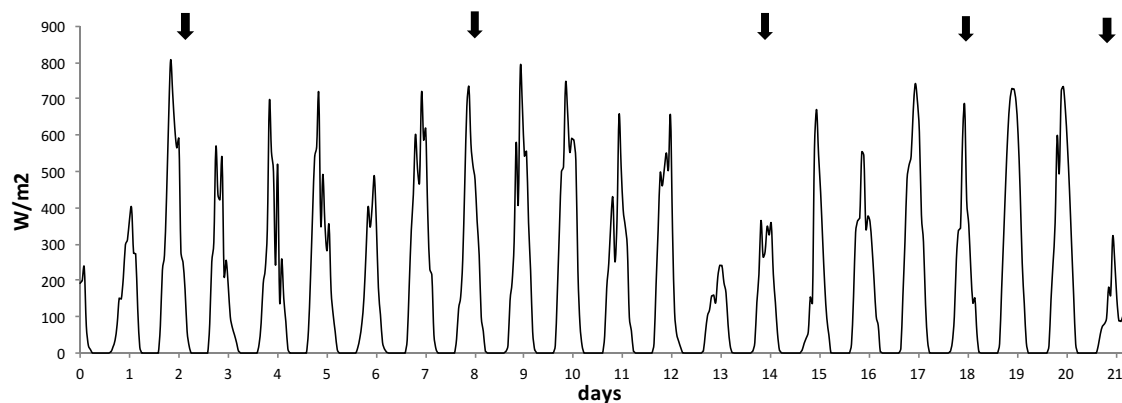


Figure 5-3. Solar irradiation data in W/m^2 (measured at Coleshill, UK – located at N 52° 28' 57'' latitude and W 1° 41' 46'' longitude – obtained from MetOffice) for outdoor exposure time period, black arrows indicate the five sampling points.

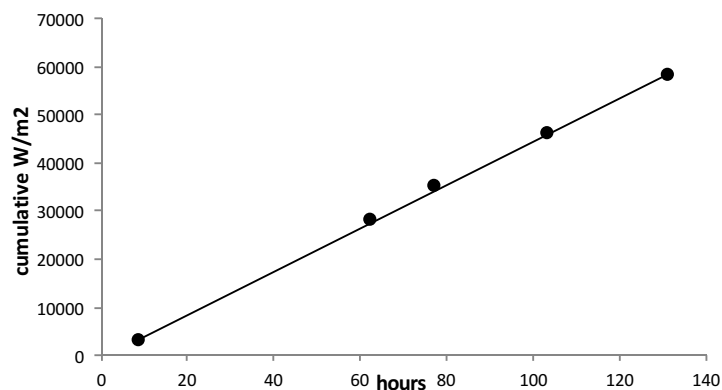


Figure 5-4. Cumulative irradiation in W/m^2 of five samples taken during outdoor exposure

5.2. Exposure Experiments

5.2.1. Indoor exposure

Results for indoor exposure experiments for EH-TBB, BEH-TEBP, BTBPE and DBPDE in toluene, hexane and methanol indicate degradation of parent compounds over the exposure period and degradants were identified. First-order kinetics did fit the decay of the compounds only to a certain degree, as judged by the linearity (R^2) of the decay, thus these results have to be interpreted with caution. Graphs of the kinetics and degradation can be found in Appendix III.

Table 5-1. Photodegradation kinetics for indoor exposure experiments for EH-TBB, BEH-TEBP, BTBPE and DBPDE, including half-lives $t_{1/2}$ and linearity of the decay R^2

analyte	solvent	rate constant k (h^{-1})	$t_{1/2}$ (h^{-1})	R^2
EH-TBB	toluene	0.0022	315	0.88
	hexane	0.0007	990	0.55
	methanol	0.0015	462	0.84
BEH-TEBP	toluene	0.0010	693	0.85
	hexane	0.0004	1732	0.83
	methanol	0.0026	267	0.96
BTBPE	toluene	0.0025	277	0.62
	hexane	0.0012	578	0.73
	methanol	0.0015	462	0.85
DBDPE	toluene	0.0037	187	0.86
	hexane	0.0034	204	0.85
	methanol	0.0053	131	0.78

5.2.2. Outdoor solar irradiation exposure

Resulting degradation rate constants and half-lives for outdoor solar exposure experiments for EH-TBB, BEH-TEBP, BTBPE and DBPDE in toluene, hexane and methanol are summarised in Table 5-2. Degradation followed first-order kinetics (except for BTBPE in methanol with a R^2 value of 0.69). Again, graphs of kinetics and decay can be found in Appendix III. When, comparing these with the values obtained for indoor experiments, half-lives are an order of magnitude higher indoors, except for BTBPE where degradation values were found to be

comparable between indoor and outdoor exposure and might relate to a more stable structure needing more energy input to form transformation products. Degradation rates for all compounds were comparable in toluene and hexane, while a faster transformation was observed in methanol.

Table 5-2. Photodegradation kinetics for outdoor sunlight exposure experiments for EH-TBB, BEH-TEBP, BTBPE and DBDPE, including half-lives $t_{1/2}$ and linearity of the decay R^2

analyte	solvent	rate constant k (h^{-1})	$t_{1/2}$ (h^{-1})	R^2
EH-TBB	toluene	0.049	14.1	0.98
	hexane	0.045	15.4	0.97
	methanol	0.063	11.0	0.98
BEH-TEBP	toluene	0.030	23.1	0.98
	hexane	0.035	19.8	0.98
	methanol	0.066	10.5	0.95
BTBPE	toluene	0.002	346	0.94
	hexane	0.002	346	0.93
	methanol	0.003	231	0.69
DBDPE	toluene	0.030	23.1	0.89
	hexane	0.035	19.8	0.96
	methanol	0.066	10.5	0.97

Davis *et al.* reported half-lives of EH-TBB in toluene and methanol with 2.7 and 1.6 h^{-1} , respectively, while for BEH-TEBP half-lives of 2.4 and 3.7 h^{-1} were calculated in these solvents [103]. These values are 3 to 10 times lower compared to our findings, likely caused by differences in the experimental conditions and set-up.

5.2.3. UV-exposure

Degradation kinetics of UV-B/C exposure experiments for EH-TBB, BEH-TEBP, BTBPE and DBPDE in methanol are summarised in Table 5-3. Degradation rate constants were higher and half-lives shorter for all compounds, compared to the indoor / outdoor exposure experiments. However, except for BTBPE, no significant difference in kinetics between UV-B and UV-C exposure was visible. Differences for BTBPE might result from its chemical structure and

stability of the compound, compared to the other investigated NBRs. This difference was also observed for outdoor solar irradiation experiments for BTBPE as shown earlier in Table 5-2. UV-C energy input however seems sufficiently high to compensate for these differences between BTBPE and the other compounds. Detailed graphs used for calculation are shown in Appendix III.

Table 5-3. Photodegradation kinetics (rate constant k and half-life $t_{1/2}$) for UV-B / UV-C exposure experiments calculated for EH-TBB, BEH-TEBP, BTBPE and DBDPE in methanol, including degradation rate constant k , half-lives $t_{1/2}$ and linearity of the decay R^2

analyte	UV-B			UV-C		
	k (h^{-1})	$t_{1/2}$ (h^{-1})	R^2	k (h^{-1})	$t_{1/2}$ (h^{-1})	R^2
EH-TBB	0.150	4.6	0.92	0.141	4.9	0.99
BEH-TEBP	0.145	4.8	0.99	0.147	4.7	0.98
BTBPE	0.019	36.5	0.93	0.141	4.9	0.99
DBDPE	0.138	5.0	0.91	0.133	5.2	0.95

5.3. Degradation products

Degradation products in this chapter were identified based on a combination of the bromine trace and elemental composition suggestions obtained from Xcalibur (as explained in 3.2.1), as well as earlier reported transformation products found in literature.

5.3.1. EH-TBB (2-ethylhexyl-2,3,4,5-tetrabromobenzoate)

Degradation products identified for EH-TBB are listed in Table 5-4. Two main degradation products were formed through stepwise reductive debromination, with the loss of 1 and 2 bromines. XICs for identified products are shown in Figure 5-5 and Figure 5-6 for UV-C and outdoor solar exposure, respectively. Both the outdoor and UV-C exposure experiment indicate the formation of comparable degradation products. The presence of several peaks for P1 and P2 in the XIC traces possibly relates to the difference in the position specific arrangement of the bromine atoms in the compound, as the formation of different stereoisomers for di- and tribrominated EH-TBB is possible. Differences between solar

outdoor exposure and UV-C experiment can be observed for these stereoisomers and thus the type of energy source has to be taken into account when conducting photolysis experiments. In the XIC of degradation product P1 in both Figure 5-5 and Figure 5-6 a peak at retention time 7.85 is visible, eluting after the parent compound at 7.79. The formation of this was observed in all experiments, but not in the dark control samples. Normally, the formation of degradation products lighter in mass than the parent compound leads to earlier elution and the observed peak can currently not be explained.

As shown in the bromine trace of Figure 5-5, compared to Figure 5-6, two peaks at retention times of 2.76 and 2.95 indicate the presence of brominated degradation products with comparatively low masses and/or increased polarity for the UV-C irradiation only. However, no transformation product could be positively identified at the indicated retention times. The presence of these in the UV-C experiments only, could be explained by the difference in energy source input between these two experiments.

Table 5-4. Identified EH-TBB (C₁₅H₁₈Br₄O₂) degradation products, including measured accurate mass-to-charge and mass deviation; tentative formula and measured ion

#	Accurate m/z	degradation products	formula	measured ion	ion formed	ppm
	484.87856	EH-TBB	C ₁₅ H ₁₈ Br ₄ O ₂	[C ₁₅ H ₁₈ Br ₃ O ₃] ⁻	[M-Br+O] ⁻	-3.7
P1	406.96860	tribrominated EH-TBB	C ₁₅ H ₁₉ Br ₃ O ₂	[C ₁₅ H ₁₉ Br ₂ O ₃] ⁻	[M-Br+O] ⁻	-3.9
P2	327.06013	dibrominated EH-TBB	C ₁₅ H ₂₀ Br ₂ O ₂	[C ₁₅ H ₂₀ BrO ₃] ⁻	[M-Br+O] ⁻	-4.0

These two debrominated degradation products P1 and P2 have been tentatively reported earlier by Davis *et al.* [103] and de Jourdan *et al.* [247], in both cases measured on GC-MS instrumentation. Additionally, it was reported that several other brominated transformation products were detected in their experiments, but structures could not be elucidated and molecular ion peaks determined. Further investigation in our full scan data is required, along with the need for authentic standards of these degradants.

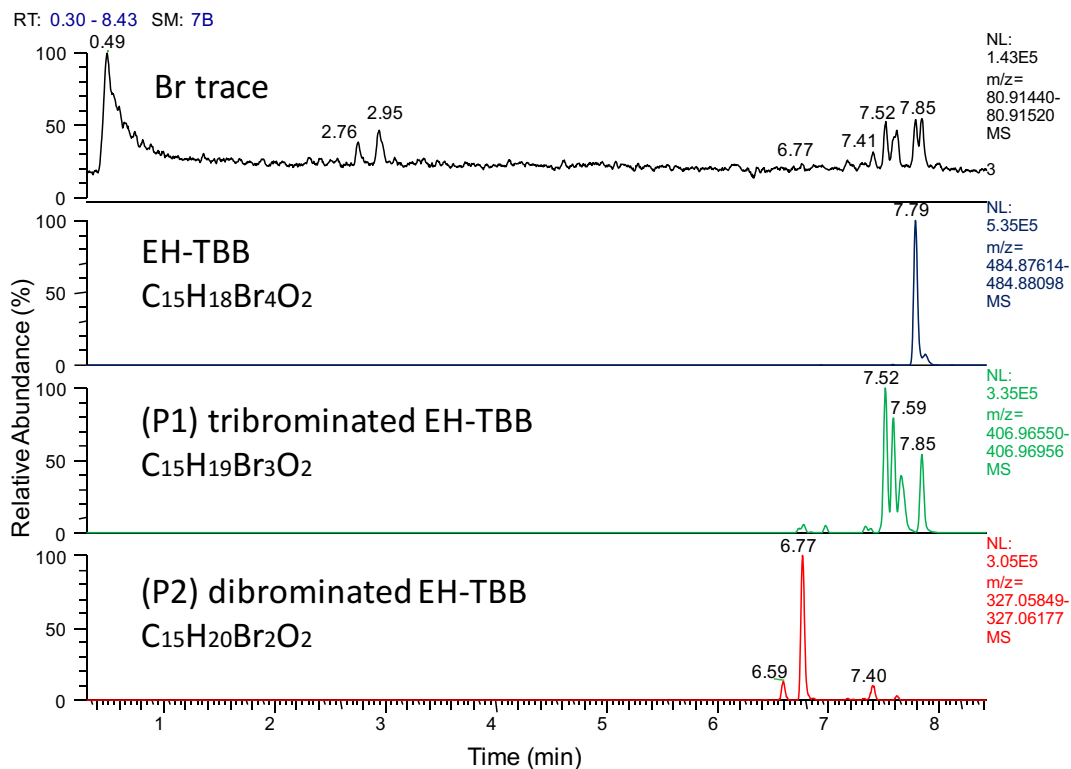


Figure 5-5. XICs of EH-TBB and identified photodegradation products P1 (tribrominated) and P2 (dibrominated) in methanol after 22 h of UV-C irradiation

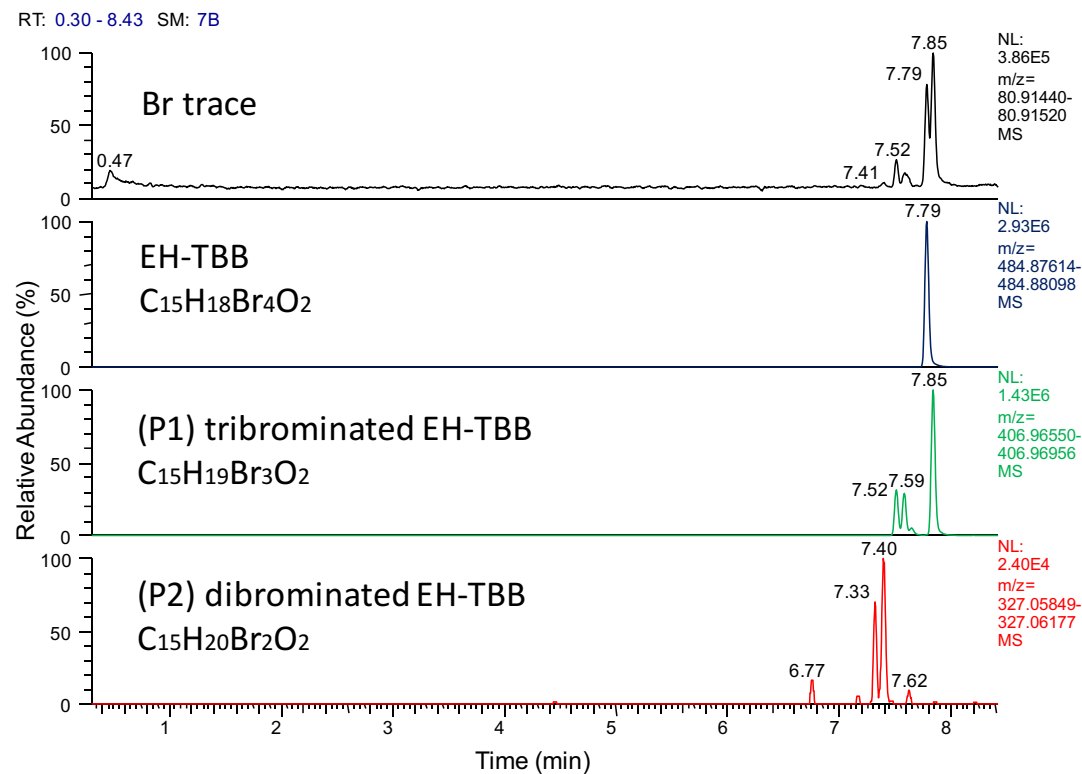


Figure 5-6. XICs of EH-TBB and identified photodegradation products P1 (tribrominated) and P2 (dibrominated) in methanol after 9 h of outdoor solar exposure

Formation of debromination products P1 and P2 for EH-TBB is illustrated in Figure 5-6, indicating a step-wise reaction with initial formation of P1, followed by a subsequent decline with an increased formation of P2. These products were quantified based on the same external calibration used for the parent compound, under the error-prone assumption of the same response factor. The sum of all areas in a mass trace was used for calculations, but further differentiation might be necessary for a more profound understanding. The relative amount indicated in the figure, was then calculated by dividing the concentration of transformation products by the initial concentration of the parent compound. Corrections however were made to account for the difference in molecular weight of parent and degradant, by multiplying the obtained percentage degradation by the ratio of molecular weight of the proposed degradant formula divided by the original molecular weight of the respective parent compound. Further research and the availability of standards of these degradation products are needed to facilitate quantification and better understanding on the formation of these degradants. Therefore, caution should be exerted when interpreting these graphs for EH-TBB and the other NBFs investigated in this chapter.

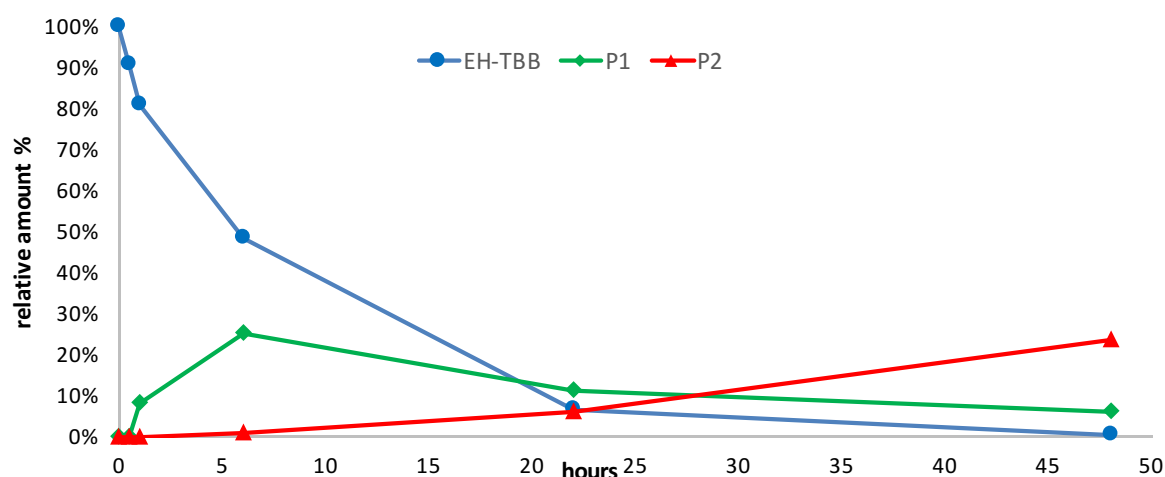


Figure 5-7. Relative amount of EH-TBB and its debromination products in methanol at different UV-C irradiation times

5.3.2. BEH-TEBP (bis(2-ethylhexyl)tetrabromophthalate)

Degradation products for BEH-TEBP are listed in Table 5-4. Three main degradation products P1, P2 and P3 were formed through stepwise reductive debromination as with EH-TBB, but with the loss of up to 3 bromines. Identified products are shown in Figure 5-8 and Figure 5-9 for UV-C and outdoor solar exposure, respectively, while Figure 5-10 show the stepwise formation of these degradation products over time. Davis *et al.* [103] also reported the presence of di- and tribrominated BEH-TEBP, but not monobrominated. Further, the group reported the presence of several other di- and tribrominated analogues, while most of them were missing both alkane branches. Our data does not indicate the presence of the latter compounds, but further investigation might be necessary. De Jourdan *et al.* proposed the formation of an anhydride in his photo transformation experiments as shown in Figure 5-11 [247]. However, this was not detected in any of our conducted experiments. Their experiments were conducted in an aquatic mesocosm, where interactions and factors influencing photolysis differ from our experiments. Similar to EH-TBB, degradation products P1 and P2 form several peaks, thus indicating the possible presence of stereoisomers of the debrominated BEH-TEBP.

Table 5-5. Identified BEH-TEBP (C₂₄H₃₄Br₄O₄) degradation products, including measured accurate mass-to-charge and mass deviation; tentative formula and measured ion

#	m/z	Degradation products	formula	measured ion	ion formed	ppm
	640.99165	BEH-TEBP	C ₂₄ H ₃₄ Br ₄ O ₄	[C ₂₄ H ₃₄ Br ₃ O ₅] ⁻	[M-Br+O] ⁻	-3.9
P1	563.08142	tribrominated BEH-TEBP	C ₂₄ H ₃₅ Br ₃ O ₄	[C ₂₄ H ₃₅ Br ₂ O ₅] ⁻	[M-Br+O] ⁻	-3.9
P2	483.17358	dibrominated BEH-TEBP	C ₂₄ H ₃₆ Br ₂ O ₅	[C ₂₄ H ₃₆ BrO ₅] ⁻	[M-Br+O] ⁻	-3.3
P3	405.26294	monobrominated BEH-TEBP	C ₂₄ H ₃₇ BrO ₅	[C ₂₄ H ₃₇ O ₅] ⁻	[M-Br+O] ⁻	-4.2

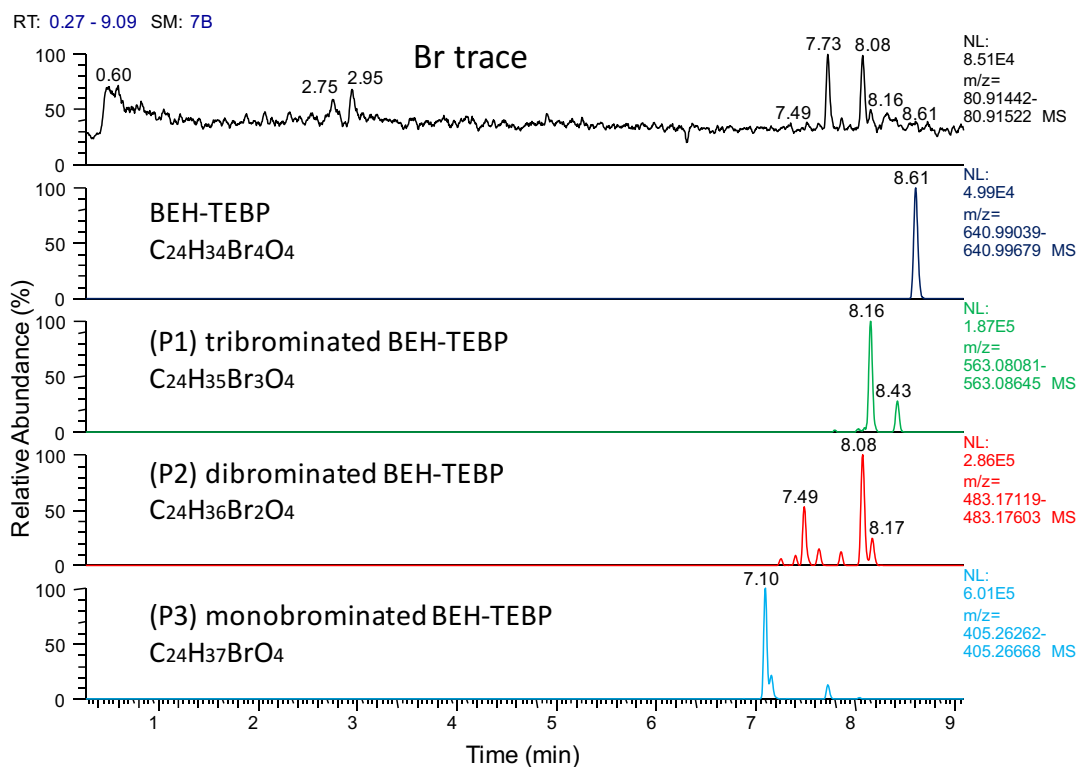


Figure 5-8. XICs of BEH-TEBP and its photodegradation products P1 (tribrominated), P2 (dibrominated) and P3 (monobrominated) in methanol after 22 h of UV-C irradiation

Similarly, like for EH-TBB, the Br trace for BEH-TEBP in Figure 5-8, in comparison to Figure 5-9, indicates the presence of brominated degradants at lower retention times 2.75 and 2.95, which could however not be elucidated. However, due to the structural similarity of EH-TBB and BEH-TEBP the formation of similar transformation products seems plausible. The formation of the three debrominated products in Figure 5-10 again indicates a stepwise reaction with sequential debromination occurring.

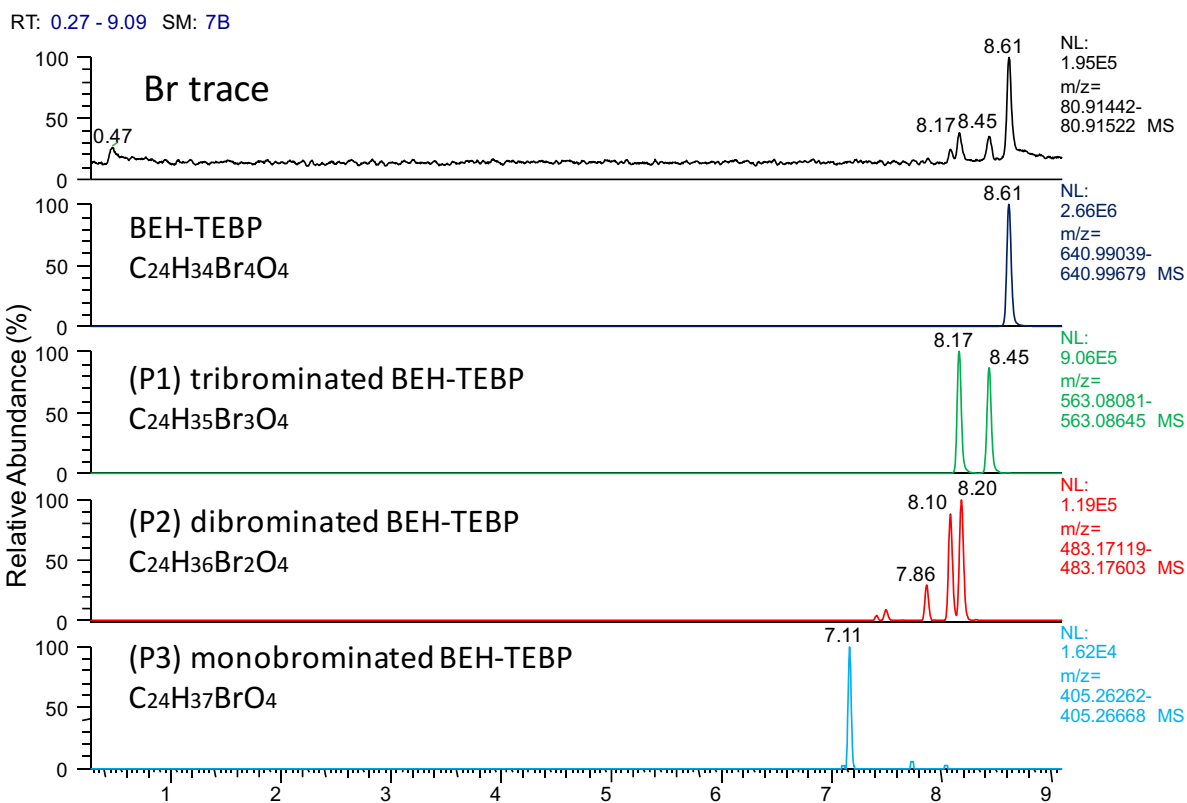


Figure 5-9. XICs of BEH-TEBP and its photodegradation products P1 (tribrominated), P2 (dibrominated) and P3 (monobrominated) in methanol after 9 h of outdoor solar exposure

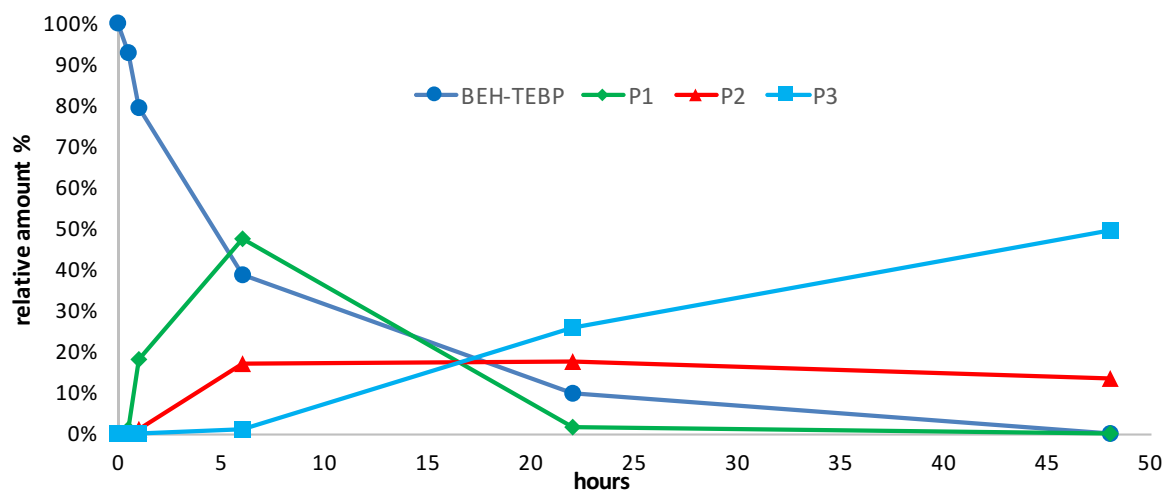


Figure 5-10. BEH-TEBP and its debromination products in methanol at different UV-C irradiation times

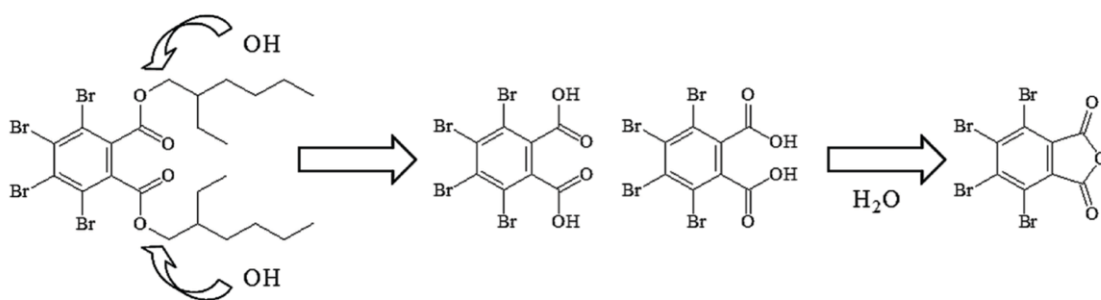


Figure 5-11. Proposed degradation pathway of BEH-TEBP through hydrolysis of the ester groups and formation of an anhydride, adapted from [247]

5.3.3. BTBPE

Degradation products for BTBPE are listed in Table 5-6. Three main degradation products P1, P2/3 and P4 were formed through stepwise reductive debromination as with EH-TBB and BEH-TEBP, with the loss of up to 3 bromines. Identified products are shown in Figure 5-12 and Figure 5-13 for UV-C exposure. Zhang *et al.* proposed a photodegradation pathway for BTBPE as shown in Figure 5-15 [250]. Numbering and nomenclature of our degradation products is based on their formation findings. Figure 5-12 and Figure 5-13 shows the tentative presence of the majority of the reported products. However, selected photolysis products of BTBPE were not detected in our experiments, namely ethyl-2,4,6-tribromophenoxy ether (P8), vinyl-2,4,6-tribromophenyl ether (P10), ethyl-2,4,6-tribromophenoxy ether (P11) and ethyl-4-bromophenoxy ether (P13). The group used a 500W mercury lamp with a higher energy input, again indicating how the differences in experimental set-up might lead to dissimilar results. These photolysis products have not been reported in environmental media to date and investigation into their degradation mechanism when bound to matrix (i.e. soil, dust, sediment) is needed. This might give a better understanding of their impact in the environment and the necessity for toxicological studies of these degradation products.

Table 5-6. Identified BTBPE (C₁₄H₈Br₆O₂) degradation products, including measured accurate mass-to-charge and mass deviation; tentative formula and measured ion

#	m/z	degradation products	formula	measured ion	ion formed	ppm
	328.76266	BTBPE	C ₁₄ H ₈ Br ₆ O ₂	[C ₆ H ₂ Br ₃ O] ⁻	[C ₆ H ₂ Br ₃ O] ⁻	-3.6
P1	544.72497	pentabrominated BTBPE	C ₁₄ H ₉ Br ₅ O ₂	[C ₁₄ H ₉ Br ₄ O ₃] ⁻	[M-Br+O] ⁻	-3.5
P2/3	464.81651	tetrabrominated BTBPE	C ₁₄ H ₁₀ Br ₄ O ₂	[C ₁₄ H ₁₀ Br ₃ O ₃] ⁻	[M-Br+O] ⁻	-4.3
P4	386.90600	tribrominated BTBPE	C ₁₄ H ₁₁ Br ₃ O ₂	[C ₁₄ H ₁₁ Br ₂ O ₃] ⁻	[M-Br+O] ⁻	-2.5
P5	310.87366	2-ethanol-2,4,6-tribromophenoxy ether	C ₈ H ₇ Br ₃ O ₂	[C ₈ H ₇ Br ₂ O ₃] ⁻	[M-Br+O] ⁻	-3.6
P6	308.85905	2-ethenol-2,4,6-tribromophenoxy ether	C ₈ H ₅ Br ₃ O ₂	[C ₈ H ₅ Br ₂ O ₃] ⁻	[M-Br+O] ⁻	-3.4
P7	292.86323	2-ethenol-2,4-dibromophenoxy ether	C ₈ H ₆ Br ₂ O ₂	[C ₈ H ₅ Br ₂ O ₂] ⁻	[M-H] ⁻	-3.1
P9	328.76285	2,4,6-tribromophenol	C ₆ H ₃ Br ₃ O	[C ₆ H ₂ Br ₃ O] ⁻	[M-H] ⁻	-3.7
P12	250.85235	2,4-dibromophenol	C ₆ H ₄ Br ₂ O	[C ₆ H ₃ Br ₃ O] ⁻	[M-H] ⁻	-4.6

P1: 1-(2,4,6-tribromophenoxy)-2-(2,4-dibromophenoxy)ethane

P2/3: 1,2-bis(2,4-dibromo-phenoxy) ethane / 1-(2,4,6-tribromophenoxy)-2-(4-bromophenoxy)ethane

P4: 1-(2,4-dibromophenoxy)-2-(4-bromophenoxy)ethane

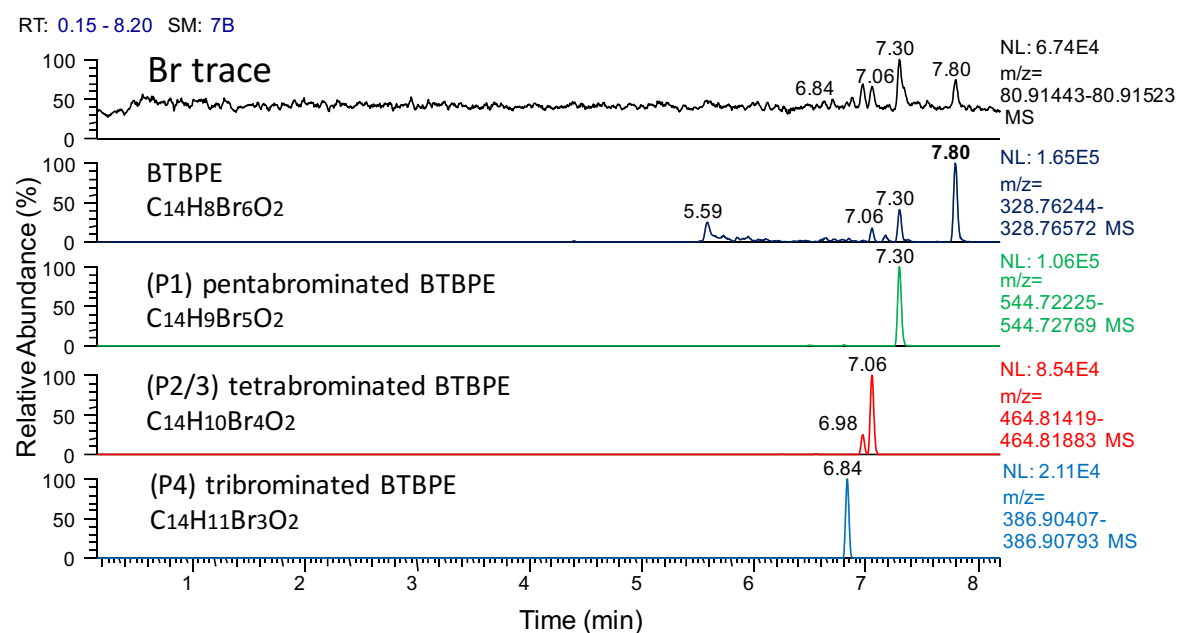


Figure 5-12. XICs of BTBPE (peak at 7.8 marked in bold) and its photodegradation products P1 (1-(2,4,6-tribromophenoxy)-2-(2,4-dibromophenoxy)ethane), P2/3 (1,2-bis(2,4-dibromo-phenoxy) ethane / 1-(2,4,6-tribromophenoxy)-2-(4-bromophenoxy)ethane and P4 (1-(2,4-dibromo-phenoxy)-2-(4-bromophenoxy)ethane) in methanol after 48 h of UV-C irradiation

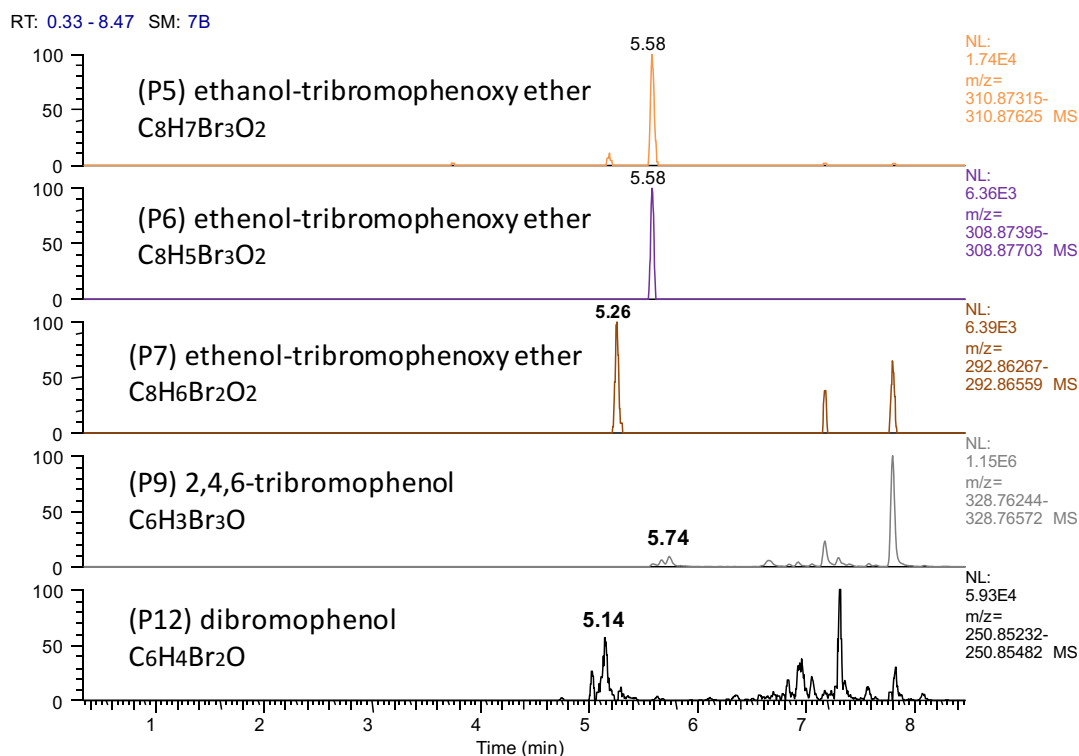


Figure 5-13. XICs of further BTBPE photodegradation products P5 (2-ethanol-2,4,6-tribromophenoxy ether), P6 (2-ethenol-2,4,6-tribromophenoxy ether), P7 (2-ethenol-2,4-dibromophenoxy ether), P9 (2,4,6-tribromophenol) and P12 (2,4-dibromophenol) in methanol after 48 h of UV-C irradiation, for P7 (RT 5.26), P9 (RT 5.74) and P12 (5.14) the described compounds are marked in bold.

When interpreting the results of Figure 5-12 and Figure 5-13, it becomes visible that for certain XICs, several peaks are shown (for BTBPE; P7, P9 and P12). This is caused by the fact that during instrumental measurements in-source fragmentation occurs and higher molecular weight compounds form lower ones. Thus, retention time and the use of standards, where available, along with the comparison to other measurements were used to identify the peak of interest (marked in bold). Further, P2/3 in Figure 5-12 represents the tetrabrominated BTBPE and due to the location of the bromine atoms on the molecule can either form 1,2-bis(2,4-dibromophenoxy) ethane or 1-(2,4,6-tribromophenoxy)-2-(4-bromophenoxy)ethane, indicated by the presence of two peaks in the mass trace. According to Figure 5-15, the formation of product P3 has been reported to follow the main pathway and thus would suggest that the peak at

retention time 7.06 in Figure 5-12 belongs to P3, while the minor one at 6.98 to P2. The ratio between the area of these two peaks is comparable throughout the irradiation experiment. However, further investigation in to the exact mechanism is needed.

Figure 5-14 shows the formation of the identified transformation products. Due to their low relative amount, the degradation of the parent compound was not included. Results reveal that P1 and P2/3 are mainly formed initially, together with P12 towards the end of the irradiation experiments. However, a longer exposure time above 50 hours is needed to obtain a better insight into the photodegradation mechanism, especially of products P4-P9 in order to understand if the proposed degradation pathway shown in Figure 5-15 is generally valid.

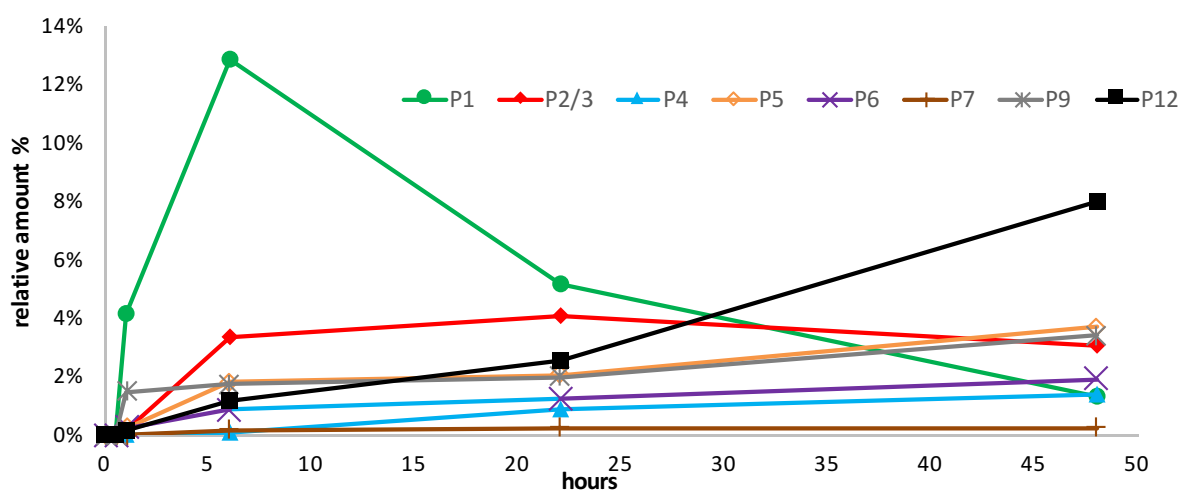


Figure 5-14. Relative amount debromination products of BTBPE in methanol at different UV-C irradiation times

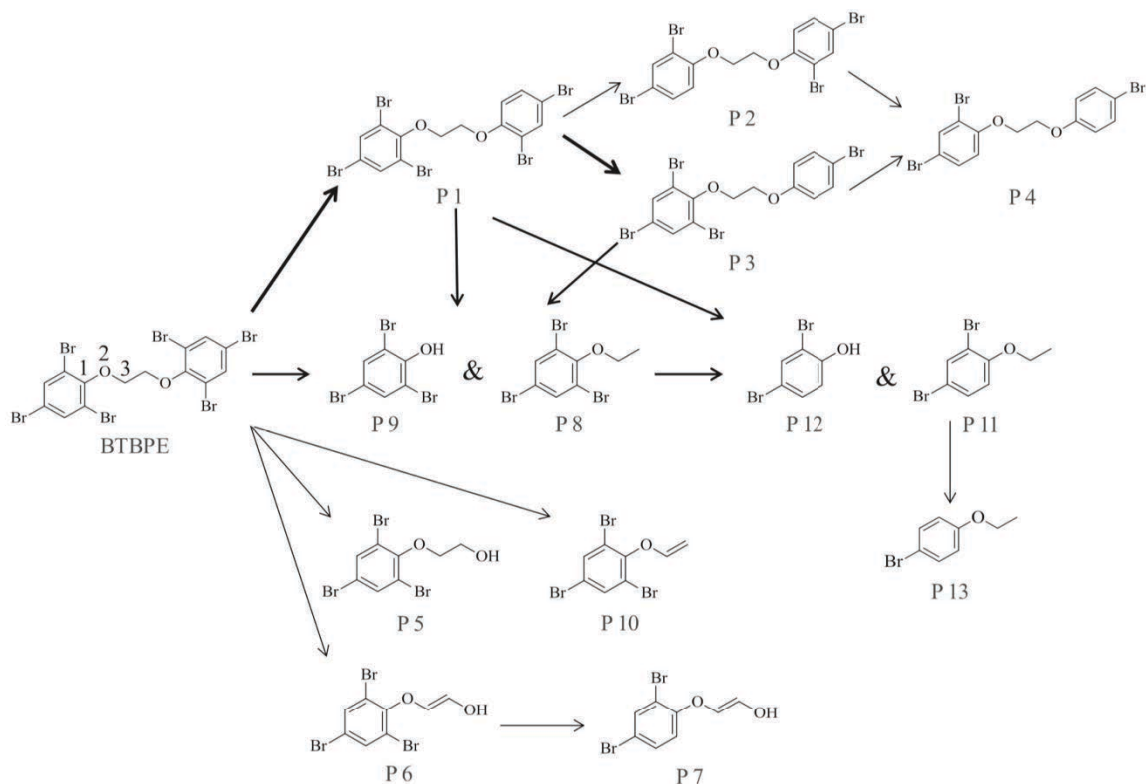


Figure 5-15. Proposed degradation pathway of BTBPE, bold arrows mark the main pathway, adapted from [250]

5.3.4. DBDPE

Degradation products for DBDPE are listed in Table 5-7. Several main degradation products (P1-P7) were formed through stepwise reductive debromination as with EH-TBB, BEH-TEBP and BTBPE, but with the loss of up to 7 bromines to form tri-BDPE. Identified products are shown in Figure 5-16. Further, Table 5-7 lists other four tentative transformation products P8-P11 with similar structure, but only debromination occurring down to hexa-BDPE (as also shown in Figure 5-18 and Figure 5-19 for UV-C and outdoor exposure experiments). This needs to be further investigated and exact mechanism and formations understood. Similar to BTBPE, the presence of these DBDPE degradation products in environmental samples has not been reported and needs to be investigated to take decisions on future research directions and possible toxicological studies in order to assess the degradants adverse potential.

Table 5-7. Identified DBDPE (C₁₄H₄Br₁₀) degradation products, including measured accurate mass-to-charge and mass deviation; tentative formula and measured ion

#	m/z	degradation products	formula	measured ion	ion formed	ppm
	906.28333	DBDPE	C ₁₄ H ₄ Br ₁₀	[C ₁₄ H ₄ Br ₉ O] ⁻	[M-Br+O] ⁻	-0.3
P1	826.35560	nona-BDPE	C ₁₄ H ₃ Br ₉ O	[C ₁₄ H ₃ Br ₈ O ₂] ⁻	[M-Br+O] ⁻	-2.2
P2	762.44189	octa-BDPE	C ₁₄ H ₄ Br ₈ O	[C ₁₄ H ₄ Br ₇ O ₂] ⁻	[M-Br+O] ⁻	-3.8
P3	684.53174	hepta-BDPE	C ₁₄ H ₅ Br ₇ O	[C ₁₄ H ₅ Br ₆ O ₂] ⁻	[M-Br+O] ⁻	-2.4
P4	604.62335	hexa-BDPE	C ₁₄ H ₆ Br ₆ O	[C ₁₄ H ₆ Br ₅ O ₂] ⁻	[M-Br+O] ⁻	-2.6
P5	525.71277	penta-BDPE	C ₁₄ H ₇ Br ₅ O	[C ₁₄ H ₇ Br ₄ O ₂] ⁻	[M-Br+O] ⁻	-3.1
P6	446.80447	tetra-BDPE	C ₁₄ H ₈ Br ₄ O	[C ₁₄ H ₈ Br ₃ O ₂] ⁻	[M-Br+O] ⁻	-3.3
P7	368.89393	tri-BDPE	C ₁₄ H ₉ Br ₃ O	[C ₁₄ H ₉ Br ₂ O ₂] ⁻	[M-Br+O] ⁻	-4.1
Further degradation products						
P8	828.37048	nona-BDPE	C ₁₄ H ₅ Br ₉	[C ₁₄ H ₅ Br ₈ O] ⁻	[M-Br+O] ⁻	-3.2
P9	748.46191	octa-BDPE	C ₁₄ H ₆ Br ₈	[C ₁₄ H ₆ Br ₇ O] ⁻	[M-Br+O] ⁻	-3.6
P10	670.55176	hepta-BDPE	C ₁₄ H ₇ Br ₇	[C ₁₄ H ₇ Br ₆ O] ⁻	[M-Br+O] ⁻	-3.5
P11	589.64453	hexa-BDPE	C ₁₄ H ₈ Br ₆	[C ₁₄ H ₈ Br ₅ O] ⁻	[M-Br+O] ⁻	-1.9

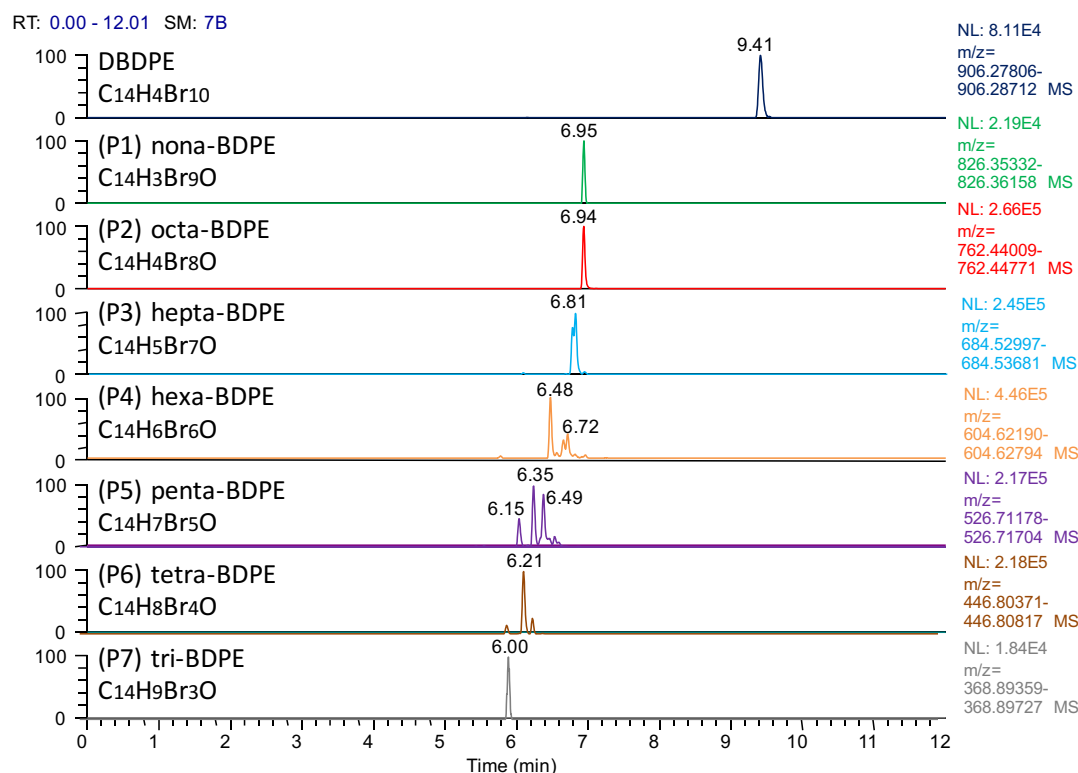


Figure 5-16. XICs of DBDPE and its photodegradation products P1-P7 (nona- to tri-BDPE) in methanol after 9 h (for DBDPE, P1 and P2) and 130 h (P3-P7) of outdoor solar irradiation

Figure 5-17 similarly to the other NBFRs investigated, illustrates the stepwise reductive debromination process for DBDPE. While, nona-BDPE appears fairly unstable and/or is rapidly formed and further debrominated, the other degradation products P2, P3, P4 are stepwise formed and further debrominated. P5 appears to reach its maximum relative amount, while to see the same effect for P6 and P7 longer irradiation is needed, along with a tentative formation of even lower brominated species.

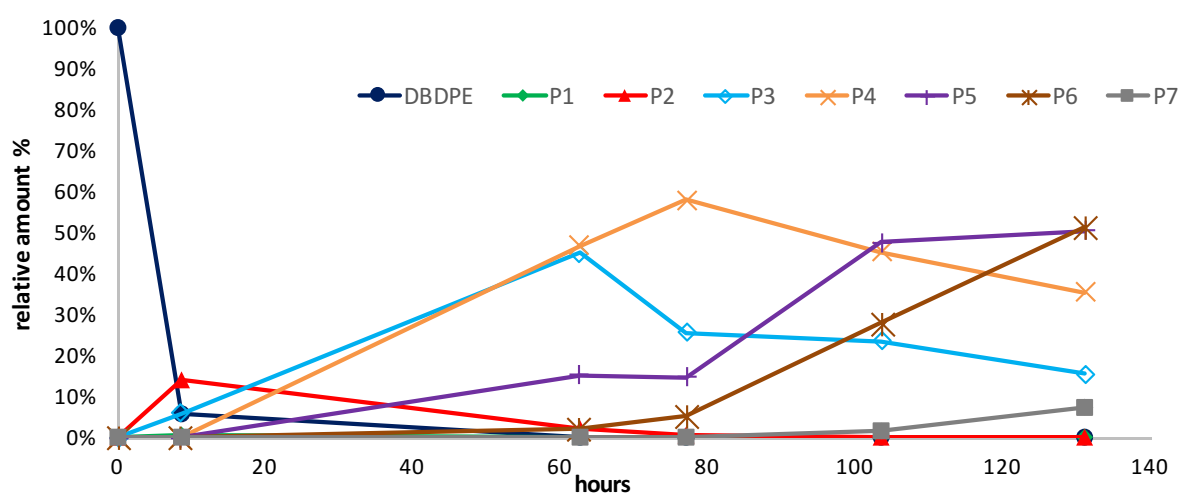


Figure 5-17. Relative amounts of DBDPE and its debromination products in methanol at different UV-C irradiation times

For DBDPE debromination to form nona-, octa- and hepta-BDPEs has been reported [248]. Our study however suggests that further debromination down to tri-BDPE is possible in outdoor solar irradiation experiments. This is of particular interest, since research has shown that the structurally similar BDE-209 undergoes debromination to form more toxic and bioavailable congeners [112]. A very recent study has shown that oxidative KMnO_4 degradation of DBDPE in a sulfuric acid system leads to the formation of 28 different degradants, following two main pathways. ECOSAR (Ecological Structure Activity Relationships) for estimating aquatic toxicity showed that the adverse effects of DBDPE and its products should not be overlooked, although DBDPE seemed to be more toxic than its transformation products [252].

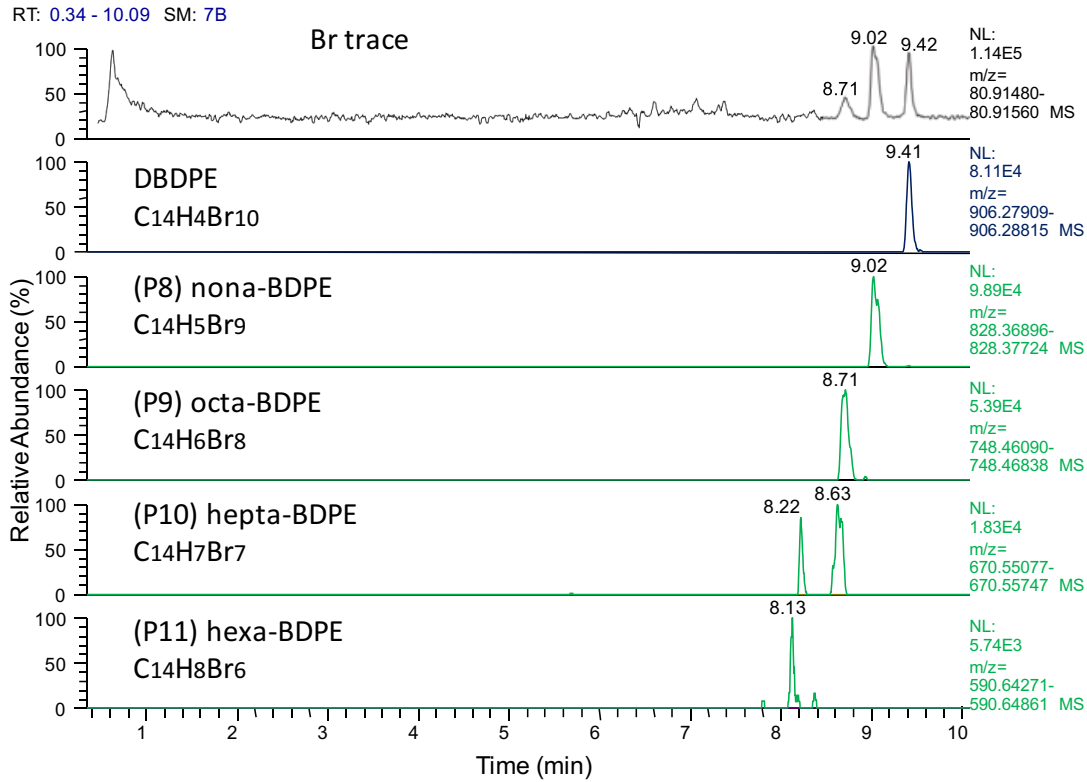


Figure 5-18. XICs of DBDPE and further photodegradation products nona- to hexa-BDPE) in methanol after 9 h of outdoor solar irradiation

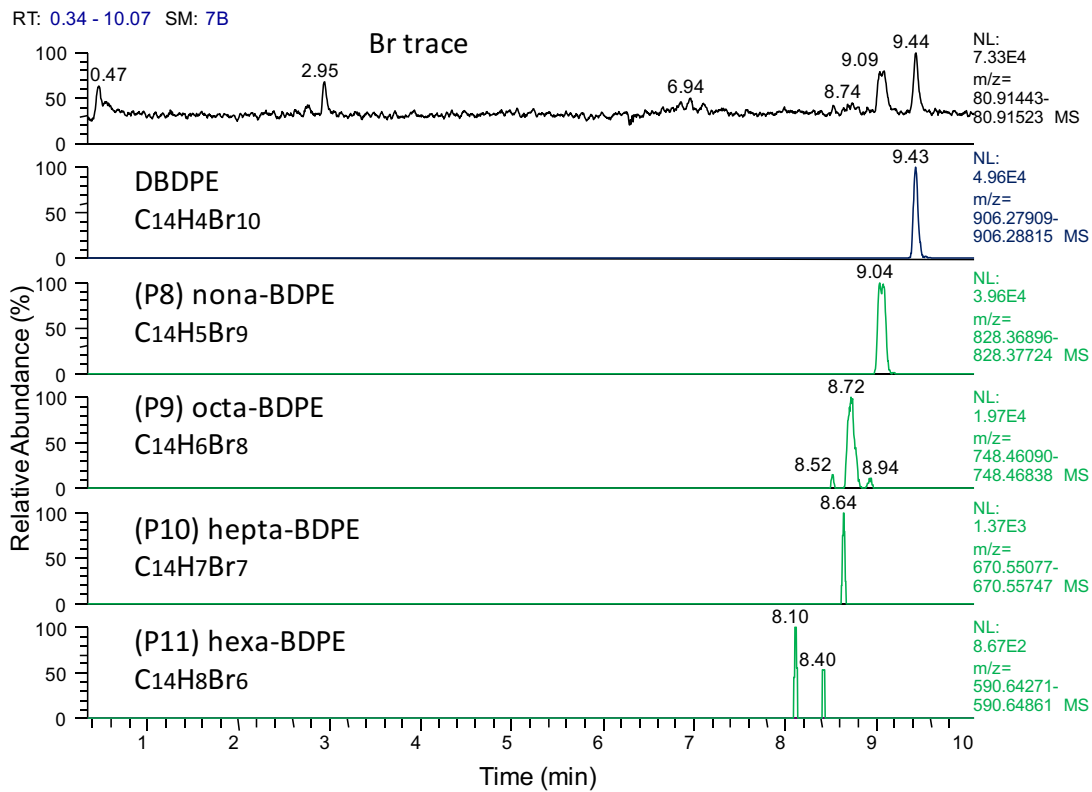


Figure 5-19. XICs of DBDPE and further photodegradation products nona- to hexa-BDPE) in methanol after 22 h of UV-C irradiation

5.4. Conclusions

The photodegradation experiments conducted had the aim of identify primary degradation products as markers that can be used to trace environmental degradation processes. These can aid in future studies to investigate whether parent compounds transform to more toxic and biologically available substances and regulatory steps have to be taken. It was not the aim of this study to examine nor determine the exact mechanisms by which these compounds are photodegraded in different solvents at this stage.

Indoor exposure experiments did not always show first-order kinetics for the decay of the compounds, while half-times of the decay were an order of magnitude greater compared to outdoor experiments. The latter experiments and UV-A and UV-B irradiation followed first-order decay kinetics. Half-lives were an order of magnitude lower for outdoor experiments compared to UV exposure. This difference between experiments is expected, since the light energy input increases in the following order indoor < outdoor < UV lamp. While EH-TBB, BEH-TEBP and DBDPE had comparable degradation constants within each experiment, BTBPE degraded comparatively slower, with the exception for UV-C exposure, where the irradiation energy probably was large enough to compensate for the higher structural stability of the compound. Further investigations into the exact mechanisms and kinetics of the degradation reactions seems appropriate.

Photolysis experiments conducted with all four compounds indicated the sequential debromination reaction to form lower brominated compounds. For EH-TBB di- and tribrominated products were formed, BEH-TEBP showed formation of mono-, di- and tribrominated degradants, while DBDPE showed the presence of tri- to nona-brominated-BDPE. BTBPE did not only form tri-, tetra- and penta- brominated products, but also several other di- and tribrominated degradants were tentatively identified. This is of special interest,

since lower brominated compounds have shown to be more toxic and biologically available [112], hence the ban of the technical PentaBDE and OctaBDE mixture, as well as recently DecaBDE, which has the potential to form lower brominated species. It is of special importance to conduct field-based fate experiments in relevant environmental matrixes (i.e. dust, plastics and textiles for indoor environment, soil and sediments for outdoor environment) and understand how they compare to our findings. However, it has to be noted that these results might differ significantly, as for example no debromination products were formed in plastic samples containing DBDPE exposed to natural sunlight [249]. Differences may originate from the fact that compounds are matrix bound and energy transfer mechanism differ (absorbance of energy by the matrix, shielding effects etc.). It is important to also consider the use of validated procedures, which are capable of extracting both parent and transformation products from the matrix. Here, the availability of authentic standards of degradants further allows for better identification and mass balance calculations, together with the use of labelled standards for method recovery determination.

Finally, when conducting future experimental design, following guidance documents such as the OECD protocols for direct phototransformation of chemicals in water [253] and soil [254] appears warranted.

Chapter VI – *In vitro* biotransformation of NBFRs by trout liver microsomes

6.1. Overview

In vitro experiments can act as an initial screening tool to identify metabolites and obtain an assessment of the main biotransformation pathways of drugs and other xenobiotics. These studies are relatively inexpensive and readily carried out, and can serve as a basis for further *in vivo* testing. For *in vitro* studies generally, metabolizing recombinant enzymes, subcellular fractions or cellular organelles are employed [255]. The general focus in these experiments is liver tissue, since the liver is the main site of drug metabolism. However, when considering other biological and exposure pathways, experiments using lung, intestine or skin cells have also been reported [256].

When focusing on subcellular fractions, these can be further divided into 3 categories as shown in Table 6-1. While S9 fractions contain both the microsomal and cytosolic fractions of cells, which allow to obtain information on both phase I and phase II metabolic pathways, the microsomal fraction (insoluble membrane proteins) provides information about phase I metabolism, while the cytosolic fraction (soluble proteins) address phase II transformations [190].

Table 6-1. Metabolic enzymes in different liver subcellular fractions (adapted from ¹):

Metabolic enzymes	Liver Microsomes	Liver Fractions	S9	Liver Cytosol
Aldehyde Oxidase (AO)			X	X
Cytochromes P450 (CYP)	X	X		
Flavin Monooxygenases (FMO)	X	X		
Glutathione Transferase (GST)		X		
Monoamine Oxidase (MAO)		X		
Sulfotransferase (SULT)		X		X
Uridine Glucuronide Transferase (UGT)	X	X		

¹<https://www.thermofisher.com/at/en/home/industrial/pharma-biopharma/drug-discovery-development/microsomes-s9-fractions-cytosol.html>

Comparison between exposure studies in different species can provide specific information on characteristics, degree of metabolism and formation of metabolites in selected species. This can aid the assessment of risk for human and environmental health, through the understanding of toxic effects of formed metabolites and the choice of model species for toxicological studies [115]. Several studies have compared specific metabolism of species, including fish, rodents and mammals [115, 190, 257, 258], as well as differences between *in vitro* and *in vivo* experiments [112].

While the focus in this chapter is on microsome studies, a brief overview on other *in vitro* and *in vivo* studies available when assessing the metabolism of (N)BFRs will be given.

6.1.1. PBDEs, HBCDDs and TBBPA

For PBDEs, studies have shown that metabolic pathways can occur either based on reductive debromination, or as oxidative metabolism, leading to the formation of lower brominated congeners and hydroxylated PBDEs (HO-PBDE), respectively [4]. It was indicated for example that in fish, PBDEs tend to be reductively debrominated [259-261], while mammals and rodents primarily form HO-PBDE through oxidative processes [259, 260, 262]. HO-PBDE

metabolites are of special toxicological interest, since they often show greater biological activity compared to their parent compounds [130, 263] and possible endocrine disrupting potential [23].

Several studies have focused on the bioaccumulation and metabolic pathways of PBDEs, mainly investigating BDE-47 [263, 264], BDE-99 [262-265], BDE-100 [266] and BDE-209 [112, 114, 264, 267-269].

For HBCDDs, the metabolism of the three stereoisomers was investigated by human liver microsomes (HLM) [270], as well as rat and trout liver S9 fractions [190]. Metabolites formed include mono- and dihydroxylated HBCDDs, pentabromocyclododecenes (PBCDDs) and tetrabromocyclododecadienes (TBCDDs) through reductive debromination, as well as monohydroxylated forms of PBCDDs and TBCDDs. Some of these metabolites were also reported in rat and wildlife samples [271]. Further, it was observed that there is a shift of the diastereomeric pattern of HBCDD towards enrichment of the α stereoisomer when exposed to liver microsomes of harbour seals [272].

6.1.2. NBFRs

Few studies have explored the metabolism of NBFRs in different species to date. The *in vivo* and *in vitro* metabolism by different species has been investigated for EH-TBB and BEH-TEBP [73, 115, 257], BTBPE [273, 274] and DBE-DBCH [275-278]. Details on the results of these studies will be discussed in the course of this chapter along with the results of the experiments conducted.

6.2. Screening for metabolite formation of NBFRs

Female rainbow trout (*Oncorhynchus mykiss*) liver microsomes (TLM) were challenged with EH-TBB, BEH-TEBP, DBE-DBCH and BTBPE for initial screening purposes. In the literature, a number of studies have employed trout liver microsomes and other related subcellular fractions for the investigation of the metabolism of HBCDDs [190] and BDE-209 [112], as well as conducted *in vivo* studies on rainbow trout for understanding the metabolism of BDE-209 [267-269] and DEHP [279]. A general experiment to assess bioaccumulation through basal-level enzyme activities and hepatic intrinsic clearance rates of trout was also conducted [258]. Other studies on EH-TBB and BEH-TEBP were obtained by exposing fathead minnow and common carp to said substances [73, 115].

6.2.1. EH-TBB and BEH-TEBP

Initially, full scan experiments were conducted to obtain a general overview of the presence of metabolites. All ion fragmentation (AIF) was performed in parallel to obtain a Br ion trace and aid in metabolite identification. As shown in Figure 6-2, the major metabolite for EH-TBB could be identified as 2,3,4,5-tetrabromobenzoic acid (TBBA). TBBA had to be measured in HESI where the characteristic $[M-H]^-$ quasi molecular ion was formed, since in APCI, only weak ionization of the acidic compound was observed. Structural confirmation was conducted by the injection of a reference standard of the metabolite, including comparison of accurate mass, retention time, isotopic pattern and MS/MS fragmentation spectra. Further, TBBA was quantified in follow-up temperature experiments by the addition of ^{13}C -TBBA as internal standard. The formation of TBBA has also been reported in *in vitro* studies employing human and rat liver microsomes and intestinal subcellular fractions [257], through cleavage of the 2-ethylhexyl chain in all experiments as shown in Figure 6-1. Interestingly, another study

suggested the formation of 2,3,4,5-tetrabromomethylbenzoate (TBMB), with TBBA acting only as an intermediate metabolite. This study used subcellular fractions of fathead minnow, common carp, mouse and snapping turtle, where the formation of TBMB was attributed to the methylation of TBBA via methyl transferase phase II enzymes [115].

For BEH-TEBP on the other hand, a reduction of the initial dose of the parent compound after treatment with trout liver microsomes was observed, but no stable ions for potential metabolites were confirmed after data analysis of both APCI and HESI measured extracts. Figure 6-3 presents the parent compound after exposure to TLM and several bromine containing peaks in the bromine trace, which could not be further identified.

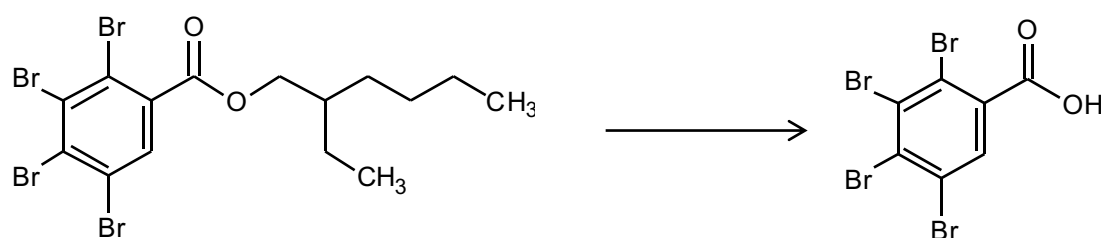


Figure 6-1. Formation of 2,3,4,5 tetrabromobenzoic acid (TBBA) from EH-TBB through cleavage of the 2-ethylhexyl chain.

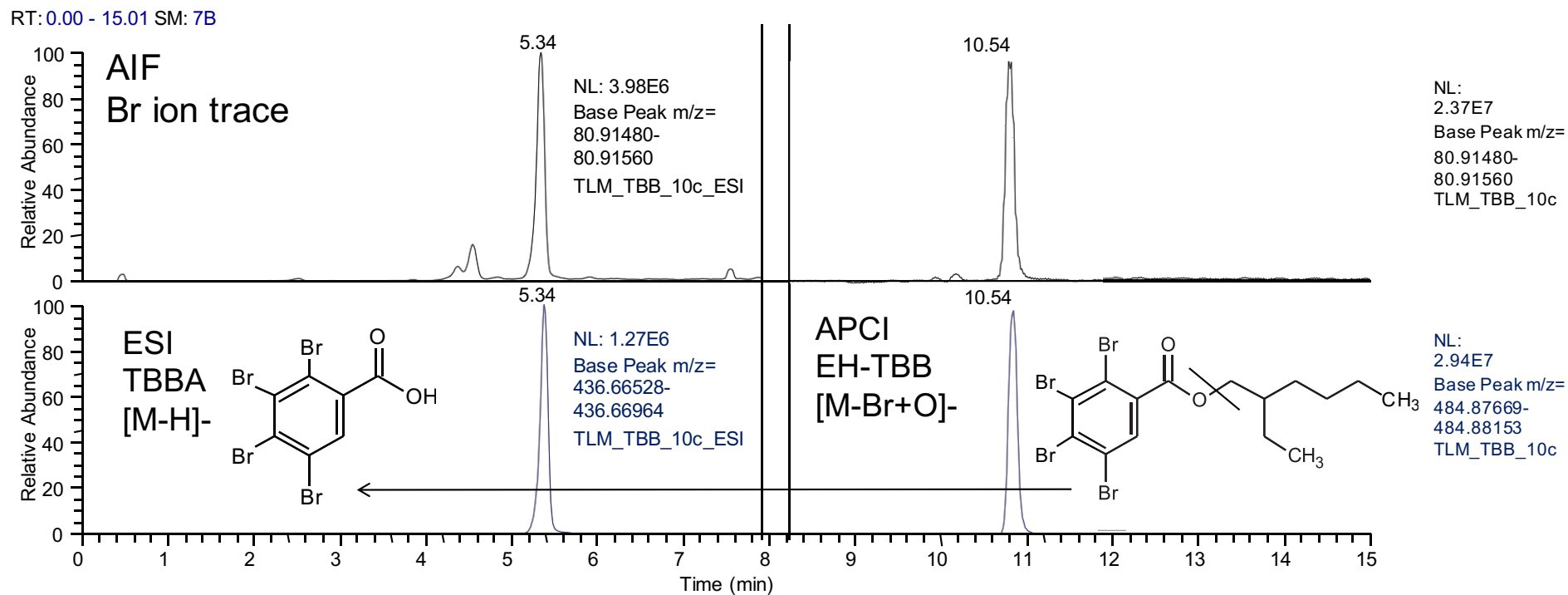


Figure 6-2. Selected UPLC–Orbitrap–MS XIC of EH-TBB (APCI) and its metabolite TBBA (ESI) formed by TLM exposure to 10 μ M EH-TBB for 60 min., including Br ion trace from all ion fragmentation (AIF)

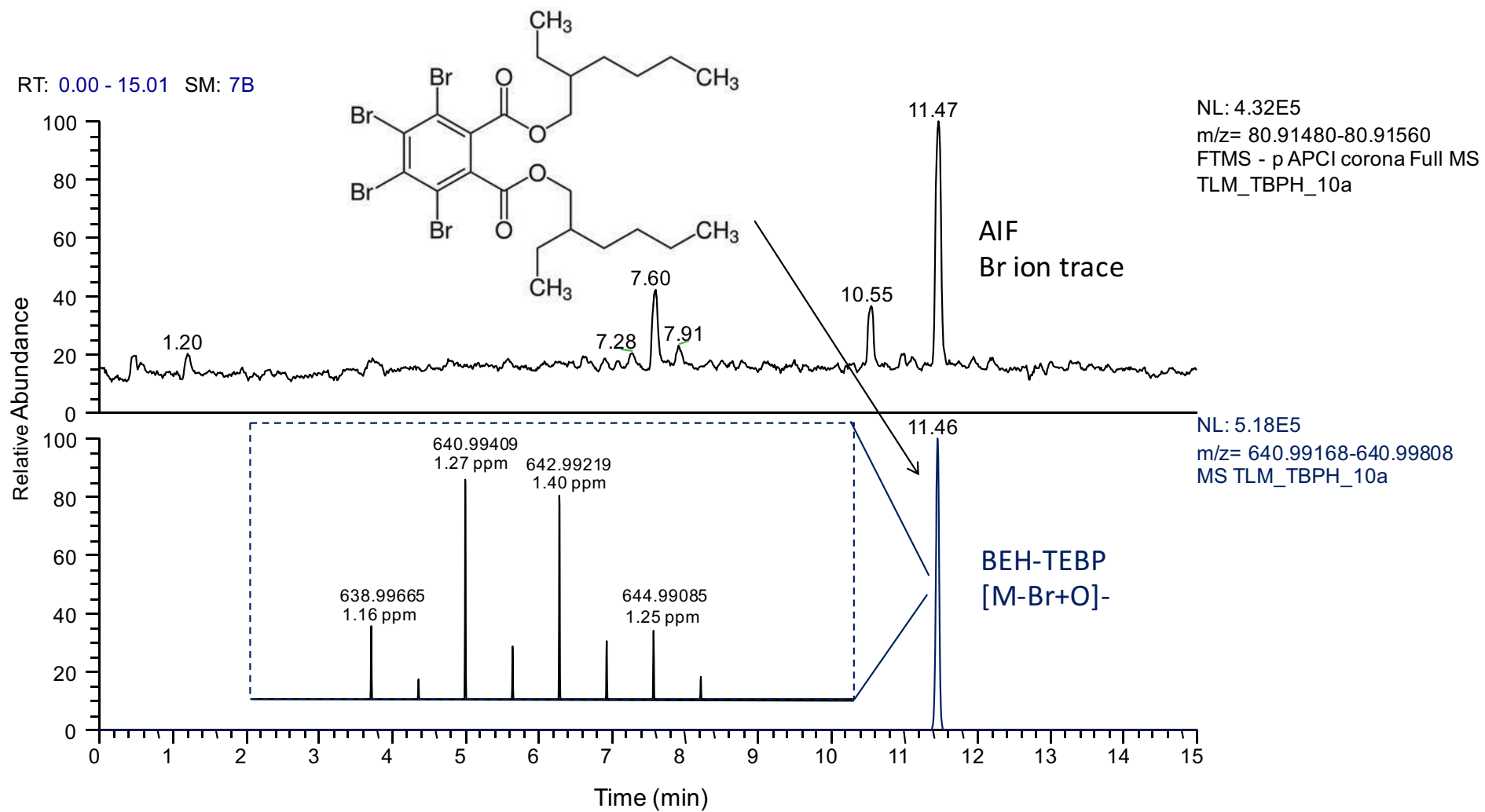


Figure 6-3. Selected UPLC–Orbitrap–MS XIC of BEH-TEBP after TLM exposure to 10 μ M BEH-TEBP for 60 min, including Br ion trace from all ion fragmentation (AIF)

The first study to investigate the *in vivo* metabolism and bioavailability of EH-TBB and BEH-TEBP in fathead minnow reported that dietary exposure led to accumulation in fish tissue (1 % of daily dosage) and the formation of unidentified brominated metabolites for EH-TBB only. Both compounds induced non-lethal DNA damage in the hepatic tissue of the fish [73]. Further investigation of this group led to an *in vitro* study in the fathead minnow, common carp, mouse and snapping turtle, whereby different hepatic subcellular fractions (S9, microsomes and cytosol) were challenged with EH-TBB and BEH-TEBP [115]. Metabolic loss of these parent compounds was observed in all species, except for EH-TBB in snapping turtle. While no metabolites were identified for BEH-TEBP, it was suggested that EH-TBB metabolizes to form TBMB with TBBA as an intermediate product. Another study, exposing human and rat liver and intestinal subcellular fractions to EH-TBB and BEH-TEBP, similarly did not detect any metabolites for BEH-TEBP. However, they reported the formation of mono(2-ethylhexyl) tetrabromophthalate (TBMEHP), when exposing BEH-TEBP to purified porcine carboxylesterase [257]. Contrasting to the above, for EH-TBB they found TBBA to be the main metabolite formed.

When comparing the metabolite formation of EH-TBB and the lack of reported biotransformation for BEH-TEBP, a possible explanation could be the open ring site of EH-TBB which enables enzymatic activity to occur [73], while BEH-TEBP has a more bulky, closed structure.

The metabolism of di(2-ethylhexyl)phthalate (DEHP), a structural analogue of BEH-TEBP lacking the four bromine atoms, has been studied in rainbow trout [279], as well as human and rat liver fractions [280]. Metabolites include mono(2-ethylhexyl) phthalate (MEHP), as well as several other transformation products formed. Extrapolation to possible metabolism of BEH-TEBP has to be done with caution, since the addition of the bromine atoms result in a

larger and more hydrophobic compound and thus might inhibit enzyme accessibility and/or activity. Further, a study for PBDEs reported that the number of bromine within a molecule is inversely correlated to the metabolic reaction rate [281].

6.2.2. Temperature studies for EH-TBB

In vivo and *in vitro* studies employing trout are conducted at different temperatures, when comparing experimental design in literature, as summarised in Table 6-2. It becomes evident that temperatures commonly cover a range from 10 to 25 °C when working with trout or fish in general. One study, in which trout were kept in outdoor waters, monitored the temperature for the time of the experiment and reported values from 10.5 to 23.5 °C for the period June to September in Stockholm, Sweden [269], thus indicating, that fish and their metabolism have to adapt to varying temperatures over the year. This is in contrast to rodent or animal studies, which generally are conducted at a constant 37 °C.

Table 6-2. Selection of *in vitro* / *in vivo* studies of trout (rainbow and juvenile brown)

Type of study	Tissue / subcellular fraction	Compound / test	Temperature °C	Ref.
<i>in vivo</i>	blood / muscle / liver	BDE-209	10.5-23.5	[269]
<i>in vivo</i>	TLM / S9	Enzyme activity	10	[258]
<i>in vivo</i>	TLM	13 BDEs	12	[282]
<i>in vivo</i>	bile / urine	DEHP	12	[279]
<i>in vitro</i>	thyroid	β-DBE-DBCH	12 – 15	[278]
<i>in vitro</i>	S9	HBCDD	15	[190]
<i>in vivo</i>	liver / blood / kidney	BDE-209	15 ± 2	[267, 268]
<i>in vivo</i> / <i>in vitro</i>	liver / blood / intestine	BDE-209	25	[112]

To examine the temperature dependency of metabolite formation, TLM were exposed to EH-TBB for 60 min at temperatures of 10, 15, 20 and 30 °C. TBBA formation and reduction in EH-TBB were quantified (using ¹³C-TBBA and ¹³C-EH-TBB as internal standard, respectively), as illustrated in Figure 6-4. Results indicate an increase of the enzyme's catalytic activity with increasing temperature, while the optimal temperature might be above 30 °C. However, since

trout are rarely exposed to water temperatures of 30 °C and above, this might not be indicative of real world exposure conditions. Nevertheless, temperature influences metabolism as expected with enzymatic reactions and has to be considered in experimental design.

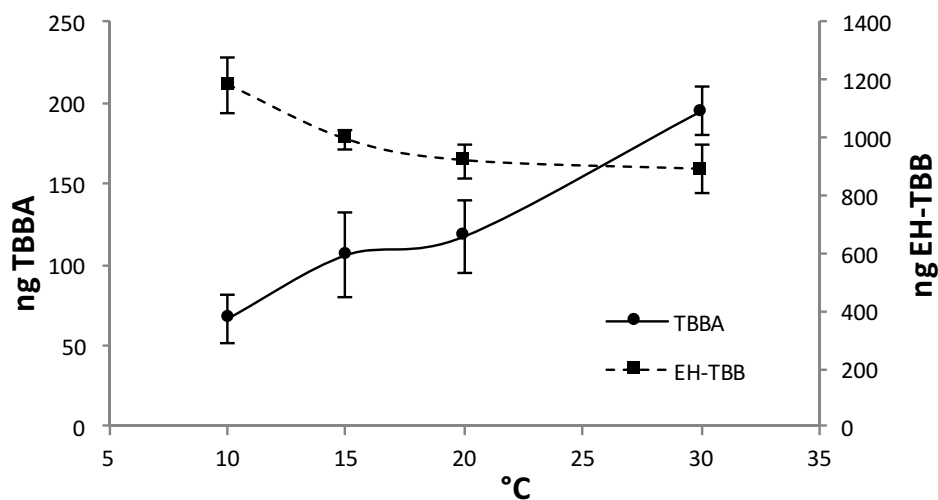


Figure 6-4. Temperature dependent formation of metabolite TBBA from the parent compound EH-TBB exposed to trout liver microsomes for 60 min.

6.2.3. BTBPE

Similar to EH-TBB and BEH-TEBP initial full scan experiments were conducted to screen for possible metabolites. The Br ion trace was used as a mean to aid in metabolite identification. Screening results for BTBPE indicated no reduction of the initial dose after treatment with TLM and thus likely no *in vitro* metabolism.

An *in vivo* study on male Sprague-Dawley rats reported several metabolites in fecal excretions when exposed to BTBPE. This could be explained by species-specific differences and variances between *in vivo* / *in vitro* results. Metabolites included mono- and dihydroxylated moieties, as well as those debrominated on a single or both aromatic rings and combinations thereof, as well as cleavage of the ether linkage to form tribromophenol and tribromophenoxyethanol [274]. Further, a study comparing the effects of dietary exposure of BTBPE and EH-TBB in

juvenile rainbow trout [273] concluded that while EH-TBB is rapidly depurated and/or metabolised, BTBPE is accumulated (detection in fish carcass of 76 % of the daily dosage versus 2 % for EH-TBB). Results for BTBPE also indicate the impact on immune related gene transcription, as well as oxidative stress and endocrine disruption potential. EH-TBB on the other hand did not affect the transcriptional response of the fish an exposure period of 28 days. This might explain, why EH-TBB in our TLM experiments is metabolized, while for BTBPE no metabolic activity was shown. Further studies are needed to better understand the species specific differences for the metabolism of BTBPE.

6.2.4. DBE-DBCH

Screening based on Full Scan experiments and the use of the Br ion trace of DBE-DBCH showed the formation of two major metabolites (Table 6-3) for the technical DBE-DBCH mixture (panel d and f) while only one for β -DBE-DBCH (panel e) as shown in Figure 6-5. Metabolite were identified using a Thermo Fisher Compound Discoverer™ 2.0 workflow (see Figure 2-21) for the detection of metabolites from parent compounds, as described in 2.6.5 and shown in Figure 2-22 (for monohydroxy-DBE-DBCH). Structural confirmation was based on molecular weight, isotopic pattern matching and that the compound is not present in the negative control. Monohydroxy-DBE-DBCH has previously been reported for experiments conducted with rat and human liver microsomes [275, 276], while monohydroxy-triDBE-DBCH has only recently been reported in the same study on human liver microsomes [276]. It was suggested that the latter metabolite is formed through a combination of debromination and hydroxylation. This again demonstrates species-specific variations in metabolism of NBRs. The isobaric isomers in the technical DBE-DBCH mixture cannot be separated by means of LC as shown in Figure 6-5 (panel b), however purified β -DBE-DBCH is commercially available and was studied separately (panel c) to aid in the interpretation of results. Therefore, the

assumption was taken that the metabolite at retention time 7.57 min in panel d belongs to β -DBE-DBCH, while the other two are associated with α -DBE-DBCH. Interestingly no monohydroxy- β -triDBE-DBCH was formed in our experiments, which could possibly be explained by weaker enzymatic affinity of TLM for β -DBE-DBCH.

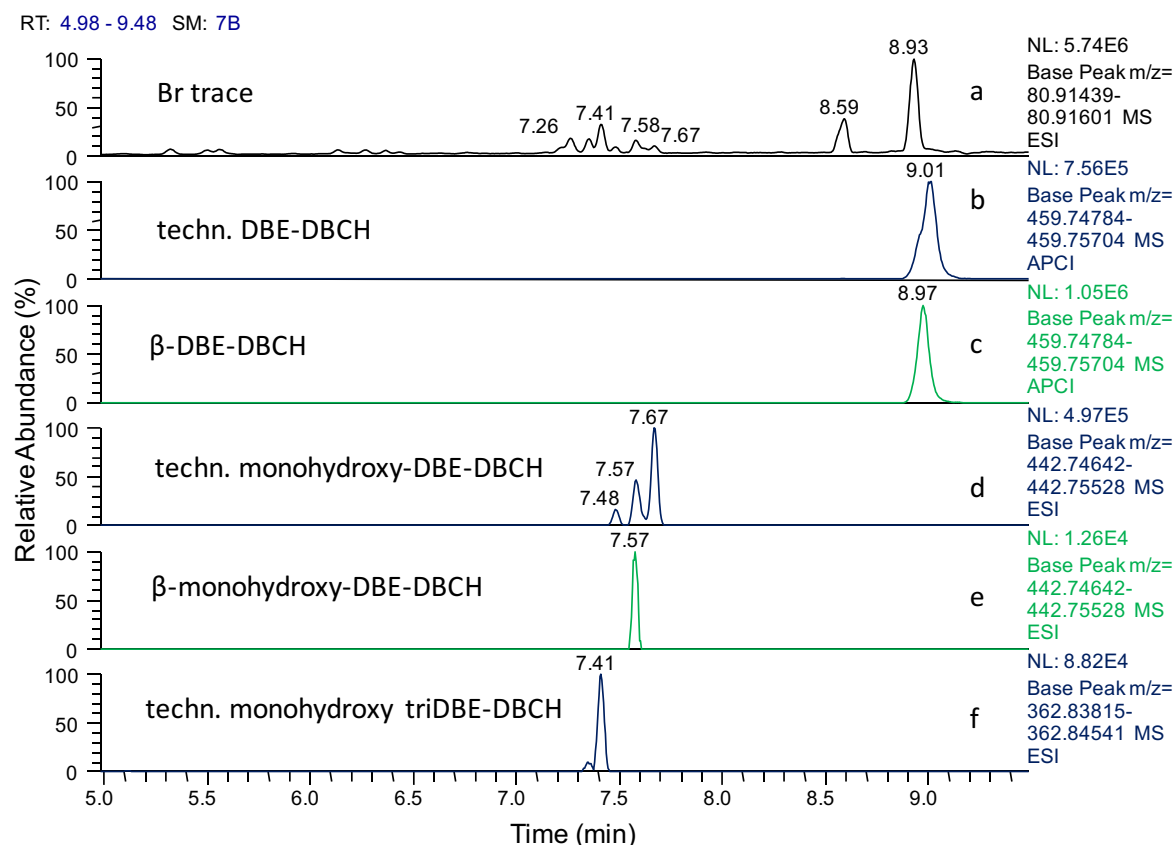
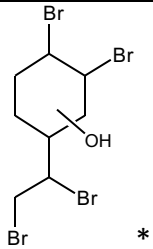
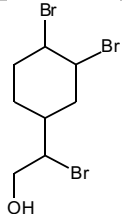


Figure 6-5. Selected UPLC-Orbitrap-MS XIC of DBE-DBCH and its metabolites formed by TLM exposure to 10 μ M of technical DBE-DBCH (panels b, d and f) and β -DBE-DBCH (panels c and e) for 60 min. Parent compounds (panel b and c) are measured in APCI, metabolites and Br trace (panels a and d-f) in ESI

Table 6-3. List of identified DBE-DBCH metabolites produced after incubation of technical DBE-DBCH with TLM for 60 min.

Accurate mass [M-H] ⁻	Mass accuracy ppm	Predicted formula	name	Plausible structure
442.74997	-1.8	C ₈ H ₁₂ Br ₄ O	Monohydroxy-DBE-DBCH	 *
362.84175	-1.3	C ₈ H ₁₃ Br ₃ O	Monohydroxy-tri-DBE-DBCH	
* the exact position of the hydroxyl group could not be specified via the applied standard protocol.				

6.3. Kinetic studies on DBE-DBCH

To further investigate the kinetics of the metabolite formation, both the technical DBE-DBCH and β-DBE-DBCH were exposed to TLM at increasing substrate concentrations (1, 2, 5, 10 and 15 μM). Concentrations of metabolites were semi-quantitatively calculated based on the response factors of the parent compounds, since no authentic standard was commercially available. Further, summed areas of all peaks were used for quantification of metabolite formation. Kinetic modelling was applied to the resulting concentrations using the SigmaPlot™ Enzyme Kinetics Module. Non-linear regression models Michaelis–Menten, Hill and substrate-inhibition were tested, based on the kinetic model in Equation 6-1, 6-2 and 6-3, respectively.

$$v = \frac{V_{max} \times [S]}{K_m + [S]} \quad \text{(Equation 6-1)}$$

$$v = \frac{V_{max} \times [S]^n}{K' + [S]^n} \quad \text{(Equation 6-2)}$$

$$v = \frac{V_{max}}{1 + \frac{K_m + [S]}{[S]} + \frac{K_i}{[S]}} \quad \text{(Equation 6-3)}$$

where v is initial velocity of the reaction, V_{max} is the maximal velocity, $[S]$ is the substrate concentration, K_m is the Michaelis-Menten constant, K' is the Hill dissociation constant, n is the Hill coefficient and K_i is the inhibitory dissociation constant.

As a mean for the best fitting model the following two statistical criteria were evaluated: Akaike Information Criterion corrected for small sample size (AICc) and standard deviation of the residuals ($Sy.x$). The model with the lowest values for these both was chosen, which was the Michaelis–Menten for all metabolites formed, as shown in Figure 6-6 and Figure 6-7.

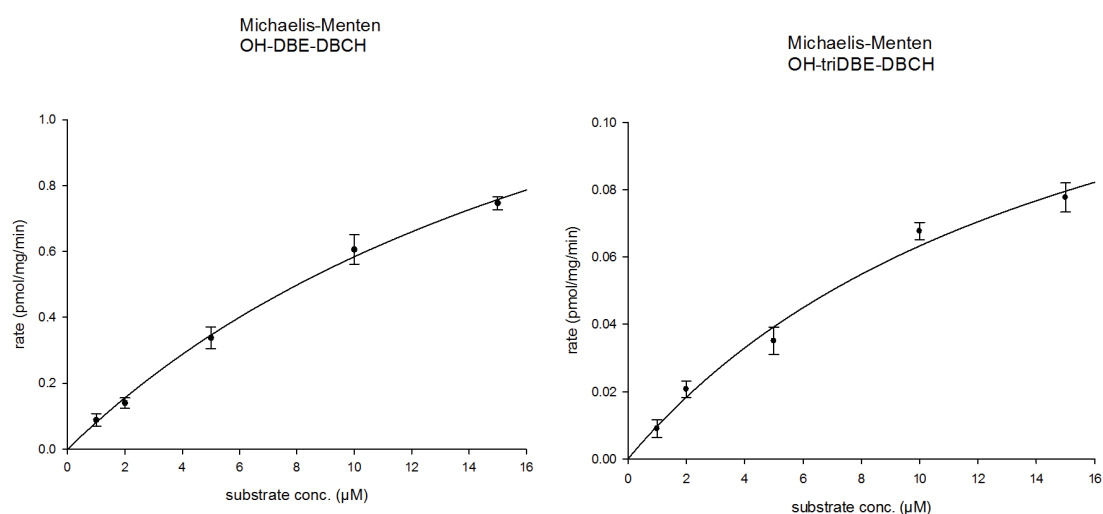


Figure 6-6. Kinetic study of technical DBE-DBCH metabolite formation fit to a Michaelis–Menten model following 60 min incubation with TLM at various substrate concentrations. Data are means \pm SD ($n = 3$)

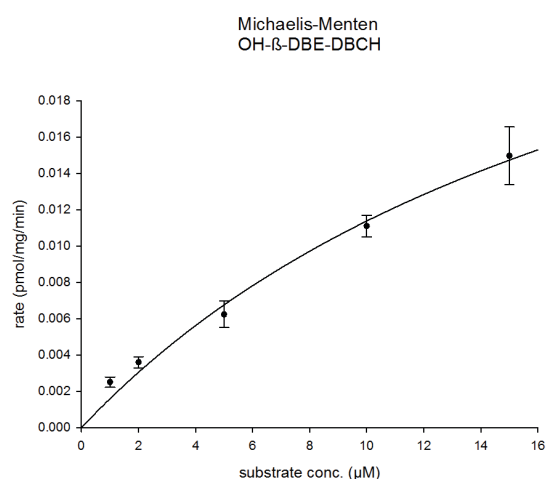


Figure 6-7. Kinetic study of β -DBE-DBCH metabolite formation fit to a Michaelis–Menten model following 60 min incubation with TLM at various substrate concentrations. Data are means \pm SD ($n = 3$)

Kinetic parameters derived from this are listed Table 6-4. When looking at these results it has to be noted that monohydroxy-DBE-DBCH was regarded as primary metabolite, while further research and the availability of metabolite standards are needed to confirm whether monohydroxy-triDBE-DBCH is a primary or secondary metabolite [276]. Kinetic parameters calculated for monohydroxy-triDBE-DBCH are based on the assumption of being a primary metabolite and hence caution should be exerted when interpreting these results.

Table 6-4. Kinetic parameters derived from Michaelis–Menten model for the formation of DBE-DBCH metabolites following incubation of technical DBE-DBCH and β -DBE-DBCH with TLM for 60 Min.

Metabolite	K_m (μM) \pm SD	V_{max} ($\text{pmol min}^{-1} \text{mg protein}^{-1}$) \pm SD
<i>technical DBE-DBCH</i>		
OH-DBE-DBCH	22.0 \pm 6.6	1.9 \pm 0.4
OH-triDBE-DBCH	15.8 \pm 4.9	0.16 \pm 0.03
<i>β-DBE-DBCH</i>		
OH- β -DBE-DBCH	21.5 \pm 10	0.04 \pm 0.01

For technical DBE-DBCH, the maximum metabolic rate v_{max} indicates that monohydroxy-DBE-DBCH is formed primarily and at a faster rate than monohydroxy-triDBE-DBCH, with a value an order of magnitude lower, 1.9 and 0.16 $\text{pmol min}^{-1} \text{mg protein}^{-1}$, respectively.

For β -DBE-DBCH the formation rate of the monohydroxylated metabolite is even slower, with only 0.04 $\text{pmol min}^{-1} \text{mg protein}^{-1}$. When comparing these results to the study on human liver microsomes [276], it becomes evident that the maximum metabolic rate in trout is two orders of magnitude lower for the technical DBE-DBCH than for HLM. Contrary to human liver microsomes, β -DBE-DBCH in TLM seems to be metabolised by TLM at a much slower rate. This, together with comparatively higher K_M values could indicate that the affinity and metabolic rate of the species specific-enzymes in TLM for DBE-DBCH in an *in vitro* setting are generally lower. However, an *in vivo* study in juvenile brown trout reported the rapid metabolism of

β -DBE-DBCH and depuration following first-order kinetics in their experiment [277], but could not detect any metabolites produced, albeit focusing only on two potential dibrominated metabolites. A similar study exposing the same species to environmentally relevant concentrations of β -DBE-DBCH equally failed to detect any debrominated or dehydrobrominated metabolites and provided no indication of isomerization to other isoform. While no details metabolic/depuration rates were specified, the group reported that β -DBE-DBCH may modulate the thyroid axis in fish [278].

6.4. Conclusion

The HRAM Q-Exactive Orbitrap employed in this work provides sensitive, reliable detection and identification of metabolites of NBFRs despite the low, environmentally-relevant concentrations used in this study. Further, it gives valuable information and insight into the metabolic pathways of these chemicals. This demonstrates the ability of this platform as a sensitive, selective and HR platform for metabolic studies in this field of science. In addition, the software Compound Discoverer can aid in the identification of metabolites, also in more complex metabolite studies.

Results indicate, that species-specific differences and variations in the metabolism of NBFRs can be observed. For EH-TBB, the metabolite 2,3,4,5 tetrabromobenzoic acid (TBBA) appears to be a suitable biomarker to detect this NBFR in biota samples. Further, 2,3,4,5-tetrabromomethylbenzoate (TBMB) should also be included in future monitoring, as a study suggest that TBBA acts only as an intermediate metabolite [115]. For BEH-TEBP on the other hand, no metabolite was found and can be suggested at this stage, but metabolic loss of this NBFR has been reported in a study with common carp hepatic subcellular fractions [115]. More studies on the accumulation, metabolism and genotoxicity of both compounds in fish and their possible adverse effects to aquatic species have to be conducted. Both EH-TBB and BEH-TEBP have been detected in marine mammals, which is especially of concern, since they were found in top-trophic-level marine organisms [75]. It would be interesting to investigate the presence of TBBA and TBMB in these marine species, bearing in mind possible metabolic differences between mammals and fish. However, TBBA was also reported as main metabolite in human and rat liver microsome experiments [257].

For BTBPE no metabolite can be suggested, since no metabolic activity was observed in our experiments. In a dietary exposure of BTBPE in juvenile rainbow trout, similarly no metabolite formation was detected and BTBPE was accumulated in the tissue. Results for BTBPE indicate the impact on immune related gene transcription, as well as oxidative stress and endocrine disruption potential [273]. Since BTBPE has been detected in fish [43, 50], further studies investigating its adverse effects and any possible metabolite formation.

The DBE-DBCH *in vitro* study showed the formation of two metabolites, monohydroxy-DBE-DBCH and monohydroxy-triDBE-DBCH, which are suggested to be used as biomarkers in future research studies. Since DBE-DBCH has been detected in UK diet samples, including fish [67], further studies are needed to understand the toxicity of these metabolites and investigate their presence in fish samples.

Possible non-metabolic sources of the metabolites identified in our study are not reported in literature, but have to be considered if conducting such experiments, as they would falsify any results and conclusions taken. Several negative controls were included with each of our experiment to avoid any false positives. Further research is necessary to understand the potential differences between observations made in *in vivo* and *in vitro* studies, as well as to understand which metabolites are formed and where, how they compare to their parent compounds in terms of toxicity, as well how they are possibly eliminated from the organism. Especially, when considering that these contaminants and their metabolites can be magnified through the food chain to reach top-trophic-level organism or end up in food for human consumption. With this information and as a next step, biota samples (or samples from feeding studies) can then be analysed and the presence and toxicity of the suggested biomarkers investigated.

Chapter VII – Summary and future perspectives

The principal aim of this thesis was to gain a greater understanding of the levels and behaviour of LBFRs and NBFRs as well as investigate their transformation reactions in the environment, making use of state-of-the-art high resolution accurate mass instrumentation.

7.1. Summary and Conclusions

The aims and objectives of this thesis were accomplished by:

- Developing a multi-residue analysis method for the detection of LBFRs and NBFRs based on a UPLC-HRMS Orbitrap system, and subsequently testing its suitability for the intended purpose. This was evaluated by screening for halogenated compounds in a complex data set of organic contaminants and exploiting their characteristic mass defect with the use of high resolution accurate mass measurements. The set included 60 compounds (10 PBDEs, HBCDDs, TBBPA, 15 NBFRs, 6 Dechloranes, 3 OPFRs, as well as 8 PCBs and 16 PAHs). The UPLC-Orbitrap positively identified 44 compounds, with the exception of PAHs which cannot be detected on the present instrument. Mass defect plots of an extracted dust and sediment samples revealed the presence of both LBFRs (PBDEs and HBCDDs), as well as NBFRs (DBDPE and BEH-TEBP). In addition, through the use of accurate mass and isotope pattern matching, the presence of e.g. polychlorinated biphenyls (PCBs), chlorinated paraffins (CP), chlorinated terphenyls, as well as bromo- and chlorophenols was suggested within these samples. MD plots can be exploited as a screening and untargeted analysis tool for environmental samples. The results can serve to draw attention to halogenated ions that do not correspond to targeted compounds and would otherwise be very challenging to discover. Transformed mass defect plots cannot be used to discriminate between legacy BFRs and novel BFRs, but can readily visualize the presence of potentially

novel persistent and bioaccumulative halogenated chemicals in a complex mass spectrum. Furthermore, a two-dimensional gas chromatography system (GCxGC) coupled to a time-of-flight mass spectrometer (TOF-MS) was employed and demonstrated enhanced chromatographic separation (compared to a one dimensional chromatographic system) of most contaminants (50 out of 60), followed by database searches based on fragmentation spectra for confirmation purposes.

- Establishing a protocol for the extraction, clean-up and instrumental analysis of sediment samples. These were taken along the River Thames, from central London to the North Sea, passing through the industrial area of the city. Results indicate that BDE-209 is the predominant congener in all samples, accounting for ~ 95 % of total PBDEs detected, with a concentration range of <math><0.1</math> to \Sigma_{12}BDEs in this study, as well as showing a similar concentration pattern along the river, possibly indicating a similar source input. Spatial variation analysis of the sediment samples further revealed that locations within the industrial area of London had significantly higher concentrations of Σ_{12} BDEs, HBCDDs, TBBPA, as well as BEH-TEBP, BTBPE and TBP. Therefore, it is suggested to especially track the latter three compounds as NFRs candidates in future environmental studies. Analysis of HBCDD diastereomer patterns revealed samples from three locations within the industrial area possessed

comparatively high concentrations and diastereomer profiles matching those of the technical mixture. This could possibly indicate fresh input sources at these locations. Further, the presence of bromophenols and hydroxylated PBDEs in the analysed sediments indicate the presence of transformation product in the environment and need to be further investigated. Giving a final verdict on whether these compounds in the investigated area originate from leachates from consumer products on landfill sites, sewage treatment plants or are emissions from industry cannot be confirmed at this point. A study on the industries employing BFR in their products in the investigated area is necessary to identify potential sources. Sediment can be regarded as sinks for environmental pollutants and thus can contribute to reveal which compounds are persistent and might lead to environmental concern in the future.

- Conducting controlled *in vitro* trout liver microsome experiments to better understand the metabolic reactions of NBFRs and find suitable biomarkers for the investigation of further biota sample analysis. The employed high resolution Orbitrap system provides valuable information and insight into the metabolite formation pathways of NBFRs despite the low, environmentally-relevant concentrations applied in the study design. A possible biomarker for EH-TBB was identified as 2,3,4,5 tetrabromobenzoic acid (TBBA). For DBE-DBCH monohydroxy-DBE-DBCH and monohydroxy-triDBE-DBCH were detected. Experiments for BEH-TEBP showed a reduction of the initial dose of the parent compound after treatment, but no stable ions for potential metabolites were confirmed, while screening results for BTBPE indicated no reduction of the initial dose after treatment with TLM and thus likely the absence of *in vitro* metabolism. Further research is necessary to understand the potential differences between observations made in *in vivo* and *in vitro* studies, together with the analysis of biota samples for the suggested biomarkers, as not many studies have

focused on this. Comparison of these metabolites and their parent compounds in terms of toxicity is also needed, especially when considering that both these compounds can be magnified through the food chain to reach top-trophic-level organism or end up in food for human consumption.

- Photodegradation of EH-TBB, BEH-TEBP, BTBPE and DBDPE in different solvent indicated the sequential debromination reaction to form lower brominated compounds. For EH-TBB di- and tribrominated products were formed, BEH-TEBP showed formation of mono-, di- and tribrominated degradants, while DBDPE showed the presence of tri- to nona-brominated-BDPE. BTBPE did not only form tri-, tetra- and penta- brominated products, but also several other di- and tribrominated degradants were tentatively identified. This is of special interest, since lower brominated compounds have shown to be more toxic and biologically available. It is of special importance to conduct field-based fate experiments in relevant environmental and understand how they compare to our findings. So far, photodegradation products have not been reported in environmental samples. This could be caused by the fact that degradation mechanism differs when compounds are bound and incorporated into a matrix. Therefore, conducting photodegradation experiments in environmental matrixes serves to understand if these degradants are also formed under natural conditions and can be compared to our findings. The availability of authentic standards for these transformation products further allows for better identification and quantification.

7.2. Research gaps and future perspective

Research gaps remain and further studies are required to address the following aspects:

- Enhancement of current analytical techniques and methods for analysis, with a special focus on
 - sample preparation methods, not discriminating between parent and possible transformation products,
 - availability of (internal isotopically-labelled) standards for metabolite/transformation product identification (for major metabolites and reaction products),
 - validated multi-residue methods for the analysis of NBFRs, with good analytical performance including standard reference materials for NBFRs,
 - and automated software tools for handling the amount of data produced in HR measurements.
- Increase use of high resolution instrumentation platforms and HR data acquisition, allowing for the retrospective screening of future compounds of interest in already measured data-sets (GC-Orbitrap, LC-Orbitrap), as well improvements in the capabilities (i.e. scan speed, resolution) of two dimensional chromatography systems coupled to high resolution systems (GC x GC – HR-TOF).
- Conduct more environmental studies in various matrices (e.g. dust, soil, sediment) and locations to understand which NBFRs need to be targeted and possibly regulated in the future, together with identification of sources.
- Examine the presence of transformation products (based on biomarkers identified in metabolic studies and principal degradants resulting of forced irradiation experiments) in environmental and biota samples, as well as *in vitro* / *in vivo* comparisons.

- Consider the toxic implications of the degradation / biotransformation products identified in this study and follow-up studies to understand the fate and behaviour of these chemicals, with the final aim of taking regulatory decisions where necessary.
- Investigate the potential interaction between sediment microbiome / aquatic microorganisms and various (N)BFRs and explore the potential of these organisms for aerobic / anaerobic degradation of hazardous (N)BFRs.
- Development of holistic strategies to get a better understanding of the influence of toxic chemical mixtures in sediment and river water on the aquatic biota.

References

1. D'Silva, K., A. Fernandes, and M. Rose, *Brominated Organic Micropollutants—Igniting the Flame Retardant Issue*. Critical Reviews in Environmental Science and Technology, 2004. **34**(2): p. 141-207.
2. Ezechias, M., S. Covino, and T. Cajthaml, *Ecotoxicity and biodegradability of new brominated flame retardants: A review*. Ecotoxicology and Environmental Safety, 2014. **110**: p. 153-167.
3. Shaw, S.D., et al., *Halogenated flame retardants Do the fire safety benefits justify the risks*. Organohalogen Compounds, 2010. **73**: p. 2036-2039.
4. Dirtu, A.C., et al., *Transformation Products of Brominated Flame Retardants (BFRs)*, in *Transformation Products of Emerging Contaminants in the Environment: Analysis, Processes, Occurrence, Effects and Risks*, D.A. Lambropoulou and L.M.L. Nollet, Editors. 2014, John Wiley and Sons Ltd: Chichester, United Kingdom. p. 545-576.
5. DiGangi, J., et al., *San Antonio Statement on brominated and chlorinated flame retardants*. Environmental Health Perspective, 2010. **118**(12): p. A516-8.
6. Barceló, D. and E. Eljarrat, *Brominated Flame Retardants*. Vol. 16. 2011.
7. Stockholm Convention, *Global chemical experts take science to action by moving towards phase out of toxic chemicals*. 2015: online at <http://chm.pops.int/Implementation/PublicAwareness/PressReleases/OutcomesofPOPRC11/tabid/4692/Default.aspx>.
8. UNEP, *Guidance for the inventory, of Hexabromocyclododecane (HBCD)*. 2017.
9. Abdallah, M.A., *Environmental occurrence, analysis and human exposure to the flame retardant tetrabromobisphenol-A (TBBP-A)-A review*. Environment International, 2016. **94**: p. 235-250.
10. Bergman, A., et al., *A novel abbreviation standard for organobromine, organochlorine and organophosphorus flame retardants and some characteristics of the chemicals*. Environment International, 2012. **49**: p. 57-82.
11. Babrauskas, V., et al., *Flame Retardants in Furniture Foam: Benefits and Risks*. Fire Safety Science, 2011. **10**: p. 265-278.
12. Kemmlein, S., D. Herzke, and R.J. Law, *Brominated flame retardants in the European chemicals policy of REACH-Regulation and determination in materials*. Journal of Chromatography A, 2009. **1216**(3): p. 320-33.
13. Law, R.J., et al., *Levels and trends of brominated flame retardants in the European environment*. Chemosphere, 2006. **64**(2): p. 187-208.
14. Covaci, A., et al., *Novel brominated flame retardants: a review of their analysis, environmental fate and behaviour*. Environment International, 2011. **37**(2): p. 532-56.
15. Harju, M., et al., *Emerging "new" Brominated flame retardants in flame retarded products and the environment*, N.P.C. Authority, Editor. 2009.
16. de Wit, C.A., D. Herzke, and K. Vorkamp, *Brominated flame retardants in the Arctic environment--trends and new candidates*. Science of The Total Environment, 2010. **408**(15): p. 2885-918.
17. Luo, X., et al., *Advances in the study of current-use non-PBDE brominated flame retardants and dechlorane plus in the environment and humans*. Science China Chemistry, 2010. **53**(5): p. 961-973.
18. Vorkamp, K. and F.F. Riget, *A review of new and current-use contaminants in the Arctic environment: Evidence of long-range transport and indications of bioaccumulation*. Chemosphere, 2014. **111C**: p. 379-395.
19. Urs, J., *Emerging Brominated Flame Retardants in Sediments and Soils: a Review*. Current Pollution Reports, 2016. **2**(4): p. 213-223.

20. Ma, Y., et al., *Has the phase-out of PBDEs affected their atmospheric levels? Trends of PBDEs and their replacements in the Great Lakes atmosphere*. Environmental Science & Technology, 2013. **47**(20): p. 11457-64.
21. de Wit, C.A., et al., *Emerging Brominated Flame Retardants in the Environment*, in *Brominated Flame Retardants*, E. Eljarrat and D. Barceló, Editors. 2011, Springer-Verlag: Berlin Heidelberg. p. 241-286.
22. Schymanski, E.L., et al., *Identifying small molecules via high resolution mass spectrometry: communicating confidence*. Environmental Science & Technology, 2014. **48**(4): p. 2097-8.
23. Watanabe, I. and S.-i. Sakai, *Environmental release and behavior of brominated flame retardants*. Environment International, 2003. **29**(6): p. 665-682.
24. Dirtu, A.C., et al., *Advances in the sample preparation of brominated flame retardants and other brominated compounds*. TrAC Trends in Analytical Chemistry, 2013. **43**: p. 189-203.
25. Wu, J.P., et al., *Several current-use, non-PBDE brominated flame retardants are highly bioaccumulative: evidence from field determined bioaccumulation factors*. Environment International, 2011. **37**(1): p. 210-5.
26. Wang, X., et al., *Levels and distribution of brominated flame retardants in the soil of Harbin in China*. Journal of Environmental Sciences, 2009. **21**(11): p. 1541-1546.
27. Wang, D.G., et al., *Analysis and occurrence of emerging chlorinated and brominated flame retardants in surficial sediment of the Dalian coastal area in China*. Journal of Environmental Monitoring, 2011. **13**(11): p. 3104-10.
28. Ricklund, N., A. Kierkegaard, and M.S. McLachlan, *An international survey of decabromodiphenyl ethane (deBDethane) and decabromodiphenyl ether (decaBDE) in sewage sludge samples*. Chemosphere, 2008. **73**(11): p. 1799-1804.
29. Bjorklund, J.A., et al., *Indoor air is a significant source of tri-decabrominated diphenyl ethers to outdoor air via ventilation systems*. Environmental Science & Technology, 2012. **46**(11): p. 5876-84.
30. Karlsson, M., et al., *Levels of brominated flame retardants in blood in relation to levels in household air and dust*. Environment International, 2007. **33**(1): p. 62-9.
31. Darnerud, P.O., et al., *Time trends of polybrominated diphenylether (PBDE) congeners in serum of Swedish mothers and comparisons to breast milk data*. Environmental Research, 2015. **138**: p. 352-60.
32. Wu, N., et al., *Human Exposure to PBDEs- Associations of PBDE Body Burdens with Food Consumption and House Dust Concentrations*. Environmental Science & Technology, 2007. **41**(5): p. 1584-1589.
33. Wildford, B.H., et al., *Passive Sampling Survey of Polybrominated Diphenyl Ether Flame Retardants in Indoor and Outdoor Air in Ottawa, Canada- Implications for Sources and Exposure*. Environmental Science & Technology, 2004. **38**: p. 5312-5318.
34. Harrad, S., et al., *Indoor Contamination with Hexabromocyclododecanes, Polybrominated Diphenyl Ethers, and Perfluoroalkyl Compounds: An Important Exposure Pathway for People?* Environmental Science & Technology, 2010. **44**(9): p. 3221-3231.
35. Harrad, S. and S. Hunter, *Concentrations of Polybrominated Diphenyl Ethers in Air and Soil on a Rural-Urban Transect Across a Major UK Conurbation*. Environmental Science & Technology, 2006. **40**(15): p. 4548-4553.
36. Cousins, A.P., T. Holmgren, and M. Remberger, *Emissions of two phthalate esters and BDE 209 to indoor air and their impact on urban air quality*. Science of The Total Environment, 2014. **470-471**: p. 527-35.
37. Harner, T., et al., *Passive sampler derived air concentrations of PBDEs along an urban-rural transect: spatial and temporal trends*. Chemosphere, 2006. **64**(2): p. 262-7.
38. Battermann, S.A., et al., *Concentrations and Emissions of Polybrominated Diphenyl Ethers from U.S. Houses and Garages*. Environmental Science & Technology, 2009. **43**(8): p. 2693-2700.

39. Hoh, E., L. Zhu, and R.A. Hites, *Novel Flame Retardants, 1,2-Bis(2,4,6-tribromophenoxy)-ethane and 2,3,4,5,6-Pentabromo-ethylbenzene, in United States' Environmental Samples*. Environmental Science & Technology, 2005. **39**: p. 2472-2477.
40. Qiu, X., C.H. Marvin, and R.A. Hites, *Dechlorane Plus and Other Flame Retardants in a Sediment Core from Lake Ontario*. Environmental Science & Technology, 2007. **41**: p. 6014-6019.
41. Hoh, E. and R.A. Hites, *Brominated Flame Retardants in the Atmosphere of the East-Central United States*. Environmental Science & Technology, 2005. **39**: p. 7794-7802.
42. Olukunle, O.I. and O.J. Okonkwo, *Concentration of novel brominated flame retardants and HBCD in leachates and sediments from selected municipal solid waste landfill sites in Gauteng Province, South Africa*. Waste Management, 2015.
43. Shi, T., et al., *Occurrence of brominated flame retardants other than polybrominated diphenyl ethers in environmental and biota samples from southern China*. Chemosphere, 2009. **74**(7): p. 910-6.
44. Wu, J.P., et al., *Trophodynamics of Hexabromocyclododecanes and Several Other Non-PBDE Brominated Flame Retardants in a Freshwater Food Web*. Environmental Science & Technology, 2010. **44**: p. 5490-5495.
45. Nyholm, J.R., et al., *Environmental occurrence of emerging and legacy brominated flame retardants near suspected sources in Norway*. Science of The Total Environment, 2013. **443**: p. 307-14.
46. La Guardia, M.J., et al., *Flame-Retardants and Other Organohalogenes Detected in Sewage Sludge by Electron Capture Negative Ion Mass Spectrometry*. Environmental Science & Technology, 2010. **44**: p. 4658-4664.
47. Stapleton, H.M., et al., *Detection of Organophosphate Flame Retardants in Furniture Foam and U.S. House Dust*. Environmental Science & Technology, 2009. **43**: p. 7490-7495.
48. Harrad, S., et al., *Concentrations of brominated flame retardants in dust from United Kingdom cars, homes, and offices: causes of variability and implications for human exposure*. Environment International, 2008. **34**(8): p. 1170-5.
49. Tao, F., M.A. Abdallah, and S. Harrad, *Emerging and Legacy Flame Retardants in UK Indoor Air and Dust: Evidence for Replacement of PBDEs by Emerging Flame Retardants?* Environmental Science & Technology, 2016. **50**(23): p. 13052-13061.
50. Ismail, N., et al., *Brominated and chlorinated flame retardants in Lake Ontario, Canada, lake trout between 1979 and 2004 and possible influences of food-web changes*. Environmental Toxicology and Chemistry, 2009. **28**(5): p. 910-920.
51. Law, K., et al., *Bioaccumulation and trophic transfer of some brominated flame retardants in a Lake Winnipeg (Canada) food web*. Environmental Toxicology and Chemistry, 2006. **25**(8): p. 2177-2186.
52. Gauthier, L.T., et al., *Temporal Trends and Spatial Distribution of Non-polybrominated Diphenyl Ether Flame Retardants in the Eggs of Colonial Populations of Great Lakes Herring Gulls*. Environmental Science & Technology, 2009. **47**: p. 312-317.
53. Ricklund, N., A. Kierkegaard, and M.S. McLachlan, *Levels and Potential Sources of Decabromodiphenyl Ethane (DBDPE) and Decabromodiphenyl Ether (DecaBDE) in Lake and Marine Sediments in Sweden*. Environmental Science & Technology, 2010. **44**: p. 1987-1991.
54. Zhang, X.L., et al., *Spatial distribution and vertical profile of polybrominated diphenyl ethers, tetrabromobisphenol A, and decabromodiphenylethane in river sediment from an industrialized region of South China*. Environmental Pollution, 2009. **157**(6): p. 1917-23.
55. Yang, C., *Persistent Organic Pollutants in lacustrine environments, in School of Geography, Earth and Environmental Sciences*. 2014, University of Birmingham: Birmingham.
56. Wu, F., et al., *Polybrominated diphenyl ethers and decabromodiphenylethane in sediments from twelve lakes in China*. Environmental Pollution, 2012. **162**: p. 262-8.
57. Kierkegaard, A., T. Björklund, and U. Friden, *Identification of the Flame Retardant Decabromodiphenyl Ethane in the Environment*. Environmental Science & Technology, 2004. **38**: p. 3247-3253.

58. Eljarrat, E., et al., *Occurrence of the "new" brominated flame retardant, decabromodiphenyl ethane, in sewage sludge from Spain*. *Organohalogen Compounds*, 2005. **67**: p. 459-461.
59. McCrindle, R., et al., *Native and Mass Labeled [¹³C¹⁴]-Decabromodiphenylethane (DBDPE): Characterization and Use in Determination of DBDPE in Sewage Sludge*. *Organohalogen Compounds*, 2004. **66**: p. 3744-3750.
60. Drage, D.S., et al., *Concentrations of legacy and emerging flame retardants in air and soil on a transect in the UK West Midlands*. *Chemosphere*, 2016. **148**: p. 195-203.
61. Al-Omran, L.S. and S. Harrad, *Distribution pattern of legacy and "novel" brominated flame retardants in different particle size fractions of indoor dust in Birmingham, United Kingdom*. *Chemosphere*, 2016. **157**: p. 124-131.
62. Ali, N., et al., *"Novel" brominated flame retardants in Belgian and UK indoor dust: implications for human exposure*. *Chemosphere*, 2011. **83**(10): p. 1360-5.
63. Stapleton, H.M., et al., *Alternate and New Brominated Flame Retardants Detected in U.S. House Dust*. *Environmental Science & Technology*, 2008. **42**(18): p. 6910-6916.
64. He, M.J., et al., *Bioaccumulation of polybrominated diphenyl ethers and decabromodiphenyl ethane in fish from a river system in a highly industrialized area, South China*. *Science of The Total Environment*, 2012. **419**: p. 109-15.
65. Luo, X.J., et al., *Persistent Halogenated Compounds in Waterbirds from an e-Waste Recycling Region in South China*. *Environmental Science & Technology*, 2009. **43**: p. 306-311.
66. Hu, G.-c., et al., *Brominated Flame Retardants, Polychlorinated Biphenyls, and Organochlorine Pesticides in Captive Giant Panda (*Ailuropoda melanoleuca*) and Red Panda (*Ailurus fulgens*) from China*. *Environmental Science & Technology*, 2008. **42**: p. 4704-4709.
67. Tao, F., et al., *Emerging and legacy flame retardants in UK human milk and food suggest slow response to restrictions on use of PBDEs and HBCDD*. *Environment International*, 2017. **105**: p. 95-104.
68. Wang, F., et al., *Comparative Tissue Distribution, Biotransformation and Associated Biological Effects by Decabromodiphenyl Ethane and Decabrominated Diphenyl Ether in Male Rats after a 90-Day Oral Exposure Study*. *Environmental Science & Technology*, 2010. **44**: p. 5655-5660.
69. Hardy, M.L., et al., *Studies and evaluation of the potential toxicity of decabromodiphenyl ethane to five aquatic and sediment organisms*. *Ecotoxicology and Environmental Safety*, 2012. **75**(1): p. 73-9.
70. Lam, J.C., et al., *Temporal Trends of Hexabromocyclododecanes (HBCDs) and Polybrominated Diphenyl Ethers (PBDEs) and Detection of Two Novel Flame Retardants in Marine Mammals from Hong Kong, South China*. *Environmental Science & Technology*, 2009. **43**: p. 6944-6949.
71. Al-Omran, L.S. and S. Harrad, *Within-room and within-home spatial and temporal variability in concentrations of legacy and "novel" brominated flame retardants in indoor dust*. *Chemosphere*, 2018. **193**: p. 1105-1112.
72. Betts, K., *New flame retardants detected in indoor and outdoor environments*. *Environmental Science & Technology*, 2008. **42**(18): p. 6778-6778.
73. Berr, J.S., H.M. Stapleton, and C.L. Mitchelmore, *Accumulation and DNA damage in fathead minnows (*Pimephales promelas*) exposed to 2 brominated flame-retardant mixtures, Firemaster[®] 550 and Firemaster[®] BZ-54*. *Environmental Toxicology and Chemistry*, 2010. **29**(3): p. 722-729.
74. Betts, K.S., *Tracking alternative flame retardants: hand-to-mouth exposures in adults*. *Environmental Health Perspective*, 2015. **123**(2): p. A44.
75. Lam, J.C.W., et al., *Temporal Trends of HBCDs and PBDEs and Detection of Two Novel Flame Retardants in Marine Mammals from Hong Kong, South China*. *Environmental Science & Technology*, 2013. **43**: p. 6944-6949.
76. Verreault, J., et al., *Brominated Flame Retardants in Glaucous Gulls from the Norwegian Arctic More Than Just an Issue of Polybrominated Diphenyl Ethers*. *Environmental Science & Technology*, 2007. **41**: p. 4925-4931.

77. Gauthier, L.T., et al., *Current-Use Flame Retardants in the Eggs of Herring Gulls (*Larus argentatus*) from the Laurentian Great Lakes*. Environmental Science & Technology, 2007. **41**: p. 4561-4567.
78. Klosterhaus, S.L., et al., *Brominated and chlorinated flame retardants in San Francisco Bay sediments and wildlife*. Environment International, 2012. **47**: p. 56-65.
79. Law, R.J., et al., *Alternative flame retardants, Dechlorane Plus and BDEs in the blubber of harbour porpoises (*Phocoena phocoena*) stranded or bycaught in the UK during 2008*. Environment International, 2013. **60**(0): p. 81-88.
80. Houde, M., et al., *Novel brominated flame retardants and dechloranes in three fish species from the St. Lawrence River, Canada*. Science of The Total Environment, 2014. **479–480**: p. 48-56.
81. Gorga, M., et al., *Determination of PBDEs, HBB, PBEB, DBDPE, HBCD, TBBPA and related compounds in sewage sludge from Catalonia (Spain)*. Science of The Total Environment, 2013. **444**: p. 51-59.
82. Poma, G., et al., *Concentrations and trophic interactions of novel brominated flame retardants, HBCD, and PBDEs in zooplankton and fish from Lake Maggiore (Northern Italy)*. Science of The Total Environment, 2014. **481**(0): p. 401-408.
83. Schlabach, M., *Nordic screening data relevant for PBT evaluation*. 2012, NILU.
84. Lopez, P., et al., *Optimization and development of analytical methods for the determination of new brominated flame retardants and polybrominated diphenyl ethers in sediments and suspended particulate matter*. Analytical and Bioanalytical Chemistry, 2011. **400**(3): p. 871-83.
85. Moller, A., et al., *Polybrominated diphenyl ethers (PBDEs) and alternative brominated flame retardants in air and seawater of the European Arctic*. Environmental Pollution, 2011. **159**(6): p. 1577-83.
86. Suhring, R., et al., *Fingerprint analysis of brominated flame retardants and Dechloranes in North Sea sediments*. Environmental Research, 2015. **140**: p. 569-78.
87. Yang, R., et al., *Emerging brominated flame retardants in the sediment of the Great Lakes*. Environmental Science & Technology, 2012. **46**(6): p. 3119-26.
88. Lam, J.C.W., et al., *Emerging halogenated flame retardants in coastal region of China*. Organohalogen Compounds, 2013. **75**: p. 1269-1272.
89. Zhu, B., et al., *Conventional and emerging halogenated flame retardants (HFRs) in sediment of Yangtze River Delta (YRD) region, East China*. Chemosphere, 2013. **93**(3): p. 555-60.
90. Nyholm, J.R., C. Lundberg, and P.L. Andersson, *Biodegradation kinetics of selected brominated flame retardants in aerobic and anaerobic soil*. Environmental Pollution, 2010. **158**(6): p. 2235-40.
91. von der Recke, R. and W. Vetter, *Synthesis and Characterization of 2,3-Dibromopropyl-2,4,6-tribromophenyl Ether (DPTE) and Structurally Related Compounds Evidenced in Seal Blubber and Brain*. Environmental Science & Technology, 2007. **41**: p. 1590-1595.
92. Vorkamp, K., et al., *Novel brominated flame retardants and dechlorane plus in Greenland air and biota*. Environmental Pollution, 2015. **196**: p. 284-91.
93. Newton, S., U. Sellstrom, and C.A. de Wit, *Emerging flame retardants, PBDEs, and HBCDDs in indoor and outdoor media in Stockholm, Sweden*. Environmental Science & Technology, 2015. **49**(5): p. 2912-20.
94. Poma, G., C. Roscioli, and L. Guzzella, *PBDE, HBCD, and novel brominated flame retardant contamination in sediments from Lake Maggiore (Northern Italy)*. Environmental Monitoring and Assessment, 2014. **186**(11): p. 7683-92.
95. Zhang, X.L., et al., *Spatial distribution and vertical profile of polybrominated diphenyl ethers, tetrabromobisphenol A, and decabromodiphenylethane in river sediment from an industrialized region of South China*. Environmental Pollution, 2009. **157**(6): p. 1917-23.
96. Luo, X.J., et al., *Persistent Halogenated Compounds in Waterbirds from an e-Waste Recycling Region in South China*. 2009. **43**: p. 306-311.

97. Weijs, L., et al., *Bioaccumulation and Biotransformation of Brominated Flame Retardants*, in *Persistent Organic Pollutants (POPs): Analytical Techniques, Environmental Fate and Biological Effects*, E. Zeng, Editor. 2015, Elsevier. p. 433-491.
98. Eljarrat, E., M.L. Feo, and D. Barceló, *Degradation of Brominated Flame Retardants*, in *Brominated Flame Retardants*, E. Eljarrat and D. Barceló, Editors. 2011, Springer-Verlag: Berlin Heidelberg. p. 187-202.
99. Fang, L., et al., *Photochemical degradation of six polybrominated diphenyl ether congeners under ultraviolet irradiation in hexane*. *Chemosphere*, 2008. **71**(2): p. 258-67.
100. Shih, Y.H. and C.K. Wang, *Photolytic degradation of polybromodiphenyl ethers under UV-lamp and solar irradiations*. *Journal of Hazardous Materials*, 2009. **165**(1-3): p. 34-8.
101. Harrad, S., M.A. Abdallah, and A. Covaci, *Causes of variability in concentrations and diastereomer patterns of hexabromocyclododecanes in indoor dust*. *Environment International*, 2009. **35**(3): p. 573-9.
102. Kajiwara, N., et al., *Photolysis of brominated flame retardants in textiles exposed to natural sunlight*. *Environmental Science: Processes & Impacts*, 2013. **15**(3): p. 653.
103. Davis, E.F. and H.M. Stapleton, *Photodegradation Pathways of Nonabrominated Diphenyl Ethers, 2-Ethylhexyltetrabromobenzoate and Di(2-ethylhexyl)tetrabromophthalate Identifying Potential Markers of Photodegradation*. *Environmental Science & Technology*, 2009. **43**: p. 5739-5746.
104. Balabanovich, A.I., et al., *Thermal decomposition behavior of 1,2-bis-(2,4,6-tribromophenoxy)ethane*. *Journal of Analytical and Applied Pyrolysis*, 2003. **67**: p. 95-107.
105. Stiborova, H., et al., *Dynamics of brominated flame retardants removal in contaminated wastewater sewage sludge under anaerobic conditions*. *Science of The Total Environment*, 2015. **533**: p. 439-45.
106. Gerecke, A.C., et al., *Anaerobic Degradation of Decabromodiphenyl Ether*. *Environmental Science & Technology*, 2005. **39**: p. 1078-1083.
107. He, J., K.R. Robrock, and L. Alvarez-Cohen, *Microbial Reductive Debromination of Polybrominated Diphenyl Ethers*. *Environmental Science & Technology*, 2006. **40**: p. 4429-4434.
108. Vonderheide, A.P., et al., *Rapid breakdown of brominated flame retardants by soil microorganisms*. *Journal of Analytical Atomic Spectrometry*, 2006. **21**(11): p. 1232.
109. Yen, J.H., et al., *Interaction of polybrominated diphenyl ethers (PBDEs) with anaerobic mixed bacterial cultures isolated from river sediment*. *Journal of Hazardous Materials*, 2009. **165**(1-3): p. 518-24.
110. Hakk, H. and R.J. Letcher, *Metabolism in the toxicokinetics and fate of brominated flame retardants - a review*. *Environment International*, 2003. **29**(6): p. 801-828.
111. Li, Y., et al., *Fate of tetrabromobisphenol A and hexabromocyclododecane brominated flame retardants in soil and uptake by plants*. *Chemosphere*, 2011. **82**(2): p. 204-9.
112. Stapleton, H.M., et al., *In vivo and in vitro debromination of deca- bromodiphenyl ether (BDE 209) by juvenile rainbow trout and common carp*. *Environmental Science & Technology*, 2006. **40**: p. 4653-4658.
113. Stapleton, H.M., *Brominated Flame Retardants - Assessing DecaBDE Debromination in the Environment*. 2006: EEN Epha Environment Network.
114. Noyes, P.D., D.E. Hinton, and H.M. Stapleton, *Accumulation and debromination of decabromodiphenyl ether (BDE-209) in juvenile fathead minnows (Pimephales promelas) induces thyroid disruption and liver alterations*. *Toxicological Sciences*, 2011. **122**(2): p. 265-74.
115. Berr, J.S., et al., *Species specific differences in the in vitro metabolism of the flame retardant mixture, Firemaster(R) BZ-54*. *Aquatic Toxicology*, 2012. **124-125**: p. 41-7.
116. Marsh, G., et al., *Identification of Hydroxylated and Methoxylated Polybrominated Diphenyl Ethers in Baltic Sea Salmon (Salmo salar) Blood*. *Environmental Science & Technology*, 2004. **38**(1): p. 10-18.

117. Lin, K., C. Yan, and J. Gan, *Production of hydroxylated polybrominated diphenyl ethers (OH-PBDEs) from bromophenols by manganese dioxide*. Environmental Science & Technology, 2014. **48**(1): p. 263-71.
118. Malmvärn, A., et al., *Hydroxylated and Methoxylated Brominated Diphenyl Ethers in the Red Algae *Ceramium tenuicorne* and Blue Mussels from the Baltic Sea*. Environmental Science & Technology, 2005. **39**(0): p. 2290-2997a.
119. Malmvärn, A., et al., *Hydroxylated and methoxylated polybrominated diphenyl ethers and polybrominated dibenzo-p-dioxins in red alga and cyanobacteria living in the Baltic Sea*. Chemosphere, 2008. **72**: p. 910-916.
120. Kerrigan, J.F., et al., *Quantification of Hydroxylated Polybrominated Diphenyl Ethers (OH-BDEs), Triclosan, and Related Compounds in Freshwater and Coastal Systems*. Plos One, 2015. **14**: p. 1-19.
121. Ueno, D., et al., *Hydroxylated Polybrominated Diphenyl Ethers (OH-PBDEs) in the Abiotic Environment- Surface Water and Precipitation from Ontario, Canada*. Environmental Science & Technology, 2008. **42**: p. 1657-1664.
122. Hua, W., E.R. Bennett, and R.J. Letcher, *Triclosan in waste and surface waters from the upper Detroit River by liquid chromatography-electrospray-tandem quadrupole mass spectrometry*. Environment International, 2005. **31**: p. 621-630.
123. Robrock, K., *Aerobic Biotransformation of Polybrominated Diphenyl Ethers (PBDEs) by Bacterial Isolates*. Environmental Science & Technology, 2009. **43**: p. 5705-5711.
124. Xia, X., *Microbial Degradation of Polybrominated Diphenyl Ethers- Current and Future*. Bioremediation and Biodegradation, 2013. **4**(1): p. 1-2.
125. Liu, H., et al., *Formation of 2'-hydroxy-2,3',4,5'-tetrabromodiphenyl ether (2'-HO-BDE68) from 2,4-dibromophenol in aqueous solution under simulated sunlight irradiation*. Chemosphere, 2011. **84**: p. 512-518.
126. Zhao, Q., et al., *Photochemical Formation of Hydroxylated Polybrominated Diphenyl Ethers (OH-PBDEs) from Polybrominated Diphenyl Ethers (PBDEs) in Aqueous Solution under Simulated Solar Light Irradiation*. Environmental Science & Technology, 2015. **49**: p. 9092-9099.
127. Agarwal, V., et al., *Biosynthesis of polybrominated aromatic organic compounds by marine bacteria*. Nature Chemical Biology, 2014. **10**(8): p. 640-7.
128. Wan, Y., et al., *Origin of Hydroxylated Brominated Diphenyl Ethers: Natural Compounds or Man-Made Flame Retardants?* Environmental Science & Technology, 2009. **43**: p. 7536-7542.
129. Su, G., et al., *Mechanisms of toxicity of hydroxylated polybrominated diphenyl ethers (HO-PBDEs) determined by toxicogenomic analysis with a live cell array coupled with mutagenesis in Escherichia coli*. Environmental Science & Technology, 2014. **48**(10): p. 5929-37.
130. Meerts, I.A.T.M., et al., *In Vitro Estrogenicity of Polybrominated Diphenyl Ethers, Hydroxylated PBDEs, and Polybrominated Bisphenol A Compounds*. Environmental Health Perspectives, 2001. **109**(4): p. 399-407.
131. Zota, A.R., et al., *Polybrominated diphenyl ethers, hydroxylated polybrominated diphenyl ethers, and measures of thyroid function in second trimester pregnant women in California*. Environmental Science & Technology, 2011. **45**(18): p. 7896-905.
132. Van Bostel, A.L., et al., *Microarray Analysis Reveals a Mechanism of Phenolic Polybrominated Diphenylether Toxicity in Zebrafish*. Environmental Science & Technology, 2008. **42**: p. 1773-1779.
133. Legradi, J., et al., *Disruption of oxidative phosphorylation (OXPHOS) by hydroxylated polybrominated diphenyl ethers (OH-PBDEs) present in the marine environment*. Environmental Science & Technology, 2014. **48**(24): p. 14703-11.
134. Pang, S.Y., et al., *Oxidation of flame retardant tetrabromobisphenol a by aqueous permanganate: reaction kinetics, brominated products, and pathways*. Environmental Science & Technology, 2014. **48**(1): p. 615-23.

135. Abdallah, M.A., et al., *High-resolution mass spectrometry provides novel insights into products of human metabolism of organophosphate and brominated flame retardants*. Analytical and Bioanalytical Chemistry, 2015. **407**(7): p. 1871-83.
136. Lagalante, A.F. and T.D. Oswald, *Analysis of polybrominated diphenyl ethers (PBDEs) by liquid chromatography with negative-ion atmospheric pressure photoionization tandem mass spectrometry (LC/NI-APPI/MS/MS): application to house dust*. Analytical and Bioanalytical Chemistry, 2008. **391**(6): p. 2249-56.
137. Abdallah, M.A., *Advances in Instrumental Analysis of Brominated Flame Retardants: Current Status and Future Perspectives*. International Scholarly Research Notices, 2014. **2014**: p. 1-21.
138. Portoles, T., et al., *Novel Analytical Approach for Brominated Flame Retardants Based on the Use of Gas Chromatography-Atmospheric Pressure Chemical Ionization-Tandem Mass Spectrometry with Emphasis in Highly Brominated Congeners*. Analytical Chemistry, 2015. **87**(19): p. 9892-9.
139. Megson, D., et al., *Determination of Halogenated Flame Retardants Using Gas Chromatography with Atmospheric Pressure Chemical Ionization (APCI) and a High-Resolution Quadrupole Time-of-Flight Mass Spectrometer (HRqTOFMS)*. Analytical Chemistry, 2016. **88**: p. 11406-11411.
140. Ballesteros-Gomez, A., J. de Boer, and P.E. Leonards, *Novel analytical methods for flame retardants and plasticizers based on gas chromatography, comprehensive two-dimensional gas chromatography, and direct probe coupled to atmospheric pressure chemical ionization-high resolution time-of-flight-mass spectrometry*. Analytical Chemistry, 2013. **85**(20): p. 9572-80.
141. Zhou, S.N., et al., *Development of liquid chromatography atmospheric pressure chemical ionization tandem mass spectrometry for analysis of halogenated flame retardants in wastewater*. Analytical and Bioanalytical Chemistry, 2010. **396**(3): p. 1311-20.
142. Al-Odaini, N.A., et al., *Isotopic dilution determination of emerging flame retardants in marine sediments by HPLC-APCI-MS/MS*. Analytical Methods, 2013. **5**(7): p. 1771.
143. Abdallah, M.A. and S. Harrad, *Determination of PBDEs using liquid chromatography - negative ionization-atmospheric pressure photoionisation-tandem mass spectrometry (LC-NI-APPI-MS/MS): validation and application to house dust*. 2009.
144. Debrauwer, L., et al., *Probing new approaches using atmospheric pressure photo ionization for the analysis of brominated flame retardants and their related degradation products by liquid chromatography-mass spectrometry*. Journal of Chromatography A, 2005. **1082**(1): p. 98-109.
145. Zhou, S.N., et al., *Liquid chromatography-atmospheric pressure photoionization tandem mass spectrometry for analysis of 36 halogenated flame retardants in fish*. Journal of Chromatography A, 2010. **1217**(5): p. 633-41.
146. Cariou, R., et al., *Comparison of Analytical Strategies for the Chromatographic and Mass Spectrometric Measurement of Brominated Flame Retardants: 1. Polybrominated Diphenylethers*. Journal of Chromatographic Science, 2006. **44**: p. 489-497.
147. Budakowski, W. and G. Tomy, *Congener-specific analysis of hexabromocyclododecane by high-performance liquid chromatography/electrospray tandem mass spectrometry*. Rapid Communications in Mass Spectrometry, 2003. **17**(13): p. 1399-1404.
148. Chu, S., G.D. Haffner, and R.J. Letcher, *Simultaneous determination of tetrabromobisphenol A, tetrachlorobisphenol A, bisphenol A and other halogenated analogues in sediment and sludge by high performance liquid chromatography-electrospray tandem mass spectrometry*. Journal of Chromatography A, 2005. **1097**(1-2): p. 25-32.
149. Mascolo, G., V. Locaputo, and G. Mininni, *New perspective on the determination of flame retardants in sewage sludge by using ultrahigh pressure liquid chromatography-tandem mass spectrometry with different ion sources*. Journal of Chromatography A, 2010. **1217**(27): p. 4601-11.
150. Li, D.X., et al., *Gas chromatography coupled to atmospheric pressure ionization mass spectrometry (GC-API-MS): review*. Analytica Chimica Acta, 2015. **891**: p. 43-61.

151. Papachlimitzou, A., et al., *A review of the analysis of novel brominated flame retardants*. Journal of Chromatography A, 2012. **1219**: p. 15-28.
152. Cristale, J. and S. Lacorte, *Development and validation of a multiresidue method for the analysis of polybrominated diphenyl ethers, new brominated and organophosphorus flame retardants in sediment, sludge and dust*. Journal of Chromatography A, 2013. **1305**: p. 267-75.
153. Van den Eede, N., et al., *Multi-residue method for the determination of brominated and organophosphate flame retardants in indoor dust*. Talanta, 2012. **89**: p. 292-300.
154. Sahlstrom, L.M., U. Sellstrom, and C.A. De Wit, *Clean-up method for determination of established and emerging brominated flame retardants in dust*. Analytical and Bioanalytical Chemistry, 2012. **404**: p. 454-466.
155. Ali, N., et al., *Analytical characteristics and determination of major novel brominated flame retardants (NBFRs) in indoor dust*. Analytical and Bioanalytical Chemistry, 2011. **400**(9): p. 3073-83.
156. Abdallah, M.A., et al., *Hexabromocyclododecanes in indoor dust from Canada, the United Kingdom, and the United States*. Environmental Science & Technology, 2008. **42**: p. 459-464.
157. Stapleton, H.M., et al., *Determination of polybrominated diphenyl ethers in environmental standard reference materials*. Analytical and Bioanalytical Chemistry, 2007. **387**(7): p. 2365-79.
158. Huang, Y., et al., *Metabolite Identification Using Multiple Mass Defect Filters and Higher Energy*. Spectroscopy Online, 2008.
159. Hall, M.P., et al., *"Mass defect" tags for biomolecular mass spectrometry*. Journal of Mass Spectrometry, 2003. **38**(8): p. 809-16.
160. Sleno, L., *The use of mass defect in modern mass spectrometry*. Journal of Mass Spectrometry, 2012. **47**(2): p. 226-236.
161. Ballesteros-Gomez, A., et al., *Identification of novel brominated compounds in flame retarded plastics containing TBBPA by combining isotope pattern and mass defect cluster analysis*. environmental Science & Technology, 2016.
162. Myers, A.L., et al., *Complementary nontargeted and targeted mass spectrometry techniques to determine bioaccumulation of halogenated contaminants in freshwater species*. Environmental Science & Technology, 2014. **48**(23): p. 13844-54.
163. Vetter, W., *Marine Halogenated Natural Products of Environmental Relevance*, in *Reviews of Environmental Contamination and Toxicology: Continuation of Residue Reviews*, G.W. Ware, et al., Editors. 2006, Springer New York: New York, NY. p. 1-57.
164. Jobst, K.J., et al., *The use of mass defect plots for the identification of (novel) halogenated contaminants in the environment*. Analytical and Bioanalytical Chemistry, 2013. **405**(10): p. 3289-97.
165. Ubukata, M., et al., *Non-targeted analysis of electronics waste by comprehensive two-dimensional gas chromatography combined with high-resolution mass spectrometry: Using accurate mass information and mass defect analysis to explore the data*. Journal of Chromatography A, 2015. **1395**: p. 152-9.
166. Hilton, D.C., R.S. Jones, and A. Sjodin, *A method for rapid, non-targeted screening for environmental contaminants in household dust*. Journal of Chromatography A, 2010. **1217**(44): p. 6851-6.
167. Hashimoto, S., et al., *Selective extraction of halogenated compounds from data measured by comprehensive multidimensional gas chromatography/high resolution time-of-flight mass spectrometry for non-target analysis of environmental and biological samples*. Journal of Chromatography A, 2013. **1282**: p. 183-9.
168. Pena-Abaurrea, M., et al., *Identification of Potential Novel Bioaccumulative and Persistent Chemicals in Sediments from Ontario (Canada) Using Scripting Approaches with GCxGC-TOF MS Analysis*. Environmental Science & Technology, 2014. **48**(16): p. 9591-9.
169. Peng, H., et al., *Untargeted Identification of Organo-Bromine Compounds in Lake Sediments by Ultrahigh-Resolution Mass Spectrometry with the Data-Independent Precursor Isolation and Characteristic Fragment Method*. Analytical Chemistry, 2015. **87**(20): p. 10237-46.

170. Peng, H., et al., *Untargeted Screening and Distribution of Organo-Bromine Compounds in Sediments of Lake Michigan*. Environmental Science & Technology, 2015. **50**(1): p. 321-30.
171. Kendrick, E., *A Mass Scale Based on CH₂ = 14.0000 for High Resolution Mass Spectrometry of Organic Compounds*. Analytical Chemistry, 1963. **35**(13): p. 2146-2154.
172. Fernando, S., et al., *Identification of the Halogenated Compounds Resulting from the 1997 Plastimet Inc. Fire in Hamilton, Ontario, using Comprehensive Two-Dimensional Gas Chromatography and (Ultra)High Resolution Mass Spectrometry*. Environmental Science & Technology, 2014. **48**(18): p. 10656-63.
173. Myers, A.L., et al., *Using mass defect plots as a discovery tool to identify novel fluoropolymer thermal decomposition products*. Journal of Mass Spectrometry, 2014. **49**(4): p. 291-6.
174. Kramer, R.W., E.B. Kujawinski, and P.G. Hatcher, *Identification of Black Carbon Derived Structures in a Volcanic Ash Soil Humic Acid by Fourier Transform Ion Cyclotron Resonance Mass Spectrometry*. Environmental Science & Technology, 2004. **38**(12): p. 3387-3395.
175. Sleighter, R.L. and P.G. Hatcher, *The application of electrospray ionization coupled to ultrahigh resolution mass spectrometry for the molecular characterization of natural organic matter*. Journal of Mass Spectrometry, 2007. **42**(5): p. 559-74.
176. Marshall, A.G. and R.P. Rodgers, *Petroleomics: The Next Grand Challenge for Chemical Analysis*. Accounts of Chemical Research, 2004. **37**(1): p. 53-59.
177. Zhu, M., et al., *Detection and characterization of metabolites in biological matrices using mass defect filtering of liquid chromatography/high resolution mass spectrometry data*. Drug Metabolism and Disposition, 2006. **34**(10): p. 1722-33.
178. Bateman, K.P., et al., *MSE with mass defect filtering for in vitro and in vivo metabolite identification*. Rapid Communications in Mass Spectrometry, 2007. **21**(9): p. 1485-96.
179. Nagy, K., et al., *Mass-defect filtering of isotope signatures to reveal the source of chlorinated palm oil contaminants*. Food Additives & Contaminants, 2011. **28**(11): p. 1492-500.
180. Zhang, H., et al., *Mass defect filter technique and its applications to drug metabolite identification by high-resolution mass spectrometry*. Journal of Mass Spectrometry, 2009. **44**(7): p. 999-1016.
181. Zhang, H., et al., *Mass defect profiles of biological matrices and the general applicability of mass defect filtering for metabolite detection*. Rapid Communications in Mass Spectrometry, 2008. **22**(13): p. 2082-8.
182. Cuyckens, F., et al., *Extracting metabolite ions out of a matrix background by combined mass defect, neutral loss and isotope filtration*. Rapid Communications in Mass Spectrometry, 2009. **23**(2): p. 327-32.
183. Dunn, W.B., et al., *Mass appeal: metabolite identification in mass spectrometry-focused untargeted metabolomics*. Metabolomics, 2013. **9**(S1): p. 44-66.
184. Schymanski, E.L., et al., *Non-target screening with high-resolution mass spectrometry: critical review using a collaborative trial on water analysis*. Analytical and Bioanalytical Chemistry, 2015. **407**(21): p. 6237-55.
185. Lopes dos Santos, R.A. and C.H. Vane, *Signatures of tetraether lipids reveal anthropogenic overprinting of natural organic matter in sediments of the Thames Estuary, UK*. Organic Geochemistry, 2016. **93**: p. 68-76.
186. Vane, C.H., D.J. Beriro, and G.H. Turner, *Rise and fall of mercury (Hg) pollution in sediment cores of the Thames Estuary, London, UK*. Earth and Environmental Science Transactions of the Royal Society of Edinburgh, 2015. **105**(04): p. 285-296.
187. Vane, C.H., I. Harrison, and A.W. Kim, *Polycyclic aromatic hydrocarbons (PAHs) and polychlorinated biphenyls (PCBs) in sediments from the Mersey Estuary, U.K.* Science of The Total Environment, 2007. **374**(1): p. 112-26.
188. Beriro, D.J., et al., *Effects of drying and comminution type on the quantification of Polycyclic Aromatic Hydrocarbons (PAH) in a homogenised gasworks soil and the implications for human health risk assessment*. Chemosphere, 2014. **111**: p. 396-404.

189. Abdallah, M.A., S. Harrad, and A. Covaci, *Hexabromocyclododecanes and Tetrabromobisphenol-A in Indoor Air and Dust in Birmingham, UK - Implications for Human Exposure*. Environmental Science & Technology, 2008. **42**: p. 6855–6861.
190. Abdallah, M.A., et al., *Enantioselective biotransformation of hexabromocyclododecane by in vitro rat and trout hepatic sub-cellular fractions*. Environmental Science & Technology, 2014. **48**(5): p. 2732-40.
191. Abdallah, M.A., D. Drage, and S. Harrad, *A one-step extraction/clean-up method for determination of PCBs, PBDEs and HBCDs in environmental solid matrices*. Environ Sci Process Impacts, 2013. **15**(12): p. 2279-87.
192. Alam, M.S., C. Stark, and R.M. Harrison, *Using Variable Ionization Energy Time-of-Flight Mass Spectrometry with Comprehensive GCxGC To Identify Isomeric Species*. Analytical Chemistry, 2016. **88**(8): p. 4211-20.
193. Taylor, J.K., *Quality Assurance of Chemical Measurements*. 1984.
194. Xu, Y., et al., *Evaluation of Accurate Mass and Relative Isotopic Abundance Measurements in the LTQ-Orbitrap Mass Spectrometer for Further Metabolomics Database Building*. Analytical Chemistry, 2010. **82**(13): p. 5490-5501.
195. Cariou, R., et al., *Screening halogenated environmental contaminants in biota based on isotopic pattern and mass defect provided by high resolution mass spectrometry profiling*. Analytica Chimica Acta, 2016. **936**: p. 130-8.
196. Bojes, H.K. and P.G. Pope, *Characterization of EPA's 16 priority pollutant polycyclic aromatic hydrocarbons (PAHs) in tank bottom solids and associated contaminated soils at oil exploration and production sites in Texas*. Regulatory Toxicology and Pharmacology, 2007. **47**(3): p. 288-95.
197. Moriwaki, H., et al., *Determination of Polycyclic Aromatic Hydrocarbons in Sediment by Liquid Chromatography-Atmospheric Pressure Photoionization-Mass Spectrometry*. Analytical Sciences, 2004. **20**: p. 375-377.
198. Robb, D.B., T.R. Covey, and A.P. Bruins, *Atmospheric Pressure Photoionization - An Ionization Method for Liquid Chromatography-Mass Spectrometry*. Analytical Chemistry, 2000. **72**: p. 3653-3659.
199. Marvin, C.H., et al., *Analysis of high-molecular-mass polycyclic aromatic hydrocarbons in environmental samples using liquid chromatography-atmospheric pressure chemical ionization mass spectrometry*. Journal of Chromatography A, 1999. **863**: p. 13-24.
200. Pérez, S., *Determination of Polycyclic Aromatic Hydrocarbons in Sewage Reference Sludge by Liquid Chromatography-Atmospheric-Pressure Chemical-Ionization Mass Spectrometry*. Chromatographia, 2001. **53**(9/10475-480).
201. Lien, G.W., C.Y. Chen, and C.F. Wu, *Analysis of polycyclic aromatic hydrocarbons by liquid chromatography/tandem mass spectrometry using atmospheric pressure chemical ionization or electrospray ionization with tropylium post-column derivatization*. Rapid Communications in Mass Spectrometry, 2007. **21**(22): p. 3694-700.
202. Huang, X., et al., *Fast screening of short-chain chlorinated paraffins in indoor dust samples by graphene-assisted laser desorption/ionization mass spectrometry*. Talanta, 2018. **179**: p. 575-582.
203. Hilger, B., et al., *Occurrence of chlorinated paraffins in house dust samples from Bavaria, Germany*. Environ Pollut, 2013. **175**: p. 16-21.
204. Pellizzato, F., et al., *Analysis of short-chain chlorinated paraffins: a discussion paper*. Journal of Environmental Monitoring, 2007. **9**(9): p. 924-30.
205. Eljarrat, E. and D. Barcelo, *Quantitative analysis of polychlorinated n-alkanes in environmental samples*. TrAC Trends in Analytical Chemistry, 2006. **25**(4): p. 421-434.
206. Santos, F.J., J. Parera, and M.T. Galceran, *Analysis of polychlorinated n-alkanes in environmental samples*. Analytical and Bioanalytical Chemistry, 2006. **386**(4): p. 837-57.

207. Wester, P.G. and J. de Boer, *Determination of Polychlorinated Terphenyls in Aquatic Biota and Sediment with Gas Chromatography:Mass Spectrometry Using Negative Chemical Ionization*. Environmental Science & Technology, 1996. **30**(2): p. 473-480.
208. Zushi, Y., et al., *Retrospective analysis by data processing tools for comprehensive two-dimensional gas chromatography coupled to high resolution time-of-flight mass spectrometry: a challenge for matrix-rich sediment core sample from Tokyo Bay*. Journal of Chromatography A, 2014. **1338**: p. 117-26.
209. Hashimoto, S., et al., *Global and selective detection of organohalogenes in environmental samples by comprehensive two-dimensional gas chromatography-tandem mass spectrometry and high-resolution time-of-flight mass spectrometry*. Journal of Chromatography A, 2011. **1218**(24): p. 3799-810.
210. Alam, M.S. and R.M. Harrison, *Recent advances in the application of 2-dimensional gas chromatography with soft and hard ionisation time-of-flight mass spectrometry in environmental analysis*. Chemical Science, 2016. **7**(7): p. 3968-3977.
211. Kind, T. and O. Fiehn, *Metabolomic database annotations via query of elemental compositions: mass accuracy is insufficient even at less than 1 ppm*. BMC Bioinformatics, 2006. **7**: p. 234.
212. Segev, O., A. Kushmaro, and A. Brenner, *Environmental impact of flame retardants (persistence and biodegradability)*. International Journal of Environmental Research and Public Health, 2009. **6**(2): p. 478-91.
213. Yang, C., et al., *Hexabromocyclododecanes, polybrominated diphenyl ethers, and polychlorinated biphenyls in radiometrically dated sediment cores from English lakes, ~1950-present*. Science of The Total Environment, 2016. **541**: p. 721-728.
214. Harrad, S., et al., *Current-Use Brominated Flame Retardants in Water, Sediment, and Fish from English Lakes*. Environmental Science & Technology, 2009. **43**: p. 9077-9083.
215. Rippey, B., et al., *An assessment of toxicity in profundal lake sediment due to deposition of heavy metals and persistent organic pollutants from the atmosphere*. Environment International, 2008. **34**(3): p. 345-56.
216. Allchin, C.R., R.J. Law, and S. Morris, *Polybrominated diphenylethers in sediments and biota downstream of potential sources in the UK*. Environmental Pollution, 1999. **105**: p. 197-207.
217. Barber, J.L., et al., *Halogenated flame retardants in UK sediments*. Organohalogen Compounds, 2014. **76**(1348): p. 1348-1351.
218. Morris, S., et al., *Distribution and Fate of HBCD and TBBPA Brominated Flame Retardants in North Sea Estuaries and Aquatic Food Webs*. Environmental Science & Technology, 2004. **38**: p. 5497-5504.
219. Lu, Q., et al., *Persistent Organic Pollutants in sediment and fish in the River Thames Catchment (UK)*. Science of The Total Environment, 2017. **576**: p. 78-84.
220. Webster, L., et al., *An assessment of persistent organic pollutants in Scottish coastal and offshore marine environments*. Journal of Environmental Monitoring, 2011. **13**(5): p. 1288-307.
221. Russell, M., et al., *Persistent organic pollutants and trace metals in sediments close to Scottish marine fish farms*. Aquaculture, 2011. **319**(1-2): p. 262-271.
222. Vane, C.H., et al., *Increasing polybrominated diphenyl ether (PBDE) contamination in sediment cores from the inner Clyde Estuary, UK*. Environmental Geochemistry and Health, 2010. **32**(1): p. 13-21.
223. Webster, L., et al., *Preliminary assessment of polybrominated diphenyl ethers (PBDEs) in the Scottish aquatic environment, including the Firth of Clyde*. Journal of Environmental Monitoring, 2008. **10**(4): p. 463-73.
224. Harrad, S., *A meta-analysis of recent data on UK environmental levels of POP-BFRs in an international context: Temporal trends and an environmental budget*. Emerging Contaminants, 2015. **1**(1): p. 39-53.
225. La Guardia, M.J., R.C. Hale, and B. Newman, *Brominated flame-retardants in Sub-Saharan Africa: burdens in inland and coastal sediments in the eThekweni metropolitan municipality, South Africa*. Environmental Science & Technology, 2013. **47**(17): p. 9643-50.

226. Knudsen, G.A., et al., *Estimation of human percutaneous bioavailability for two novel brominated flame retardants, 2-ethylhexyl 2,3,4,5-tetrabromobenzoate (EH-TBB) and bis(2-ethylhexyl) tetrabromophthalate (BEH-TEBP)*. Toxicology and Applied Pharmacology, 2016. **311**: p. 117-127.
227. Baron, E., E. Eljarrat, and D. Barcelo, *Gas chromatography/tandem mass spectrometry method for the simultaneous analysis of 19 brominated compounds in environmental and biological samples*. Analytical and Bioanalytical Chemistry, 2014. **406**(29): p. 7667-76.
228. Suhring, R., et al., *Distribution of brominated flame retardants and dechloranes between sediments and benthic fish--A comparison of a freshwater and marine habitat*. Science of The Total Environment, 2016. **542**(Pt A): p. 578-85.
229. Kolic, T.M., et al., *The Analysis of Halogenated Flame Retardants by GC-HRMS in the Environment*. Journal of Chromatographic Science, 2009. **47**: p. 83-91.
230. Pope, N.D. and W.J. Langston, *Sources, distribution and temporal variability of trace metals in the Thames Estuary*. Hydrobiologia, 2011. **672**(1): p. 49-68.
231. Tye, A.M., J. Rushton, and C.H. Vane, *Distribution and speciation of phosphorus in foreshore sediments of the Thames estuary, UK*. Marine Pollution Bulletin, 2018. **127**: p. 182-197.
232. Stapleton, H.M. and N. Dodder, *Photodegradation of DecaBDE in house dust by natural sunlight*. Environmental Toxicology and Chemistry, 2008. **27**(2): p. 306-312.
233. La Guardia, M.J., R.C. Hale, and E. Harvey, *Detailed PBDE Congener Composition of the Widely Used Penta-, Octa-, and Deca-PBDE Technical Flame-retardant Mixtures*. Environmental Science & Technology, 2006. **40**: p. 6247-6254.
234. Chen, D., R.C. Hale, and R.J. Letcher, *Photochemical and microbial transformation of emerging flame retardants: cause for concern?* Environmental Toxicology and Chemistry, 2015. **34**(4): p. 687-99.
235. Su, G., et al., *Photolytic degradation products of two highly brominated flame retardants cause cytotoxicity and mRNA expression alterations in chicken embryonic hepatocytes*. Environmental Science & Technology, 2014. **48**(20): p. 12039-46.
236. Pan, Y., et al., *The photodegradation of polybrominated diphenyl ethers (PBDEs) in various environmental matrices: Kinetics and mechanisms*. Chemical Engineering Journal, 2016. **297**: p. 74-96.
237. Wei, H., et al., *Photolytic debromination pathway of polybrominated diphenyl ethers in hexane by sunlight*. Environmental Pollution, 2013. **174**: p. 194-200.
238. Söderström, G., et al., *Photolytic Debromination of Decabromodiphenyl Ether (BDE 209)*. Environmental Science & Technology, 2004. **38**: p. 127-132.
239. Wang, R., et al., *Formation and degradation of polybrominated dibenzofurans (PBDFs) in the UV photolysis of polybrominated diphenyl ethers (PBDEs) in various solutions*. Chemical Engineering Journal, 2018. **337**: p. 333-341.
240. Bendig, P. and W. Vetter, *UV-induced formation of bromophenols from polybrominated diphenyl ethers*. Environmental Science & Technology, 2013. **47**(8): p. 3665-70.
241. Erickson, P.R., et al., *Photochemical Formation of Brominated Dioxins and Other Products of Concern from Hydroxylated Polybrominated Diphenyl Ethers (OH-PBDEs)*. Environmental Science & Technology, 2012. **46**: p. 8174-8180.
242. Zhao, H., et al., *Monohydroxylated Polybrominated Diphenyl Ethers (OH-PBDEs) and Dihydroxylated Polybrominated Biphenyls (Di-OH-PBBs): Novel Photoproducts of 2,6-Dibromophenol*. Environmental Science & Technology, 2015. **49**(24): p. 14120-8.
243. Eriksson, J., et al., *Photochemical Decomposition of 15 Polybrominated Diphenyl Ether Congeners in Methanol:Water*. Environmental Science & Technology, 2004. **38**: p. 3119-3125.
244. Santos, M.S.F., A. Alves, and L.M. Madeira, *Chemical and photochemical degradation of polybrominated diphenyl ethers in liquid systems - A review*. Water Research, 2016. **88**: p. 39-59.
245. Abdallah, M.A., et al., *Comparative evaluation of liquid chromatography-mass spectrometry versus gas chromatography-mass spectrometry for the determination of*

- hexabromocyclododecanes and their degradation products in indoor dust*. Journal of Chromatography A, 2008. **1190**(1-2): p. 333-41.
246. Eriksson, J., et al., *Photochemical transformations of tetrabromobisphenol A and related phenols in water*. Chemosphere, 2004. **54**(1): p. 117-126.
247. de Jourdan, B.P., et al., *Environmental fate of three novel brominated flame retardants in aquatic mesocosms*. Environmental Toxicology and Chemistry, 2013. **32**(5): p. 1060-8.
248. Wang, J., et al., *Photolytic degradation of decabromodiphenyl ethane (DBDPE)*. Chemosphere, 2012. **89**(7): p. 844-9.
249. Kajiwarra, N., Y. Noma, and H. Takigami, *Photolysis Studies of Technical Decabromodiphenyl Ether (DecaBDE) and Ethane (DeBDethane) in Plastics under Natural Sunlight*. Environmental Science & Technology, 2008. **42**: p. 4404-4409.
250. Zhang, Y.N., et al., *Photochemical transformation of five novel brominated flame retardants: Kinetics and photoproducts*. Chemosphere, 2016. **150**: p. 453-60.
251. Wang, R., et al., *Photodebromination behaviors of polybrominated diphenyl ethers in methanol/water systems: Mechanisms and predicting descriptors*. Science of The Total Environment, 2017. **595**: p. 666-672.
252. Chen, J., et al., *Mechanism insights into the oxidative degradation of decabromodiphenyl ethane by potassium permanganate in acidic conditions*. Chemical Engineering Journal, 2018. **332**: p. 267-276.
253. OECD, *Test No. 316: Phototransformation of Chemicals in Water – Direct Photolysis*. 2008.
254. OECD, *Phototransformation of Chemicals on Soil Surfaces*. 2002.
255. Jia, L. and X. Liu, *The Conduct of Drug Metabolism Studies Considered Good Practice II - In Vitro experiments*. Current Drug Metabolism, 2007. **8**(8): p. 822-829.
256. Ahmad, M., et al., *In-vitro Metabolism of Retinoic Acid by Different Tissues from Male Rats*. Journal of Pharmacy and Pharmacology, 2000. **52**: p. 511-515.
257. Roberts, S.C., L.J. Macaulay, and H.M. Stapleton, *In vitro metabolism of the brominated flame retardants 2-ethylhexyl-2,3,4,5-tetrabromobenzoate (TBB) and bis(2-ethylhexyl) 2,3,4,5-tetrabromophthalate (TBPH) in human and rat tissues*. Chemical Research in Toxicology, 2012. **25**(7): p. 1435-41.
258. Han, X., et al., *Liver microsomes and s9 from rainbow trout (oncorhynchus mykiss): comparison of basal-level enzyme activities with rat and determination of xenobiotic intrinsic clearance in support of bioaccumulation assessment*. Environmental Toxicology and Chemistry, 2009. **28**(3): p. 481-488.
259. Stapleton, H.M., R.J. Letcher, and J.E. Baker, *Debromination of Polybrominated Diphenyl Ether Congeners BDE 99 and BDE 183 in the Intestinal Tract of the Common Carp (Cyprinus carpio)*. Environmental Science & Technology, 2004. **38**: p. 1954-1061.
260. Stapleton, H.M., et al., *Dietary accumulation and metabolism of polybrominated diphenyl ethers by juvenile carp*. Environmental Toxicology and Chemistry, 2004. **23**(8): p. 1939-1946.
261. Roberts, S.C., et al., *Species-specific differences and structure-activity relationships in the debromination of PBDE congeners in three fish species*. Environmental Science & Technology, 2011. **45**(5): p. 1999-2005.
262. Noyes, P.D., et al., *Characterizing the in vitro hepatic biotransformation of the flame retardant BDE 99 by common carp*. Aquatic Toxicology, 2010. **97**(2): p. 142-50.
263. Erratico, C.A., S.C. Moffatt, and S.M. Bandiera, *Comparative oxidative metabolism of BDE-47 and BDE-99 by rat hepatic microsomes*. Toxicological Sciences, 2011. **123**(1): p. 37-47.
264. Yang, J. and K.M. Chan, *Evaluation of the toxic effects of brominated compounds (BDE-47, 99, 209, TBBPA) and bisphenol A (BPA) using a zebrafish liver cell line, ZFL*. Aquatic Toxicology, 2015. **159**: p. 138-47.
265. Hakk, H., G. Larsen, and E. Klasson-Wehler, *Tissue disposition, excretion and metabolism of 2,2',4,4',5-pentabromodiphenyl ether (BDE-99) in the male Sprague-Dawley rat*. Xenobiotica, 2002. **32**(5): p. 369-382.

266. Hakk, H., et al., *Tissue disposition, excretion and metabolism of 2,2',4,4',6-pentabromodiphenyl ether (BDE-100) in male Sprague–Dawley rats*. *Xenobiotica*, 2006. **36**(1): p. 79-94.
267. Feng, C., et al., *Metabolic pathways of decabromodiphenyl ether (BDE209) in rainbow trout (Oncorhynchus mykiss) via intraperitoneal injection*. *Environmental Toxicology and Pharmacology*, 2015. **39**(2): p. 536-44.
268. Feng, C., et al., *Relationship between BDE 209 metabolites and thyroid hormone levels in rainbow trout (Oncorhynchus mykiss)*. *Aquatic Toxicology*, 2012. **122-123**: p. 28-35.
269. Kierkegaard, A., et al., *Dietary Uptake and Biological Effects of Decabromodiphenyl Ether in Rainbow Trout (Oncorhynchus mykiss)*. *Environmental Science & Technology*, 1999. **33**(10): p. 1612-1617.
270. Erratico, C., et al., *Stereoselective Metabolism of alpha-, beta-, and gamma-Hexabromocyclododecanes (HBCDs) by Human Liver Microsomes and CYP3A4*. *Environmental Science & Technology*, 2016. **50**(15): p. 8263-73.
271. Brandsma, S., et al., *Identification of Hydroxylated Metabolites of HBCD in Wildlife and 28-days Exposed Wistar Rats*. *Environmental Science & Technology*, 2009. **43**: p. 6058-6063.
272. Zegers, B.N., et al., *Levels of hexabromocyclododecane in harbor porpoises and common dolphins from western European seas, with evidence for stereoisomer-specific biotransformation by cytochrome p450*. *Environmental Science & Technology*, 2005. **39**(7): p. 2095-2100.
273. Giraud, M., et al., *Effects of food-borne exposure of juvenile rainbow trout (Oncorhynchus mykiss) to emerging brominated flame retardants 1,2-bis(2,4,6-tribromophenoxy)ethane and 2-ethylhexyl-2,3,4,5-tetrabromobenzoate*. *Aquatic Toxicology*, 2017. **186**: p. 40-49.
274. Hakk, H., G. Larsen, and J. Bowers, *Metabolism, tissue disposition, and excretion of 1,2-bis(2,4,6-tribromophenoxy)ethane (BTBPE) in male Sprague-Dawley rats*. *Chemosphere*, 2004. **54**(10): p. 1367-74.
275. Chu, S., L.T. Gauthier, and R.J. Letcher, *Alpha and beta isomers of tetrabromoethylcyclohexane (TBECH) flame retardant: depletion and metabolite formation in vitro using a model rat microsomal assay*. *Environmental Science & Technology*, 2012. **46**(18): p. 10263-70.
276. Nguyen, K.H., et al., *Biotransformation of the Flame Retardant 1,2-Dibromo-4-(1,2-dibromoethyl)cyclohexane (TBECH) in Vitro by Human Liver Microsomes*. *Environmental Science & Technology*, 2017. **51**(18): p. 10511-10518.
277. Gemmill, B., et al., *Toxicokinetics of tetrabromoethylcyclohexane (TBECH) in juvenile brown trout (Salmo trutta) and effects on plasma sex hormones*. *Aquatic Toxicology*, 2011. **101**(2): p. 309-17.
278. Park, B.J., et al., *Thyroid axis disruption in juvenile brown trout (Salmo trutta) exposed to the flame retardant beta-tetrabromoethylcyclohexane (beta-TBECH) via the diet*. *Environmental Science & Technology*, 2011. **45**(18): p. 7923-7.
279. Barron, M.G., P.W. Albro, and W.L. Hayton, *Biotransformation of Di(2-Ethylhexyl)phthalate by rainbow trout*. *Environmental Toxicology and Chemistry*, 1995. **14**(5): p. 873-876.
280. Choi, K., et al., *In vitro metabolism of di(2-ethylhexyl) phthalate (DEHP) by various tissues and cytochrome P450s of human and rat*. *Toxicology In Vitro*, 2012. **26**(2): p. 315-22.
281. Cheng, S.W., K. Randall, and A.T. Kotchevar, *In Vitro Metabolism Studies of Polybrominated Diphenyl Ethers Using Rat and Human Liver Microsomes*. *American Journal of Biochemistry and Biotechnology*, 2008. **4**(3): p. 295-303.
282. Tomy, G.T., et al., *Bioaccumulation, Biotransformation, and Biochemical Effects of Brominated Diphenyl Ethers in Juvenile Lake Trout (Salvelinus namaycush)*. *Environmental Science & Technology*, 2004. **38**(5): p. 1496-1504.

Appendix I

SUMMARY OF ANALYTICAL METHODS AND ASSOCIATED QUALITY ASSURANCE/QUALITY CONTROL (QA/QC) PROCEDURES FOR SEMI-VOLATILE ORGANIC COMPOUNDS

Prepared by: Dr. Stuart Harrad,
Organic Pollutants Research group,
Division of Environmental Health & Risk Management,
University of Birmingham

Overview

This document describes the generically applicable methods and procedures that all researchers within the group must follow to ensure the reliability of their analytical data. Methods that apply only to a specific group of pollutants are not covered here. If you have any questions about anything relating to analysis, please ask your supervisor or an experienced member of the Research Group for advice.

Instrument Calibration

A full 5-point calibration must be conducted at the beginning of any measurement campaign. The exact concentrations and content of the calibration standard mixes will vary according to the pollutant class being measured but as a guide, the table below gives a typical example.

<i>Compound</i>	<i>Standard A</i>		<i>Standard B</i>		<i>Standard C</i>		<i>Standard D</i>		<i>Standard E</i>	
	<i>Concn</i>	<i>(pg μl^{-1})</i>	<i>Concn</i>	<i>(pg μl^{-1})</i>	<i>Concn</i>	<i>(pg μl^{-1})</i>	<i>Concn</i>	<i>(pg μl^{-1})</i>	<i>Concn</i>	<i>(pg μl^{-1})</i>
All "native" ¹ standards	20		50		200		500		1000	
Internal standards,	200		200		200		200		200	
Sampling										
Evaluation										
standards,										
recovery										
determination										
standards										

¹ "native" refers to the ¹²C or ¹H isotope of the target compound. The term is used to distinguish it from the ¹³C or ²D (deuterated) isotope used as the internal standard.

Appendix I

These standards are used to calculate relative response factors (RRFs) for each of the “target” compounds. The RRF is defined as the instrument response for a unit amount of target pollutant relative to the instrument response obtained for the same amount of the internal standard (IS). For example, if the response of a unit amount of the target compound is 1.5 times that for the same amount of the internal standard, the RRF =1.5. It is calculated as in equation 1.

$$RRF = \frac{A_{NAT}}{A_{IS}} \times \frac{C_{IS}}{C_{NAT}} \text{ (equation 1)}$$

where A_{NAT} is the peak area for the “native” compound in the standard; A_{IS} is the peak area of the internal standard in the standard; C_{NAT} is the concentration of the “native” compound in the standard; and C_{IS} is the concentration of the internal standard in the standard.

Calculation of RRFs for each of the standards A-E, should reveal them to be essentially identical in each standard. Ideally, the relative standard deviation (*i.e.* $(\sigma_{n-1}/\text{average}) \times 100\%$) of RRFs for a given target compound should not exceed 10%. If they do, consult your supervisor before proceeding.

A full 5-point calibration typically only needs to be conducted infrequently, or when an on-going accuracy check proves unsatisfactory. The average RRF for any subsequent full calibration should be within $\pm 10\%$ of the average RRF obtained for the 1st 5-point calibration. If they do not, then you must consult your supervisor immediately.

Before each batch of samples are analysed on the GC/MS, one of the calibration standards (usually Standard C, but others are fine) must be run. The RRFs obtained from this analysis must be within $\pm 25\%$ of the RRFs obtained for that standard in the initial 5-point calibration. If they do not, please consult your supervisor before proceeding. At the end of each batch of samples, the same calibration standard must be run. The RRFs obtained from this analysis must be within $\pm 25\%$ of the RRFs obtained for that standard in the initial 5-point calibration. The RRFs that must be used for calculating concentrations in samples in that batch will be an average of those obtained for the 2 standards run for that batch.

GC/MS tuning tips

At the start of each session, an autotune should be run. The results should be printed out and a record kept. Following the autotune (which should detect any major problems with the GC/MS), a manual tune must be conducted. The purpose of the manual tune is to maximise sensitivity and instrument performance for the particular group of compounds you are targeting. As a general rule, while during tuning the detector voltage should be set at 200V, you should set the detector voltage to 450V (*i.e.* that necessary to detect compounds in the concentration range 10-1000 pg/component) in your acquisition file used when running

standards and samples. You should also tune with the oven temperature at a temperature similar to that at which your target compounds will elute from the GC column. Typically for a DB-5 type column it will be 250°C, but may be lower for other columns (DO NOT EXCEED THE MAXIMUM ALLOWABLE ISOTHERMAL OPERATING TEMPERATURE FOR THE COLUMN). You should choose the m/z values most appropriate to the mass range of the pollutants which you are targeting – your supervisor will be able to advise you on the best choice. The autotune uses m/z 69, 219, and 502 – this is not appropriate for PCBs for example, which lie in the mass range 256 to 394, and the manual tune should be based on tuning masses 219, 264, and 414.

Determination of Internal Standard Recoveries

It is important to note that use of the internal standard quantification method means that NO correction of concentrations for recovery is required. However, it is important that recoveries of internal standards are calculated for each sample as a QA/QC measure. Typically, such recoveries should be around 70%, but they may routinely fall in the range 30%-150%. If values exceed 150%, the sample extract should be re-analysed and the recovery recalculated. If recoveries are below 30%, then the signal to noise (S:N) ratio of the internal standard must be calculated. The data are acceptable provided that the S:N ratio exceeds 20:1. If it is less than 20:1 the sample extract should be re-analysed and the recovery recalculated. If the recovery percentage and S:N ratio is still unacceptable then data for that sample must be considered invalid.

Internal standard (IS) recoveries are calculated thus:

$$\% \text{ IS Recovery} = \left[\left(\frac{A_{IS}}{A_{RDS}} \right)_S \times \left(\frac{A_{RDS}}{A_{IS}} \right)_{STD} \times \left(\frac{C_{IS}}{C_{RDS}} \right)_{STD} \times \left(\frac{C_{RDS}}{C_{IS}} \right)_S \right] \times 100 \text{ (equation 2)}$$

where $(A_{IS}/A_{RDS})_S$ = ratio of internal standard peak area to recovery determination standard peak area in the sample; $(A_{RDS}/A_{IS})_{STD}$ = ratio of recovery determination standard peak area to internal standard peak area in the calibration standard (the average of values obtained for both calibration standards run for a batch of samples is used); $(C_{IS}/C_{RDS})_{STD}$ = ratio of concentration of internal standard to concentration of recovery determination standard in the calibration standard; and $(C_{RDS}/C_{IS})_S$ = ratio of concentration of recovery determination standard to concentration of internal standard in the sample (assuming 100% recovery). Note that this can be calculated as the amount of internal or recovery determination standard added to the sample divided by the volume of the sample extract used for GC/MS analysis (typically 25-50 μ l).

Determination of Sampling Evaluation Standard Recoveries

Recoveries of sampling evaluation standards (*i.e.* those added to the PUF plug in air or aqueous sample analysis) are calculated for each sample as QA/QC measure. Note that SESs are NOT added to solid samples like soil or grass. Typically, such recoveries should be around 70%, but they may routinely fall in the range 30%-150%. Note that although SES recoveries should be recorded for every sample, they are a QA/QC check only, and are NOT used to correct concentrations for sampling losses. If values exceed 150%, the sample extract should be re-analysed and the recovery recalculated. If it still exceeds 150%, then data for that sample must be considered invalid. If recoveries are below 30%, then the signal to noise (S:N) ratio of the sampling evaluation standard must be calculated. The data are acceptable provided that the S:N ratio exceeds 20:1. If it is less than 20:1 the sample extract should be re-analysed and the recovery recalculated. If the recovery percentage and S:N ratio is still unacceptable then data for that sample must be considered invalid.

Sampling evaluation standard (SES) recoveries are calculated thus:

$$\% \text{ SES Recovery} = \left[\left(\frac{A_{SES}}{A_{RDS}} \right)_S \times \left(\frac{A_{RDS}}{A_{SES}} \right)_{STD} \times \left(\frac{C_{SES}}{C_{RDS}} \right)_{STD} \times \left(\frac{C_{RDS}}{C_{SES}} \right)_S \right] \times 100 \text{ (equation 3)}$$

where $(A_{SES}/A_{RDS})_S$ = ration of sampling evaluation standard peak area to recovery determination standard peak area in the sample; $(A_{RDS}/A_{SES})_{STD}$ = ratio of recovery determination standard peak area to sampling evaluation standard peak area in the calibration standard (the average of values obtained for both calibration standards run for a batch of samples is used); $(C_{SES}/C_{RDS})_{STD}$ = ratio of concentration of sampling evaluation standard to concentration of recovery determination standard in the calibration standard and $(C_{RDS}/C_{SES})_S$ = ratio of concentration of recovery determination standard to concentration of sampling evaluation standard in the sample (assuming 100% recovery). Note that this can be calculated as the amount of sampling evaluation or recovery determination standard added to the sample divided by the volume of the sample extract used for GC/MS analysis (typically 25-50 μ l).

Determination and On-Going Monitoring of Accuracy

The principal means of determining method accuracy is *via* analysis of one or more certified or standard reference materials (CRMs or SRMs). Your supervisor will recommend a suitable CRM/SRM. Before you commence analysis of any samples as part of your research, you must conduct 5 replicate analyses of a suitable CRM or SRM, and obtain satisfactory data for these analyses. Essentially a CRM or SRM is a sample that has been analysed a large number of expert laboratories worldwide and that has had agreed concentrations of target pollutants assigned to it. These values are usually cited as an average \pm a standard deviation. The values

Appendix I

you obtain will be compared with these. You must discuss your data with your supervisor and will only be allowed to proceed with analysis of your samples once acceptable accuracy of data are obtained.

As an ongoing measure of accuracy, you must analyse 1 aliquot of the same CRM/SRM for every 20 samples – *i.e.* every 21st sample you analyse must be a CRM/SRM. If satisfactory data are not obtained, then you must consult your supervisor immediately.

Additional means of evaluating accuracy include participation in interlaboratory comparisons. Your supervisor will advise you as and when such comparisons are to take place.

Determination of Precision

This is defined as the relative standard deviation (*i.e.* $100 \times \sigma_{n-1}/\text{average}$) of concentrations obtained from 5 replicate analyses of the same sample. Usually, this is a CRM/SRM. Typically, precision should be no more than 30%, but you must discuss your data with your supervisor.

Determination of Blank Concentrations

This is defined as the concentration of a target pollutant present in an analysis where the sample is omitted, but internal standards etc. are added. Note that for air analyses, a blank should consist of analysis of a clean PUF plug and filter paper. For calculation of blank sample concentrations, you should assume the sample mass or volume to be that typically used – *e.g.* 1,000 m³ for air samples, 50g for soil or grass samples. One blank analysis must be conducted for every 5 samples – *i.e.* every 6th analysis you perform must be a blank. Where the concentration of a target pollutant in a blank for a given batch of samples is 5-20% of the concentration in a sample from that batch, the blank concentration must be subtracted from that in the sample. Where the concentration in the blank exceeds 20% of that in a sample from that batch, data for that target pollutant in that sample must not be reported.

Determination of Detection limits

Two categories of detection limits exist.

1. instrument detection limit (IDL)
2. sample detection limit (SDL)

The IDL is defined as that amount of pollutant that gives a signal to noise ratio of 3:1. It is best determined by calculating the signal to noise ratio for the pollutant in your calibration standard A. To illustrate, if the concentration of a target pollutant in that standard = 20 pg/ μ l and 1 μ l is injected, then if a signal to noise ratio of 50:1 is obtained, then the IDL = $20 \times (3/50) = 1.2$ pg/injection.

Appendix I

The SDL can then be calculated as in equation 4:

$$SDL = \frac{IDL \times FEV}{VFEI \times SS} \times \frac{100}{\%IS Recovery} \quad (\text{equation 4})$$

Where FEV = final extract volume (μl), VFEI = volume of final extract injected (μl); SS = sample size (m^3 or g); and %IS recovery = percentage recovery of internal standard used to quantify the target pollutant in a particular sample.

To illustrate, if the IDL = 1.2 pg/injection, the final extract volume for a sample is 50 μl , 1 μl is injected; the sample size is 1,000 m^3 , and the percentage internal standard recovery in that sample = 70%, then the SDL = $((1.2 \times 50) / (1 \times 1000)) \times 100/70 = 0.086 \text{ pg m}^{-3}$.

Where the concentration in the sample blank exceeds the SDL calculated as above, the effective SDL is the blank concentration. This is not an unusual occurrence.

Calculation of concentrations in samples

Concentrations in samples may be calculated *via* the equation below:

$$Concn. = \frac{A_{NAT}}{A_{IS}} \times \frac{1}{RRF} \times \frac{M_{IS}}{SS} \quad (\text{equation 5})$$

Where A_{IS} = peak area of internal standard in sample; A_{NAT} = peak area of target pollutant in sample; RRF = relative response factor for the target pollutant (see equation 1); M_{IS} = mass of internal standard added to sample (pg) and SS = sample size (m^3 or g).

To illustrate, where A_{NAT} = 10,000 units; A_{IS} = 20,000 units; RRF = 1.5; M_{IS} = 20,000 pg; and SS = 50 g, the concentration of the target pollutant will be $(10,000/20,000) \times (1/1.5) \times (20,000/50) = 133.33 \text{ pg g}^{-1}$.

Correct Storage of Calibration and internal standards

Once prepared in CERTAN vials, all standards should be stored in a freezer unless required for analysis. You should record the weight of the CERTAN vial and contents before and after each use. Before weighing, allow the vial and contents to reach room temperature, and wipe off any condensation before weighing. If at any time, the weight before use is less than 5% of the weight after recorded after the previous use, you must consult your supervisor immediately.

Criteria for Quantification of a Peak as a Target pollutant

For a given peak to be identified as a target pollutant in a sample, various criteria must be met. These are:

1. the signal to noise ratio of the peak must exceed 3:1

Appendix I

2. the relative retention time (RRT) of the peak in the sample must be within 0.2% of the average value determined for the 2 calibration standards run for the sample batch. Note $RRT = \text{retention time of target pollutant} / \text{retention time of internal standard used to quantify target pollutant}$.

The above criteria apply to all target pollutants. For organochlorine and organobromine pollutants, the following criterion also applies.

- the isotope ratio of the peak in the sample must be within 20% of the average value determined for the 2 calibration standards run for that sample batch. If it falls outside this range, then you must consult your supervisor, but it is likely that the peak cannot be quantified due to a co-eluting interference. For example, for trichlorinated PCBs, where 2 m/z values are monitored (*i.e.* 255.95 and 257.95) the isotope ratio = area of peak for 255.95 trace/area of peak for 257.95 trace. Note that for calculating RRFs and concentrations, the m/z value providing the largest peak must be used.

Appendix II

Table 10-1. Distance from Teddington Lock, TOC and site name for Thames Estuary surface sediments

Sample Location	Site Name	TOC (%)¹	Approx. distance from Teddington Lock (km)
1	Grand Union, Brentford	5.28	8.0
2	Chiswick Bridge	3.00	11.0
3	Barnes Bridge	2.44	13.0
4	Hammersmith Bridge	1.32	15.0
5	Chelsea Creek	2.08	22.0
6	Vauxhall Bridge	2.78	26.0
7	Lambeth Bridge	2.42	27.0
8	Millenium Bridge	0.55	30.0
9	Butlers Wharf	3.12	32.0
10	Cuckold's Point	6.05	34.0
11	Millwall	1.22	36.0
12	Deptford Creek	3.43	37.0
13	Blackwall Tunnel	5.86	38.0
14	Greenwich Pier	1.96	40.0
15	Bow Creek	3.09	41.0
16	Bugsby's Reach	2.25	42.0
17	Silvertown	2.09	43.5
18	Gallions Reach N	2.95	47.0
19	Gallions Reach S	2.50	48.0
20	Beckton Creek	2.89	49.0
21	Barking	3.44	51.0
22	Crossness	3.23	52.0
23	Dagenham Ford Pier	2.41	53.0
24	Fairview Industrial Park	1.99	54.0
25	Erith	2.24	56.5
26	Dartford	2.70	58.0
27	Dartford Marshes	1.27	60.0
28	Purfleet	1.87	61.0
29	Dartford Tunnel	1.22	61.5
30	Queen Elizabeth II Bridge	1.16	62.0
31	St Clement's Reach	1.69	64.5
32	Swanscombe Marshes	6.35	65.0
33	Swanscombe 2	3.11	65.5
34	Tilbury Power Station	1.00	73.0
35	Tilbury	2.75	74.0
36	Mucking Flats	0.75	79.0

Table 10-1 continued

37	Shorne	3.59	75.0
38	Cliffe	3.87	82.0
39	Halstow	4.07	77.0
40	Mucking	1.25	83.0
41	Canvey Island 1	0.67	83.5
42	Yantlet Flats 2	0.10	94.0
43	Yantlet Flats 1	0.65	95.0
44	Grain Spit 3	0.25	100.0
45	Maplin Sands	0.26	110.0

¹ Data from Vane et al., 2015 [186]

Table 10-2. Calibration standards CS1 to CS5, with native compounds, internal standards (IS) and syringe standard (SS – recovery determination standard)

	CS1	CS2	CS3	CS4	CS5
	pg/ul	pg/ul	pg/ul	pg/ul	pg/ul
BDE17	20	50	200	500	1000
BDE28	10	25	100	250	500
BDE47	5	12.5	50	125	250
aDP	5	12.5	50	125	250
sDP	5	12.5	50	125	250
abTBEC	100	250	1000	2500	5000
DBDPE	20	50	200	500	1000
BDE99	1	4	20	80	400
BDE100	1	4	20	80	400
BDE153	1	4	20	80	400
BDE154	1	4	20	80	400
BDE183	1	4	20	80	400
BDE196	1	4	20	80	400
BDE197	1	4	20	80	400
BDE206	1	4	20	80	400
BDE207	1	4	20	80	400
BDE208	1	4	20	80	400
BDE209	1	4	20	80	400
HBCDs	1	4	20	80	400
TBBPA	1	4	20	80	400
HBB	1	4	20	80	400
EHTBB	1	4	20	80	400
BEHTEBP	2	8	40	160	800
BTBPE	2	8	40	160	800
PBEB	2	8	40	160	800
TBP	0.5	2	10	40	200
BB153	1	4	20	80	400

Table 10-2 continued					
IS	pg/ul	pg/ul	pg/ul	pg/ul	pg/ul
MBDE28	100	100	100	100	100
BDE77	100	100	100	100	100
BDE128	100	100	100	100	100
MBDE209	200	200	200	200	200
MEHTBB	200	200	200	200	200
MBEHTBP	200	200	200	200	200
MBTBPE	200	200	200	200	200
MHBCD	100	100	100	100	100
MTBBPA	100	100	100	100	100
SS	pg/ul	pg/ul	pg/ul	pg/ul	pg/ul
MBDE-100	200	200	200	200	200

Appendix II

Table 10-3. Summary of the concentrations ($\mu\text{g kg}^{-1}$ dry weight / organic carbon) of PBDE congeners in sediments from the River Thames

Congener	DF (%)	Median	Average	Range	Median	Average	Range
		values in $\mu\text{g kg}^{-1}$ dry weight			values in $\mu\text{g kg}^{-1}$ organic carbon		
BDE-17	24	<0.4	<0.4	n.d. – <0.4	<0.4	<0.4	n.d. – <0.4
BDE-28	27	<0.2	0.4	n.d. – 4.0	<0.2	12	n.d. – 116
BDE-47	53	<0.03	0.2	n.d. – 2.5	<0.03	6.7	n.d. – 48
BDE-99	71	0.5	0.8	n.d. – 4.4	15	28	n.d. – 130
BDE-100	60	0.05	0.2	n.d. – 1.1	<0.01	4.2	n.d. – 21
BDE-153	16	<0.01	0.03	n.d. – 0.6	<0.01	1.2	n.d. – 33
BDE-154	22	<0.03	<0.03	n.d. – 0.2	<0.03	<0.03	n.d. – 10
BDE-183	71	0.05	0.1	n.d. – 0.7	0.4	3.3	n.d. – 23
BDE-196	64	0.02	0.1	n.d. – 2.2	1.0	4.4	n.d. – 41
BDE-197	51	<0.04	0.5	n.d. – 5.0	<0.04	15	n.d. – 95
BDE-206	96	2.6	3.3	n.d. – 11.7	115	135	n.d. – 389
BDE-207	58	0.06	0.4	n.d. – 2.3	3.6	13	n.d. – 60
BDE-209	100	148	174	0.03 - 535	6800	7673	0.03– 20762

* n.d. - not detected

* < indicates the value of the LOD

Appendix II

Table 10-4. Summary of concentrations in ng g⁻¹ dry weight for all PBDE congeners analysed in all 45 sediment samples

Nr	BDE17	BDE28	BDE47	BDE99	BDE100	BDE153	BDE154	BDE183	BDE196	BDE197	BDE206	BDE207	BDE209
1	0	0	2.51	4.44	1.11	0.55	0.23	0.72	2.15	5.02	9.51	2.32	352.88
2	0	0	0.47	1.78	0.37	<LOQ	<LOQ	0.19	0	1.92	5.17	1.05	278.55
3	0	0	0.69	1.44	0.24	0	0	0.04	0.01	1.83	4.72	0.69	209.28
4	0	0	<LOD	0.16	0.04	0	0	<LOQ	0	1.23	0.38	0.01	33.36
5	0	0	0	0.2	0	0	0	0	0.02	0.41	2.87	0.31	148.46
6	0	0	0	0.36	0.03	0	0	0	0	0.68	2.13	0.05	148.35
7	0	0	0.12	0.86	0.1	0	0	<LOQ	0.03	0.19	3.18	0.15	195.59
8	0	0	0	0	0	0	0	<LOQ	0	0	0	0	4.63
9	<LOD	2.26	1.08	2.61	0.5	<LOQ	0.13	0.22	0.34	<LOQ	11.72	1.87	534.90
10	0	0	0.18	1.72	0.28	0	<LOQ	<LOQ	0.01	0.84	6.98	0.97	380.40
11	0	0	0	0	0	0	0	<LOQ	0.02	<LOQ	0.49	0	54.12
12	<LOD	1.81	0.1	0.27	0.12	0	<LOQ	0.33	0.2	2.23	3.12	0.79	117.41
13	0	0	0	0	0	0	0	<LOQ	0	0	0	0	0.64
14	<LOD	<LOQ	0.37	0.94	0.24	0.22	0.2	0.45	0.02	<LOD	5.47	0.89	214.46
15	0	<LOQ	0.09	2	0.42	0	<LOQ	0.13	0.07	0.44	7.77	0.48	409.82
16	<LOD	0	0.26	1	0.25	<LOQ	<LOQ	<LOQ	0.02	1.67	7.09	0.77	313.95
17	0	<LOD	0	0	0	0	0	0	0	<LOQ	0.41	0	57.64
18	<LOD	2.6	0.17	1.42	0.24	0	0	0.13	0.04	0.49	9.73	0.67	507.25
19	<LOD	0	0	<LOQ	0	0	0	<LOQ	0.14	0.3	1.53	0.09	116.88
20	<LOD	2.92	0.21	1.95	0.39	0	<LOQ	0.11	0.02	<LOQ	8.49	1.62	389.33
21	0	3.99	1.31	2.07	0.53	0	0	0.07	0.06	<LOQ	7.09	1.32	350.64
22	0	1.89	0.3	2.06	0.39	0	0	0.12	0.81	1.89	8.92	1.63	427.37
23	0	0	0.19	0.17	0.07	0	0	<LOQ	0.01	0.48	2.78	0.22	163.87
24	0	0	<LOQ	0.56	0.08	0	0	0.03	0.13	0	6.6	0.25	332.54
25	<LOD	0	0	0.46	<LOQ	0	0	0.03	0.11	0.11	5.09	0.25	255.98
26	0	0	0	0	0	0	0	0.03	0.03	0	0	0	0.41

Appendix II

Table 10-4 continued													
27	0	0	0.19	0.49	0.05	0.42	<LOQ	0	0	0	2.65	0	247.41
28	0	0	0	0.93	0.11	0	0	0.04	0	0	3.53	0.06	236.64
29	0	0	<LOD	0.38	<LOQ	0	0	0.1	0.06	0	2.61	0	155.76
30	<LOD	0	0.51	1.51	<LOQ	<LOQ	0	0.05	0.01	0	1.65	0.19	127.33
31	0	0	0	0.72	0	0	0	0.05	0.07	0	5.24	0.09	292.85
32	0	0	0	0	0	0	0	<LOQ	0	0	0	0	0.10
33	0	1.12	0	<LOQ	0	0	0	0.64	0.47	0.85	0.23	0	37.38
34	0	0	0	0.17	0	0	0	<LOQ	0.02	0	3.89	0	207.62
35	0	<LOD	0.1	1.49	0.24	0	0	0	0.11	0	1.37	0	86.51
37	0	0	<LOD	<LOQ	0	0	0	<LOQ	0	0	0.04	0	29.14
39	<LOD	<LOQ	<LOQ	0.46	0.09	0	0	<LOQ	0.67	0	1.51	0	87.39
36	0	0	0	0	0	0	0	0.06	0	0	0	0	7.12
38	0	0	0	0	0	0	0	0.03	0	0	0	0	53.03
40	0	0	0	0.29	<LOQ	0	0	<LOQ	0.24	0	1.96	0.15	133.62
41	0	0	0	<LOQ	<LOQ	0	0	<LOQ	0.04	0	0.7	0.04	68.51
42	0	0	0	0	0	0	0	0	0	0	0	0	0.00
43	<LOD	0	0	0	0	0	0	0.04	0	0	0.08	0	37.91
44	0	0	0	0	0	0	0	0	0	0	0	0	0.56
45	0	0	0	0	0	0	0	0.03	0.03	0	0	0	0.71

0 – not detected

<LOD – below the limit of detection

<LOQ – below the limit of quantification

Appendix II

Table 10-5. Summary of concentrations in ng g⁻¹ dry weight for (N)BFRs analysed in all 45 sediment samples

Nr	HBCDDs	TBBPA	TBP	BEH-TEBP	BTBPE	DBDPE	PBEB	asDP	EH-TBB / $\alpha\beta$ -DBE-DBCH / BB153 / HBB
1	3.54	0.87	0.14	5.65	1.94	0	0	65.94	0
2	1.86	0.63	0.09	3.23	<LOQ	22.49	0	0	0
3	2.27	0.71	<LOQ	3.75	<LOQ	0	0	0	0
4	0.24	0.3	<LOQ	0.42	0	0	0	0	0
5	1.48	0.27	0.09	1.29	0	24.01	0	0	0
6	2.76	0.6	0.06	0.59	0	0	0	1.50	0
7	1.95	0.52	0	2.24	<LOQ	0	0	0.81	0
8	0.02	2.62	0	0	0	0	0	0	0
9	6.43	0.45	0.11	10.09	0.46	<LOD	0	0	0
10	13.29	0.9	0	6.57	0	<LOD	0	0	0
11	0.17	0.61	0	0	0	0	0	0.31	0
12	0.73	1.11	0.14	<LOQ	0.13	0	47.50	0	0
13	0.02	<LOQ	0	0	0	0	0	0.14	0
14	3.58	0.39	0.07	3.52	<LOQ	0	0	17.96	0
15	9.78	0.97	0.17	13.74	<LOQ	<LOQ	0	0	0
16	2.32	0.62	0	5.04	<LOQ	0	0	0	0
17	0.88	0.23	0.16	0	0	0	0	0	0
18	38.19	1.09	0.16	12.08	0.17	0	0	0	0
19	0.54	0.42	0	6.65	<LOQ	0	0	0	0
20	4.83	1.51	0.14	11.37	<LOQ	0	14.47	0	0
21	6	0.69	0.24	11.72	3.53	<LOD	0	0.27	0
22	6.24	1.39	0.22	12.34	0.1	0	0	0	0
23	0.65	1	0.05	1.5	<LOD	0	0	0	0
24	3.6	0.69	0.13	5.51	<LOQ	0	0	0	0
25	3.43	0.62	0.18	9.03	0	0	0	0	0
26	0.09	0	0.16	0	3.47	0	12.87	0	0

Appendix II

Table 10-5 continued									
27	3.7	0.65	0.43	2.27	1.81	0	0	0.27	0
28	2.08	0.8	0.05	5.23	<LOQ	0	0	0	0
29	2.23	0.77	0.19	2.72	<LOD	0	0	0	0
30	2.39	0.32	0.07	2.21	0	0	0	0	0
31	22.93	0.68	0.16	3.92	<LOD	<LOD	0	0	0
32	0	<LOQ	0.12	0	0	<LOD	0	0	0
33	0.7	0.62	0.42	0.35	3.84	0	0	0	0
34	7.9	0.35	0.18	1.1	0	0	0	0	0
35	2.82	0.45	0.13	1.5	0	0	0	0	0
37	0.83	0.25	0.17	0.36	0	0	0	0	0
39	1.82	0.25	0.36	1.19	0.16	<LOD	0	0	0
36	0.04	<LOQ	0.04	<LOQ	0	0	0	0	0
38	1.41	0.06	0	0	3.8	<LOD	0	0	0
40	0.44	0.2	0	2.11	<LOD	0	0	0	0
41	0.22	0.18	0	1.09	0	<LOD	0	0	0
42	0	<LOQ	0	0	0	0	0	0	0
43	0.06	<LOQ	0	0	0	0	0	0	0
44	0	<LOQ	0	0	0	0	0	0	0
45	0	0.3	0	0	0	0	0	0	0

0 – not detected

<LOD – below the limit of detection

<LOQ – below the limit of quantification

Appendix III

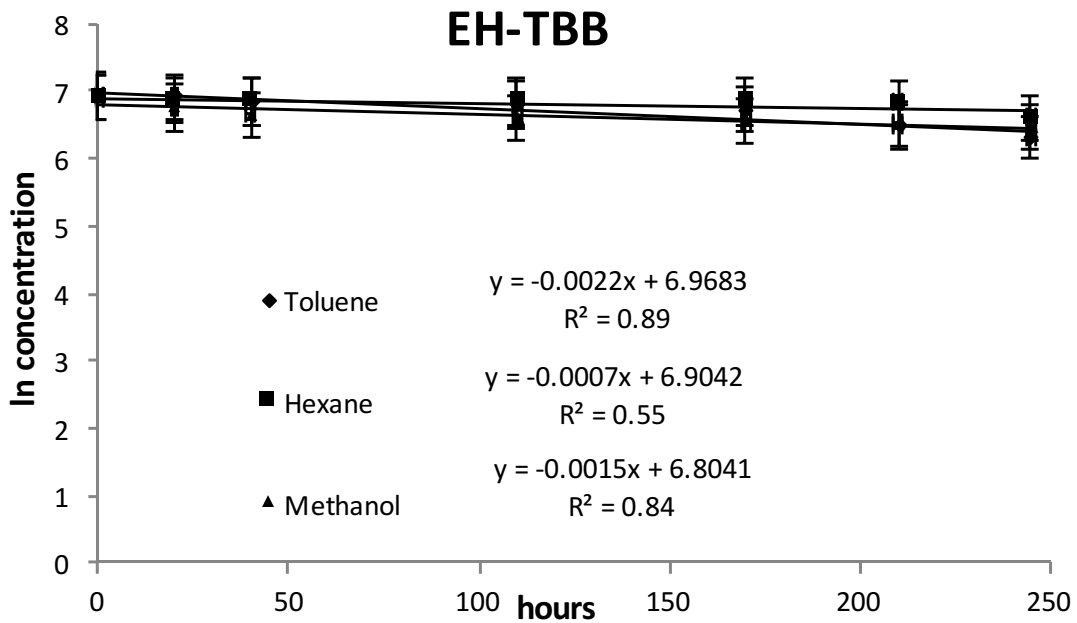
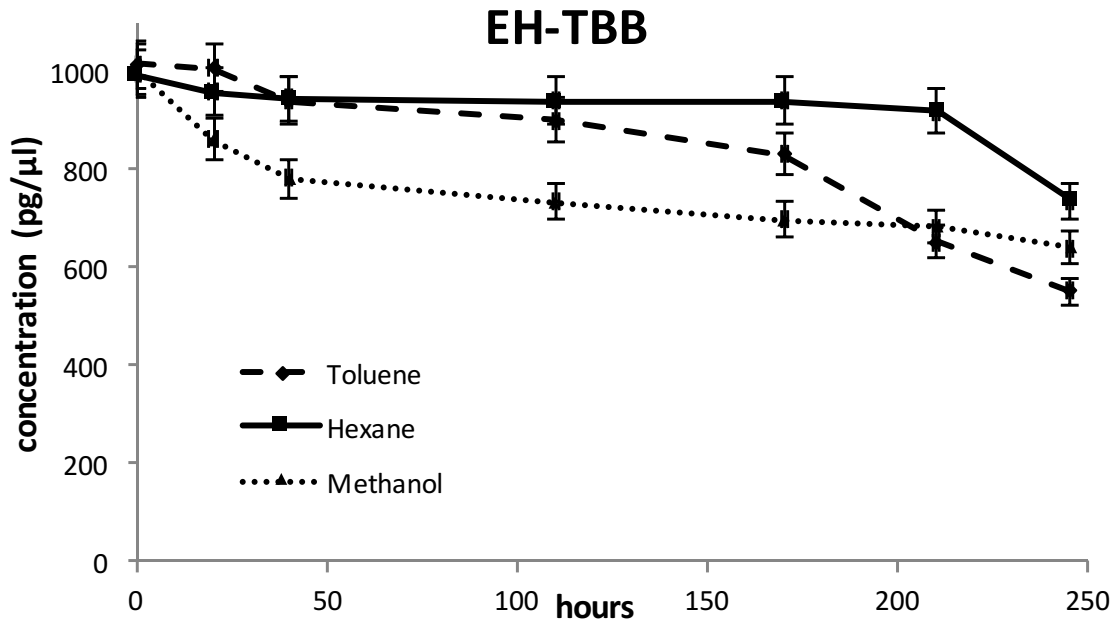


Figure 11-1. The concentration of EH-TBB at different irradiation times (top) during indoor exposure, including first order kinetic degradation rates in toluene, hexane and methanol (bottom)

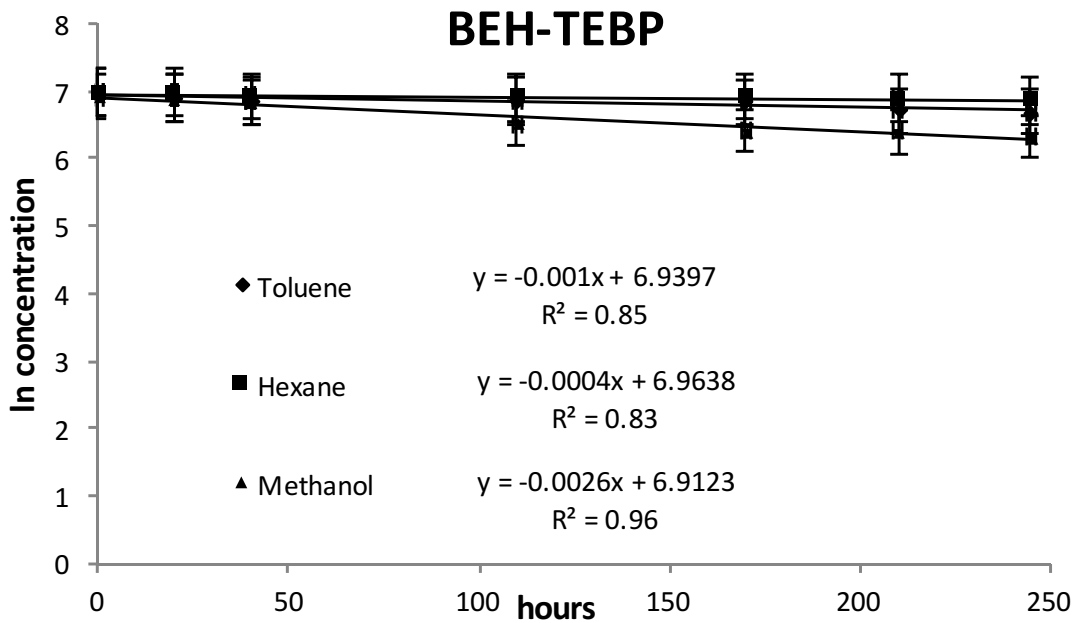
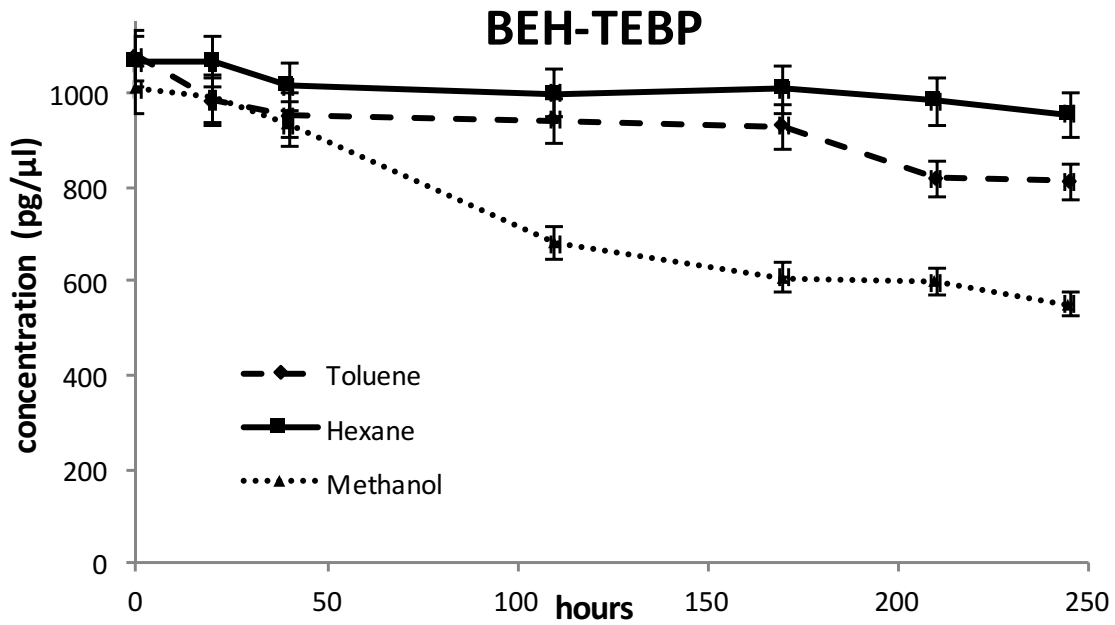


Figure 11-2. The concentration of BEH-TEBP at different irradiation times (top) during indoor exposure, including first order kinetic degradation rates in toluene, hexane and methanol (bottom)

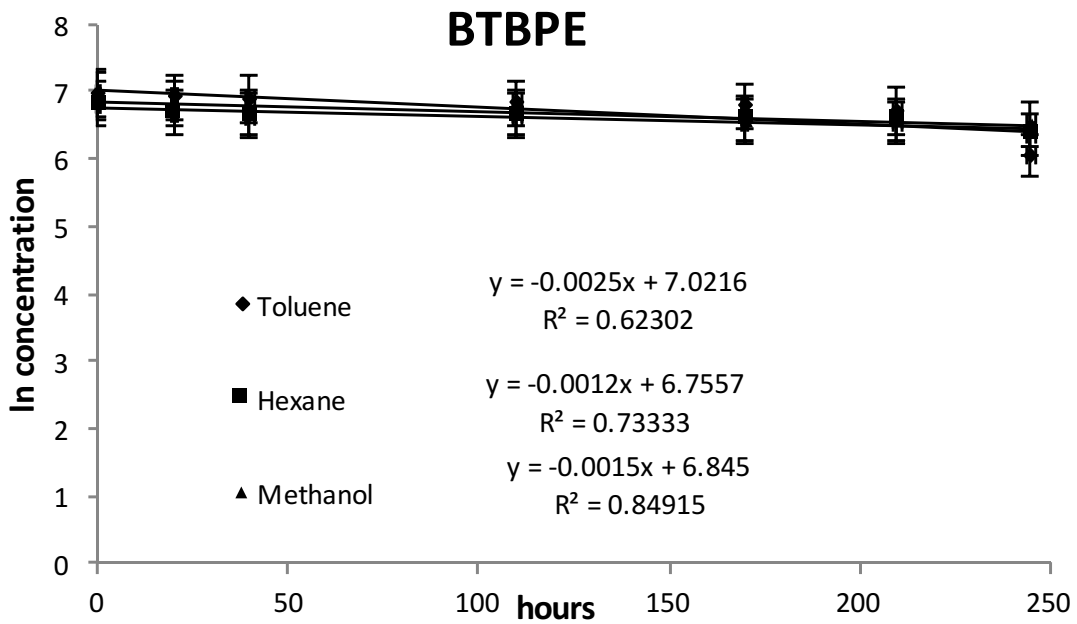
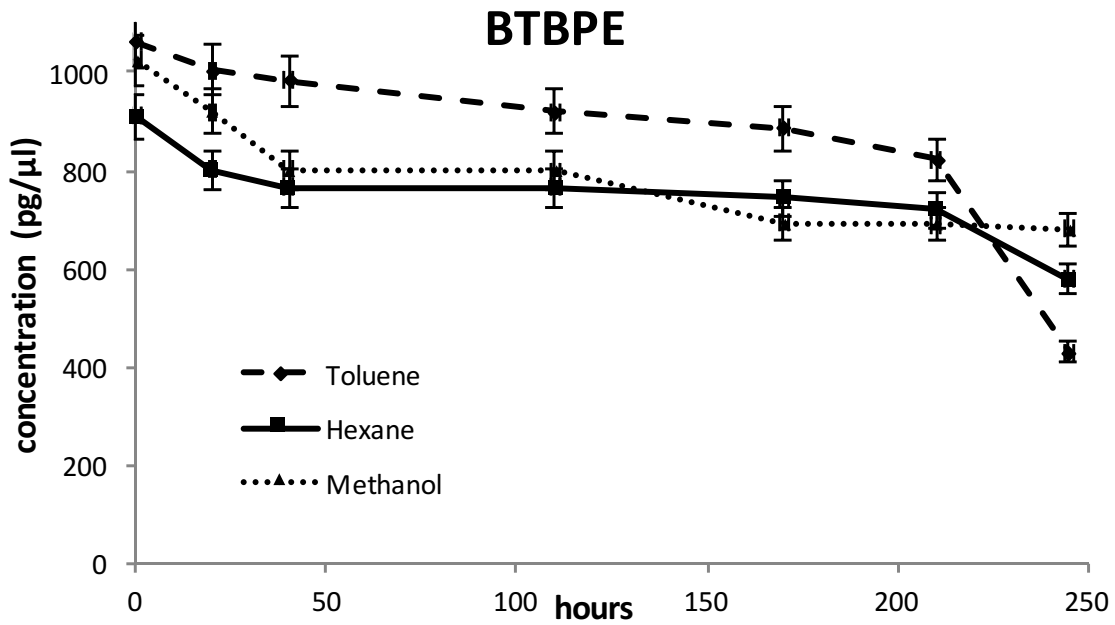


Figure 11-3. The concentration of BTBPE different irradiation times (top) during indoor exposure, including first order kinetic degradation rates in toluene, hexane and methanol (bottom)

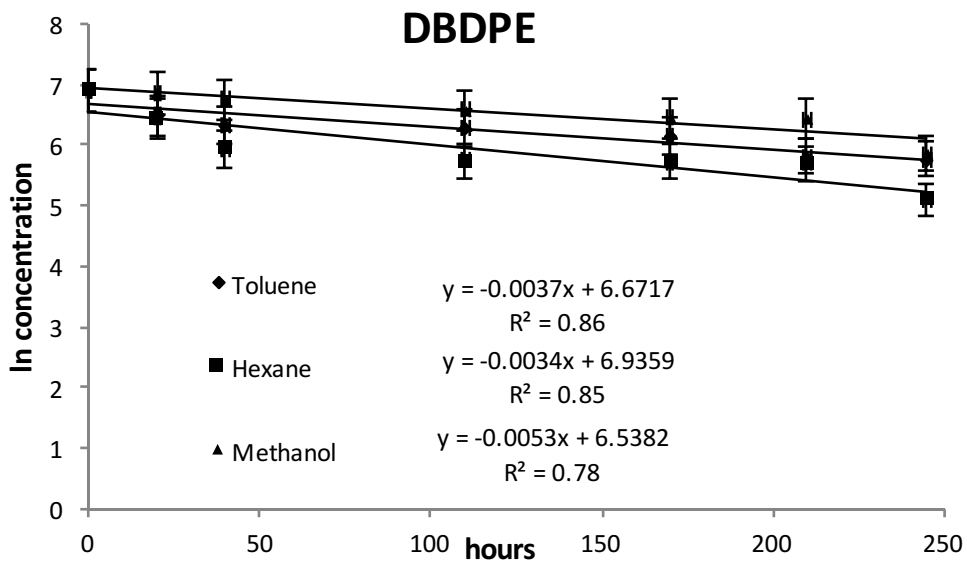
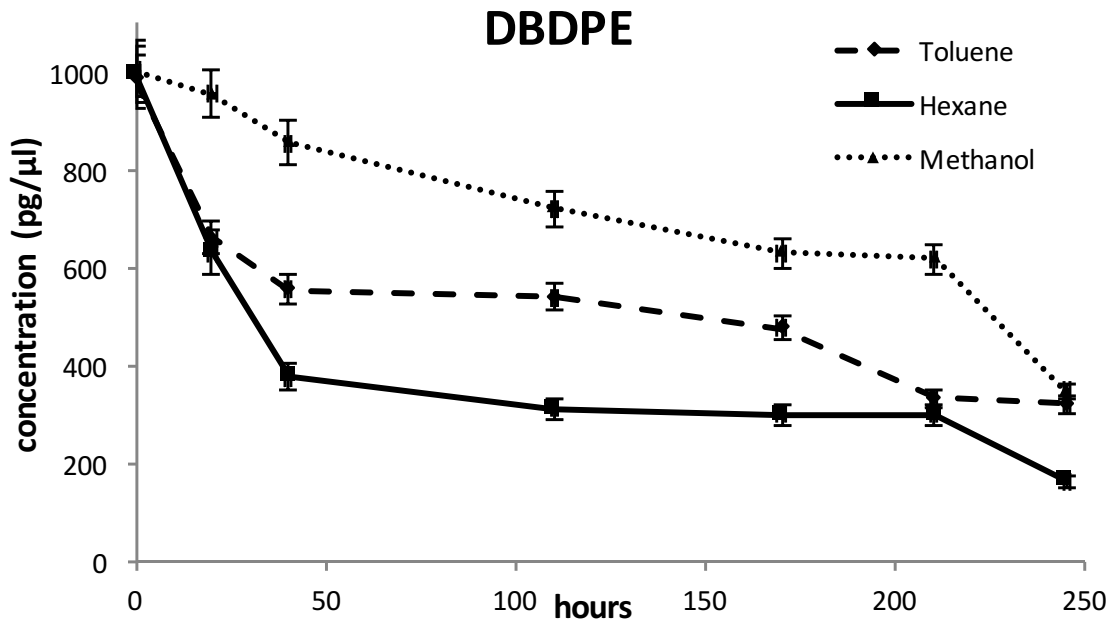


Figure 11-4. The concentration of DBDPE different irradiation times (top) during indoor exposure, including first order kinetic degradation rates in toluene, hexane and methanol (bottom)

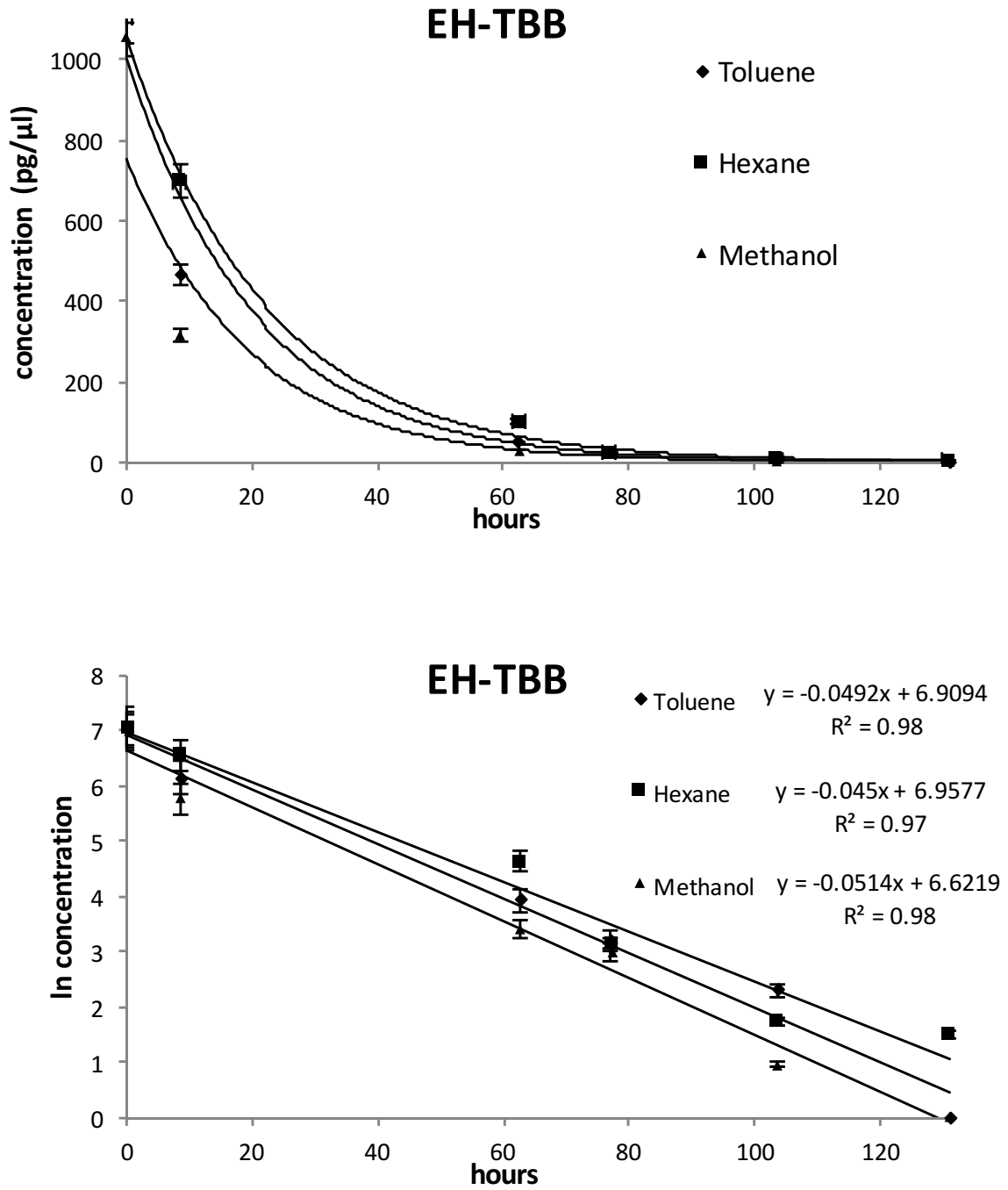


Figure 11-5. The concentration of EH-TBB different irradiation times (top) during outdoor exposure, including first order kinetic degradation rates in toluene, hexane and methanol (bottom)

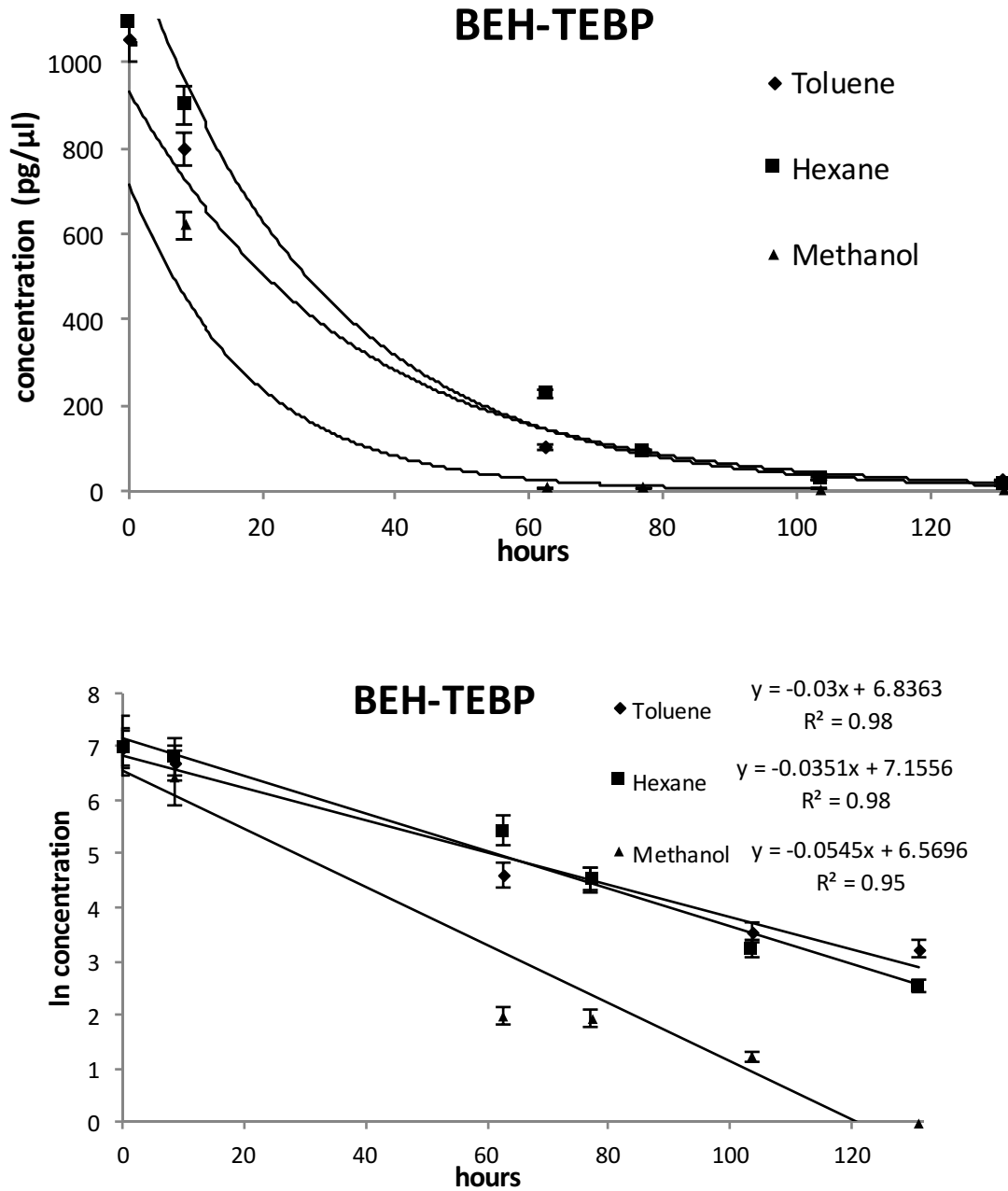


Figure 11-6. The concentration of BEH-TEBP different irradiation times (top) during outdoor exposure, including first order kinetic degradation rates in toluene, hexane and methanol (bottom)

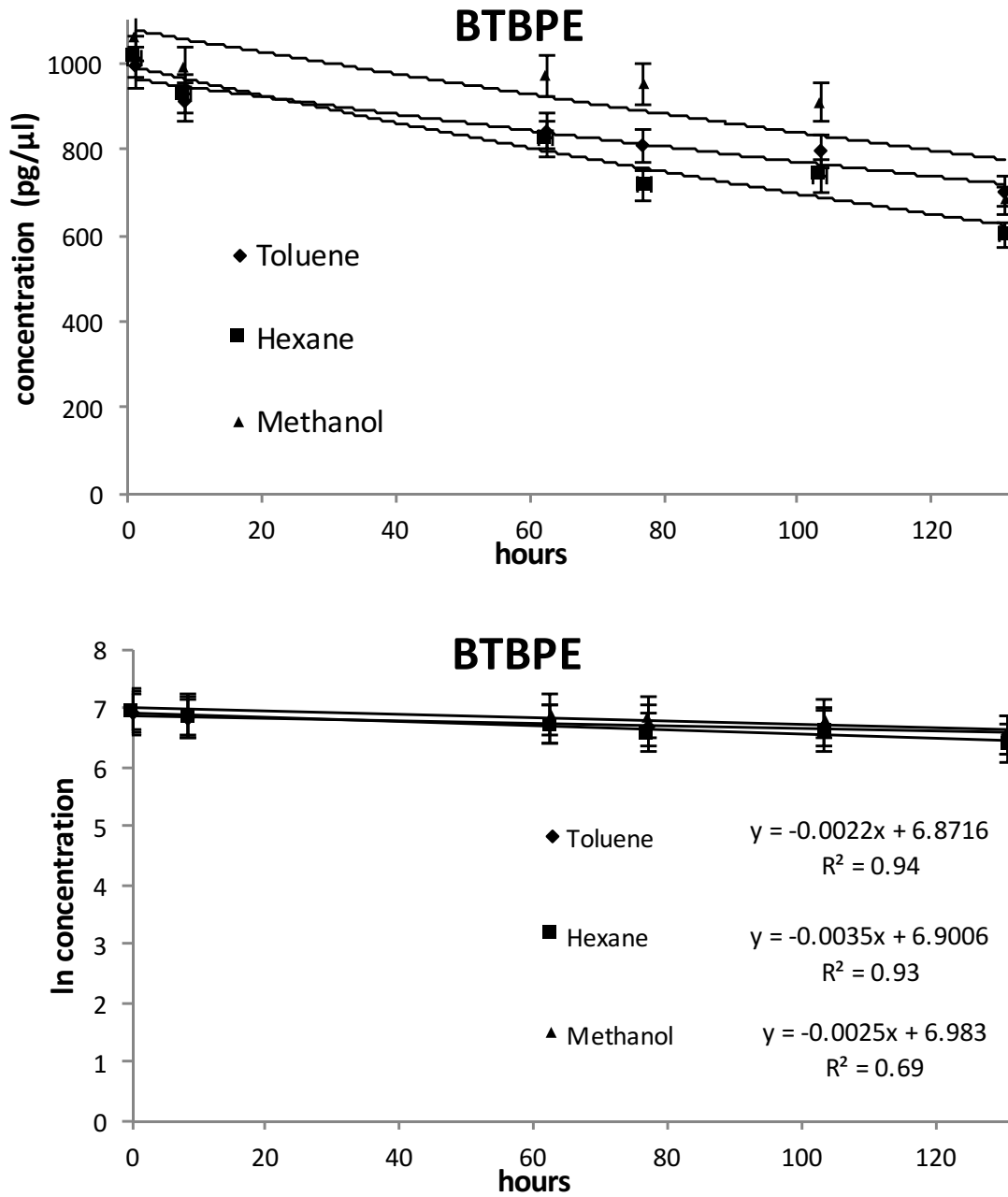


Figure 11-7. The concentration of BTBPE different irradiation times (top) during outdoor exposure, including first order kinetic degradation rates in toluene, hexane and methanol (bottom)

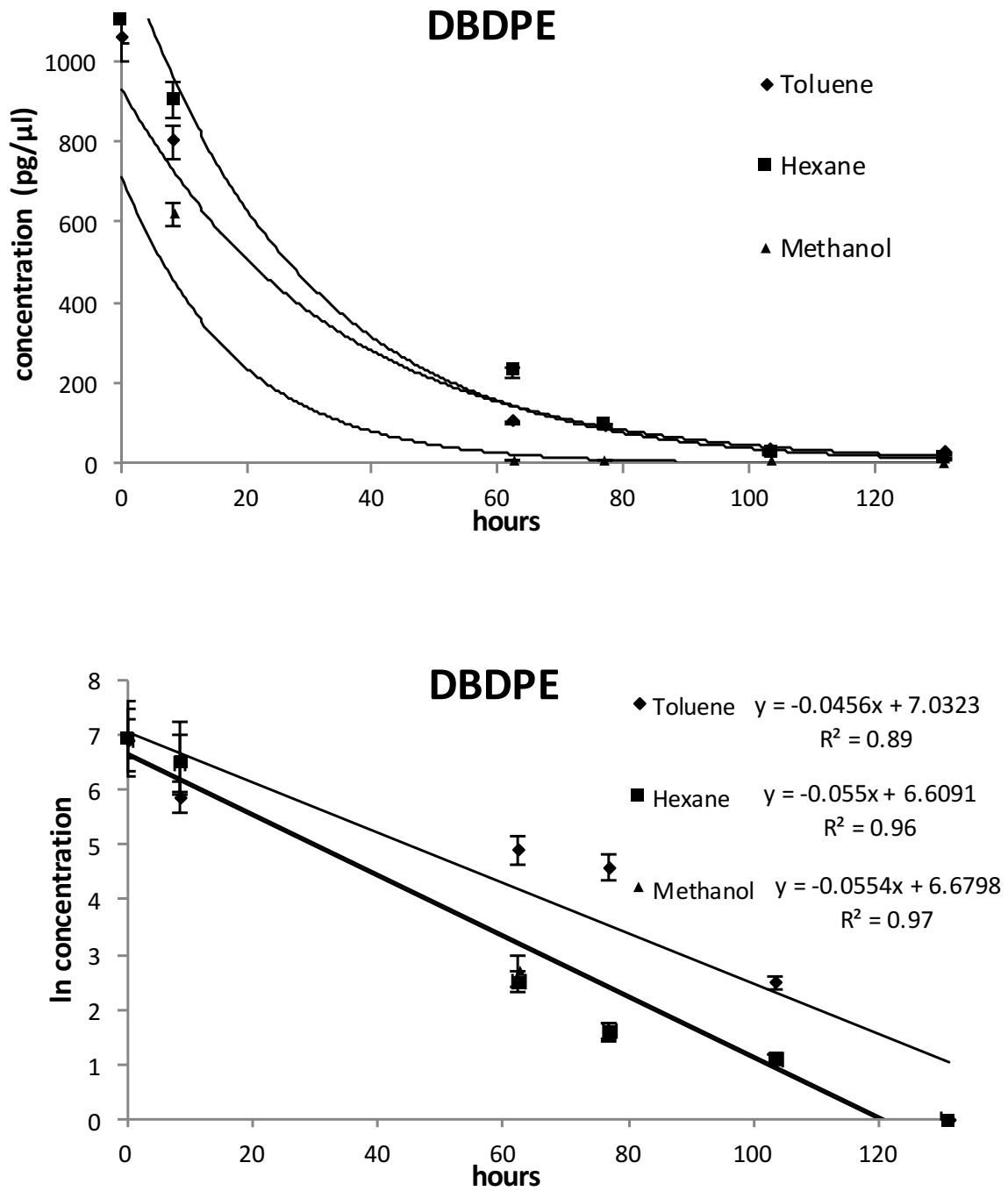


Figure 11-8. The concentration of DBDPE different irradiation times (top) during outdoor exposure, including first order kinetic degradation rates in toluene, hexane and methanol (bottom)

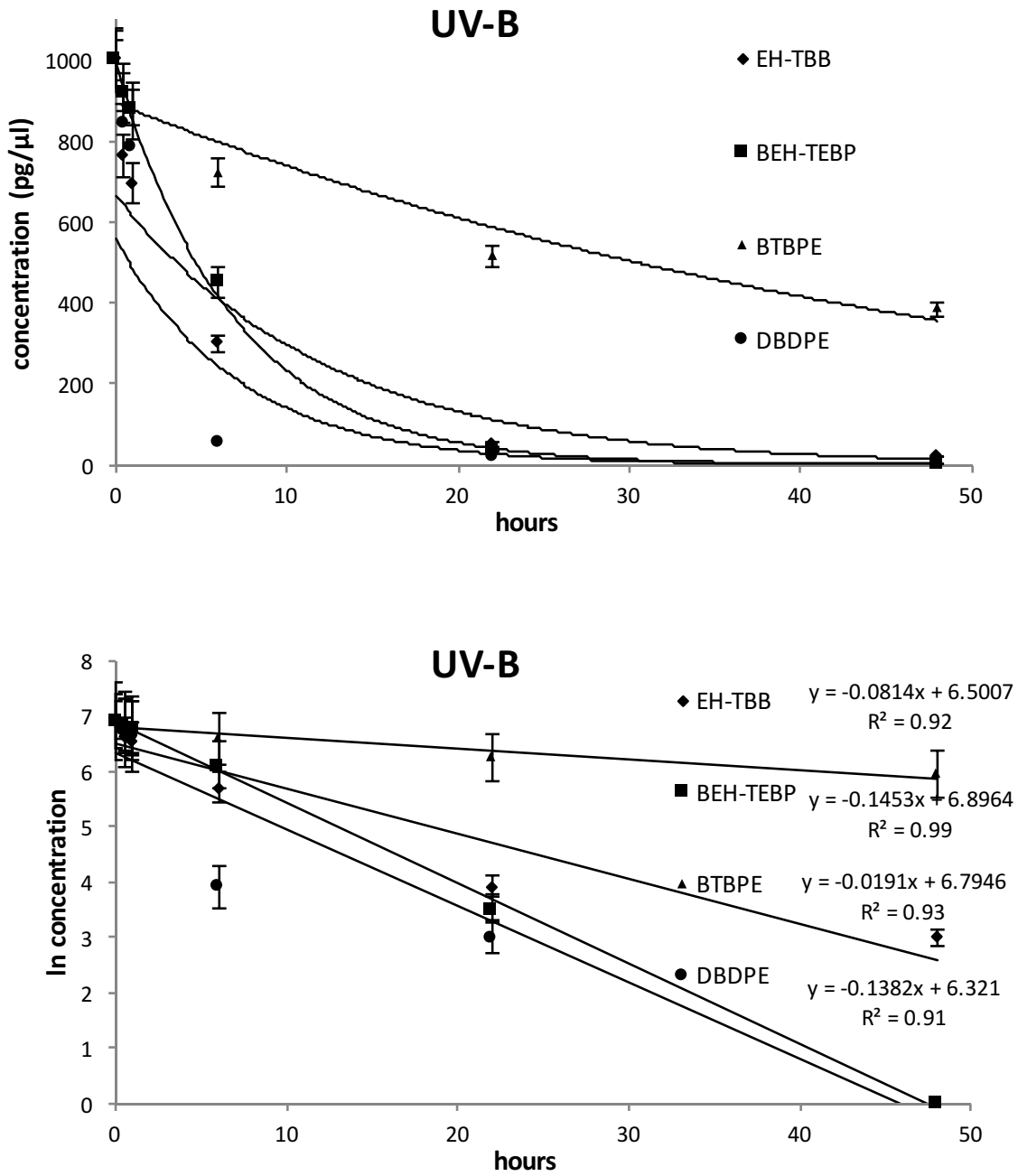


Figure 11-9. The concentration of EH-TBB, BEH-TEBP, BTBPE and DBDPE different irradiation times (top) during UV-B exposure, including first order kinetic degradation rates in methanol (bottom)

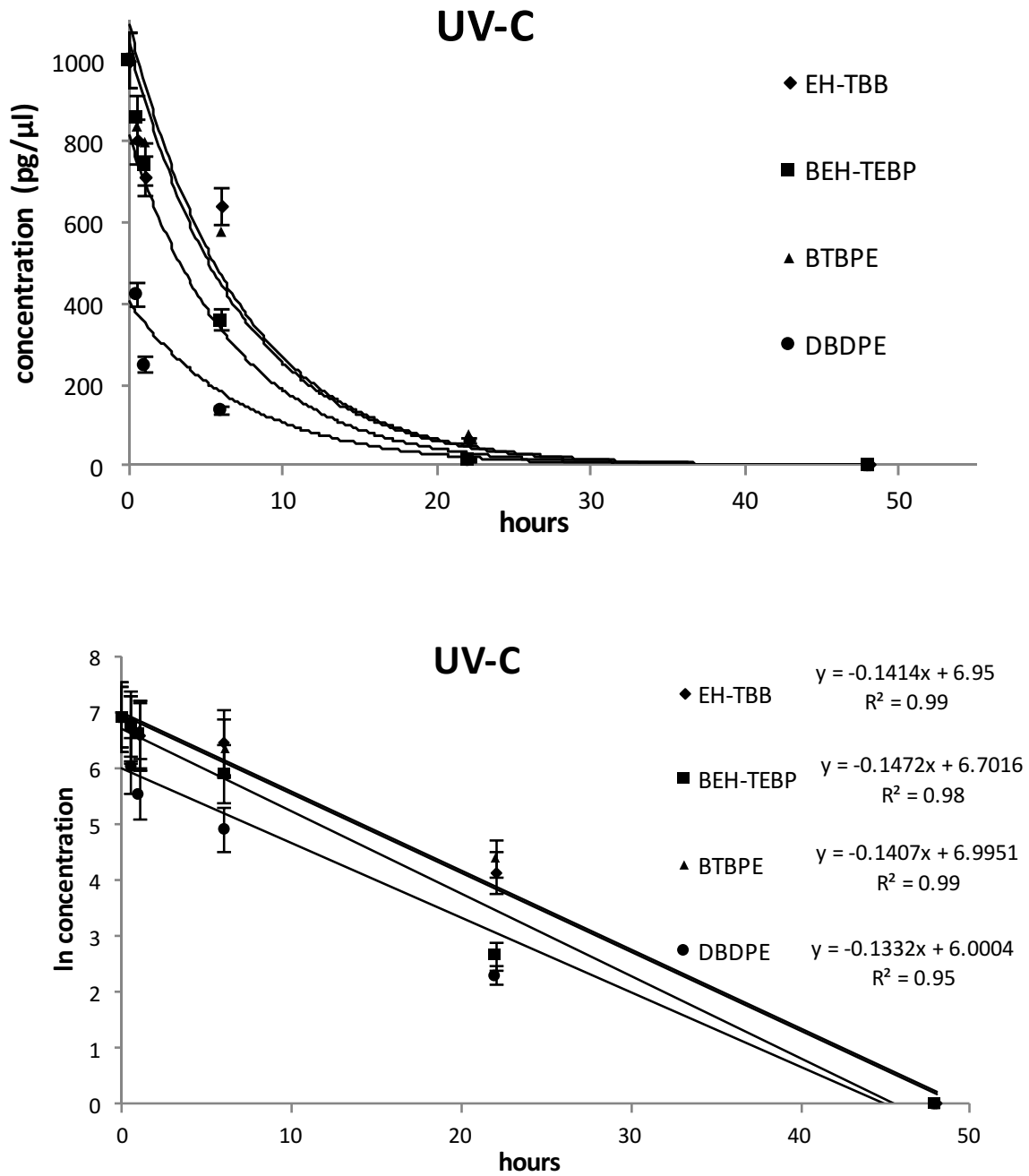


Figure 11-10. The concentration of EH-TBB, BEH-TEBP, BTBPE and DBDPE different irradiation times (top) during UV-C exposure, including first order kinetic degradation rates in methanol (bottom)